UNIVERSITY OF COPENHAGEN
FACULTY OF SCIENCE

NIELS BOHR INSTITUTE

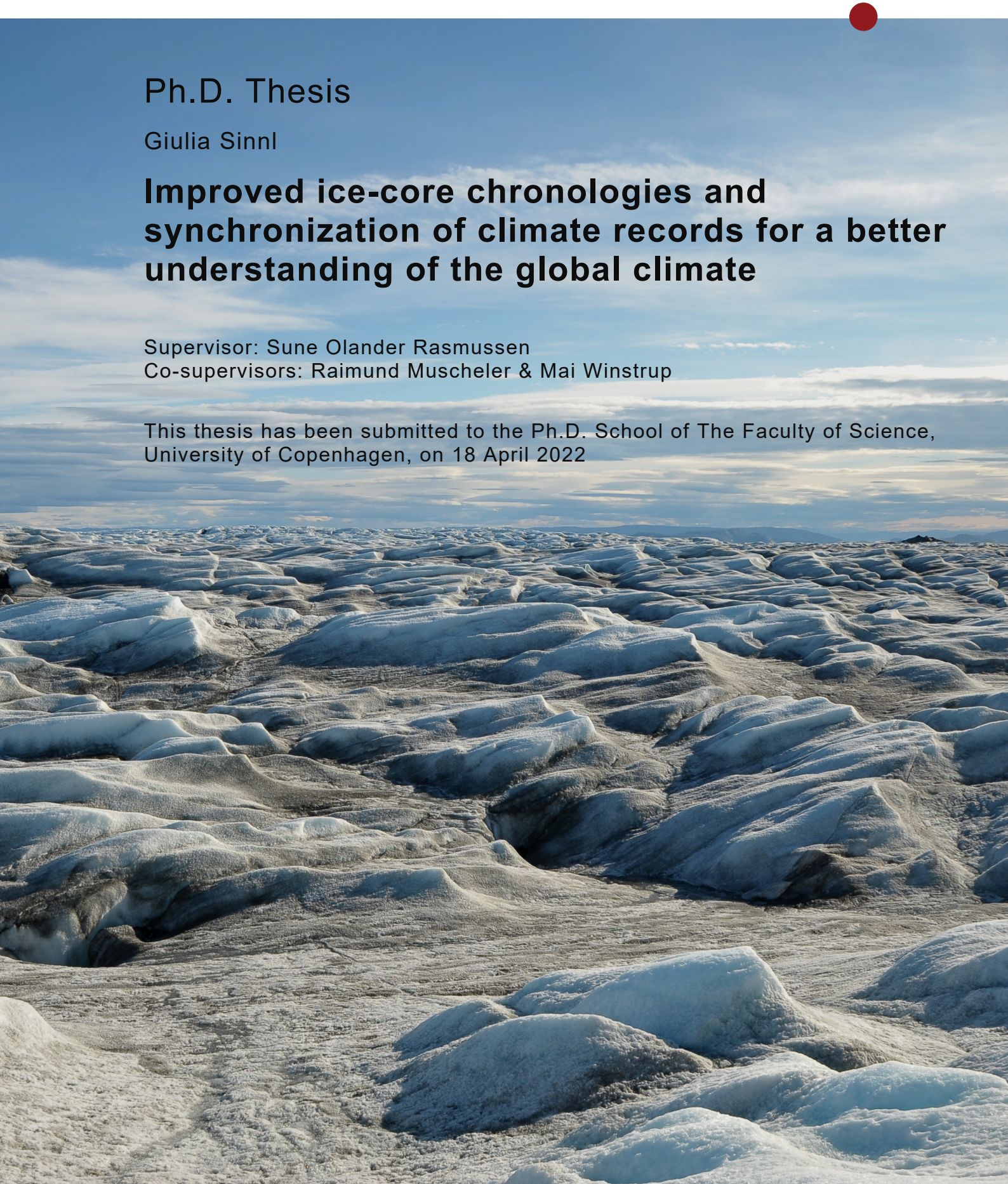

Ph.D. Thesis

Giulia Sinnl

Improved ice-core chronologies and synchronization of climate records for a better understanding of the global climate

Supervisor: Sune Olander Rasmussen
Co-supervisors: Raimund Muscheler & Mai Winstrup

This thesis has been submitted to the Ph.D. School of The Faculty of Science, University of Copenhagen, on 18 April 2022

Cover picture: Ice Cap Point 660, just outside of Kangerlussuaq in Greenland, covered in dust particles, likely deposited by the wind from the surrounding area.
(ph: Franck Hollander www.flickr.com/photos/fhollander)

Dedicated to my parents

Abstract (English)

Greenlandic ice cores contain a wealth of information thanks to the perpetual fall of snow and the chemical signals recorded in the deposited layers. The study of ice cores thus relies on the accurate time scale of these layers. Other layered archives, such as tree rings or speleothems, form by different mechanisms and are to be dated independently from ice cores.

In this thesis, I address some problems in the previously established Greenland Ice Core Chronology (GICC05). I propose a new timescale of Greenlandic ice cores covering the most recent 3800 years, which is called GICC21. The method for constructing GICC21 is based on annual layer counting between multiple ice cores. I verified the good accuracy of the new time scale against some single-ice-core time scales and the tree-ring time scale.

With the aid of the GICC21 timescale and the newly measured data from the EastGRIP and NEEM ice cores, I present a study of post-volcanic climate on the Greenlandic ice sheet. I find that, after strong tropical eruptions, the climate in Greenland is cooled down for the subsequent decade, after which the regional climate returns to its pre-eruptive state. Furthermore, I find frequent co-occurrence of warm decades in the North American continent with surface melt on the ice sheet.

In the period between 20 and 25 thousand years ago, I have analysed the concentration of the cosmogenic radionuclide Beryllium-10 in the ice from NorthGRIP (Greenland) and WAIS (Antarctica). I have compared these datasets to the concentration of cosmogenic radionuclide Carbon-14 in a Chinese speleothem. The three climatic archives are connected by the solar activity that modulates the production of these atoms, by which they can be synchronized. I find that the GICC05 timescale was dated about 400 years too young compared to the speleothem. Moreover, I add the new result that the Antarctic timescale is also too young, by about 200 years.

These time scale discrepancies may be caused by less snowfall in the coldest periods of the last glacial, the Heinrich Stadials. Thanks to the synchronization of the three time scales, I was able reconstruct the sequence of climatic events in the period between 20 and 25 thousand years ago, examining the timing of two northern-hemispheric Dansgaard Oeschger events relative to the Antarctic Isotope Maximum 2.

Abstract (Danish)

Grønlandske iskerner indeholder en stor mængde information grundet det årlige snefald som arkiver partikler og kemikalier i lag. Studier af iskerner er derfor baseret på nøjagtigheden af hvordan disse lag er dateret. Andre lagdelte arkiver, så som træringe og speleothems, dannes ved andre mekanismer og kan derfor dateres uafhængigt af iskerner.

I dette thesis adresserer jeg problemer med den tidligere grønlandsk iskerne-kronologi (GICC05). Jeg forslår en ny tidsskala for grønlandske iskerner, som dækker over de sidste 3800 år og som kaldes GICC21. Denne tidsskala er baseret ved at tælle de årlige sne lag over flere forskellige iskerner. Jeg verificerede nøjagtigheden af denne nye tidsskala ud fra enkelt iskerne tidsskalaer og trærings tidsskalaen.

Ved hjælp fra den nye GICC21 tidsskala og nye data fra EastGrip og NEEM iskernerne, præsenterer jeg et studie af post vulkansk klima af den grønlandske indlandsis. Jeg finder, at, efter en stor tropisk vulkanudbrud, det grønlandske klima vil se en nedkøling, som varer det næste årti, hvorefter local-klimaet vil blive genetableret. Derudover finder jeg flere sammenfaldene mellem smelte lag og varme årtier i det norlige amerikanske kontinent.

For perioden mellem 20 til 25 tusinde år siden har jeg analyseret koncentrationen af radionuklidet beryllium-10, som forkommer af kosmisk stråling, i iskerne fra NorthGRIP (Grønland) og WAIS (Antarktis). Jeg sammenligner dette data med koncentrationen af radionuklidet kulstof-14 i en kinesisk speleothem. Disse tre klima arkiver er forbundet af solaktiviteten, som regulerer produktionen af radionkuliderne, hvilket gør det muligt at synkronisere de tre tidsskalaer.

Jeg viser at den GICC05 tidsskala er 400 år for ung sammenlignet med speleothemen, derudover finder jeg at den Antarktiske tidsskala (WD2014) er 200 år for ung. Denne uoverensstemmelse kan skyldes den lavere mængde snefald under de koldeste perioder, Heinrich Stadials, af den sidste istid. Ud fra synkroniseringen af disse tre tidsskalaer kunne jeg rekonstruere sekvensen af klimatiske begivenheder i perioden 20 til 25 tusinde år siden.

Abstract (Italiano)

Le carote di ghiaccio groenlandesi contengono una gran varietá di informazione grazie ai segnali chimici depositati ogni anno con la neve. Lo studio dei ghiacci si fonda dunque sull'accurata datazione di questi strati di deposito nevoso. Altri archivi climatici che si accrescono di anno in anno, come ad esempio gli anelli nel legno o le stalagmiti, si formano in condizioni diverse e devono essere datati con metodi indipendenti.

In questa tesi affronto alcune delle problematiche legate alla scala temporale dei ghiacci groenlandesi giá esistente (GICC05). Propongo una nuova scala temporale dei ghiacci groenlandesi riguardante gli ultimi 3800 anni, denominata GICC21. Il metodo di costruzione della GICC21 si basa sul conteggio comparato degli anni di deposito nevoso registrati in svariate carote glaciali. Ho valutato l'accuratezza della nuova cronologia, confrontandola con le scale temporali di due singole carote glaciali e con la scala temporale dendrocronologica.

Grazie alla GICC21 e ai nuovi dati misurati nelle piú recenti carote glaciali EastGRIP e NEEM, propongo uno studio del clima registratosi in Groenlandia negli anni successivi ad alcune delle piú drammatiche eruzioni vulcaniche. Dimostro che, dopo le eruzioni tropicali piú forti, il clima groenlandese si raffredda per una decade, per poi riassestarsi nuovamente sui livelli medi pre-eruttivi. Verifico inoltre la coincidenza molto frequente di decadi con elevate temperature nel continente nordamericano con eventi di scioglimento superficiale in Groenlandia.

Nel periodo dai 20 ai 25 mila anni fa ho analizzato il contenuto di atomi cosmogenici radioattivi di berillio-10 nel ghiaccio proveniente dal sito NorthGRIP, in Groenlandia, e dal sito WAIS, in Antartide. Ho confrontato questi dati con il contenuto di atomi cosmogenici radioattivi di carbonio-14 in una particolare stalagmite cinese. Questi tre archivi climatici, pur trovandosi in regioni distanti, sono connessi dall'attivitá solare che modula la produzione di tali atomi.

Confermo i risultati di studi precedenti affermando che la scala temporale groenlandese é in ritardo di circa 400 anni sulla scala temporale della stalagmite cinese, la quale registra etá piú antiche. Aggiungo il nuovo risultato che anche la scala temporale antartica é in ritardo di circa 200 anni rispetto alla stalagmite cinese. Le ragioni di queste incongruenze temporali sono associabili a particolari dinamiche climatiche in risposta ai periodi piú freddi dell'ultima era glaciale, ovvero quelli successivi agli eventi di Heinrich, periodi di frequente

distacco di iceberg nell'oceano Nord Atlantico. Grazie a questo confronto cronologico, sono in grado di ricostruire la sequenza climatica del periodo, esaminando le tempistiche di due eventi di Dansgaard-Oeschger in Groenlandia rispetto al secondo Massimo Isotopico in Antartide.

Acknowledgments

First and foremost, I would like to thank my supervisor, Sune, who has helped me in so many ways in the past four years that I cannot even recount. Thanks to him, I got to make this Ph.D. a rewarding and full experience and I have learned how to present myself as a scientist. I could not have hoped for a more generous, supportive, competent, and honest supervisor.
A big thank you goes to Raimund for the support of my research and the time I could spend at the Lund Laboratory. Thank you also to Chiara for the help and the hospitality in Lund.
Thank you to Mai for the many fine-tuning sessions and the help with the StratiCounter algorithm. Thank you to Anders for much support about time scales and for organizing the very useful stratigraphy meetings.
Next, I would like to thank the Ph.D. students and junior colleagues at PICE that I have had the luck to meet and call my friends in the past three years: Iben, Meg, Jesper, Marta, Nicholas, Eliza, and all the others. Thanks, in particular, to Julien, Tamara, and Jia-Mei for these years of shared office and for always helping each other in this adventure.
Thanks to Hjalte for meeting me during this amazing time and for all the support. Thanks to my flatmates and friends, Gabriele and Theresa, for being there. Thanks to the Tangospirer community for keeping me sane!
Thanks to my mother, my father, my sister, my grandparents, and the rest of my family, for supporting me in my choice of moving away.
Thanks to Paolo for having fought the hardest battle, we will miss you.

Table of Contents

Table of Figures

List of Abbreviations and Units

AICC2012	Antarctic Ice Core Chronology 2012
AMOC	Atlantic Meridional Overturning Circulation
AMS	Accelerator Mass Spectrometry
ASM	Asian Summer Monsoon
AWI	Alfred Wegener Institute
BC	Black Carbon
CFA	Continuous Flow Analysis
DEP	Dielectric Profiling
DRI	Desert Research Institute
EastGRIP or EGRIP	East GReenland Ice-core drilling Project
ECM	Electrical Conductivity Measurement
G2B Event	GS2.1c 10Be Event
GCR	Galactic Cosmic Rays
GI	Greenland Interstadial
GICC	Greenland Ice Core Chronology
GICC05	Greenland Ice Core Chronology 2005
GICC21	Greenland Ice Core Chronology 2021
GRIP	GReenland Ice-core drilling Project
GS	Greenland Stadial
HE	Heinrich Event
HS	Heinrich Stadial
IC	Ion Chromatography
ICP-MS	Inductively coupled plasma mass spectrometry
IntCal	Radiocarbon Calibration Curve
INTIMATE	INTegration of Ice-core, MArine and TErrestrial records
IRD	Ice Rafted Debris
ITCZ	Intertropical Convergence Zone
LGM	Last Glacial Maximum
MCE	Maximum Counting Error of GICC05
NAO	North Atlantic Oscillation
NEEM	North Greenland Eemian Ice Drilling Project
NEEM-2011-S1	Shallow core S1 drilled in 2011 at NEEM
NEGIS	North East Greenland Ice stream
NH	Northern Hemisphere
NorthGRIP or NGRIP	North GReenland Ice-core drilling Project
NS1-2011	NEEM-2011-S1 Ice Core Chronology
ppb	Parts per billion
ppbv	Parts per billion by volume
RECAP	Renland Ice Cap Ice core
RSMD	Root-mean-square deviation
SC	StratiCounter
SH	Southern Hemisphere
SPE	Solar Proton event
SVF	Sigl et al. (2015) volcanic forcing dataset
TSI	Total Solar Irradiance
U/Th	Uranium/Thorium
VEI	Volcanic Explosivity Index
VS	Visual Stratigraphy
WAIS	West-Antarctic Ice Divide
WD2014	WAIS Divide Ice Core Chronology 2014
WDC	WAIS Divide Ice Core
b2k	Years before 2000 CE
BP	Years before present (1950 CE)
CE/BCE	Years (Before) Common Era
µeq./kg	micro equivalents per kilogram
‰	permille

List of Papers

Paper I (co-author) "A first chronology for the East Greenland Ice-core Project (EastGRIP) over the Holocene and last glacial termination"
Authors: Seyedhamidreza Mojtabavi, Frank Wilhelms Eliza Cook, Siwan M. Davies, **Giulia Sinn**l, others, and Sune Olander Rasmussen
Status: Published (2020) Climate of the Past, 16(6), 2359-2380.
https://doi.org/10.5194/cp-16-2359-2020

Paper II (co-author) "Upstream flow effects revealed in the EastGRIP ice core using Monte Carlo inversion of a two-dimensional ice-flow model"
Authors: Tamara Annina Gerber, Christine Schøtt Hvidberg, Sune Olander Rasmussen, Steven Franke, **Giulia Sinnl**, others, and Dorthe Dahl-Jensen
Status: Published (2021) The Cryosphere, 15(8), 3655-3679.
https://doi.org/10.5194/tc-15-3655-2021

Paper III (main author) "A multi-ice-core, annual-layer-counted Greenland ice-core chronology for the last 3800 years: GICC21"
Authors: Giulia Sinnl, Mai Winstrup, Tobias Erhardt, Eliza Cook, Camilla Jensen, Anders Svensson, Bo Møllesøe Vinther, Raimund Muscheler, and Sune Olander Rasmussen
Status: Accepted (Mar 2022) Climate of the Past Discussions, 1-34.
https://doi.org/10.5194/cp-2021-155

Paper IV (co-author) "Melt in the Greenland EastGRIP ice core reveals Holocene warming events"
Authors: Julien Westhoff, **Giulia Sinnl**, others, and Ilka Weikusat
Status: Second review round (Feb 2022) Climate of the Past Discussions, 1-36.
https://doi.org/10.5194/cp-2021-89

Paper V (main author) "Synchronizing ice-core and U/Th time scales in the Last Glacial Maximum using Hulu Cave ^{14}C and new ^{10}Be measurements from Greenland and Antarctica"
Authors: Giulia Sinnl, Raimund Muscheler, Florian Adolphi, Marcus Christl, Kees Welten, Thomas Woodruff, Marc Caffee, Anders Svensson, Sune Olander Rasmussen
Status: Submission planned to Climate of the Past

Preface — Aim of Research and How To read this Thesis

During my PhD, I have gathered a lot of formative experiences which I hope have made me a reliable scientist, although I started with very little background in the field of glaciology. Because of the pandemic, the opportunities for dissemination have been limited, therefore this thesis is particularly dear to me as a record of my work in the last 3.5 years at Copenhagen University within the Physics of Ice and Climate group (PICE).
Luckily, I had the chance to teach about annual-layer counting at the ICAT summer school (Copenhagen 2019) and I talked about my research at INQUA (Dublin 2019), at the EastGRIP steering committee in 2019, and at the EastGRIP seminar in March 2022.
I personally travelled to EastGRIP to witness the ice drilling in the summer of 2019 and to work in the water isotope lab: this part of my work will be absent from this thesis because of its practical traits and because none of it resulted yet in a conclusive scientific outcome specific to my project.

In this thesis, I have conducted an intensive and demanding analysis of large amounts of ice core data mostly from Greenland and, in one case, from Antarctica. The aim of my PhD project has been, since the very early days of my enrolment, an investigation about possible revisions to be made to the Greenlandic Ice Core Chronology (GICC05). As GICC05 has been the result of many efforts by esteemed colleagues, my aim has been to identify where constructive criticism could be useful to the community. Here, I plan to demonstrate at least two cases where I have found reasons to improve the GICC in the hope to encourage others to revise the chronology in the future, although it will not be easy. The advantages of such an effort are many, because a better time scale will provide new insight on the ice core data and on global climate. It simply has to be done!

In accordance with the PhD thesis guidelines of the University of Copenhagen, I prepared this thesis as a synopsis with manuscripts of papers or already published papers attached.
This thesis contains six chapters and is structured as follows.
Chapter 1 describes state-of-the-art research as well as foundational theory about the general topic of this thesis, in order to provide a review of important references that have guided my work.
Chapter 2 contains a description of how to compare ice core data with the goal of finding common isochrones. I co-authored two papers on the topic of matching EastGRIP to other ice cores in order to extend GICC05 to the newly drilled ice core (Paper I and Paper II). The

content of the sections I have collaborated on will be reproduced here, but one can access the entire papers at the DOI of the publications.

Chapter 3 briefly introduces and reproduces Paper III in its entirety.

Chapter 4 describes some unpublished work I have conducted that I did not yet bring into a publication but which I believe is worth describing before moving on to other topics. It contains an analysis on post-volcanic climate signals and a possible age-range for the Thera eruption. It contains a part of Paper IV which I have personally contributed to regarding melt at EastGRIP.

Chapter 5 briefly introduces and reproduces Paper V in its entirety.

Chapter 6 presents conclusions and outlook.

1 Introduction to Climate and Time Scales

Accurate time scales are of fundamental importance to paleoclimatic studies. The construction of time scales is, sometimes, a tedious operation of classification, but without them we would not have any clue about cause-effect relationships in climatology. For example, how would we discover that it was a period of sustained volcanic cooling that contributed to the political uprisings in the late Roman Republic? (McConnell et al., 2020)
Such fascinating links between our human development and cataclysmic events are relevant not only to archaeologists but to us all, for we can prepare better for the future if we understand our past. Fortunately for us, there is a lot of information to be gathered in nature about events that happened a long time ago. For example, by collecting paleoclimatic examples of climate change, we can better understand the possible scenarios of anthropogenic warming and use this knowledge to constrain climate models (Fischer et al., 2018).
In this thesis, I am investigating paleo timescales across the climate system, with a special focus on Greenlandic ice cores. The periods I was most interested in were the Late Holocene and a limited section of the glacial called the Last Glacial Maximum (LGM). I was mostly captured by those aspects of time scales that have a direct impact on the paleoclimatic interpretations. In this introduction, I will review the sources that I have found most useful during my research.

1.1 Past Climate as recorded in Greenlandic Ice Cores

Ice sheets today cover large parts of Greenland and Antarctica, although at times in the past they extended over North and South America, parts of the Eurasian continent, and portions of Australia and New Zealand (Batchelor et al., 2019; Gowan et al., 2021). The ice in Greenland is in a precarious state because of climate change and its dramatic effects (Meredith et al., 2019, i.e. IPCC6 Report, Chapter 3), which could imply losing information about past climate.
Ice sheets register years of continuous precipitation of snow that contains particles and chemicals from several sources, such as marine sodium, terrestrial calcium, biogenic ammonium, volcanic ashes, and more. The snow itself is composed of ice with a ratio of heavy and light isotopes of oxygen and hydrogen atoms, which tells us about the history of temperature and moisture (Dansgaard et al., 1964). Moreover, the snow traps the gasses from

past atmospheres, although the initial exchange of air with the surface makes the trapped gas younger than the surrounding ice (Blunier et al. 1995; Buizert et al. 2015).

As snow falls every year, the older snow gets compressed to firn by the overlying weight. The firn, a middle step before ice, gets further transformed because of the compression, first by closing off the bubbles of gas, and then by becoming compact ice, with a density of 0.917 g/cm^3 (Herron & Langway, 1980). Within some critical depth range, the gas bubbles are charged with very high pressures so that, when they are retrieved to the surface, they effectively explode, making the ice almost unusable for measurements (Neff et al., 2014). This ice is called brittle for obvious reasons and is often located within the part of Greenlandic ice younger than 12'000 years, i.e. the Holocene.

Through very ambitious and lengthy drilling projects, ice cores from the ice sheets of Greenland are retrieved to the surface to study all the information recorded by the old and deep ice (some examples are shown in Figure 1.1a). The deepest ice cores are more than 3000 m long and were usually drilled close to the ice divide, the highest dorsal of Greenland. The very low surface velocity on the ice divide and the thickness of the ice sheet makes these ice cores most useful for their preserved stratigraphy and their old age at depth.

The most recent ice-core drilling on Greenland is the EastGRIP project, which was started in 2016. The EastGRIP site is located in the North-East Greenland Ice Stream (NEGIS), which is a river of ice flowing at very high surface velocities of the order of ~50 m/year (Hvidberg et al., 2020). The unique configuration of the NEGIS makes EastGRIP a very important tool for understanding the flow properties of ice. Furthermore, the EastGRIP ice core contains a brittle zone of better quality, thanks to improved core handling (field report Dahl Jensen et al., 2019). Measurements on the brittle ice of EastGRIP, located between 650 and 950 m (Westhoff et al.,2021a), produced chemical measurements of unprecedented quality in the period of the Holocene (Jensen, 2021).

1.1.1 The Holocene climate recorded in Greenland

About half of central Greenlandic ice was formed during the Holocene, the current geological era which started around 11.7 ka b2k (Rasmussen et al., 2014). As shown in Figure 1.1b-f, the regional climate of Greenland during the Holocene can be described by the proxies recorded in the ice cores. Isotope records (^{18}O, ^{17}O, ^{2}H, ^{3}H), briefly mentioned above, are partly related to temperature changes but are also influenced by elevation, moisture, and precipitation-source changes (Jouzel et al., 1997; Vinther et al., 2010; Læpple et al., 2018). Hence, they provide vital information about climate. However, as explained by

Vinther et al. (2009), the water isotopes of central-Greenlandic ice cores may not be suited as the best proxy for temperature because of an apparent flatness and stability of the signal. This is because the ice sheet was subjected to elevation changes which counterbalanced the temperature changes.

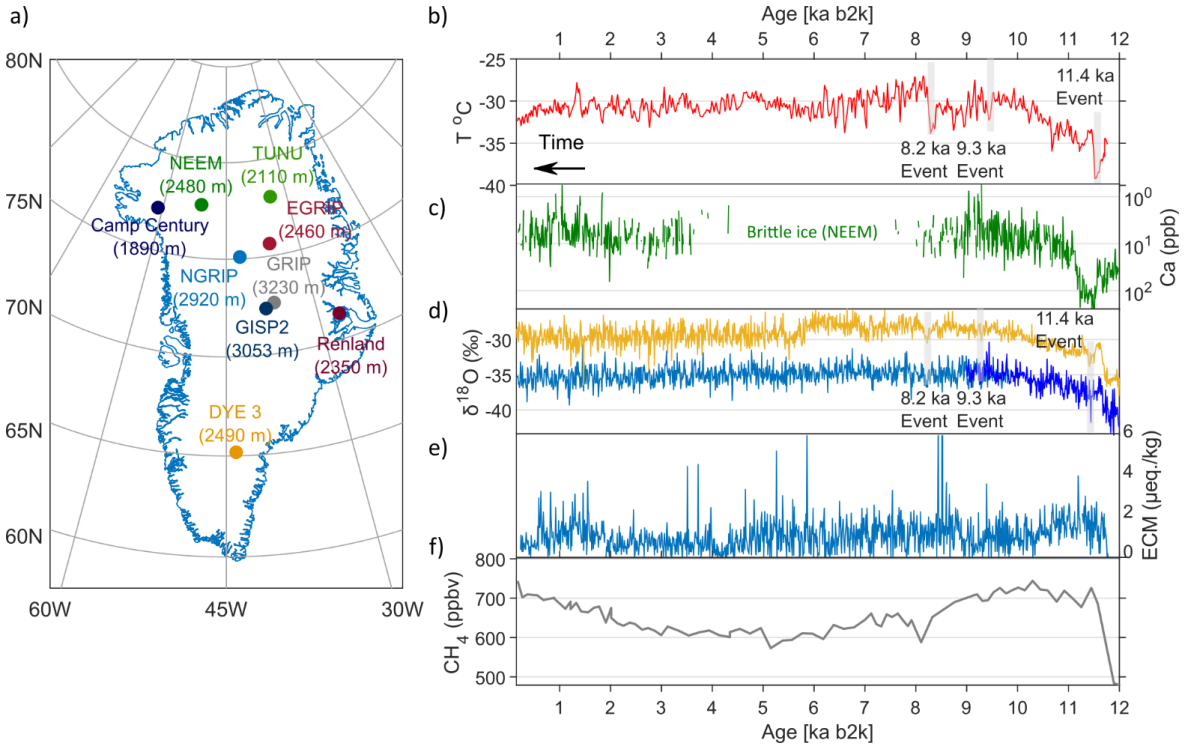

Figure 1.1 Ice-core drilling sites in Greenland (a) and Holocene climate overview (pre-1850 CE) (b-f).

(a) Map of Greenland showing the ice-core drilling sites mentioned in this thesis, and their respective elevation. Except for TUNU and Renland, these ice cores are more than 2000 m long.

(b) A temperature reconstruction of the Holocene period by Kobashi et al. (2017) presents the general ~2 °C cooling that Greenland has experienced since the Holocene thermal maximum, about 8 ka b2k (thousands of years before the year 2000 CE). It also shows three Early Holocene cooling events at 8.2, 9.3, and 11.4 ka b2k. Note the time direction from right to left, usual in this thesis.

(c) The calcium record from NEEM (Erhardt et al., 2021), a proxy for dryness, windiness, and dust loading in Greenland, presents a wide data gap because of the brittle-ice zone, located within the Holocene.

(d) A relatively stable water isotope record ($\delta^{18}O$) was preserved in all Greenlandic ice cores over the Holocene[1] (including EastGRIP, for which the isotopic record is being processed by Morris et al. at the University of Colorado Boulder). The $\delta^{18}O$ of DYE-3 (yellow), and NorthGRIP (blue; darker blue for the NorthGRIP2 part[2]) are shown (Rasmussen et al., 2007). Differences between the $\delta^{18}O$ records between the ice cores exist because of their distant geographic location.

(e) The electrical conductivity record (ECM) of NorthGRIP (Rasmussen et al., 2013) is a proxy of the many volcanic eruptions which left an imprint on the Greenlandic ice sheet.

(f) The methane record from GRIP (Blunier, 1999) is an example of the gas contained in the bubbles trapped in the ice.

Useful temperature reconstructions can be obtained from ice cores by measuring the gravitational fractionation of nitrogen isotopes or by borehole temperature inversion techniques (Kobashi et al., 2017; Dahl-Jensen et al., 1998). From these methods, we can infer that Greenland Holocene temperatures were generally 15-25 ºC warmer than in the glacial (Cuffey et al., 1997; Dahl-Jensen et al., 1998; Buizert et al., 2014). Moreover, a significant amount of melt layers has been documented in the central Greenland GISP2 core (Alley and Anandakrishnan, 1995), which constitutes a direct trace of the warm climatic conditions of this era.

The history of Greenlandic climate during the Holocene presents complex dynamics, both on long and shorter time scales. It started with the deglaciation, a prolonged period of global warming that began as early as 14 ka b2k and ended at about 9.5 ka b2k. Holocene temperatures peaked during the thermal maximum, occurring around 8 ka b2k. Since then, the average temperatures have been decreasing steadily until the Industrial Age (Vinther et al., 2009). Over the general decreasing trend, brief warmer periods of centennial duration have been identified in the GISP2 water isotope record (Easterbrook, 2016) like, for example, the Minoan Warming at around 3.3 ka b2k. Likewise, some centennial-scale cooling events have punctuated the relatively warm climate of this era, such as the Little Ice Age period (1570-1850 CE; Kjær, 2022) or the 8.2, 9.3, and 11.4 ka events (Rasmussen et al., 2006).

On the decadal to multiannual scale, it has been shown that Greenlandic climate is heavily affected by the North Atlantic Oscillation (NAO) which is one of the leading modes of atmospheric circulation over the North Atlantic (e.g. Visbeck et al., 2001). The NAO index describes the pressure difference between Iceland and the Azores; a positive NAO index generally indicates cooler and drier conditions in Greenland. Greenlandic accumulation rates of ice cores can be used to reconstruct the history of the NAO (Appenzeller et al., 1998). Connections with solar variability and volcanoes have both been examined as causes for NAO instability during the Holocene (Sjolte et al., 2018).

---

[1] The $\delta^{18}O$ quantity indicates the fraction of ^{18}O to ^{16}O isotopes, relative to a standard.

[2] NorthGRIP2 was drilled next to NorthGRIP1 after the first drill got stuck in 1997 (Rasmussen et al., 2006). NorthGRIP2 is used for depths beyond 1370 m (9812 years b2k) because the NorthGRIP1 core terminates. The two cores have about 30 m of overlap for continuous synchronization.

The consequences of global warming and climate oscillations during the Holocene were many. On an atmospheric level, methane in ice cores increased during the deglaciation, decreased until 5 ka b2k, and then increased again. This is likely because of changes in the wetland surface over time, which is the main natural source of this gas (Blunier et al., 1995). The global CO_2 levels, measured in Antarctic ice cores, have had a different trend (Monnin et al., 2004), with a steady increase from 8 ka b2k until the Industrial Age by about 20 ppm, with several explanation possible, such as the increase in vegetation cover (Brovkin et al., 2019). The average levels of soluble ions measured in the ice, such as the marine and terrestrial salts in GISP2 (O'Brien et al., 1995), show centennial to decadal climatic oscillations, likely in response of regional changes of circulation patterns, although in this thesis we are more focused on their annual variations.

Arguably, the most important consequence of the Holocene climatic conditions was that they favoured the development and thriving of the human civilization. Evidence of human activity has been found in the record of lead and copper preserved in GRIP ice, indicating periods of intense mining pollution dating back to 3000 years b2k (McConnell et al., 2018).

Finally, thanks to the emission of sulfate into the atmosphere, volcanic eruptions increase the ice acidity and the sulfate content (Gautier et al., 2016). In Figure 1.1e, we can observe many volcanic spikes in the ECM of NorthGRIP. The identity of the volcanic eruption can only be discovered with the aid of volcanic glass particles (tephra). In Greenland, the vast majority of tephra are from Icelandic eruptions and only a dozen has ever been assigned to other geographic sources (Abbott and Davies, 2012; Lin et al., 2021). The influence of volcanic eruptions on climate and human civilization during the Holocene will be examined further in section 1.2.2.

In conclusion to this paragraph, the Holocene climate was innately complex and this brief introduction cannot contain all the information about it. The main challenge from the perspective of time scales is to obtain the highest possible accuracy and precision to compare the many records available from Greenland and other regions.

1.1.2 The last glacial and the Dansgaard-Oeschger events

By measuring the water oxygen isotopes in the deeper ice, a complex history of abrupt climate changes was discovered (Dansgaard et al., 1982), such as the ones shown in Figure 1.2. It became clear that the Earth has seen periods of abrupt climate change within the last

glacial period that are of non-orbital source[3]. The Dansgaard-Oeschger (D-O) events are saw-tooth shaped water-isotope anomalies that indicate an abrupt northern-hemispheric warming of about ~10 ºC over a few decades, followed by a more gradual return to a glacial climate (Steffensen et al., 2008; Kindler et al., 2014). D-O events happened more than 25 times during the last glacial period. The signature of D-O events can be investigated in several Greenlandic proxies other than water isotopes, for example in the ECM, the marine and terrestrial aerosols (e.g. Na^+ and Ca^{2+}), and in the measured thickness of the annual layers. A study has shown that the onset of D-O events is almost synchronous in all these proxies (Erhardt et al., 2019b).

Many D-O events were at first colloquially designated by nicknames such as "the three sisters" or "the man with his dog" (J.P. Steffensen talk, 2021). More appropriately, the alternating periods of mild and cold climate were renamed by the 'Integration of Ice-core, Marine and Terrestrial records' stratigraphy working group (INTIMATE; Rasmussen et al., 2014), establishing the current nomenclature of Greenland Stadials (GS: cold periods) and Interstadials (GI: warm periods). In this thesis, GI is used as a synonym of D-O event. The GI/GS onsets and terminations have been dated with the aid of the current Greenland Ice Core Chronology (GICC05; Svensson et al., 2008, and references therein; Seierstad et al., 2014).

The cause of the GIs is subject to intense debate and investigation, as they likely implied very large reorganizations of the global climate since their impact is observed widely across the globe. The current interpretation attributes GIs to changes in the strength of the Atlantic meridional overturning circulation (AMOC) affecting the heat transport to Greenland (e.g. Peltier and Vettoretti, 2014). The climate system oscillates between the two quasi-stable states, the GSs and the GIs.

There is debate concerning whether these shifts are self-sustained or externally forced. Each GI presents some peculiarities; therefore, the likely cause of the system oscillation is a combination of multiple coupled climatic feedback mechanisms (Capron et al., 2021). It has also been observed that large bipolar eruptions occur more frequently around GI onsets (Lohmann and Svensson, 2022, in review), hence volcanoes could play a significant role in triggering the events.

[3] Orbital forcing causes the glacial-interglacial cycles (Milankovitch, 1941).

From a modelling perspective, Vettoretti et al. (2022) determined that atmospheric CO_2 levels control the stability and duration of GI/GS stages, which are self-sustained. The transitions may thus occur either because of stochastic noise internal to the system, or because of low amplitude signals from external forcing, such as the solar activity or volcanic eruptions.

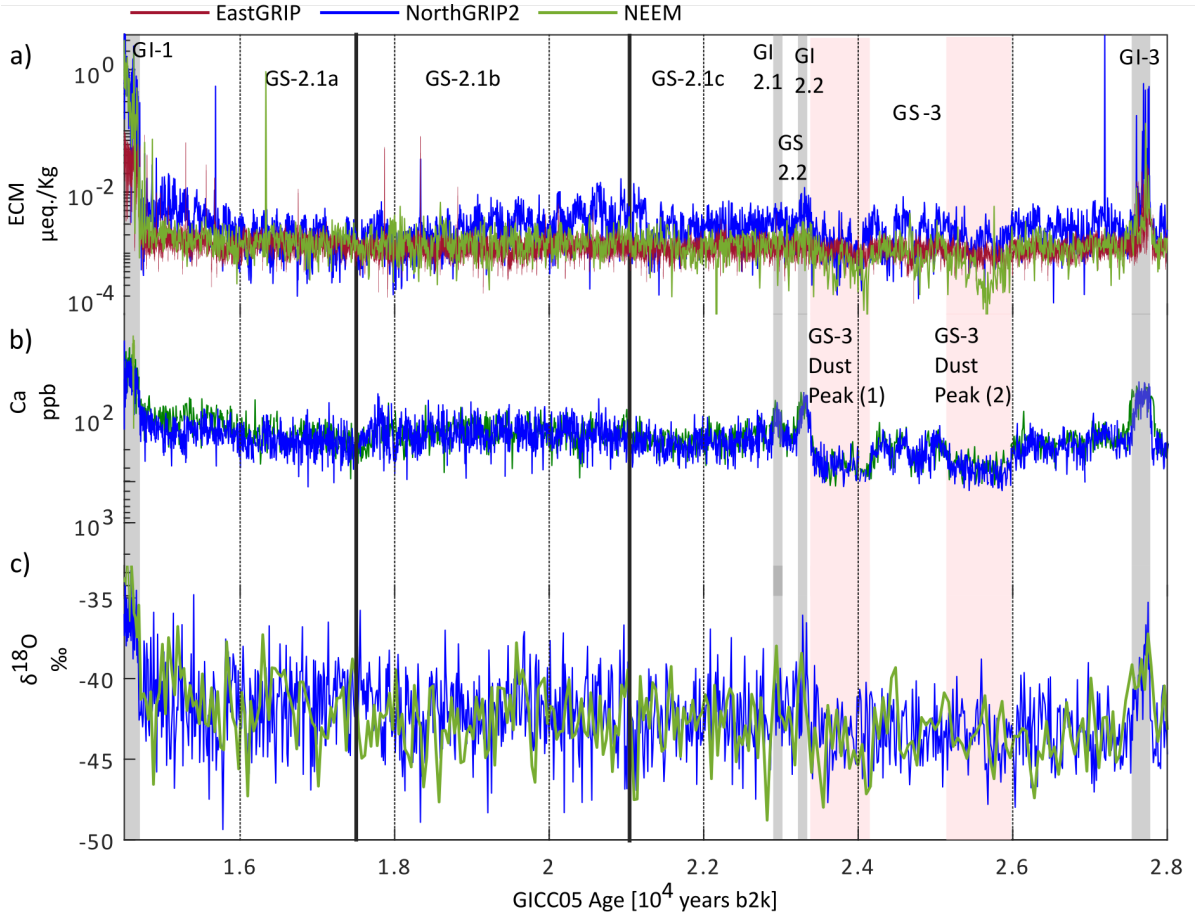

Figure 1.2 Section of the INTIMATE ice-core stratigraphy framework, adapted here from Rasmussen et al. (2014) to include NEEM and EastGRIP data.
Between 15 and 28 ka b2k, several climatic periods are highlighted by vertical bars and shaded areas.
The sequence of GSs (white shading) and GIs (grey shading), is numbered progressively as we go back in time. On the very left, we have the beginning of the Bølling-Allerød period, GI-1, which started about 14.7 ka ago. The sub-division of GS-2.1 in three parts follows empirical evidence of the proxies behaving differently (Rasmussen et al., 2014).
(a) The ECM is sensitive to the alternating climate periods, because of the higher alkaline dust flux during stadials. It also records some strong volcanic peaks. (b) Calcium records of NEEM and NorthGRIP, on an inverted log scale, contain the signature of two dust peaks (red shading), as well as GI events and the signature identifying GS 2.1a. (c) The water isotopes are qualitatively used as a proxy of temperature, and hence show the short-lived GI-2.2 and the prominent GI-1 and GI-3.

By comparing water isotope records from both poles, an anti-phase dynamic between the GI events in Greenland and the Antarctic Isotope Maxima (AIM) in Antarctica was observed.

The shape of the AIMs is characterized by a much more gradual increase and decrease than the GI/GS abrupt transitions, which led to believe that the Antarctic ice sheet was slowly responding to northern-hemispheric climate.

This counterbalanced effect between the global North and South is explained by the action of the bipolar seesaw (Stocker and Johnsen, 2003; Pedro et al. 2018), a model that describes how the shutdown of the AMOC during a GS prevents heat advection from South to North, causing warming in Antarctica. During a GI, on the other hand, the AMOC is predicted to be stronger and Antarctica starts to cool down. However, the original model by Stocker & Johnsen does not account for a delay in transmission of the temperature signal between the two ice sheets. The analysis by Pedro et al. (2018) expands on the atmospheric and oceanic components of the model, explaining that a delay between the AMOC collapse and the Antarctic warming is likely present, due to heat accumulation in the Antarctic Circumpolar Current.

The average delay between the onset of a GI and the decline of the corresponding AIM was measured as 218±92 years (WAIS project members, 2015) or as 122±24 years (Svensson et al., 2020). The approach used in the first case was a synchronization between Antarctic methane and Greenland $\delta^{18}O$ since globally mixed methane closely follows the GI/GS transitions. This method is subject to the age uncertainties of the gas chronology (Buizert et al., 2015). In the study by Svensson et al., on the other hand, a more precise synchronization was obtained using bipolar eruptions to synchronize Antarctic and Greenlandic $\delta^{18}O$.

1.1.3 The Last Glacial Maximum

During the last glacial era, the LGM was the last period when the ice sheets were at their largest extent before the deglaciation into the Holocene (Clark et al., 2009). During this time, the global mean temperature was about 6 ºC colder than today (Tierney et al., 2020), causing global desertification and low sea levels.

The onset and termination of this period depend on the choice of regional records, as each region responded differently. Hence, a common stratigraphic definition of the LGM is still lacking (Hughes & Gibbard, 2015).

In general, one can locate the LGM within the broader Marine Isotope Stage 2 (MIS-2; 14-29 ka b2k) of marine climate records (Lisiecki & Raimo, 2005). For Greenland, a stratigraphic definition locates the LGM within GS-3 (23.3-27.5 ka b2k; Hughes & Gibbard, 2015). The Antarctic dust flux, possibly a proxy for vegetation cover (Harrison et al., 2001), also peaks within GS-3 and hence supports this definition (Hughes & Gibbard, 2015).

Marine sediments, which allow reconstructions of the sea level, record the LGM between 19 and 23 ka b2k (Yokoyama et al., 2000; Clark et al., 2009), thus signifying that globally meaningful definitions of the LGM are hard to produce.

As this is the period in focus in Paper V, more information on the LGM can be found in Chapter 5.

1.1.4 Heinrich events

At times during the last glacial, massive icebergs were injected into the North Atlantic Ocean, so much that the term 'armada' is sometimes used to describe the behaviour of the iceberg formation travelling the waters (Heinrich, 1988). The icebergs transported debris from the location of the ice sheet to very distant destinations, therefore the method of detection is generally based on the Ice Rafted Debris records (IRD) measured in marine sediments (Broecker et al., 1992). There is debate about what constitutes the 'true' Heinrich event (HE; Andrews & Voelker, 2018), what caused them and what climate they associate with. One theory is that during and following HEs, especially the Laurentide-born ones[4], the Northern Hemisphere climate was extremely cold and dry, possibly because the icebergs injected a lot of fresh water into the ocean, producing a more complete shutdown of the AMOC and thereby an even more lowered heat transport toward the northern regions (Vidal et al., 1997).

Each HE may thus correspond to a broader period of climate change, the Heinrich Stadial (HS), although this distinction is not always applicable (Andrews & Voelker, 2018). In Paper V, we will focus on HS-1 and HS-2 as these appear to be closely connected to challenges for the ice-core chronologies within the LGM.

In particular, the HS-1 is also roughly synchronous with the "mystery interval" between 14.5 and 17.5 ka b2k (Denton et al., 2006), where Greenland experienced very cold winters, the Asian monsoon was weakened, the Atlantic Intertropical Convergence Zone (ITCZ) moved to more southern locations, and the Antarctic ice sheet started its deglaciation. Hence, the occurrence of the HE-1 by a combination of at least two pulses in the IRD record (Bard et al., 2000) is linked to global climatic changes. For HS-2, the global climatic signal is less clear, possibly because of chronological issues that hamper the reconstruction of the sequence of events (Adolphi et al., 2018).

---

[4] The Laurentide Ice Sheet largely covered Canada and Northern US during the last glacial period.

1.2 Strengthening climatic connections around the globe

The global climate is a system that is subject to external forcing affecting the energetic budget, for example because of changes in the astronomical parameters. As we have seen in the case of the bipolar seesaw, the system can present internal shifts across regions because of counteracting effects that aim at keeping the system in equilibrium.

The lead-lag dynamics within the climate system cannot be ascertained without precise chronological markers. Synchronous and short-term events are always needed to compare records from distant locations to reconstruct such internal shifts. In this thesis, chronological markers play an extensive role in reaching conclusive results about climate. There are two important types of chronological markers in ice cores that need to be introduced here: cosmogenic radionuclide signals and volcanic eruption signals.

1.2.1 Cosmogenic radionuclides and solar activity

Cosmogenic radionuclides are produced via the interaction of the atmosphere with particles from Galactic Cosmic Rays (GCR) or Solar Proton Events (SPE). The production is modulated by the helio- and geomagnetic fields, which may fluctuate in time. The magnetic fields shield the Earth from the GCRs and are therefore inversely proportional to the strength of the interaction. The atomic cascade synchronously produces, amongst others, ^{14}C, ^{10}Be, and ^{36}Cl, with proportional amplitudes depending, for example, on the atmospheric budget of their parent atoms.

After production, the atoms are mixed in the atmosphere and deposited on Earth via several mechanisms (Figure 1.3). ^{10}Be and ^{36}Cl are globally well-mixed and they deposit on the surface of the Earth by gravity or are scavenged by precipitation, all within 1-2 years after production (Raisbeck et al., 1981). They are deposited on the ice sheet either because they are diluted in the snow (wet deposition) or because they are attached to dust particles that precipitated (dry deposition).

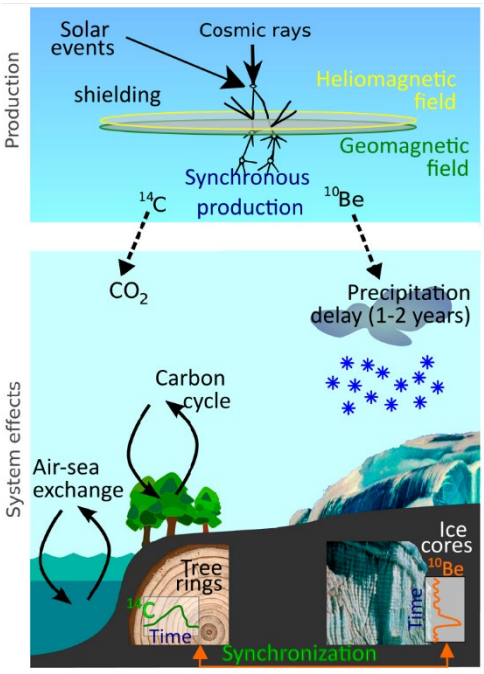

modified from: Steinhilber, et al., 2012

Figure 1.3 Schematic of the depositional dynamics of cosmogenic radionuclides.

On the other hand, ^{14}C further enters the hemispheric carbon cycle, which results in a delay and smoothing of the production signal (Siegenthaler et al., 1980).

As the production of radionuclides is closely linked to the solar activity of the past, their measurement can tell us about solar cycles, irradiance changes, and the occurrence of SPEs (Steinhilber et al., 2012; Miyake et al., 2015).

Changes in the solar activity may affect the climate, trough the modulation of the total solar irradiance (TSI). Across the 11-year Schwabe cycle, for example, the TSI varies by ±0.5 kW/m^2, around an average TSI of about 1361 kW/m^2 (Kopp & Lean, 2011). Cycle superposition may produce periods of complete sun-spot absence, called solar minima (Vecchio et al., 2017). Across a solar minimum such as the Maunder Minimum (1645–1715; Eddy, 1976), the variation of TSI can reach 0.24 %, depending on the reconstructions applied (e.g. Kopp, 2016). The climate is related to such solar activity, however, these changes in TSI are small and are thought to be enhanced within the climate system by amplification feedback mechanisms (Sundquist et al., 2013; Previdi et al., 2021). As a result, during the LGM, a persistent solar-climate connection was proved by analysing correlations between the radionuclide signal and the isotopic ice-core record (Adolphi et al., 2014) although the amount of solar impact is yet to be proven.

1.2.2 Volcanic eruptions and human civilization

Another source of external forcing are volcanic eruptions[5], which can have a brief cooling effect on the climate because of the emitted aerosols shielding the solar radiation (Robock, 2000).

Many eruptions are recorded synchronously in Greenland and Antarctica (Svensson et al., 2020), representing an important synchronization tool across the climate system.

The record of eruptions and their climate forcing has recently been extended to the entire Holocene thanks to ice-core data (Sigl et al., 2015; Sigl et al., 2022). The impact of tropical eruptions is proven to cool the tree-ring record for about 10 years (Sigl et al., 2015) and to produce around 1 °C of summer cooling (Stoffel et al., 2015).

---

[5] The classification of volcanic eruptions as external forcing may be questioned, because volcanoes are internal to the climate system as they are scattered on the Earth's surface. However, the random occurrence of eruptions and their ability to cause climate alterations independently from other factors support the external forcing definition. On longer geological timescales, however, the average effect of volcanic eruptions is often considered as an internal factor.

The impact of large volcanic eruptions on human civilization is known to be catastrophic. The Okmok eruption in Alaska (43 BCE) likely impacted the historic course of the Roman empire (McConnell et al., 2020) because of the strong cooling followed by crop failures and famine, as well as because of visually spectacular solar dimming that could have been interpreted as signs for political change in the ancient societies. However, the latter was likely originated by an Etna eruption the year before.

The eruption of Thera on the island of Santorini in Greece (16^{th}-17^{th} century BCE) likely caused the end of the Minoan civilization and great political shifts in the Mediterranean region (Warburton et al., 2009; Manning et al., 2014). One can only imagine the impact of the Thera eruption, having a high VEI[6] of 7, on the local population. Dating the Thera eruption would allow linking archaeological chronologies of the Mediterranean region. One way to establish the most accurate date of this eruption has been to search for evidence in the ice cores and their tephra record. Now rejected, the initial ice-core identification of Thera in Greenland suggested an age of the eruption in strong disagreement with the archaeological and radiocarbon evidence (Hammer et al., 1987). Unfortunately, the eruption hasn't been confirmed in any ice core yet. For more on the matter, we will examine the case of Thera in Chapter 4.

1.3 Ice-core time scales

The ice-core records we have encountered until now improved the current interpretation of paleoclimate mainly because an age was assigned to the signals. To precisely reconstruct the history of the Greenlandic climate, several methods have been developed to estimate how old the ice is at depth.

The preferred method for the age-depth estimation in ice cores is layer counting, which may be done manually or by an automated approach. The StratiCounter algorithm has shown great results for this task (Winstrup et al., 2012). When layers become too thin to be recognized, the ice-core time scales can be created by modelling ice thinning and flow (Johnsen et al., 2001; Wolff et al., 2010).

Ice-core layers are recorded, for example, in the visual stratigraphy (VS) and the ECM of ice. The VS is a relatively simple measurement of the light scattered by the ice, yet it can

[6] Volcanic explosivity index retrieved from the Smithsonian volcanic catalogue: https://volcano.si.edu/volcano.cfm?vn=212040

contain a lot of useful information (Svensson et al., 2005; Westhoff et al., 2021b). For example, the spring-peaking dust produces light bands that can be used to count annual layers. Similarly, the high ion deposition of the summer months produces an annual signal in the ECM (Andersen et al., 2006). It is not only annual layers we observe; the VS and the ECM will also register intense peaks with a volcanic eruption because of the high ion/ash loading in the corresponding year (Svensson et al., 2005).

A further indication of the annual layers in the ice can be obtained by chemical analysis of soluble ions and detection of the insoluble dust fraction in the melted samples. For this, longitudinal pieces of the ice core are melted continuously, producing high-resolution continuous flow analysis records (CFA[7]; Kaufmann et al., 2008). Alternatively, one can produce discrete measurements by cutting regular intervals of ice: if the resolution is high enough, the layers can still be seen.

In the Holocene, the ions peak in different seasons (Figure 1.4). Sodium, for example, is related to the advection of salt aerosols from the Arctic sea ice, which has its largest extent in the winter (Rhodes et al., 2017). Calcium and dust, on the other hand, are gathered by winds passing over the Eurasian continent in the dryer spring months (Fuhrer et al., 1999). Ammonium and nitrate are related to the degassing of wetlands and biogenic activity, as well as to wildfires, which are all most intense in the summer months (Fisher et al., 2015; Legrand et al., 2016). The water isotopic signal of ice can also be used to count annual layers. This is only possible if the diffusion within the firn and ice has not obliterated the water isotope signal (Vinther et al., 2006).

In the colder GSs, the seasonal signals were much different, with basically no spring and no autumn recorded, which implies all summer ions peaking together. ECM and VS become much more useful here since they present one intense peak each summer and they are non-destructive measurements, much easier to perform (Andersen et al., 2006). Nonetheless, the warmer GIs have layers more similar to the Holocene, motivating CFA measurements in the glacial (Rasmussen et al., 2006).

[7] CFA only describes the practice of melting the ice continuously. The actual measurements may be done by several techniques, such as ion chromatography (IC; Cole-Dai et al., 2006) or inductively coupled plasma mass spectrometry (ICP-MS; Erhardt et al., 2019a)

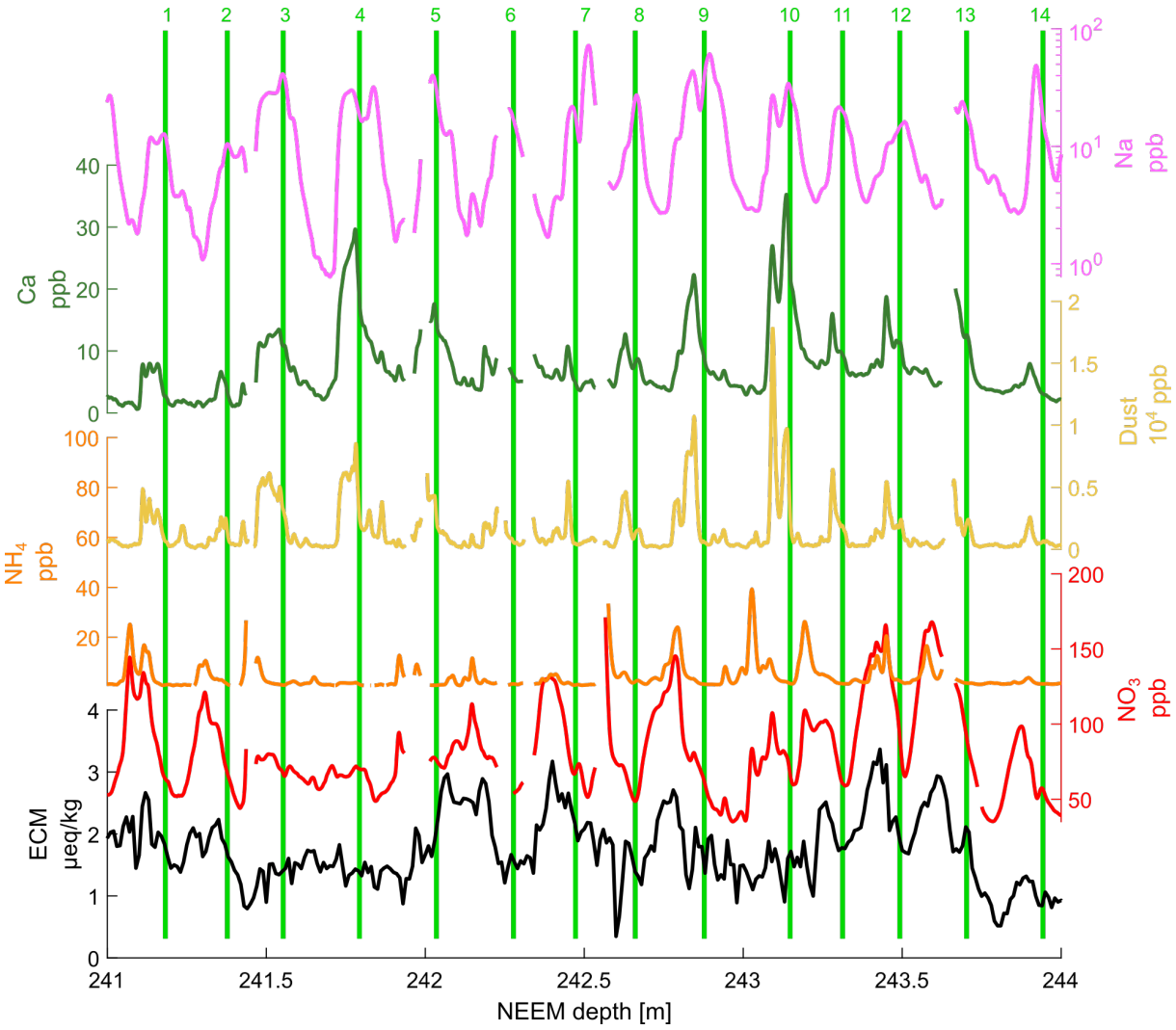

Figure 1.4 - Holocene annual layers in the NEEM ice core (Erhardt et al., 2021). Vertical bars indicate the start of each annual layer.
Ice-core layers are not perfect: each year has its peculiarities. In general, sodium (pink) is used to define the start of the year, since it is believed that this species peaks in the nominal months of December/January (Rhodes et al., 2017). Calcium (green) is strongly linked to dust (yellow) and hence they have similar patterns, as do the summer-peaking ammonium and nitrate (orange and red). The ECM (black) captures the signal of all ions present in the ice and is generally peaking in the summer because of higher anion loading in the summer months. It is useful to visualize data on the log-scale (e.g. the Na series) because the deposition varies within the year by about one order of magnitude.

1.3.1 The GICC05 timescale

Until 60 ka ago, the Greenlandic ice cores show well-resolved annual layers that have been counted manually to construct the GICC05, a complex and long operation that was conducted by many researchers together, using the ice-core data available at the time. The manual layer counting was divided into sections of time depending on the ice-core data availability, quality, and resolution. The Holocene until about 8.2 ka b2k (Vinther et al.,

2006) was dated on compared ice-core isotope data from three locations in Greenland: DYE-3, GRIP, and NorthGRIP (see the introduction of Paper III). The brittle ice gap affects this section, but fortunately the three ice cores have non-overlapping brittle zones.

For the last deglaciation, until ~14 ka b2k, the GICC05 was constructed by Rasmussen et al. (2006), using CFA ion data and ECM from NorthGRIP and GRIP. For a good part of the glacial, the timescale is described in Andersen et al. (2006) and compared to other records in Svensson et al. (2006; see the introduction of Paper V). The effort of manual counting is concluded at 60 ka ago by Svensson et al. (2008) employing NorthGRIP data. The uncertainty on the time scale was defined as the Maximum Counting Error (MCE; Rasmussen et al., 2006) on which we will return again in Paper III.

The time scale beyond 60 ka b2k was extended via modelling (GICC05modelext; Wolff et al., 2010). The extension of the time scale was obtained by adapting the ss09sea model (Johnsen et al., 2001) to match the layer counted age at 60 ka b2k. The model had been applied to date the NorthGRIP core (NGRIP members, 2004). The extended time scale was later applied to GRIP and GISP2 by volcanic matching (Seierstad et al., 2014).

1.3.2 Other ice-core time scales

A counterpart to the GICC05, the Antarctic Ice Core Chronology (AICC2012; Veres et al., 2013) synchronizes several ice cores from the Antarctic ice sheet and uses a probabilistic approach. Using time constraints such as bipolar volcanic tie points to the GICC05, the authors used inverse modelling to infer the best time scale compromise, adjusting the results of ice-flow models. By construction, the two polar chronologies are closely linked together and provided the basis for measuring the AIM-GI distance in the bipolar seesaw context.

Most other ice-core time scales are constructed on a single ice core. The NS1-2011 time scale until 2500 years ago (Sigl et al., 2015) was constructed on the NEEM-2011-S1 shallow core, drilled close to the NEEM site. StratiCounter was applied to independently check the manual count. The DRI_NGRIP2 time scale (McConnell et al., 2018) was constructed manually on a new CFA dataset of the NorthGRIP 2 ice core, covering the age range from ~750 years ago to ~3500 years ago.

The WD2014 chronology is a recent standard for Antarctic climate studies and defines a time scale for the recently drilled ice core WDC (Sigl et al., 2016; Buizert et al., 2015). Thanks to the high accumulation at the WDC site, this ice core aims at improving the understanding of the Antarctic climate. For this time scale as well, Straticounter was applied to check the manual count independently. For the Holocene, the good agreement with the

tree-ring time scale (see next paragraph) is claimed as substantial proof that WD2014 is very accurate. However, the WD2014 time scale shows some inconsistencies in the LGM, which are introduced in Paper V.

1.4 The IntCal calibration curve, tree rings, and speleothems

Comparison of records from Polar and other regions requires knowledge about other types of dating methods. It is therefore useful to introduce some basic notions about the topic of radiocarbon dating and other types of layered archives, such as tree rings and speleothems.
Radiocarbon dating measures the decayed fraction of ^{14}C to ^{12}C to infer the absolute age of any sample that contains carbon, such as organic material, corals, speleothems, archaeological artefacts, and so on. The challenge of radiocarbon dating is that the original amount of ^{14}C varied in time. Therefore, one needs to reconstruct the history of the initial ^{14}C content in the original reservoir, which is done by establishing appropriate calibration curves (Reimer, 2021).
To reconstruct the calibration curve, one measures ^{14}C in samples that can also be dated independently by other means, e.g. dendrochronology or U/Th dating.
Dendrochronology is the method of dating rings of annual growth in trees. For the Northern Hemisphere, the tree-ring chronology reaches back to ~13 ka ago (Hughes, 2002) and hence provides a way to compare to ice-core chronologies in the Holocene (Sigl et al., 2015; Sigl et al., 2016). The tree-ring chronology carries very small uncertainties thanks to the cross-dating of thousands of trees.
For ages until ~450 ka years ago, one can use the relative ratio of the decay products of Uranium to date samples containing calcium carbonate. More specifically, one can measure the decaying dis-equilibrium of unstable ^{238}U and its product ^{230}Th (Wendt et al., 2021). Speleothems formed in caves around the world, especially stalagmites, show high potential for accurate dating using this method; because ^{230}Th is insoluble in water, the water forming the speleothem is originally thorium-free and, hence, all the ratios measured stem from the decaying fraction of ^{238}U (Bradley, 2015).
The latest versions of the atmospheric calibration curve are called IntCal20 (Reimer et al., 2020) for the Northern Hemisphere, and SHCal20 (Hogg et al., 2020) for the Southern Hemisphere. Samples that are retrieved in the ocean (e.g. corals or seashells) contain carbon that is much older than the atmospheric one, because of the diffusion processes that occur in the deep waters. Therefore, one should use Marine20 for marine samples because of the apparent ageing effects (Heaton et al, 2020).

Speleothems register climate through the content of oxygen isotopes in the calcite ($\delta^{18}O_c$). In very general terms, there is an inverse relationship between temperature changes in the cave and the amount of fractionation of the isotopes (-0.24 ‰ $^{o}C^{-1}$, O'Neil et al., 1969), which is the opposite trend of water isotopes in ice cores. However, this trend can be counterbalanced by the isotopic ratio of the precipitation, which increases with temperature. That is why the water isotope signal of speleothems can look very different from the one registered by ice cores, although the temperature history might have gone in similar directions at both sites, e.g. because of a D-O event.

Asian speleothems, in particular, record the history of the Asian Summer Monsoon (ASM; Wang et al., 2001; Zhao et al., 2015) which is an important mechanism of transport of heat and moisture across the Asian continent. The ASM can be compared to other climate records, as it was shown that ASM-records resemble traits of both Northern and Southern ice caps (Zhang et al., 2019). However, each speleothem will show different signatures according to the local isotopic depletion dynamics. Nonetheless, one can infer the lag between the Greenlandic D-O events and similar events recorded in Asian speleothems (Nguyen et al., 2020). We will examine the very important Chinese Hulu Cave speleothems in Paper V to infer the connection between the U/Th time scale of this cave and the GICC05 in the LGM.

1.5 Problems in the GICC05

Some studies have demonstrated that one problem with the GICC05 time scale lies in a strong bias about certain layers. This is the case of the Vesuvius eruption (79 CE), which was thought to be recorded in ice cores but was later shown not to be compatible with tephra evidence (Plunkett et al., 2022). We will elaborate on the Holocene issues of the GICC05 in Paper III (Chapter 3). Another problem of the GICC05 might lie in layers changing their pattern unexplainably, which is what can happen in the glacial where there is a higher risk of missing annual layers due to very low precipitation. Finally, ice-core timescales have intrinsic uncertainties because there are only few ice cores to compare, hence new information from more recently drilled ice cores should be used to improve the precision of the timescale.

As early as 2008, Baillie proposed the GICC05 should be moved to younger ages by 7 years at 536 CE, because of a better alignment with the tree ring record. Important work was done by Sigl et al. (2015) who conclusively proved the offset at Vesuvius to be 8 years, meaning that the GICC05 was dated too old in the Late Holocene because of a systematic over-counting of layers. Two separate studies further used ice-core ^{10}Be and tree-ring ^{14}C to

compare the GICC05 to the IntCal13 curve in the Holocene (Adolphi et al., 2016; Muscheler et al., 2014). They both found that the GICC05 is dated towards older ages with a progressively increasing offset reaching 25 years at 8 ka ago and then 65 years at 11 ka ago. Their study is compatible with individual tie points, for example the Saksunarvatn ash layer of 10260 years b2k, found to be 86 ± 36 years younger than the GICC05 age of the corresponding layer by independent carbon dating (Lohne et al., 2013).
Given the evidence of the GICC05 ages exceeding those of other chronologies, it is time to revise the GICC05 by including the new deep ice cores drilled since its creation, namely NEEM and EastGRIP, which is the topic of Paper III.

In the glacial period between 13 ka ago and 44 ka b2k, Adolphi et al. (2018) conducted a study that further investigated the offset between the GICC05 and the speleothem time scale underlying IntCal13. The offset was measured almost 0 years at 13 ka b2k, 500 years at 22 ka b2k in the LGM, and 250 years at 44 ka b2k. These three tie points were connected using a Monte-Carlo simulation to construct a continuous transfer function between the GICC05 and IntCal13 over the glacial, with uncertainty bounds guided by the MCE. Their study suggests that the GICC05 is dated younger than IntCal13 because of a systematic under-counting of layers, as opposed to the Holocene. At 31 ka b2k, they find their results compatible with the study of Turney et al. (2016), who measured an offset of about 110 years around HS-3. Muscheler et al. (2020) later re-evaluated some of these tie points in light of the newly published IntCal20 calibration curve (Reimer et al., 2020), finding good agreement with Adolphi et al.
The offset function of Adolphi et al. (2018) in the glacial is mostly compatible with a zero offset except around the LGM. As much as their demonstration is solid, the relatively small amount of independent evidence makes us want to investigate the LGM better, which is the topic of Paper V.

1.6 References

Abbott, P. M., & Davies, S. M. Volcanism and the Greenland ice-cores: the tephra record. Earth-Science Reviews, 115(3), 173-191. https://doi.org/10.1016/j.earscirev.2012.09.001, 2012

Adolphi, F., Muscheler, R., Svensson, A., Aldahan, A., Possnert, G., Beer, J., ... & Thieblemont, R. Persistent link between solar activity and Greenland climate during the Last Glacial Maximum. Nature Geoscience, 7(9), 662-666. https://doi.org/10.1038/ngeo2225, 2014

Adolphi, F., & Muscheler, R. Synchronizing the Greenland ice core and radiocarbon timescales over the Holocene–Bayesian wiggle-matching of cosmogenic radionuclide records. Climate of the Past, 12(1), 15-30. https://doi.org/10.5194/cp-12-15-2016, 2016

Adolphi, F., Bronk Ramsey, C., Erhardt, T., Edwards, R. L., Cheng, H., Turney, C. S., ... & Muscheler, R. Connecting the Greenland ice-core and U/Th timescales via cosmogenic radionuclides: testing the synchroneity of Dansgaard–Oeschger events. Climate of the Past, 14(11), 1755-1781. https://doi.org/10.5194/cp-14-1755-2018, 2018

Alley, R. B., & Anandakrishnan, S. Variations in melt-layer frequency in the GISP2 ice core: implications for Holocene summer temperatures in central Greenland. Annals of Glaciology, 21, 64-70. doi:10.3189/S0260305500015615, 1995

Andersen, K. K., Svensson, A., Johnsen, S. J., Rasmussen, S. O., Bigler, M., Röthlisberger, R., ... & Clausen, H. B. The Greenland ice core chronology 2005, 15–42 ka. Part 1: constructing the time scale. Quaternary Science Reviews, 25(23-24), 3246-3257. https://doi.org/10.1016/j.quascirev.2006.08.002, 2006

Andrews, J. T., & Voelker, A. H. "Heinrich events"(& sediments): A history of terminology and recommendations for future usage. Quaternary Science Reviews, 187, 31-40. https://doi.org/10.1016/j.quascirev.2018.03.017, 2018

Appenzeller, C., Stocker, T. F., & Anklin, M. North Atlantic Oscillation dynamics recorded in Greenland ice cores. Science, 282(5388), 446-449. doi: 10.1126/science.282.5388.446, 1998

Baillie, M. G. Proposed re-dating of the European ice core chronology by seven years prior to the 7th century AD. Geophysical Research Letters, 35(15). https://doi.org/10.1016/j.quascirev.2006.08.002, 2008

Bard, E., Rostek, F., Turon, J. L., & Gendreau, S. Hydrological impact of Heinrich events in the subtropical northeast Atlantic. Science, 289(5483), 1321-1324. doi: 10.1126/science.289.5483.1321, 2000

Batchelor, C. L., Margold, M., Krapp, M., Murton, D. K., Dalton, A. S., Gibbard, P. L., ... & Manica, A. The configuration of Northern Hemisphere ice sheets through the Quaternary. Nature communications, 10(1), 1-10. https://doi.org/10.1038/s41467-019-11601-2, 2019

Blunier, T., Chappellaz, J., Schwander, J., Stauffer, B., & Raynaud, D. Variations in atmospheric methane concentration during the Holocene epoch. Nature, 374(6517), 46-49. https://doi.org/10.1038/374046a0, 1995

Blunier, Thomas GRIP Methane Data (Bern). PANGAEA, https://doi.org/10.1594/PANGAEA.55087, 1999

Bradley, R. S. Paleoclimatology: reconstructing climates of the Quaternary. Elsevier. ISBN: 9780123869951. Retrieved from: https://www.sciencedirect.com/book/9780123869135/paleoclimatology, 2015

Briner, J. P., McKay, N. P., Axford, Y., Bennike, O., Bradley, R. S., de Vernal, A., ... & Wagner, B. Holocene climate change in Arctic Canada and Greenland. Quaternary Science Reviews, 147, 340-364. https://doi.org/10.1016/j.quascirev.2016.02.010, 2016

Broecker, W., Bond, G., Klas, M., Clark, E., & McManus, J. Origin of the northern Atlantic's Heinrich events. Climate Dynamics, 6(3), 265-273. https://doi.org/10.1007/BF00193540, 1992

Brovkin, V., Lorenz, S., Raddatz, T., Ilyina, T., Stemmler, I., Toohey, M., & Claussen, M. What was the source of the atmospheric CO 2 increase during the Holocene?. Biogeosciences, 16(13), 2543-2555. https://doi.org/10.5194/bg-16-2543-2019, 2019

Buizert, C., Gkinis, V., Severinghaus, J. P., He, F., Lecavalier, B. S., Kindler, P., ... & Brook, E. J. Greenland temperature response to climate forcing during the last deglaciation. Science, 345(6201), 1177-1180. doi: 10.1126/science.1254961, 2014

Buizert, C., Cuffey, K. M., Severinghaus, J. P., Baggenstos, D., Fudge, T. J., Steig, E. J., ... & Taylor, K. C. The WAIS Divide deep ice core WD2014 chronology–Part 1: Methane synchronization (68–31 ka BP) and the gas age–ice age difference. Climate of the Past, 11(2), 153-173. https://doi.org/10.5194/cp-11-153-2015, 2015

Cain, W. F., & Suess, H. E. Carbon 14 in tree rings. Journal of Geophysical Research, 81(21), 3688-3694. https://doi.org/10.1029/JC081i021p03688, 1976

Capron, E., Rasmussen, S. O., Popp, T. J., Erhardt, T., Fischer, H., Landais, A., ... & White, J. W. C. The anatomy of past abrupt warmings recorded in Greenland ice. Nature communications, 12(1), 1-12. https://doi.org/10.1038/s41467-021-22241-w, 2021

Clark, P. U., Dyke, A. S., Shakun, J. D., Carlson, A. E., Clark, J., Wohlfarth, B., ... & McCabe, A. M. The last glacial maximum. Science, 325(5941), 710-714. doi: 10.1126/science.1172873, 2009

Cole-Dai, J., Budner, D. M., & Ferris, D. G. High speed, high resolution, and continuous chemical analysis of ice cores using a melter and ion chromatography. Environmental science & technology, 40(21), 6764-6769.
https://doi.org/10.1021/es061188a, 2006

Cuffey, K. M., & Clow, G. D. Temperature, accumulation, and ice sheet elevation in central Greenland through the last deglacial transition. Journal of Geophysical Research: Oceans, 102(C12), 26383-26396.
https://doi.org/10.1029/96JC03981, 1997

Dahl-Jensen, D., Mosegaard, K., Gundestrup, N., Clow, G. D., Johnsen, S. J., Hansen, A. W., & Balling, N. Past temperatures directly from the Greenland ice sheet. Science, 282(5387), 268-271.
doi: 10.1126/science.282.5387.268, 1998

Dahl-Jensen, D., Kirk, M., Koldtoft, I., Popp, T., and P, S. J.: Field seasonst GReenland Ice core Project (EGRIP) 2015-2020: Third year of EGRIP deep drilling. Prepared by Ice and Climate Group, NBI for The EGRIP project responsibles and participants and Danish and Greenlandic authorities.
https://eastgrip.nbi.ku.dk/documentation/2019/EGRIP2019FieldPlan_1stVersion.pdf, 2019

Dansgaard, W. Stable isotopes in precipitation. tellus, 16(4), 436-468. https://doi.org/10.3402/tellusa.v16i4.8993, 1964

Dansgaard, W., Clausen, H. B., Gundestrup, N., Hammer, C. U., Johnsen, S. F., Kristinsdottir, P. M., & Reeh, N. A new Greenland deep ice core. Science, 218(4579), 1273-1277. doi: 10.1126/science.218.4579.1273, 1982

Dansgaard, W., et al. Evidence for general instability of past climate from a 250-kyr ice-core record, Nature, 364, 218–220. https://doi.org/10.1038/364218a0, 1993

Denton, G. H. The mystery interval 17.5 to 14.5 kyrs ago. PAGES News Letter, 14, 14-16.
https://doi.org/10.22498/pages.14.2.14, 2006

Easterbrook, D. J. Temperature fluctuations in Greenland and the arctic. In Evidence-Based Climate Science (pp. 137-160). Elsevier. https://doi.org/10.1016/B978-0-12-804588-6.00008-2, 2016

Eddy, J. A. The Maunder Minimum: The reign of Louis XIV appears to have been a time of real anomaly in the behavior of the sun. Science, 192(4245), 1189-1202. doi: 10.1126/science.192.4245.1189, 1976

Erhardt, T., Jensen, C. M., Borovinskaya, O., & Fischer, H. Single particle characterization and total elemental concentration measurements in polar ice using continuous flow analysis-inductively coupled plasma time-of-flight mass spectrometry. Environmental science & technology, 53(22), 13275-13283. https://doi.org/10.1021/acs.est.9b03886, 2019a

Erhardt, T., Capron, E., Rasmussen, S. O., Schüpbach, S., Bigler, M., Adolphi, F., & Fischer, H. Decadal-scale progression of the onset of Dansgaard–Oeschger warming events. Climate of the Past, 15(2), 811-825. https://doi.org/10.5194/cp-15-811-2019, 2019b

Erhardt, T., Bigler, M., Federer, U., Gfeller, G., Leuenberger, D., Stowasser, O., ... & Fischer, H. High resolution aerosol concentration data from the Greenland NorthGRIP and NEEM deep ice cores. Earth System Science Data Discussions, 1-25. https://doi.org/10.5194/essd-2021-324, 2021

Fischer, H., Schüpbach, S., Gfeller, G., Bigler, M., Röthlisberger, R., Erhardt, T., . . . Wolff, E. Millennial changes in North American wildfire and soil activity over the last glacial cycle. Nature Geoscience, 8(9), 723-727.
https://doi.org/10.1038/ngeo2495, 2015

Fischer, H., Meissner, K. J., Mix, A. C., Abram, N. J., Austermann, J., Brovkin, V., ... & Zhou, L. Palaeoclimate constraints on the impact of 2 C anthropogenic warming and beyond. Nature geoscience, 11(7), 474-485.
https://doi.org/10.1038/s41561-018-0146-0, 2018

Fuhrer, K., Wolff, E. W., & Johnsen, S. J. Timescales for dust variability in the Greenland Ice Core Project (GRIP) ice core in the last 100,000 years. Journal of Geophysical Research: Atmospheres, 104, 31043–31052. https://doi.org/10.1029/1999jd900929, 1999

Gautier, E., Savarino, J., Erbland, J., Lanciki, A., & Possenti, P. Variability of sulfate signal in ice core records based on five replicate cores. Climate of the Past, 12(1), 103-113. https://doi.org/10.5194/cp-12-103-2016, 2016

Gowan, E. J., Zhang, X., Khosravi, S., Rovere, A., Stocchi, P., Hughes, A. L., ... & Lohmann, G. A new global ice sheet reconstruction for the past 80 000 years. Nature communications, 12(1), 1-9. https://doi.org/10.1038/s41467-021-21469-w, 2021

Hammer, C. U. Acidity of polar ice cores in relation to absolute dating, past volcanism, and radio–echoes. Journal of Glaciology, 25(93), 359-372. https://doi.org/10.1017/s0022143000015227, 1980

Harrison S.P. , K.E. Kohfeld, C. Roelandt, T. Claquin. The role of dust in climate changes today, at the Last Glacial Maximum and in the future. Earth-Science Reviews, 54 pp. 43-80. doi: 10.1016/S0012-8252(01)00041-1, 2001

Heaton, T. J., Köhler, P., Butzin, M., Bard, E., Reimer, R. W., Austin, W. E., ... & Skinner, L. C. Marine20—the marine radiocarbon age calibration curve (0–55,000 cal BP). Radiocarbon, 62(4), 779-820. doi:10.1017/RDC.2020.68, 2020

Heinrich, H. Origin and consequences of cyclic ice rafting in the northeast Atlantic Ocean during the past 130,000 years. Quaternary research, 29(2), 142-152. doi:10.1016/0033-5894(88)90057-9, 1988

Herron, M. M., & Langway, C. C. Firn densification: an empirical model. Journal of Glaciology, 25(93), 373-385. doi:10.3189/S0022143000015239, 1980

Hogg, A. G., Heaton, T. J., Hua, Q., Palmer, J. G., Turney, C. S., Southon, J., ... & Wacker, L. SHCal20 Southern Hemisphere calibration, 0–55,000 years cal BP. Radiocarbon, 62(4), 759-778. doi:10.1017/RDC.2020.59, 2020

Hughes, M. K. Dendrochronology in climatology–the state of the art. Dendrochronologia, 20(1-2), 95-116. https://doi.org/10.1078/1125-7865-00011, 2002

Hughes, P. D., & Gibbard, P. L. A stratigraphical basis for the Last Glacial Maximum (LGM). Quaternary International, 383, 174-185. https://doi.org/10.1016/j.quaint.2014.06.006, 2015

Hvidberg, C. S., Grinsted, A., Dahl-Jensen, D., Khan, S. A., Kusk, A., Andersen, J. K., ... & Vallelonga, P. Surface velocity of the Northeast Greenland Ice Stream (NEGIS): assessment of interior velocities derived from satellite data by GPS. The Cryosphere, 14(10), 3487-3502. https://doi.org/10.5194/tc-14-3487-2020, 2020

Jensen, C. M. Continuous high-resolution aerosol record from the East Greenland Ice Core Project covering the entire Holocene (Doctoral dissertation, Institute for Climate and Environmental Physics and Oeschger Centre for Climate Change Research, University of Bern). https://boris.unibe.ch/158023/, 2021

Johnsen, S. J., Dahl-Jensen, D., Gundestrup, N., Steffensen, J. P., Clausen, H. B., Miller, H., . . . White, J. Oxygen isotope and palaeotemperature records from six Greenland ice-core stations: Camp Century, Dye-3, GRIP, GISP2, Renland and NorthGRIP. Journal of Quaternary Science: Published for the Quaternary Research Association, 16, 299–307. https://doi.org/10.1002/jqs.622, 2001

Jouzel, J., Alley, R. B., Cuffey, K. M., Dansgaard, W., Grootes, P., Hoffmann, G., ... & White, J. Validity of the temperature reconstruction from water isotopes in ice cores. Journal of Geophysical Research: Oceans, 102(C12), 26471-26487. https://doi.org/10.1029/97JC01283, 1997

Kaufmann, P. R., Federer, U., Hutterli, M. A., Bigler, M., Schüpbach, S., Ruth, U., ... & Stocker, T. F. An improved continuous flow analysis system for high-resolution field measurements on ice cores. Environmental science & technology, 42(21), 8044-8050. https://doi.org/10.1021/es8007722, 2008

Kindler, P., et al. Temperature reconstruction from 10 to 120 kyr b2k from the NGRIP ice core. Clim. Past, 10, 887–902. doi:10.5194/cp-10-887-2014, 2014

Kjær, K. H., Bjørk, A. A., Kjeldsen, K. K., Hansen, E. S., Andresen, C. S., Siggaard-Andersen, M-L., Khan, S. A., Søndergaard, A. S., Colgan, W., Schomacker, A., Woodroffe, S., Funder, S., Rouillard, A., Jensen, J. F., & Larsen, N. K. Glacier response to the Little Ice Age during the Neoglacial cooling in Greenland. EarthScience Reviews, 227, [103984]. DOI: 10.1016/j.earscirev.2022.103984, 2022

Kobashi, T., Menviel, L., Jeltsch-Thömmes, A., Vinther, B. M., Box, J. E., Muscheler, R., . . . others. Volcanic influence on centennial to millennial Holocene Greenland temperature change. Scientific reports, 7, 1–10. https://doi.org/10.1038/s41598-017-01451-7, 2017

Kopp, G., & Lean, J. L. A new, lower value of total solar irradiance: Evidence and climate significance. Geophysical Research Letters, 38(1). https://doi.org/10.1029/2010GL045777, 2011

Kopp, G. Magnitudes and timescales of total solar irradiance variability. Journal of space weather and space climate, 6, A30. https://doi.org/10.1051/swsc/2016025, 2016

Laepple, T., Münch, T., Casado, M., Hoerhold, M., Landais, A., & Kipfstuhl, S. On the similarity and apparent cycles of isotopic variations in East Antarctic snow pits. The Cryosphere, 12(1), 169-187. https://doi.org/10.5194/tc-12-169-2018, 2018

Legrand, M., McConnell, J., Fischer, H., Wolff, E. W., Preunkert, S., Arienzo, M., ... & Flannigan, M. Boreal fire records in Northern Hemisphere ice cores: a review. Climate of the Past, 12(10), 2033-2059. https://doi.org/10.5194/cp-12-2033-2016, 2016

Li, T. Y., Wu, Y., Shen, C. C., Li, J. Y., Chiang, H. W., Lin, K., ... & Edwards, R. L. High precise dating on the variation of the Asian summer monsoon since 37 ka BP. Scientific reports, 11(1), 1-14. https://doi.org/10.1038/s41598-021-88597-7, 2021

Lin, J., Svensson, A., Hvidberg, C. S., Lohmann, J., Kristiansen, S., Dahl-Jensen, D., ... & Mulvaney, R. Magnitude, frequency and climate forcing of global volcanism during the last glacial period as seen in Greenland and Antarctic ice cores (60–9 ka). Climate of the Past Discussions, 1-45. https://doi.org/10.5194/cp-18-485-2022, 2021

Lisiecki, L. E., & Raymo, M. E. A Pliocene-Pleistocene stack of 57 globally distributed benthic δ18O records. Paleoceanography, 20(1). https://doi.org/10.1029/2004PA001071, 2005

Lohmann, J. and Svensson, A. Ice core evidence for major volcanic eruptions at the onset of Dansgaard-Oeschger warming events, Clim. Past Discuss. [preprint]https://doi.org/10.5194/cp-2022-1, 2022

Lohne, Ø. S., Mangerud, J. A. N., & Birks, H. H. Precise 14 C ages of the Vedde and Saksunarvatn ashes and the Younger Dryas boundaries from western Norway and their comparison with the Greenland Ice Core (GICC 05) chronology. Journal of Quaternary Science, 28(5), 490-500. https://doi.org/10.1002/jqs.2640, 2013

Manning, S. W., Höflmayer, F., Moeller, N., Dee, M. W., Ramsey, C. B., Fleitmann, D., ... & Wild, E. M. Dating the Thera (Santorini) eruption: archaeological and scientific evidence supporting a high chronology. Antiquity, 88(342), 1164-1179. doi:10.1017/S0003598X00115388, 2014

Matthews, J. A., & Briffa, K. R. The 'Little Ice Age': re-evaluation of an evolving concept. Geografiska Annaler: Series A, Physical Geography, 87(1), 17-36. hhtp://www.jstor.org/stable/3554259, 2005

McConnell, J. R., Wilson, A. I., Stohl, A., Arienzo, M. M., Chellman, N. J., Eckhardt, S., ... & Steffensen, J. P. Lead pollution recorded in Greenland ice indicates European emissions tracked plagues, wars, and imperial expansion during antiquity. Proceedings of the National Academy of Sciences, 115(22), 5726-5731. https://doi.org/10.1073/pnas.1721818115, 2018

McConnell, J. R., Sigl, M., Plunkett, G., Burke, A., Kim, W. M., Raible, C. C., ... & Steffensen, J. P. Extreme climate after massive eruption of Alaska's Okmok volcano in 43 BCE and effects on the late Roman Republic and Ptolemaic Kingdom. Proceedings of the National Academy of Sciences, 117(27), 15443-15449. https://doi.org/10.1073/pnas.2002722117, 2020

Meredith, M., M. Sommerkorn, S. Cassotta, C. Derksen, A. Ekaykin, A. Hollowed, G. Kofinas, A. Mackintosh, J. Melbourne-Thomas, M.M.C. Muelbert, G. Ottersen, H. Pritchard, and E.A.G. Schuur, Polar Regions. In: IPCC Special Report on the Ocean and Cryosphere in a Changing Climate [H.-O. Pörtner, D.C. Roberts, V. Masson-Delmotte, P. Zhai, M. Tignor, E. Poloczanska, K. Mintenbeck, A. Alegría, M. Nicolai, A. Okem, J. Petzold, B. Rama, N.M. Weyer (eds.)]. In press. Retrieved from : https://www.ipcc.ch/srocc/chapter/chapter-3-2/, 2019

Miyake, F., Suzuki, A., Masuda, K., Horiuchi, K., Motoyama, H., Matsuzaki, H., ... & Nakai, Y. Cosmic ray event of AD 774–775 shown in quasi-annual 10Be data from the Antarctic Dome Fuji ice core. Geophysical Research Letters, 42(1), 84-89. https://doi.org/10.1002/2014GL062218, 2015

Monnin, E., Steig, E. J., Siegenthaler, U., Kawamura, K., Schwander, J., Stauffer, B., ... & Fischer, H. Evidence for substantial accumulation rate variability in Antarctica during the Holocene, through synchronization of CO2 in the Taylor Dome, Dome C and DML ice cores. Earth and Planetary Science Letters, 224(1-2), 45-54. https://doi.org/10.1016/j.epsl.2004.05.007, 2004

Muscheler, R., Adolphi, F., & Knudsen, M. Assessing the differences between the IntCal and Greenland ice-core time scales for the last 14,000 years via the common cosmogenic radionuclide variations. Quaternary Science Reviews, 106, 81-87. http://dx.doi.org/10.1016/j.quascirev.2014.08.017, 2014

Muscheler, R., Adolphi, F., Heaton, T. J., Ramsey, C. B., Svensson, A., Van Der Plicht, J., & Reimer, P. J. Testing and improving the IntCal20 calibration curve with independent records. Radiocarbon, 62, 1079–1094. https://doi.org/10.1017/rdc.2020.54, 2020

Neff, P. D. A review of the brittle ice zone in polar ice cores. Annals of Glaciology, 55(68), 72-82. doi:10.3189/2014AoG68A023, 2014

Nguyen, D. C., Chen, Y. G., Chiang, H. W., Shen, C. C., Wang, X., Doan, L. D., ... & Kuo, Y. T. A decadal-resolution stalagmite record of strong Asian summer monsoon from northwestern Vietnam over the Dansgaard–Oeschger events 2–4. Journal of Asian Earth Sciences: X, 3, 100027. https://doi.org/10.1016/j.jaesx.2020.100027, 2020

North Greenland Ice Core Project members. High resolution record of Northern Hemisphere climate extending into the last interglacial period. Nature, 431(7005), 147-151. https://doi.org/10.1038/nature02805, 2004

O'Brien, S. R., Mayewski, P. A., Meeker, L. D., Meese, D. A., Twickler, M. S., & Whitlow, S. I. Complexity of Holocene climate as reconstructed from a Greenland ice core. Science, 270(5244), 1962-1964. doi: 10.1126/science.270.5244.1962, 1995

O'Neil, J. R., Clayton, R. N., & Mayeda, T. K. Oxygen isotope fractionation in divalent metal carbonates. The Journal of Chemical Physics, 51(12), 5547-5558. https://doi.org/10.1063/1.1671982, 1969

Pedro, J. B., Jochum, M., Buizert, C., He, F., Barker, S., & Rasmussen, S. O. Beyond the bipolar seesaw: Toward a process understanding of interhemispheric coupling. Quaternary Science Reviews, 192, 27-46. https://doi.org/10.1016/j.quascirev.2018.05.005, 2018

Peltier, W. R., & Vettoretti, G. Dansgaard-Oeschger oscillations predicted in a comprehensive model of glacial climate: A “kicked” salt oscillator in the Atlantic. Geophysical Research Letters, 41(20), 7306-7313. https://doi.org/10.1002/2014GL061413, 2014

Plunkett, G., Sigl, M., Schwaiger, H., Tomlinson, E., Toohey, M., McConnell, J. R., . . . Siebe, C. No evidence for tephra in Greenland from the historic eruption of Vesuvius in 79 CE: Implications for geochronology and paleoclimatology. Climate of the Past, 18, 45–65. https://doi.org/10.5194/cp-2021-63, 2022

Previdi, M., Smith, K. L., & Polvani, L. M. Arctic amplification of climate change: a review of underlying mechanisms. Environmental Research Letters. Https://doi.org/10.1088/1748-9326/ac1c29, 2021

Raisbeck, G. M., Yiou, F., Fruneau, M., Loiseaux, J. M., Lieuvin, M., & Ravel, J. C. Cosmogenic 10Be/7Be as a probe of atmospheric transport processes. Geophysical Research Letters, 8(9), 1015-1018. https://doi.org/10.1029/GL008i009p01015, 1981

Rasmussen, S. O., Andersen, K. K., Svensson, A. M., Steffensen, J. P., Vinther, B. M., Clausen, H. B., . . . others. A new Greenland ice core chronology for the last glacial termination. Journal of Geophysical Research: Atmospheres, 111. https://doi.org/10.1029/2005JD006079, 2006

Rasmussen, S. O., Vinther, B. M., Clausen, H. B., & Andersen, K. K. Early Holocene climate oscillations recorded in three Greenland ice cores. Quaternary Science Reviews, 26(15-16), 1907-1914. https://doi.org/10.1016/j.quascirev.2007.06.015, 2007

Rasmussen, S. O., Abbott, P. M., Blunier, T., Bourne, A. J., Brook, E., Buchardt, S. L., . . . others. A first chronology for the North Greenland Eemian Ice Drilling (NEEM) ice core. Climate of the Past, 9, 2713–2730. https://doi.org/10.5194/cp-9-2713-2013, 2013

Rasmussen, S. O., Bigler, M., Blockley, S. P., Blunier, T., Buchardt, S. L., Clausen, H. B., ... & Winstrup, M. A stratigraphic framework for abrupt climatic changes during the Last Glacial period based on three synchronized Greenland ice-core records: refining and extending the INTIMATE event stratigraphy. Quaternary Science Reviews, 106, 14-28. https://doi.org/10.1016/j.quascirev.2014.09.007, 2014

Reimer, P. J., Austin, W. E., Bard, E., Bayliss, A., Blackwell, P. G., Ramsey, C. B., . . . others. The IntCal20 Northern Hemisphere radiocarbon age calibration curve (0–55 cal kBP). Radiocarbon, 62, 725–757. https://doi.org/10.1017/rdc.2020.41, 2020

Reimer, P. J. Evolution of radiocarbon calibration. Radiocarbon, 1-17. doi:10.1017/RDC.2021.62, 2021

Rhodes, R. H., Yang, X., Wolff, E. W., McConnell, J. R., & Frey, M. M. Sea ice as a source of sea salt aerosol to Greenland ice cores: a model-based study. Atmospheric Chemistry and Physics, 17(15), 9417-9433. https://doi.org/10.5194/acp-17-9417-2017, 2017

Robock, A. volcanic eruptions and climate. Reviews of Geophysics, vol. 38, issue 2, 191-219. https://doi.org/10.1029/1998RG000054, 2000

Schüpbach, S., Fischer, H., Bigler, M., Erhardt, T., Gfeller, G., Leuenberger, D., ... & Wolff, E. W. Greenland records of aerosol source and atmospheric lifetime changes from the Eemian to the Holocene. Nature communications, 9(1), 1-10. https://doi.org/10.1038/s41467-018-03924-3, 2018

Seierstad, I. K., Abbott, P. M., Bigler, M., Blunier, T., Bourne, A. J., Brook, E., ... & Vinther, B. M. Consistently dated records from the Greenland GRIP, GISP2 and NGRIP ice cores for the past 104 ka reveal regional millennial-scale δ18O gradients with possible Heinrich event imprint. Quaternary Science Reviews, 106, 29-46. https://doi.org/10.1016/j.quascirev.2014.10.032, 2014

Siegenthaler, U., Heimann, M., & Oeschger, H. 14C variations caused by changes in the global carbon cycle. Radiocarbon, 22(2), 177-191. doi:10.1017/S0033822200009449, 1980

Sigl, M., Winstrup, M., McConnell, J. R., Welten, K. C., Plunkett, G., Ludlow, F., … Woodruff, T. E. Timing and climate forcing of volcanic eruptions for the past 2,500 years. Nature, 523(7562), 543–549. https://doi.org/10.1038/nature14565, 2015

Sigl, M., Fudge, T. J., Winstrup, M., Cole-Dai, J., Ferris, D., McConnell, J. R., ... & Sowers, T. A. The WAIS Divide deep ice core WD2014 chronology–Part 2: Annual-layer counting (0–31 ka BP). Climate of the Past, 12(3), 769-786. https://doi.org/10.5194/cp-12-769-2016, 2016

Sigl, M., Toohey, M., McConnell, J. R., Cole-Dai, J., & Severi, M. n review). Volcanic stratospheric sulfur injections and aerosol optical depth during the Holocene (past 11,500 years) from a bipolar ice core array. Earth System Science Data Discussions, 1-45. https://doi.org/10.5194/essd-2021-422, 2022

Sjolte, J., Sturm, C., Adolphi, F., Vinther, B. M., Werner, M., Lohmann, G., & Muscheler, R. Solar and volcanic forcing of North Atlantic climate inferred from a process-based reconstruction. Climate of the Past, 14(8), 1179-1194. https://doi.org/10.5194/cp-14-1179-2018, 2018

Steffensen, J. P., Andersen, K. K., Bigler, M., Clausen, H. B., Dahl-Jensen, D., Fischer, H., ... & White, J. W. High-resolution Greenland ice core data show abrupt climate change happens in few years. science, 321(5889), 680-684. https://doi.org/10.1126/science.1157707, 2008

Steinhilber, F., Abreu, J. A., Beer, J., Brunner, I., Christl, M., Fischer, H., ... & Wilhelms, F. 9,400 years of cosmic radiation and solar activity from ice cores and tree rings. Proceedings of the National Academy of Sciences, 109(16), 5967-5971. https://doi.org/10.1073/pnas.1118965109, 2012

Stocker, T. F., & Johnsen, S. J. A minimum thermodynamic model for the bipolar seesaw. Paleoceanography, 18(4). doi: 10.1029/2003PA000920, 2003

Stoffel, M., Khodri, M., Corona, C., Guillet, S., Poulain, V., Bekki, S., ... & Masson-Delmotte, V. Estimates of volcanic-induced cooling in the Northern Hemisphere over the past 1,500 years. Nature Geoscience, 8(10), 784-788. https://doi.org/10.1038/ngeo2526, 2015

Sundqvist, H. S., Holmgren, K., Fohlmeister, J., Zhang, Q., Matthews, M. B., Spötl, C., & Körnich, H. Evidence of a large cooling between 1690 and 1740 AD in southern Africa. Scientific Reports, 3(1), 1-6. https://doi.org/10.1038/srep01767, 2013

Svensson, A., Nielsen, S. W., Kipfstuhl, S., Johnsen, S. J., Steffensen, J. P., Bigler, M., ... & Röthlisberger, R. Visual stratigraphy of the North Greenland Ice Core Project (NorthGRIP) ice core during the last glacial period. Journal of Geophysical Research: Atmospheres, 110(D2). https://doi.org/10.1029/2004JD005134, 2005

Svensson, A., Andersen, K. K., Bigler, M., Clausen, H. B., Dahl-Jensen, D., Davies, S. M., ... & Vinther, B. M. The Greenland ice core chronology 2005, 15–42 ka. Part 2: comparison to other records. Quaternary Science Reviews, 25(23-24), 3258-3267. doi:10.1016/j.quascirev.2006.08.003, 2006

Svensson, A., Andersen, K. K., Bigler, M., Clausen, H. B., Dahl-Jensen, D., Davies, S. M., ... & Vinther, B. M. A 60 000 year Greenland stratigraphic ice core chronology. Climate of the Past, 4(1), 47-57. https://doi.org/10.5194/cp-4-47-2008, 2008

Svensson, A., Dahl-Jensen, D., Steffensen, J. P., Blunier, T., Rasmussen, S. O., Vinther, B. M., ... & Bigler, M. Bipolar volcanic synchronization of abrupt climate change in Greenland and Antarctic ice cores during the last glacial period. Climate of the Past, 16(4), 1565-1580. https://doi.org/10.5194/cp-16-1565-2020, 2020

Tierney, J. E., Zhu, J., King, J., Malevich, S. B., Hakim, G. J., & Poulsen, C. J. Glacial cooling and climate sensitivity revisited. Nature, 584(7822), 569-573. https://doi.org/10.1038/s41586-020-2617-x, 2020

Turney, C. S., Palmer, J., Ramsey, C. B., Adolphi, F., Muscheler, R., Hughen, K. A., ... & Hogg, A. High-precision dating and correlation of ice, marine and terrestrial sequences spanning Heinrich Event 3: Testing mechanisms of interhemispheric change using New Zealand ancient kauri (Agathis australis). Quaternary Science Reviews, 137, 126-134. https://doi.org/10.1016/j.quascirev.2016.02.005, 2016

Vecchio, A., Lepreti, F., Laurenza, M. O. N. I. C. A., Alberti, T., & Carbone, V. Connection between solar activity cycles and grand minima generation. Astronomy & Astrophysics, 599, A58. https://doi.org/10.1051/0004-6361/201629758, 2017

Veres, D., Bazin, L., Landais, A., Toyé Mahamadou Kele, H., Lemieux-Dudon, B., Parrenin, F., ... & Wolff, E. W. The Antarctic ice core chronology (AICC2012): an optimized multi-parameter and multi-site dating approach for the last 120 thousand years. Climate of the Past, 9(4), 1733-1748. https://doi.org/10.5194/cp-9-1733-2013, 2013

Vettoretti, G., Ditlevsen, P., Jochum, M., & Rasmussen, S. O. Atmospheric CO2 control of spontaneous millennial-scale ice age climate oscillations. Nature Geoscience, 1-7. https://doi.org/10.1038/s41561-022-00920-7, 2022

Vidal, L., Labeyrie, L., Cortijo, E., Arnold, M., Duplessy, J. C., Michel, E., ... & Van Weering, T. C. E. Evidence for changes in the North Atlantic Deep Water linked to meltwater surges during the Heinrich events. Earth and Planetary Science Letters, 146(1-2), 13-27. https://doi.org/10.1016/S0012-821X(96)00192-6, 1997

Vinther, B., Clausen, H., Johnsen, S., Rasmussen, S., Andersen, K., Buchardt, S., . . . Heinemeier, J. A synchronized dating of three Greenland ice cores throughout the Holocene. Journal of Geophysical Research Atmospheres. https://doi.org/10.1029/2005jd006921, 2006

Vinther, B. M., Buchardt, S. L., Clausen, H. B., Dahl-Jensen, D., Johnsen, S. J., Fisher, D. A., ... & Svensson, A. M. Holocene thinning of the Greenland ice sheet. Nature, 461(7262), 385-388. https://doi.org/10.1038/nature08355, 2009

Vinther, B. M., Jones, P. D., Briffa, K. R., Clausen, H. B., Andersen, K. K., Dahl-Jensen, D., & Johnsen, S. J. Climatic signals in multiple highly resolved stable isotope records from Greenland. Quaternary Science Reviews, 29(3-4), 522-538. doi:10.1016/j.quascirev.2009.11.002, 2010

Visbeck, M. H., Hurrell, J. W., Polvani, L., & Cullen, H. M. The North Atlantic Oscillation: past, present, and future. Proceedings of the National Academy of Sciences, 98(23), 12876-12877. https://doi.org/10.1073/pnas.231391598, 2001

WAIS Divide Project Members. Precise interpolar phasing of abrupt climate change during the last ice age. Nature, 520(7549), 661-665. https://doi.org/10.1038/nature14401, 2015

Walker, M. J., Berkelhammer, M., Björck, S., Cwynar, L. C., Fisher, D. A., Long, A. J., ... & Weiss, H. Formal subdivision of the Holocene Series/Epoch: A Discussion Paper by a Working Group of INTIMATE (Integration of ice-core, marine and terrestrial records) and the Subcommission on Quaternary Stratigraphy (International Commission on Stratigraphy). Journal of Quaternary Science, 27(7), 649-659. https://doi.org/10.1002/jqs.2565, 2012

Wang, Y. J., Cheng, H., Edwards, R. L., An, Z. S., Wu, J. Y., Shen, C. C., & Dorale, J. A. A high-resolution absolute-dated late Pleistocene monsoon record from Hulu Cave, China. Science, 294(5550), 2345-2348. doi: 10.1126/science.1064618, 2001

Warburton, D. A. (Ed.). Time's Up! Dating the Minoan Eruption of Santorini: Acts of the Minoan Eruption Chronology Workshop, Sandbjerg, November 2007 (Vol. 10). ISD LLC.ISSN: 1397-1433 (print), 2009

Wendt, K. A., Li, X., & Edwards, R. L. Uranium–thorium dating of speleothems. Elements: An International Magazine of Mineralogy, Geochemistry, and Petrology, 17(2), 87-92. https://doi.org/10.2138/gselements.17.2.87, 2021

Westhoff, J., Sinnl, G., Svensson, A., Freitag, J., Kjær, H. A., Vallelonga, P., ... & Weikusat, I. n review). Melt in the Greenland EastGRIP ice core reveals Holocene warming events. Climate of the Past Discussions, 1-36. https://doi.org/10.5194/cp-2021-89, 2021a

Westhoff, J., Stoll, N., Franke, S., Weikusat, I., Bons, P., Kerch, J., ... & Dahl-Jensen, D. A stratigraphy-based method for reconstructing ice core orientation. Annals of Glaciology, 62(85-86), 191-202. https://doi.org/10.1017/aog.2020.76, 2021b

Winstrup, M., Svensson, A. M., Rasmussen, S. O., Winther, O., Steig, E. J., & Axelrod, A. E. An automated approach for annual layer counting in ice cores. Climate of the Past, 8(6), 1881-1895. https://doi.org/10.5194/cp-8-1881-2012, 2012

Wolff, E. W., Chappellaz, J., Blunier, T., Rasmussen, S. O. and Svensson, A.: Millennial-scale variability during the last glacial: the ice core record, Quat. Sci. Rev. 29, p. 2828–2838 , 2010

Yokoyama, Y., Lambeck, K., De Deckker, P., Johnston, P., & Fifield, L. K. Timing of the Last Glacial Maximum from observed sea-level minima. Nature, 406(6797), 713-716. https://doi.org/10.1038/35021035, 2000

Zhang, H., Ait Brahim, Y., Li, H., Zhao, J., Kathayat, G., Tian, Y., ... & Cheng, H. The Asian summer monsoon: Teleconnections and forcing mechanisms—A review from Chinese speleothem δ18O records. Quaternary, 2(3), 26. https://doi.org/10.3390/quat2030026, 2019

Zhao, K., Wang, Y., Edwards, R. L., Cheng, H., Liu, D., & Kong, X. A high-resolved record of the Asian Summer Monsoon from Dongge Cave, China for the past 1200 years. Quaternary Science Reviews, 122, 250-257. https://doi.org/10.1016/j.quascirev.2015.05.030, 2015

2 Matching EastGRIP to other ice cores

Without a depth-age relationship, ice cores would not be of much use and the comparison to other archives would not be possible. Since the release of GICC05, the standard procedure to date newly drilled Greenlandic ice cores has become to synchronize them to previously dated ice cores by finding appropriate isochrones in the ice.

For NEEM, the transfer of GICC05 was achieved by Rasmussen et al. (2013), while for EastGRIP, I had the chance to contribute to the establishment of appropriate tie points to NEEM, NorthGRIP1, and NorthGRIP2.

As to what constitutes a good isochrone or tie point, these are events that left a discernible trace in the ice that can be used for absolute or relative dating: volcanic eruptions, solar storms, wildfires, bomb testing traces, and any other signal that can be considered as a synchronous and instantaneous event. Not so good for ice-core matching are climate changes observed in the ice, such as the GI onsets and terminations, as it is more important to test whether they are synchronous across ice cores (Blaauw, 2012; Rasmussen et al., 2014).

Conductivity and permittivity measurements (ECM and DEP) are conducted in the field to assess the acidity and other properties of the extracted ice (Hammer, 1980; Moore et al., 1994). The climatic transitions are observed in the ECM and DEP signals because of the different impurity loading occurring across stadial-interstadial transitions (Rasmussen et al., 2006). These measurements also record peaks representing volcanic eruptions, which can be used to synchronize the ice cores (Hammer, 1980). The signature of volcanic eruptions is sufficiently uniform over Greenland to allow for accurate synchronization, although there can be spatial variability in the shape of the eruption signals (e.g. Clausen et al., 1997).

2.1 Collaboration for Paper I – Pre-processing of ECM and EastGRIP synchronization

After the field season of 2018, about 1760 m of EastGRIP had been drilled. The brittle ice of EastGRIP (about 600-950 m) was processed the year following the drilling, as the ice was stored for one winter in order to allow the ice core to relax by letting the gas adapt to the surrounding atmosphere (Dahl Jensen et al., EastGRIP field report, 2019).

A group of four ice-core matchers formed by myself, S.O. Rasmussen, M. Jensen, and S. Mojtabavi had the goal of transferring the GICC05 chronology to EastGRIP. We first had to process the raw ECM and DEP data, since the two measurements are registered in the field and sometimes contain some irregularities because of the manual procedure of measuring

the data (Hammer, 1980). Moreover, the 1.65 m long sections of drilled ice may be interrupted by gaps of missing ice, breaks between adjacent pieces, and, of course, the pieces' top and bottom ends. These occurrences are both manually logged and visible in the data as abrupt declines.

The DEP was processed at AWI, while the ECM was processed in Copenhagen. We decided to keep the DEP synchronization independent from the ECM synchronization to verify the agreement between the methods, as DEP is sensitive not only to the anions in the ice but also to neutral salts and cations (such as NH_4^+) and has different properties than ECM (Moore et al., 1994).

Since the NEEM drilling campaign, the ECM system had been mounted to a slider, replacing the hand-held electrodes with a more stable setup (Larsen et al., NEEM field report, 2010). Nonetheless, the measurement relies on the manual operation of the slide, hence uncertainties in the depth assignment are to be expected.

In synthesis, the method of pre-processing the ECM involves converting the arbitrary x-coordinate measured by the instrument to a depth in centimetres, based on the system calibration and the ice-core logging performed in the field. The ECM measurements had been repeated 2-3 times on each ice piece, hence we selected the measurement with less noise and better signal appearance. The method is reported in detail in the master thesis by Mathias S. Jensen (2019) and in Mojtabavi et al. (2020). It is worth repeating that each ECM measurement has to be manually trimmed for unnecessary data at the ends of each 1.65 m ice-core piece and over core breaks and gaps, the location of which is also logged in the field. Each observer processed the ECM independently and, after solving cases of disagreement and verifying that the depth agreement was within 1 cm, much less than 1 year in the Holocene, the version of the ECM produced by one observer was upgraded to be the released ECM dataset.

The search of common ECM spikes was performed manually with a strong focus on finding patterns of eruptions, rather than single and isolated events as this may lead to bias. The Matlab GUI "Matchmaker" facilitates the visualization of long data stretches and computes relevant parameters to evaluate the quality of the match, such as the relative depth difference and the ratio between annual layer thicknesses (Rasmussen et al., 2006; Rasmussen, et al., 2013). A set of climatic tie points, identifying the Holocene and the GIs, was used as an initial guide for the matching but was later replaced by volcanoes, at a much better resolution.

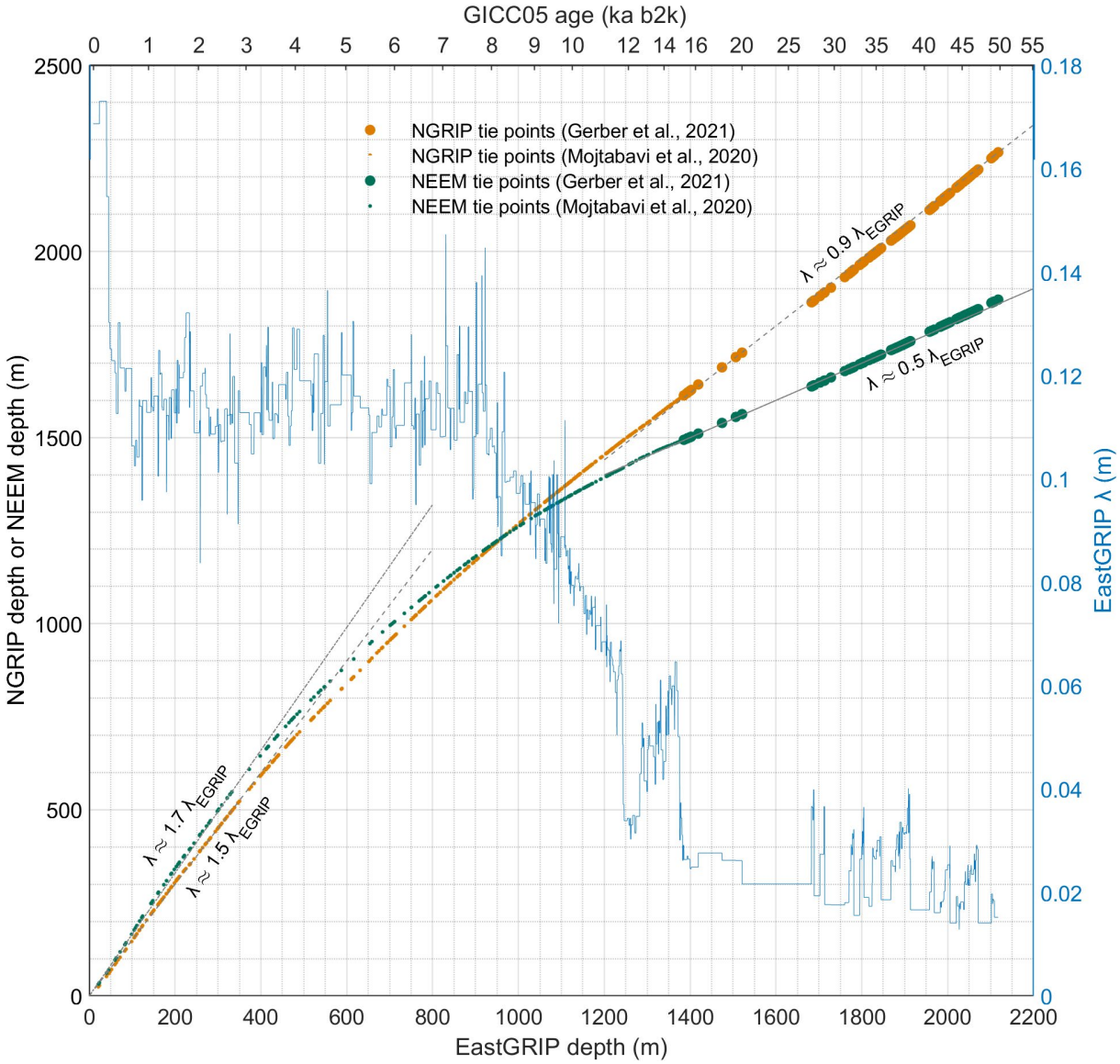

Figure 2.1 Synchronization between the EastGRIP, NorthGRIP, and NEEM ice cores. Comparison of tie points obtained in Mojtabavi et al. (2020; small dots) and Gerber et al. (2021; large dots). The annual layer thickness (λ, in blue) of EastGRIP was computed after transferring GICC05 ages by linear interpolation to the EastGRIP ice core. The proportionality of the ice-core layer thicknesses is highlighted by linear trends superposed to the tie points.

The process of ice-core matching may suffer from subjective bias. Challenges to the correctness of the match include: different shapes of eruptions across ice cores; a lack, at this stage, of tephra and/or annually resolved data to support the tie points; visualization issues related to the layer thickness difference of the ice cores; stretches of data without appropriate tie points.

Hence, an iterative comparison is key. We conducted several independent rounds of matching, after which we compared and selected a subset of tie points we agreed on. We also compared the DEP tie points and the ECM tie points and found some depth-assignment

inconsistencies that needed to be resolved before incorporating the DEP tie points. In the end, a common consensus was reached about the tie points (Figure 2.1).

For Paper I, we selected 381 tie points, of which 257 within NorthGRIP1 depths and 124 within NorthGRIP2 depths. We could include brittle-ice tie points, as the brittle ice had fortunately been processed at this time. The oldest tie point was selected at an EastGRIP depth of 1383.84 m, at 14966 years b2k (MCE = 196 years; Rasmussen et al., 2014), implying an average spacing between volcanic tie points of ~40 years. The 381st tie point was found at the termination of Greenland stadial GS-2; the glacial period between 1383 m and 1750 m (~28 ka b2k) was problematic to match because of sparse volcanic tie points, hence we postponed it until we obtained more ECM data.

2.2 Collaboration for Paper II – Extending the chronology of EastGRIP from GS-2 to GI-14

In 2019, as the depth of the borehole reached 2120 m, new EastGRIP ice became available for measurement. Again, the ECM was pre-processed in Copenhagen. For Paper II, we extended the match of EastGRIP to NorthGRIP and NEEM. The matching group was formed by myself, S. Rasmussen and T. Gerber.

A total of 262 match points was identified between 1383.84 m and 2106.65 m, adding to the previous 381 match points. The match curves between EastGRIP and the other two cores are shown in Figure 2.1, representing all the volcanic tie points. The age of the deepest match point was established to be 49200 years b2k, at the end of GS-14, with an MCE of 2026 years.

The accumulation history of EastGRIP depends on the flow properties in the NEGIS. The location of EastGRIP originated from the Summit area (GRIP), more than 300 km upstream. The depth-depth graph in Figure 2.1 highlights the relative ice-core thinning regimes. The tie points are characterized by a steady ratio over the Late Holocene, followed by a gradual change of slope over the deglaciation. Initially, EastGRIP layers are thinner than the other ice cores, while in the glacial the layer thickness at EastGRIP is higher.

The thinner Holocene layers of EastGRIP result from a lower accumulation rate; on average it snows 0.12 m (ice equivalent) each year at EastGRIP, although this number may have changed as the core location moved with the ice stream. Presently, at NEEM it snows about ~1.7 times as much, at NorthGRIP ~1.5 times, and at GRIP ~1.9 times as much (see Table

3.1 of Paper III and references reported there). Wider layers in the top lead to more compression by flow and thus thinner layers in the bottom of the ice core, and that is why the other ice cores thin more rapidly than at EastGRIP.

The layer thickness of EastGRIP is very peculiar in the Holocene. After the firn zone ends, at around 100 m, and until 900 m (~8 ka b2k), the layers maintain a constant thickness of 0.11 ± 0.1 m, as opposed to the linearly decreasing thickness of other ice cores (Vinther et al., 2006; Rasmussen et al., 2013). In case of constant accumulation rate, ice flow models predict a linearly decreasing thickness (Dansgaard & Johnsen, 1969 ; Dahl Jensen et al., 1993), which agrees with Holocene observations in ice cores from the ice divide region.

The flatness of the EastGRIP layer thickness is currently being explained as the fortuitous balance between thinning and increasing upstream accumulation during the Holocene (Gerber et al., 2021). Because of the NEGIS flow, the accumulation at the ice-core location decreased as it moved further away from the divide, while the thinning kept increasing with depth, which resulted in an overall constant layer thickness down to 900 m depth.

Severe scarcity of common match points was observed across the long GS-2 and GS-3 and across every older GS. The weak nature of volcanic signals across stadial periods should not be attributed to a diminished global volcanic activity but rather to enhanced alkaline dust deposition and lower snow deposition, caused by much colder and drier climatic conditions (Rasmussen, et al., 2013; Schüpbach et al., 2018). The largest distance between match points was observed across GS-2 and GS-3 and spans about 162 m of EastGRIP ice.

2.3 References

Blaauw, M. Out of tune: the dangers of aligning proxy archives. Quaternary Science Reviews, 36, 38-49. https://doi.org/10.1016/j.quascirev.2010.11.012, 2012

Clausen, H. B., Hammer, C. U., Hvidberg, C. S., Dahl-Jensen, D., Steffensen, J. P., Kipfstuhl, J., & Legrand, M. A comparison of the volcanic records over the past 4000 years from the Greenland Ice Core Project and Dye 3 Greenland ice cores. Journal of Geophysical Research: Oceans, 102(C12), 26707-26723. https://doi.org/10.1029/97JC00587 , 1997

Dahl-Jensen, D., Johnsen, S. J., Hammer, C. U., Clausen, H. B., and Jouzel, J.: Past Accumulation rates derived from observed annual layers in the GRIP ice core from Summit, Central Greenland, Ice in the Climate System, 112, 517–532, https://doi.org/10.1007/978-3-642-85016-5_29, 1993.

Dahl-Jensen, D., Kirk, M., Koldtoft, I., Popp, T., and P, S. J.: Field season 2019 East GReenland Ice core Project (EGRIP) 2015-2020: Third year of EGRIP deep drilling. Prepared by Ice and Climate Group, NBI for The EGRIP project responsibles and participants and Danish and Greenlandic authorities. https://eastgrip.nbi.ku.dk/documentation/2019/EGRIP2019FieldPlan_1stVersion.pdf, 2019

Dansgaard, W., & Johnsen, S. J. A flow model and a time scale for the ice core from Camp Century, Greenland. Journal of Glaciology, 8(53), 215-223. doi:10.3189/S0022143000031208, 1969

Gerber, T. A., Hvidberg, C. S., Rasmussen, S. O., Franke, S., Sinnl, G., Grinsted, A., . . . Dahl-Jensen, D. Upstream flow effects revealed in the EastGRIP ice core using a Monte Carlo inversion of a two-dimensional ice-flow model. The Cryosphere, 15(8), 3655-3679. https://doi.org/10.5194/tc-15-3655-2021 , 2021

Hammer, C. U. Acidity of polar ice cores in relation to absolute dating, past volcanism, and radio–echoes. Journal of Glaciology, 25(93), 359-372. https://doi.org/10.1017/s0022143000015227 , 1980

Larsen L.B., Sheldon S.G., Steffensen J.P. Field season 2010 North Greenland Eemian Ice drilling (NEEM) 2007-2012: NEEM 2nd season of deep ice core drilling and core processing. Prepared by Ice and Climate Group, NBI for The NEEM Steering Committee and Danish and Greenlandic authorities. https://neem.dk/billeder/NEEM2010FieldPlan.pdf/, 2010

Mathias Skov Jensen. Electrical conductivity, Volcanoes and Climate ; Master thesis at Copenhagen University (Retrieved from the author) , 2019

Mojtabavi, S., Wilhelms, F., Cook, E., Davies, S., Sinnl, G., Skov Jensen, M., . . . Rasmussen, S. A first chronology for the East Greenland Ice-core Project (EGRIP) over the Holocene and last glacial termination. Climate of the Past, 16(6). https://doi.org/10.5194/cp-16-2359-2020 , 2020

Moore, J. C., Wolff, E. W., Clausen, H. B., Hammer, C. U., Legrand, M. R., and Fuhrer, K.: Electrical response of the Summit-Greenland ice core to ammonium, sulphuric acid, and hydrochloric acid, Geophys. Res. Lett., 21, 565–568, https://doi.org/10.1029/94GL00542, 1994.

Rasmussen, S. O., Abbott, P. M., Blunier, T., Bourne, A. J., Brook, E., Buchardt, S. L., . . . others. A first chronology for the North Greenland Eemian Ice Drilling (NEEM) ice core. Climate of the Past, 9, 2713–2730. https://doi.org/10.5194/cp-9-2713-2013, 2013

Rasmussen, S. O., Andersen, K. K., Svensson, A. M., Steffensen, J. P., Vinther, B. M., Clausen, H. B., . . . others. A new Greenland ice core chronology for the last glacial termination. Journal of Geophysical Research: Atmospheres, 111(D6). https://doi.org/10.1029/2005JD006079, 2006

Rasmussen, S. O., Bigler, M., Blockley, S. P., Blunier, T., Buchardt, S. L., Clausen, H. B., ... & Winstrup, M. A stratigraphic framework for abrupt climatic changes during the Last Glacial period based on three synchronized Greenland ice-core records: refining and extending the INTIMATE event stratigraphy. Quaternary Science Reviews, 106, 14-28. https://doi.org/10.1016/j.quascirev.2014.09.007, 2014

Schüpbach, S., Fischer, H., Bigler, M., Erhardt, T., Gfeller, G., Leuenberger, D., ... & Wolff, E. W. Greenland records of aerosol source and atmospheric lifetime changes from the Eemian to the Holocene. Nature communications, 9(1), 1-10. https://doi.org/10.1038/s41467-018-03924-3, 2018

Vinther, B., Clausen, H., Johnsen, S., Rasmussen, S., Andersen, K., Buchardt, S., . . . Heinemeier, J. A synchronized dating of three Greenland ice cores throughout the Holocene. Journal of Geophysical Research Atmospheres. https://doi.org/10.1029/2005jd006921, 2006

3 A multi-ice-core, annual-layer-counted Greenland ice-core chronology for the last 3800 years: GICC21

Giulia Sinnl[1], Mai Winstrup[2], Tobias Erhardt[3,4], Eliza Cook[1], Camilla Jensen[4], Anders Svensson[1], Bo Møllesøe Vinther[1], Raimund Muscheler[5], and Sune Olander Rasmussen[1]

[1] Physics of Ice, Climate, and Earth, Niels Bohr Institute, University of Copenhagen, Denmark.

[2] DTU Space, National Space Institute, Technical University of Denmark, Kongens Lyngby, Denmark

[3] Alfred Wegener Institute, Helmholtz Centre for Polar and Marine Research, Bremerhaven, Germany

[4] Climate and Environmental Physics, Physics Institute and Oeschger Center for Climate Change Research, University of Bern, Switzerland

[5] Quaternary Sciences, Department of Geology, Lund University, Sweden

3.1 Preface to Paper III

The paper presented from section 3.2 to 3.15 in this thesis is the revised version of the preprint currently available at https://doi.org/10.5194/cp-2021-155. This revised version was accepted by Climate of the Past. The "Appendix A" and the "Supplementary Information" , both accepted by the journal, are reproduced at the end of this chapter (sec. 3.13 and 3.14) to facilitate the correspondence with the numbering of figures, tables, and sections.

This work comprises the first 2 years of research I have conducted in my PhD studies. The core idea of the project is that the GICC05 revision has to be initiated from the top of the chronology, as the expected inaccuracies arise from the most recent centuries of the chronology.

Since there are many ice cores to compare, a very large amount of ice-core data needs to be visualized and analysed. The first tool needed to visualize the ice-core data is the MatchMaker GUI written and described by Rasmussen et al. 2006. I modified the GUI to include some tools to facilitate the work of timescale construction. I included the possibility of visualizing annual layers, comparing new and old sets of layers, including tephra horizons as reminders of where they should be considered for matching, and other adjustments.

The second tool needed to work on the ice-core timescale is the StratiCounter algorithm for layer recognition, written and described by Mai Winstrup (2011), to which I added a feature to provide a continuous output of probability when running the program on adjacent batches of data. As it turns out, this was not necessary for estimating the uncertainty of the timescale, but nonetheless the study was done using the modified version, hence I felt it was important to report on its use in the supplementary material of the paper.

3.2 Abstract

Ice-core timescales are vital for the understanding of past climate; hence they should be updated whenever significant amounts of new data become available. Here, the Greenland ice-core chronology GICC05 was revised for the last 3835 years by synchronizing six deep ice cores and three shallow ice cores from the central Greenland ice sheet. A new method was applied by combining automated counting of annual layers on multiple parallel proxies and manual fine-tuning. A layer-counting bias was found in all ice cores because of site-specific signal disturbances, therefore the manual comparison of all ice cores was deemed necessary to increase timescale accuracy. After examining sources of error and their correlation lengths, the uncertainty rate was quantified to be one year per century.

The new timescale is younger than GICC05 by about 13 years at 3835 years ago. The most recent 800 years are largely unaffected by the revision. Between 800 and 2000 years ago, the offset between timescales increases steadily, with the steepest offset occurring between 800 and 1100 years ago. Moreover, offset-oscillations of about 5 years around the average are observed between 2500 and 3800 years ago. The non-linear offset behavior is attributed to previous mismatches of volcanic eruptions, to the much more extensive data set available to this study, and to the finer resolution of the new ice-core ammonium matching. By analysis of the common variations of cosmogenic radionuclides, the new ice-core timescale is found to be in alignment with the IntCal20 curve.

3.3 Introduction

Paleoclimatic chronologies allow the comparison of proxy records from different geographic locations, thereby providing a fundamental tool for the understanding of the Earth's climate. In the Late Holocene, from 4.2 thousand years ago to today (Walker et al., 2012), the large amount of well-resolved data makes it possible to construct very precise and accurate timescales. Late Holocene timescales are constructed by a large variety of methods depending on the typology of the sample, from dendrochronology to radio-isotopic measurements, from tephrochronology to chemical analysis of ice cores.

Timescale methods fall into two main categories: absolute methods providing an absolute age of the sample, such as radiocarbon dating (Bronk-Ramsey, 2008), and relative or comparative methods, such as stratigraphic comparison of isochrones in ice cores (Rasmussen et al., 2008). For the case of ice-core dating in Greenland, annual-layer counting

is a privileged method for the construction of a relative sequence of events, thanks to well-resolved annual layers recognizable well into the last glacial in the chemical and optical measurements of the ice (Andersen et al., 2006).

Once the independent timescales from different geographic locations are set up and compared, it may be possible to investigate lead-lag dynamics within the broader climate system. In the Holocene, recent studies investigated the comprehensive impact of volcanic eruptions, suggesting for example a 10-year cooling in European summer temperatures (Sigl et al., 2015) or a 5-year positive North Atlantic Oscillation (NAO) (Sjolte et al., 2018), both observed after tropical eruptions. Other examples of such inter-regional comparative studies, dependent on timescale accuracy, are the study of bi-polar timing of climate changes in the last glacial (WAIS Members, 2015; Pedro et al., 2018; Svensson et al., 2020) or the relative timing of the Holocene onset over Greenland and Asia (Nakagawa et al., 2021).

3.3.1 Annual layers in Greenlandic ice cores

Ice cores from Greenland contain high-quality climatic information thanks to the steady deposition of snow and impurities and to the inclusion of air bubbles in the ice, processes which have occurred continuously since the formation of the ice sheet. The deposited snow contains a variety of chemical compounds, such as sodium, calcium, or ammonium ions, and water-insoluble particles, like dust and volcanic ashes, which may all be interpreted as proxies for climatic conditions and processes (Fuhrer et al., 1999; Rhodes et al., 2018). Moreover, the isotopic composition of the deposited snow is an important indication for temperature and moisture at the drill sites, although the link between climate and isotopes is intrinsically complex, especially on shorter timescales (Dansgaard, 1964; Johnsen et al., 1989; Laepple et al., 2018).

Some proxies follow a clear annual cycle that can be observed if the layer thickness and the analytical measurement method provide sufficient resolution. The seasonal patterns of ice-core proxies are determined by complex depositional dynamics that control the transport from the sources to the ice sheet (Gfeller et al., 2014, Whitlow et al., 1992, Beer et al., 1991, Fischer et al., 1998, Fuhrer et al., 1996). For example, sodium (Na^+) has a strong winter peak because of increased advection of marine air masses (Herron, 1982), which can be used to define the start of the ice-core layer. Relative to sodium, calcium (Ca^{2+}) peaks in the spring because of enhanced transport from terrestrial reservoirs (Whitlow et al., 1992); ammonium (NH_4^+) has a maximum in the late spring/summer because of enhanced biogenic activity in the North American continent (Fischer et al., 2015); nitrate (NO_3^-), which is also related to

biogenic processes, peaks in the summer (Herron, 1982; Röthlisberger et al., 2002). Water isotopes ($\delta^{18}O$ and δD) show a sinusoidal pattern with winter valleys and summer peaks, mainly representing temperature variations at the drill site (Jouzel et al., 1997).

The quality of the retrieved signals is highest during high-accumulation periods and especially at high-accumulation sites, since, for example, isotopes are heavily affected by diffusion (Johnsen, 1977). To correct for the isotopic diffusion, it may be necessary to apply deconvolution techniques to reconstruct the original annual layers (Vinther et al., 2006). At the Holocene onset, the accumulation rates are about double as high as in the glacial-stadial (Rasmussen et al., 2006). Furthermore, the Holocene ice roughly comprises the upper half of the central Greenland ice sheet and is not affected by ice thinning at the same level as the older, much thinner, glacial layers (Vinther et al., 2009; Gkinis et al., 2014; Gerber et al., 2021). In the Late Holocene, the isotopic signal was quite stable, an indication of a relatively constant layer record (Vinther et al., 2009).

Overall, the shape and thickness of Late Holocene layers in all ice cores is expected to be stable and well-recognizable. However, the data quality for parts of the Holocene is hampered by the brittle ice zone, which is found at depths at which high-pressure gas bubbles in the ice make the core very fragile (Neff, 2014).

3.3.2 Annual layer counting methods

Annual layers in ice cores can be counted manually, a process that has always been a challenging part of ice-core timescale reconstructions (Vinther et al., 2006; Rasmussen et al., 2006; Sigl et al., 2013; Sigl et al., 2016). Manual identification of annual layers is a time-consuming and inherently subjective task, and attempts have been made to automate the process (McGwire et al., 2008; Smith et al., 2009). StratiCounter (SC) is a software package that computes the most likely sequence of annual layers in an ice-core multi-proxy dataset (Winstrup, 2011; Winstrup et al., 2012; Winstrup, 2016).

Starting from example data provided by the user and applying a Hidden Semi-Markov Model, the algorithm learns to recognize the specific annual pattern. SC provides a layer count and a probability distribution of the recognized layer boundaries. Some initial settings determine if the program should, for example, reduce the resolution of the original data, apply some pre-processing, or give different weight to the different data series in the analysis. These requirements are both ice-core and proxy dependent.

3.3.3 Holocene stratigraphic markers

Short-term events may be used to synchronize ice cores if the corresponding horizons can be unambiguously seen in several ice cores. Volcanic eruptions constitute the most robust base for matching ice cores because they often leave a clear imprint in the ice-core signal. When available, sulfate (SO_4^{2-}) measurements are used to identify individual eruptions, because of the associated emission of sulfur compounds to the atmosphere that precipitate onto the ice sheet (Lin et al., 2021). Thanks to the acidic nature of sulfate, eruptions are also recorded as prominent peaks in the Electrical Conductivity Measurements (ECM) and in the dielectric permittivity (DEP) (Hammer, 1980; Clausen et al., 1997; Wilhelms et al., 1998; Mojtabavi et al., 2020). However, ECM and DEP volcanic peaks might be weakened or eliminated by the opposite effect of alkaline dust, hence sulfate remains the most reliable indicator of volcanic spikes (Rasmussen et al., 2008).

The identity of the volcano can be confirmed when volcanic ash layers (tephra) are found in the ice cores, and geochemically and stratigraphically matched to reference deposits from the origin site (Zielinski et al., 1994; Abbott and Davies, 2012; Bourne et al., 2015; Cook et al., 2018a). Otherwise, if the source volcano has not yet been identified, geochemical similarity of layers found in different ice cores provides evidence of synchronicity (Cook et al., 2018b, Mojtabavi et al., 2020). However, for the most part, there is no tephra associated with acidity peaks of assumed volcanic origin, and thus, for those tephra-free sections, the matching of the cores relies entirely on identification of corresponding patterns of acidity peaks.

The volcanic-eruption signal usually spans more than one year, so that one can identify the start, the maximum, and the end of the event (Clausen et al., 1997). However, the chemo-stratigraphic response to volcanic eruptions can vary between ice cores due to different depositional dynamics. The recorded shape and delay of the volcanic signal depends, for example, on the distance from the eruption site, on the balance between dry and wet deposition of sulfate, on snow redistribution, and on different noise levels at the ice-core site (Robock and Free, 1995, and references therein; Gautier et al., 2016). Therefore, it can happen that a very strong eruption signal at GRIP from e.g. an Alaskan eruption will only appear as a minor signal in the DYE-3 core, because the two drilling sites received snowfall during different meteorological situations (Clausen et al., 1997). Hence the matching cannot rely only on the position of single peaks, but must also depend on patterns of closely-spaced

eruptions. Still, the link between many historical eruptions and the corresponding ice-core acidity spikes is well-established and serves as an exact time reference (Sigl et al., 2015).

Ammonium (NH_4^+) is a proxy for biogenic activity (Fuhrer et al., 1996), and ammonium spikes have been directly linked to biomass burning events, i.e. wildfires (Fischer et al., 2015). Wildfires are also recorded in other chemical species, such as black carbon and vanillic acid (Grieman et al., 2018; Zdanowicz et al., 2018). Because of the alkaline nature of NH_4^+, the ECM will record marked dips in correspondence with ammonium spikes (Taylor et al., 1993; Rasmussen et al., 2006). Occasionally, nitrate (NO_3^-) peaks are observed to coincide with NH_4^+ spikes, but they do not provide a reliable proxy for wildfires on their own (Legrand et al., 2016). The quality of these species as a unique proxy for wildfires is debated since they are not always consistent with each other and they likely reflect different aspects of the source, the event intensity, and the trajectory to Greenland. It is not possible to find the origin of wildfires with the same certainty as for volcanic eruptions, because there is no "fingerprinting" technique for wildfires, but patterns of ammonium-rich layers can nonetheless be identified across the Greenlandic ice cores, providing an additional tool for synchronization (Rasmussen et al., 2008; Legrand et al., 2016).

Other events that serve as tie points between ice cores include variability of cosmogenic radionuclides, which are caused by solar storms or by other forms of solar variability (Muscheler et al., 2014). By measuring the co-registration of two tie-points such as the 775 CE and the 994 CE events, Sigl et al. (2015) showed that Beryllium-10 enhancements (^{10}Be) provide precise constraints of alignment between tree-ring and ice-core timescales. In the recent work by O´Hare et al. (2019), the signature of an intense solar storm was identified in ice cores, at an age of 660 BCE, which provides an added alignment point between ice cores and tree-ring timescales in the Late Holocene. As a conclusive remark, the radioactive fallout from nuclear bomb testing, which peaked in 1963, provides a reliable and very recent chronostratigraphic marker in the form of a tritium or ^{36}Cl peak, which is especially useful for shallow ice cores (Qiao et al., 2021).

3.3.4 The GICC05 timescale in the Holocene

The Greenland Ice Core Chronology 2005 (GICC05) is the most widely recognized timescale for Greenland ice-core studies (Vinther et al., 2006; Svensson et al., 2008). In the Holocene, GICC05 is based on three ice cores: the DYE-3 ice core from southern Greenland (Johnsen et al., 2001), the GRIP ice core from Summit/central Greenland (Dansgaard et al., 1993), and the NorthGRIP ice core from north-western Greenland (NGRIP members, 2004).

The ice cores were matched by recognizing common volcanic eruptions in the ECM signal, and the annual layers were manually counted using water isotopes ($\delta^{18}O$ and δD are available in overlapping sections and are equally suited for annual layer identification). In the older part of the Holocene, high-resolution impurity records were also included in the layer counting, but they were not available at the time for reconstructing the timescale for the Late Holocene (Rasmussen et al., 2006).

When the ice-core data quality was not equal between the three cores, a master chronology was produced on the best resolved record, which was then transferred to the other ice cores. Until 1813 years b2k (years before 2000 CE, same convention applied in the rest of this paper), the count was produced on isotopes from DYE-3 and deconvoluted isotopes from GRIP and NorthGRIP. From 1813 until 3835 years b2k, NorthGRIP ages were transferred from DYE-3 and GRIP, because of lacking isotope data.

In the construction of GICC05, an acidity spike attributed to the Vesuvius eruption (79 CE, Italy) was considered an exact time-marker, carrying no age uncertainty, based on a tephra deposit found in GRIP (Vinther et al., 2006; Barbante et al., 2013). Recent analysis of the NEEM-S1-2011 ice core shows that the tephra associated with the acidity peak in this core is geochemically distinct from the shards found in GRIP (Plunkett et al., 2022), and likely originates from an Alaskan eruption. Furthermore, the analysis of the original GRIP shards by Barbante et al. (2013) was criticized by Plunkett et al. as not fulfilling sufficient requirements for the attribution to Vesuvius, thus leaving the GICC05 chronology with a significant chronological weakness.

As another discussion point, Hammer (1980) and Vinther et al. (2006) attributed a prominent ECM peak in GICC05 to the massive Hekla eruption of 1104 CE. Later, Coulter et al. (2012) attempted to find confirmation in the tephra found close to this ECM peak, but neither DYE-3 nor GRIP or NorthGRIP supported the identification with Hekla. Recently, Guillet et al. (2020) proposed that the signal represents a cluster of eruptions, one of them possibly originating from Mount Asama, Japan.

Recent comparisons between Greenlandic ice cores and ^{14}C chronologies have exposed other issues with the layer count in selected sections of the timescale (Baillie,2008, 2010; Lohne et al., 2013; Torbenson et al., 2015; Muscheler et al., 2014; Sigl et al., 2015; Adolphi & Muscheler, 2016; Adolphi et al., 2018; McAneney & Baillie, 2019). In this work we aim to expand on the causes of the GICC05 mismatches and to investigate other recurring problems to be resolved, such as, for example, the uncertainty question of ice-core timescales.

A special mention for the Greenland timescale has to be made for the GISP2 ice core, drilled at Summit in the vicinity of the GRIP site. Meese et al. (1997) constructed a timescale for this ice core that remained a widely-used standard until GICC05 was released. Annual-layer counting was performed manually using a combination of visual stratigraphy, ECM, dust laser scattering, isotopes, and ion chemistry. A number of tephra samples was collected in the Holocene ice, confirming the identity of, among others, the Laki eruption of 1783 CE (Fiacco et al., 1994), the Samalas eruption of 1257 CE (Palais et al., 1992; Lavigne et al., 2013) , and the Eldjá eruption of 939 CE (Zielinski et al., 1995). Of these three eruptions, only the first two have an independent historical estimate of the age, the Samalas eruption being dated by indirect evidence of its occurrence in 1257 CE (Vidal et al., 2016). In addition, authors of GISP2 also used Vesuvius to constrain the timescale. The agreement with GICC05 has been estimated as adequate until 40 ka b2k (Svensson et al., 2008; Seierstad et al., 2014). However, over the period between 2.5 and 8 ka b2k, the GISP2 timescale is between 5 and 40 years younger than GICC05, which is outside the uncertainty limit of GICC05.

3.3.4.1 *Uncertainty estimates of GICC05 in the Holocene*

The uncertainty associated with a timescale is essential for the correct interpretation of the climatic data. The most important source of uncertainty in GICC05 was considered to be the misinterpretation of annual layers by the observers. By defining uncertain layers to be features in the ice core that could neither be dismissed nor confirmed (Vinther et al., 2006), the GICC05 uncertainty was estimated from the Maximum Counting Error (MCE), corresponding to half the sum of the uncertain layers accumulated until the corresponding age (Rasmussen et al., 2006). Thus, each uncertain layer contributes with ½ ± ½ years to the age scale, whereas certain layers contribute 1 ± 0 years.

A fundamental choice in uncertainty estimation is whether one assumes uncorrelated errors. In case the errors are uncorrelated, they should be summed in quadrature. If, on the other hand, all errors are fully correlated, then the total uncertainty is a linear sum of the individual errors. Acknowledging that for the case of ice cores the errors are likely neither fully correlated nor uncorrelated, the authors of GICC05 opted for a conservative approach and summed the MCE linearly, but in turn did not include contributions from other sources than misinterpretation of annual layers. The authors also observed that the count between 1362 CE (Öræfajökull, Iceland) and 79 CE (Vesuvius) was correct within one year, corresponding to ~0.1% of the interval. As this number was smaller than the MCE it was considered

negligible. Hence, the MCE does not consider the bias one can introduce because of e.g. misleading assumptions on the tie points or abruptly changing layer shapes.
In summary, GICC05 was considered exact for the part younger than the eruption peak previously assigned to Vesuvius, because many well-known historical eruptions tied the chronology together. Therefore, the published uncertainty until about 2.7 ka b2k is only 2 years, increasing to 5 years at 3.9 ka b2k.

3.3.5 The NS1-2011 timescale

A more recent Greenland ice-core timescale for the past 2500 years was based on new bipolar tie-points, such as volcanic tephra and solar storm data, and on new high-resolution multi-parameter impurity records (Sigl et al., 2015). This timescale will be referred to as the NS1-2011 chronology, as it was designed on the NEEM-2011-S1 ice core by lifting the Vesuvius and Hekla constraints and replacing them with newer historical evidence about volcanic tie-points at 536, 626, and 939 CE and about a solar proton event at 775 CE. StratiCounter was employed to count annual layers on the NEEM-2011-S1 shallow core and on the NEEM main/deep ice core. These ice cores were matched to NorthGRIP via numerous volcanic tie-points to allow for the comparison to GICC05. Moreover, a manual count on the NEEM main core was conducted until 500 BCE. For most of the timescale, SC was run in constrained mode using volcanic tie-points of known age. The earliest exact time marker applied for the chronology is the 536 CE eruption, prominent in the acidity and sulfate records. For ice older than 536 CE, the authors analyzed detailed records of historical, literary, and climatic evidence and found that the timescale aligns with most of the validation points, providing statistical tests to evaluate the significance of the result. Moreover, the timescale was compared to the Antarctic timescale WD2014 (Sigl et al., 2016) and to tree ring records to verify the overall good agreement of Greenland with other climatic archives. The NS1-2011 offset to GICC05 at around 79 CE was quantified to be 8 years and the age of the layer formerly attributed to Vesuvius was changed to 87/88 CE.
The uncertainty estimate of the NS1-2011 timescale was based on the SC probability estimate. The age of volcanic eruptions is reported as a weighted average of the SC-counts in NEEM-2011-S1, the NEEM main core, and WDC (West Antarctic Ice Sheet Divide Ice Core). For example, the age of the Indonesian Samalas eruption (Vidal et al., 2016) is given as 1258 ± 2 years CE. Moreover, the comparison between the manual and the automated count in NEEM amounted to a difference of 1 year over the 500-year time interval. The timescale was estimated to have a 5 year uncertainty at 2500 years b2k.

3.3.6 The need for a revised and unified Greenland ice-core chronology in the Holocene

Given the known inconsistencies between existing Greenland Holocene timescales, we find it timely to revise the GICC05 timescale to provide a new unified ice-core chronology that includes most available data from Greenlandic deep ice cores. Our dataset includes, amongst others, the new high-resolution dataset from the recent EastGRIP ice core (Mojtabavi et al., 2020; Erhardt et al., In Prep.: see ice-core data availability section at the end). Our method relies on parallel dating of multiple cores with well-resolved annual data back to 3835 years b2k, a period which ensures data coverage from at least four ice cores until the brittle ice zone starts affecting the data quality.

SC cannot presently be applied to multiple ice cores together. Hence, SC cannot at this time provide a fully automated multi-core timescale. Nevertheless, SC can be applied separately to each ice core, on their own depth scale, after which the resulting counts can be combined between cores. Furthermore, SC cannot be used to assess whether the ice-core signal is affected by disturbances that might have altered its shape, such as snow redistribution, melt layers, and multiple seasonal peaks in the proxies (Mosley-Thompson et al., 2001; Westhoff et al., 2021; Geng et al., 2014). These observations rely on a comparison of records from several ice cores. Hence, an extensive manual effort is still required to identify problematic layers and to bring a multi-ice-core timescale to a final state.

We find the MCE unsuited to apply to our timescale, since by nature it is a single-record uncertainty estimate that does not capture the complexity of the multi-core chronology: an uncertain layer in one core may be certain or absent in another, and thus a comparison of the two can solve many chronological issues. Based on the combination of statistical estimates and empirical observation, we propose a simple formula to provide the new timescale, named GICC21, with a robust, consistent, and user-friendly uncertainty estimation.

3.4 Data

Data from six deep and three shallow ice cores provide the basis for GICC21; details about each drilling site are given in Table 3.1. Resolution and quality of the data reflect not only the local climatic conditions but also the state of the technology at the time of ice-core

retrieval and measurement. Moreover, data is only available, or of sufficient resolution and quality for layer counting, at selected ice-core depth ranges (

Figure 3.1b).

Table 3.1 Specifications about the ice cores included in this study.

Ice Core	Elevation, m	Lat., °N	Long., °W	Mean Air Temp., °C	Accumulation, m_{ice} /year	Length, m	Years of Drilling	Brittle ice zone, m
EastGRIP	2458	75.38	36.00	-29‡	0.12 [e]	2150	2017–2019 (ongoing)	650-950[l]
NEEM	2479	77.25	51.09	-29 [a]	0.22[a]	2540	2008–2012[b]	609-1281[k]
NEEM-2011-S1	2450	77.45	51.06	-21[c]	0.22[d]	410*	2011[d]	
NorthGRIP1	2917	75.10	42.32	-32 [f]	0.19 [f]	1351	1996–1997 [g]	790-1200[f]
NorthGRIP2	2921	75.10	42.32	-32 [f]	0.19 [f]	3085	1997–2004[g]	790-1200[f]
GRIP	3230	72.58	37.64	-32 [f]	0.23[f]	3027	1989–1992[h]	800-1300[f]
DYE-3	2480	65.18	43.83	-20 [f]	0.56[i]	2037	1979–1981[j]	800-1200[f]
DYE-3 4B	2491	65.17	43.93	-20†	0.535[f]	174*	1983[j]	
DYE-3 18C	2620	65.03	44.39	-20†	0.44[f]	113*	1984[j]	

*Shallow ice cores. [a] (NEEM community members, 2013) [b](Rasmussen et al., 2013) [c](Faïn et al., 2014) [d](Sigl et al., 2013) [e](Gerber et al., 2021) [f](Vinther et al., 2010) [g](Dahl-Jensen et al., 2002) [h](Johnsen et al., 1992) [i](Vinther et al., 2006) [j](Clausen & Hammer, 1988) [k](Warming et al., 2013) [l](Westhoff et al., 2021) ‡estimated from PROMICE data (Ahlstrøm et al., 2008) †Assumed same as DYE-3

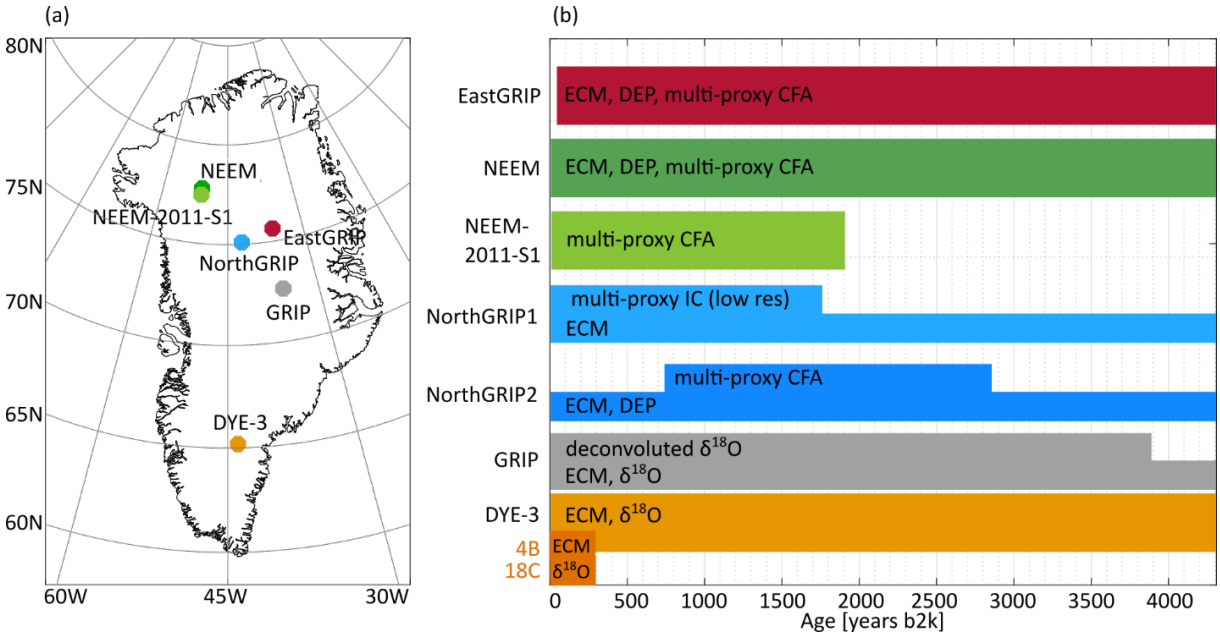

Figure 3.1 Overview of the data used for this study.
(a) Geographic locations of the ice cores, for which Table 3.1 contains the site specifications. (b) The colored patches summarize the available datasets used for annual-layer counting (e.g. continuous flow analysis, CFA) and inter-core matching (e.g. ECM), plotted on their approximate age-range.

3.4.1 EastGRIP

The East GReenland Ice-core Project (EastGRIP) is an ongoing drilling effort which in the latest field season (2019) reached a depth of about 2150 m. The ECM and DEP measurements were made in the field camp on 1.65 m long pieces of ice (Mojtabavi et al., 2020). Chemistry records of aerosol impurities were measured in Bern using the proven Continuous Flow Analysis (CFA) Setup (Kaufmann et al. 2008) coupled to an ICP-TOFMS (Erhardt et al., 2019). The chemistry data include a vast range of different species measured continuously at high sampling resolution (1 mm), with a resolving power of about 1 cm, making this dataset among the most detailed available. However, the annual accumulation rate at this site is also the lowest of the records included (Table 3.1). A detailed description of the CFA setup and the data used in this study can be found in Erhardt et al. (in prep, see Ice-core data availability section). For counting layers, we used Na, Ca, NH_4^+, and NO_3^- concentrations from 13.82 to 460.30 m depth. Water isotope records were also measured continuously but, due to the low annual accumulation, the annual signal does not survive diffusion in the firn, and therefore cannot be used for annual layer identification.

3.4.2 NEEM and NEEM-2011-S1

The North Greenland Eemian Ice Drilling (NEEM) was completed in 2012 (NEEM community members, 2013). ECM and DEP were measured in the field at 1 mm resolution (Rasmussen et al., 2013). Impurity records, measured by an international team coordinated by the University of Bern, were as well obtained in the field and have a depth resolution similar to the EastGRIP data set (Kaufmann et al., 2008) but, due to brittle ice, suffer from increasingly wide data gaps that make annual-layer identification difficult below around 750 m. Hence, we used ECM, Na^+, Ca^{2+}, NH_4^+, and NO_3^- for layer counting between 7.6 m and 727.3 m depth. A detailed description of the NEEM CFA measurements and the dataset can be found in Erhardt et al. (2021). An additional CFA-dataset was measured at DRI by Sigl et al. (2015) and provides additional data from 399 m to 500m. This dataset was not used for the SC count, but the quality of the layer count was later verified considering this additional data. Moreover, the Sigl et al. (2015) dataset contains black carbon (BC), which we used to consolidate the ammonium match.

The NEEM-2011-S1 ice core is a 410 m shallow core that was drilled about 100 m away from the NEEM main core (Sigl et al., 2013). This core reaches back until the volcanic layer

attributed in GICC05 to the Vesuvius eruption (79 CE). Chemistry data was measured at DRI for the entire core length, but the ECM of the shallow core was not measured, hence we relied on non-sea-salt sulfate (nss-S) for volcanic matching (Sigl et al., 2013). The species Na, nss-Ca, nss-Na, NH_4^+, NO_3^-, and BC were used for layer counting between 6.1 m and 410.8 m, in order to achieve a similar SC output as in Sigl et al. (2015). BC was also used to consolidate the ammonium match.

3.4.3 NorthGRIP

The NorthGRIP drilling was completed in 2004 and is composed of two ice cores: NorthGRIP1 and NorthGRIP2 (Dahl-Jensen et al., 2002). For NorthGRIP1, ECM data are available until the core ends, at about 1351 m, and discrete chemical measurements (5 cm resolution) are available uninterruptedly until 350 m and in short fragments below this (Vinther et al., 2006). Despite the resolution of only 4-5 samples per year, the annual layer pattern is clearly recognizable, and we used ECM, Na^+, Ca^{2+}, NH_4^+, NO_3^-, Cl^-, Mg^{2+}, SO_4^{2-}, and $\delta^{18}O$ for layer counting between 9.9 m and 349.1 m depth.

For the upper part (159-582 m) of NorthGRIP2, a continuous chemistry dataset was later measured at the Desert Research Institute (DRI) with a resolution of 1 cm (McConnell et al., 2018). The dataset includes a vast range of species, of which we used Na, Ca, NH_4^+, and NO_3^- for layer counting between 159.6 m to 582.4 m depth (approximately from 730 to 3200 years b2k). For volcanic matching, we mainly used a combination of ECM and DEP signals. This new record constitutes an important addition to the chronology, since it allows coverage of the NorthGRIP site until almost the end of our timescale.

3.4.4 GRIP

The drilling of the GRIP ice core (or Summit ice core) was completed in 1992 (Johnsen et al., 1992). Only ECM and isotope data are available for counting layers in this core in the late Holocene. The annual signal in the isotope data (2.5 cm resolution) is moderately affected by diffusion, but deconvolution restores a very strong sinusoidal pattern that can be used for annual counting (Johnsen et al., 2000; Vinther et al., 2003). ECM also shows an annual signal, analogous to GISP2, with a summer peak caused by enhanced acid deposition (Meese et al., 1997). Hence, we used ECM (1 mm resolution), $\delta^{18}O$, and deconvoluted $\delta^{18}O$ to count annual layers between 5.3 m and 770.1 m depth. The deconvolution is sensitive both to melt layers and to unusually wide layers. The first contain sharp gradients which create artefacts in the data, typically resulting in a series of high-amplitude oscillations that

do not correspond to real annual layers, while the second result in spurious low-amplitude oscillations. The width of these perturbations is usually 2-5 years, and they are not difficult to spot for a trained investigator (Supplementary Information Figure 3.10).

3.4.5 DYE-3

The oldest ice core in this chronology is DYE-3 whose drilling was completed in 1981 (Clausen & Hammer, 1988). The data available to our study are mainly ECM (~7mm resolution) and water isotopes (1 cm resolution) (Langway et al., 1985). The isotope record resolves the annual layers very well thanks to the high accumulation rate which provides wide layers that are safe from diffusion, and is used for counting from 0.9 to 1271.7 m depth. The ECM signal also appears to have an annual pattern (Neftel et al., 1985), hence we also used ECM to count layers from 136 m to 1271.7 m. Because of lacking setup in the first year of drilling, the ECM measurements only start after 136 m. Therefore, to construct the top chronology of DYE-3, we included two shallow cores named 4B and 18C located close to the deep core site, for which ECM and water isotopes were available for counting (Vinther et al., 2010).

3.5 Methods

The first objective of this study is the construction of a common chronology for several ice cores with data suitable for annual layer counting.
Our timescale construction method relies on three main steps:

- Automated annual-layer boundary identification using SC;
- Ice-core matching using volcanic and ammonium tie-points;
- Multi-core layer comparison by multiple observers (called fine-tuning).

We subsequently perform a study of the uncertainty of the resulting timescale.

3.5.1 The raw output: counting annual layers on each ice core with StratiCounter

To avoid the lengthy and likely somewhat inconsistent process of manual layer counting, GICC21 was based on a multi-core set of annual layers identified on each ice core by SC, which also returns an uncertainty distribution of the number of layers in each individual ice core. SC has better performances with multiple proxies, but including more than four species did not prove to make a substantial difference for the final result, because some species are

not independent of each other (e.g. those dominated by minerals with dust as primary source) and some have similar seasonal patterns. As training data, SC requires a set of annual layers manually placed by the user. We chose to place the annual layer mark on the annual sodium maximum as the best indicator of the start of a new year, except for ice cores without impurity data, where we chose the isotope annual minimum, since the two methods are roughly equivalent (Supplementary Information Figure 3.9).

Measurement gaps should be minimized using all available data to obtain an accurate layer count. Since DEP is generally measured on the full ice core, and ECM is measured on the first longitudinal cut of the core, they are both less affected by ice-core breaks than the subsequent measurements made on smaller samples or obtained from a continuous stream of melted sample. So, although the yearly pattern in the ECM signal is not always discernible and cannot be the basis of reliable annual layer identification, including it proved useful for ice cores with many small gaps, like NEEM and EastGRIP. In addition, the ECM records of DYE-3 and, to some degree, GRIP exhibit an annual ECM cycle, which helps improve the SC result. When data gaps cannot be avoided, SC makes a probabilistic estimate of the layer count considering the neighboring data.

To facilitate the pattern recognition process by SC, the datasets were preprocessed using the appropriate settings for each ice core (see Straticounter Supplement about pre-processing). The best pre-processing settings were established after testing if SC was able to accurately estimate the layers between the Laki and Samalas eruptions, within a tolerance of a few years. Elemental and ionic concentrations were treated identically, as the differences should not matter for layer identification. Even though it is possible to constrain SC to historical age markers, we chose to run SC in unconstrained mode to be able to quantify any possible biases of the algorithm. In order to account for changes in layer thickness or data quality in each ice core, a variant of SC was implemented to count on independent stretches of data (more details can be found in the Straticounter Supplement).

We observed that SC tends to under-count over data gaps, especially within longer gaps. This issue was fixed *a posteriori* by evaluating the average layer thickness around each gap and inserting the missing layers. However, too large data gaps make the timescale inaccurate. Around 3.8 ka b2k, the length of data gaps in NEEM and EastGRIP increases as both ice cores enter the brittle-ice zone. Around the same time, the effects of isotopic diffusion in GRIP gradually make recognition of the annual signal difficult, and the high-resolution

sampling was discontinued (Vinther et al., 2006). Therefore, we stopped the timescale revision at 3835 years b2k in order to abide to the multi-core data requirement.

3.5.2 Ice-core matching using synchronous events

Ice cores were matched to each other by finding patterns of assumed synchronous events that will be referred to as tie points. Previously published ice-core matches (Rasmussen et al., 2013; Seierstad et al., 2014; Sigl et al., 2015; Mojtabavi et al., 2020) were extended to all cores considering the new data sets. The manual match is facilitated using a MATLAB GUI called Matchmaker that allows for the insertion of visual bars to place stratigraphic markers on top of the data and to align data according to these markers (Rasmussen et al., 2008), of which an example is given in Figure 3.2.

The Laki eruption that happened between June 1783 and February 1784 CE is easily detected in all ice cores thanks to a pronounced acidity spike and a corresponding tephra deposit (Clausen & Hammer, 1988; Fiacco et al., 1994). Hence, we use Laki as a reference datum to calculate relative ages for the rest of the timescale. For DYE-3, however, we tie the timescale to the Öræfajökull eruption of 1362 CE, because the DYE-3 ECM measurements start below the Laki layer. Although the tephra identification of this eruption is elusive (Coulter et al., 2012), the associated peak is visible in DYE-3 and hence constitutes the most recent available candidate to tie DYE-3 to the other ice cores. Furthermore, the top chronology of DYE-3 was confirmed by comparing to two nearby shallow cores that record Laki in their ECM signal (see also the section 3.6 provided in the Supplementary Information about the DYE-3 top chronology).

When reporting historical events, we find it most convenient to use CE/BCE years (avoiding year 0). When reporting about the ice-core timescale, we will use years b2k. The conversion between the age units is easily done for rounded years:

$$Y_{CE} = 2000 - Y_{b2k}\ ;\ Y_{BCE} = 2000 - Y_{b2k} - 1$$

More details about the age conversion, similar to the one explained by McConnell et al. (2020), are provided in the Timescale Supplement. Since years b2k increase going back in time, we remark that decimal ages correspond to the inverted month order. However, we note that it may not be possible to accurately perform sub-annual dating of events, since accumulation throughout the year is not constant.

3.5.2.1 *Ammonium matching patterns*

A chemical species that shows good potential for inter-ice-core matching is ammonium, since it is regarded as a good tracer of North-American wildfires. The lifetime of ammonium in the atmosphere is very short, on the order of days, so the origin of the signal is rarely further away than Canada (Legrand et al., 2016). However, the shape of the ammonium peaks might vary across the ice sheet because of different trajectories from the source. Rasmussen et al. (2008) report on using a number of ammonium tie points in the transfer of GICC05 from NorthGRIP to GRIP and GISP2 in the glacial. Although Legrand et al. (2016) provided a 200-year long ammonium match between NEEM and GRIP, they only identify 9 possible historical events that could have originated the peaks.

To test the applicability of the ammonium matching, we examined ammonium data between sections of closely spaced volcanic eruptions and found many cases where ammonium, confirmed by black carbon, had a clear correspondence across ice cores (some examples are shown in Figure 3.2). We used black carbon data of NEEM and NEEM-2011-S1, reaching until 2500 ka b2k, to select the ammonium spikes best suited for matching, since this provides an additional criterion for the attribution of a peak to a wildfire event (Sigl et al., 2015; Legrand et al., 2016). In some cases, we observe a strong spatial variability, thus we confirmed that the ammonium matching can only have a supporting role of the volcanic match. Ammonium spikes neutralize the ECM signal, producing minima in the ECM (Robock & Free, 1995; Taylor et al., 1992). Therefore, we inverted and log-transformed the ECM record and used it as an ammonium substitute, whenever NH_4^+ was lacking for an ice core.

Beyond 2500 years b2k, patterns of NH_4^+ spikes were used to supplement the volcanic match, especially when volcanic tie points were widely spaced by many decades (Supplementary Information Figure 3.11). Here, we only select ammonium tie points that left an imprint in the ECM signal of the corresponding ice core. Overall, ammonium peaks constitute 63% of our 290 tie points over the last 3835 years, the proportion being higher in the region beyond 2500 years b2k (70%). The reason of the higher number of ammonium tie points is that we use patterns instead of single peaks. The frequency of the ammonium spikes is on the order of one in 20 years, so that, by including ammonium, we have effectively increased the resolution of the multi-core match with respect to a purely volcanic match, this latter having only 35 years average resolution.

3.5.3 Requirements for the manual fine-tuning procedure

The number of layers between synchronous tie points must be the same across ice cores. Hence, we assessed the quality of the SC output by evaluating the number of layers counted by the algorithm between historically known volcanic eruptions. Even after having chosen the best settings for SC, we observed a general tendency of under-counting in some ice cores and over-counting in others (Table 3.2).

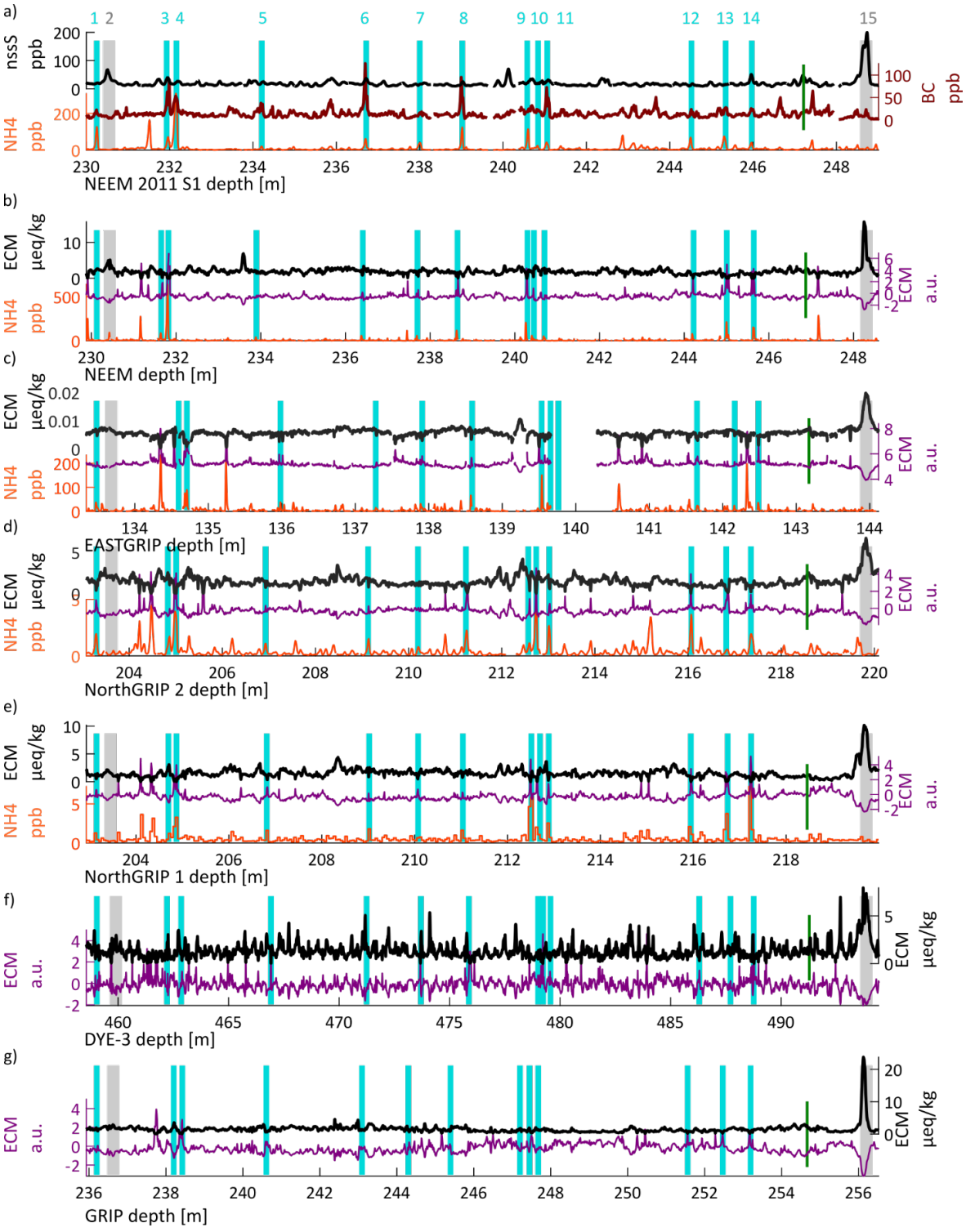

Figure 3.2 Tie points of GICC21 between two eruptions, which are highlighted by the grey vertical bars no. 2 and no. 15 (Eldjá, 939 CE).
Volcanic proxies are shown in black and the inverted log-ECM for each ice core is shown in purple. Ammonium (where available) is shown in orange and the turquoise bars highlight the patterns of ammonium that were used as supporting tie points for GICC21. a) NEEM-2011-S1: The black-carbon peaks (brown) support the choice of this subset of ammonium tie points. b-e) The co-occurrence of ammonium peaks and peaks in the log-inverted ECM provides another criterion for tie-point selection. f-g) For DYE-3 and GRIP, lack of ammonium data means that we can only use the log-inverted ECM to provide indication for the tie-points, of which nr. 3, 4, 5, 6, 11, 12, 14 are best recognizable. The green bar between 14 and 15 highlights the very subtle ECM peak associated to the Tianchi tephra (Sun et al. 2014).

These fluctuations in the layer count across ice cores are a result of the algorithm being run without age constraints, which was considered to be appropriate for using the algorithm in older sections of data, where no age constraints are known. We conclude that, although SC correctly identifies almost all annual layers, it fails to assign a sufficiently high probability to some of the thin or otherwise unusual annual
layers in each ice core, which are thereby not counted. Also, it assigns an excessive probability to other layers, which upon closer inspection cannot be confirmed as annual layers.

The cause of the under-count may be related not only to data gaps but also to partially wind-eroded layers of snow, to unusual impurity loading, or to other site-specific perturbances. In the case of DYE-3, the high accumulation makes it unlikely to miss layers in the count but, in turn, gives a higher risk of multiple isotope oscillations within one year (Supplementary Information Figure 3.12), leaving more opportunities for an over-count of the layers, which could also result from the relatively high occurrence of melt layers in this ice core. Therefore, we resort to a manual processing of the timescale, which in the following we will refer to as "fine-tuning".

We remark that our fine-tuning is not in contradiction with SC, since the algorithm attempts to derive the best layers based on the available data of each single ice core. The SC raw layers are accompanied by a probability distribution which represents the likelihood of the placement of each single layer. The fine-tuning was guided by observing where the likelihood of the layer placement is most unsure, since the SC uncertainty increases locally where the annual-layer detection quality is low. Here, the 95%-percentiles of the probability distribution register a 1-year "jump" that can be used to detect the layers that SC deemed to be most uncertain. On the other hand, we also identified the placement of "ghost layers"

where the SC-assigned probability was just below the threshold required for SC to assign an annual layer, and which may be included in the fine-tuned timescale.

The fine-tuning is performed by comparing all ice cores in parallel and using an iterative protocol. To ensure reproducibility, we adopted a ruleset to the fine-tuning process: we added layers in gaps according to the local layer thickness; we removed low-probability layers that conflicted between parallel cores; we upgraded ghost layers to full annual layers when indicated by parallel-core comparison. Some examples of how the fine-tuning was done can be found in Supplementary Information Figure 3.13.

Table 3.2 Evaluation of the SC bias of each ice core in the timescale sections constrained by historical evidence on eruption ages. The eruptions chosen for the overview were all, except for one, Icelandic: Laki (1783 CE), Bárðarbunga (1477 CE), Oræfajökull (1367 CE), and Samalas (1258 CE, Indonesia, considering a 1-year depositional delay). Within each interval, the number of expected layer boundaries is indicated by N. For each ice core, the difference from the raw SC-count indicates the amount and direction of bias. A positive value means that layers had to be added in order to reach the expected N, while a negative value means that they had to be removed. The longest interval (Laki-Samalas) shows the total layer-modifications required by each ice core. The values indicate that the 'CFA-cores' (EastGRIP, NEEM, NEEM-2011-S1) are mostly under-counted, partly because of measurement gaps, while the 'GICC05-cores' (NorthGRIP1, GRIP, DYE-3) were mostly in need of removing layers. This evaluation of bias is what eventually justifies the fine-tuning process over a purely statistical combination of SC results.

					Difference from the raw SC-count					
Event	Age [b2k]	Event	Age [b2k]	N	EastGRIP	NEEM	NorthGRIP1	NEEM-2011-S1	GRIP	DYE-3
Laki	216.5	Bárða.	522.8	306	8	7	-4	-1	-1	-3
Bárða.	522.8	Oræf.	637.3	115	0	3	-1	3	0	0
Oræf.	637.3	Samal.	741.1	104	2	0	2	0	1	-2
Laki	216.5	Samal.	741.1	525	10	10	-3	2	0	-5
	Of which layers added in gaps				2	5	0	2	0	0

Minor similarities between the records, such as minor ECM or NH_4^+ features, $\delta^{18}O$ patterns, and in some cases similar peak-shape sequences in Na^+ or Ca^{2+} for geographically-close ice cores, were used to support or reject changes in the layer count. As a consequence, some tie-points had to be re-examined because of now-apparent misalignments, and the fine-tuning was repeated to ensure consistency between the ice cores.

As a further step, two to three observers were engaged in detailed review of each section of the timescale aiming to reduce the impact of potential confirmation bias by each investigator. Whenever unanimity was lacking, the main observer (Sinnl) examined the different opinions to propose a final solution, which was then accepted or rejected again. In the end, unanimity was reached in all sections. Moreover, no previous knowledge about age was initially used

to fine-tune the timescale, except for Laki and Oræfajökull. Later, the historical part of the timescale (until Samalas) was verified with knowledge about the ages of some eruptions, finding that the fine-tuned layer count had already reached very accurate ages. Finally, we tested the correlation between DYE-3 and GRIP isotopes in the top 400 years and found an improvement of 17 % with respect to GICC05 (see Supplementary Information Table 3.4), which we take as an indication of the fine-tuning procedure reaching accurate results in the top of the timescale.

3.5.4 Uncertainty of the GICC21 chronology

An important part of our objectives for this study is to provide a simple yet empirically justified estimation of the uncertainty associated with the GICC21 timescale. Uncertainties in the layer count arise from two main sources: data issues and misinterpretation of layers (Vinther et al., 2006). In our study, data gaps are a prevailing issue because the ends of each ice-core piece are trimmed to prevent contamination during CFA measurements. This, combined with removal of small pieces around core-breaks from the drilling process, causes frequent but brief interruptions in the records. On the other hand, the misinterpretation of layers is largely accounted for by the fine-tuning of multiple parallel ice-core records.

Many factors increase the complexity of the uncertainty estimation for our new ice core timescale. We find ourselves in a mixed scenario between automated counting by SC, an algorithm that provides its own probability estimates, and our manual intervention by fine-tuning. Moreover, we have to account for possible correlations between errors, at least within a certain correlation length. A data-based error can be caused, as mentioned, by measurement gaps or also by short-term accumulation changes, unsure tie-point placement (i.e. a marker placed differently across ice cores), or a disturbed layer pattern. These errors might influence the local distribution of layers, at least within neighboring tie-points, but are very likely unrelated to errors arising elsewhere in the timescale.

Because of transport and deposition dynamics, the volcanic signals in the ice cores are affected by delays, which we quantify to be within 1 year after the event started (Robock and Free, 1995). Furthermore, we estimate that an additional contribution to the uncertainty of up to 1 year originates from possible variations in the precise position of annual layer markers relative to the tie points. We use the linear sum of these contributions as a conservative minimum uncertainty for our timescale: although some tie points are very certain because of tephra and historical reference, these represent a minority in the timescale. Moreover, any layer could have been placed too early or too late so that, although the number

of layers between tie points is correct, the actual age at any given depth is ±1 year uncertain because of the misplacement, even though the error might get re-absorbed later on.

Until the Samalas eruption (742 years b2k), the fine-tuning is constrained by well-established historical evidence on volcanic eruptions. Therefore, for the youngest part of the timescale, the uncertainty is quantified as a constant value of 2 years even though it is likely smaller near good tie points. For the rest of the timescale, we argue that the uncertainty is never below 2 years because of the aforementioned effects, and that it also increases with depth.

For the older part of the timescale, we quantified a time-dependent uncertainty based on the SC uncertainty and on the information from the fine-tuning. SC provides a probability distribution of the likely layer count between age markers for each of the ice cores, which may be averaged by a convolution. Without fine tuning, the convolution's width, which is strongly depth/age dependent because of data quality and coverage, would be a suitable candidate for the uncertainty. As described in Sec. 3.5.3 , the SC probabilities need, in any case, to be calibrated for the gap undercount, in order to reduce the width of the convolution. After correcting for the gap bias, the maximum likelihood layer number derived from the SC-convolution is expected to be closer to the fine-tuned layer count, however we observe that SC is misinterpreting some layers. We believe that fine-tuning improves the timescale, hence we regard the discrepancy between the SC result (corrected for the gap bias) and the fine-tuned result to be a conservative estimate of the age uncertainty arising from layer interpretation and data issues.

To estimate the correlation length of the uncertainties, we observed that a tie point is typically found once every 20 years. Because a layer-identification error is not likely to affect sections separated by several tie points, we find it reasonable to assume that, beyond 100 layers, errors in the fine-tuning are uncorrelated. Conversely, because the number of years between tie points must match, errors in layer identification are likely correlated over shorter intervals.

We compared the SC output in sections of 100 fine-tuned years, at continuous intervals covering the entire study period older than Samalas. In each section, we performed a SC run for every ice core, acquiring the independent probability distribution of the layer count, for which plots can be found in Supplementary Information Figure 3.14. We manually added layers in the data gaps, mostly found in EastGRIP, NEEM, and NEEM-2011-S1 (Straticounter Supplement). The ice-core distributions were convolved to provide the multi-

core average and a Gaussian curve was fitted to the convolution to obtain a mean and a standard deviation. By subtracting these means from the expected value of 100 years, we obtain the values we call δt_i^{SC} (Figure 3.3a), where i indicates the century.

The average of all δt_i^{SC} is -0.70 ± 0.04 years/century (average of absolute values: 0.84 ± 0.04 years/century; all values are reported in the Straticounter Supplement). The negative average indicates a bias towards under-counting by SC, probably related to disturbances in the layer pattern and leftover gap undercount. However, this bias appears to be reabsorbed after 2500 years, where more balanced values around 0 appear in the dataset of Figure 3.3a. This more balanced StratiCounter bias is not related to any particular horizon in the data availability and hence we exclude this effect to be caused by some lacking data. At least for the part of GICC21 exceeding NS1-2011, we can say that the effects of over- and under-counting by SC balance out, which could be a consequence of our manual gap intervention or our fine-tuning process.

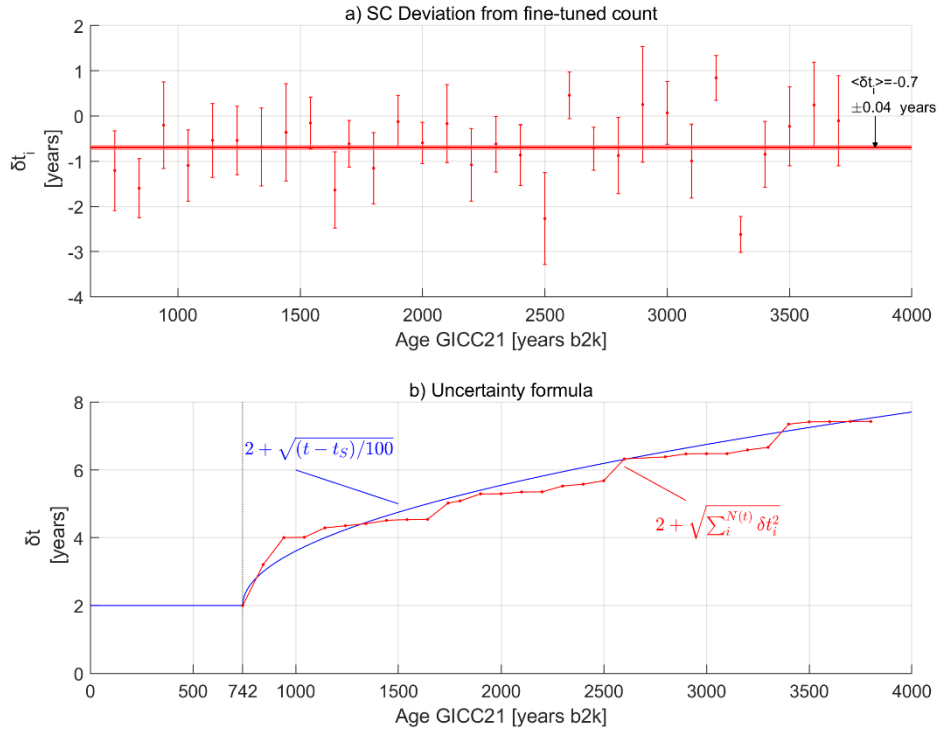

Figure 3.3 Empirical uncertainty estimation.
(a) Deviation of the gap-corrected convolutions from the expected value of 100 years. Error bars indicate the ±σ of each convolution. (b) The sum in quadrature of the measured deviations is well reproduced by our uncertainty formula.

The fine-tuning process leads to an added uncertainty, which is difficult to quantify independently, but very likely smaller than δt_i^{SC}, since we believe that the fine-tuning solves problems arising from single-core layer identification, and thus brings us closer to the true

age. Still, based on the values obtained above, we suggest a conservative empirical uncertainty of 1 year/century.

On the base of our tests, we hypothesize that our uncertainty can be represented by the following empirical formula, where the uncertainty between Samalas (t_S = 1258 CE = 742 years b2k) and any older age *t* will have an absolute uncertainty of:

$$\delta t(t\ ;\ t > t_S) = 2 + \sqrt{\frac{t - t_S}{100}}\ \text{Years} \qquad (1)$$

This formula is composed by a constant term of 2 years, which we have previously set as a conservative, lower boundary to our uncertainty, and a time-dependent term. Since we have argued that the century-errors are uncorrelated, we apply a quadrature sum to evaluate the accumulated uncertainty over time: $\delta t(t_i) = 2 + \sqrt{(1)^2 + (1)^2 + \ldots + (1)^2} = 2 + \sqrt{N_{centuries}(1)^2}$. For convenience, we hypothesize that the formula can be made continuous, obtaining equation (1), which compares well to our measured uncertainties and should be interpreted as 1σ of the GICC21 ages (Figure 3.3b). In the Supplementary Information sec. 3.14.2, we also provide an alternative demonstration of the correlation length.

3.6 The timescale offset curve

We now present a comparison between the new GICC21 timescale and the existing ice-core chronologies GICC05 (Vinther et al., 2006), GISP2 (Meese et al., 1997), DRI_NGRIP2 (McConnell et al., 2018) and NS1-2011 (Sigl et al., 2015), with the aim of investigating any dating offsets (Figure 3.4a).

To calculate the GICC21 ages at reported GICC05 depths and infer the correct offset, we linearly interpolated the GICC21-ages on the GICC05-layers of DYE-3, GRIP, and NorthGRIP1 (Vinther et al., 2006). The published volcanic matches of EastGRIP to NorthGRIP (Mojtabavi et al., 2020) and of NEEM to NorthGRIP (Rasmussen et al., 2013) allow us to find the GICC21-ages for these two cores at the published tie-points. The timescale offset of each individual ice core from GICC05 was averaged to obtain an overall transfer function of GICC21 from GICC05. The transfer function can be used to translate any age previously matched to GICC05 to the new revised GICC21 ages (provided in Timescale Supplement, see sec. 3.13 for more details on the transfer curve).

In Figure 3.4b, all ice-core individual offsets from GICC05 tend to stay close to each other, making it possible to identify a common behavior, which illustrates the result of the

timescale revision: an increasing offset from GICC05. Therefore, we recommend a timescale-calibration offset toward younger ages, when using GICC05 beyond 3835 years b2k. The amount of calibration needed is 14 years for DYE-3, 12 years for EastGRIP, 11 years for GRIP, and 12 years for any other ice core based on the average transfer curve (see sec. 3.13).

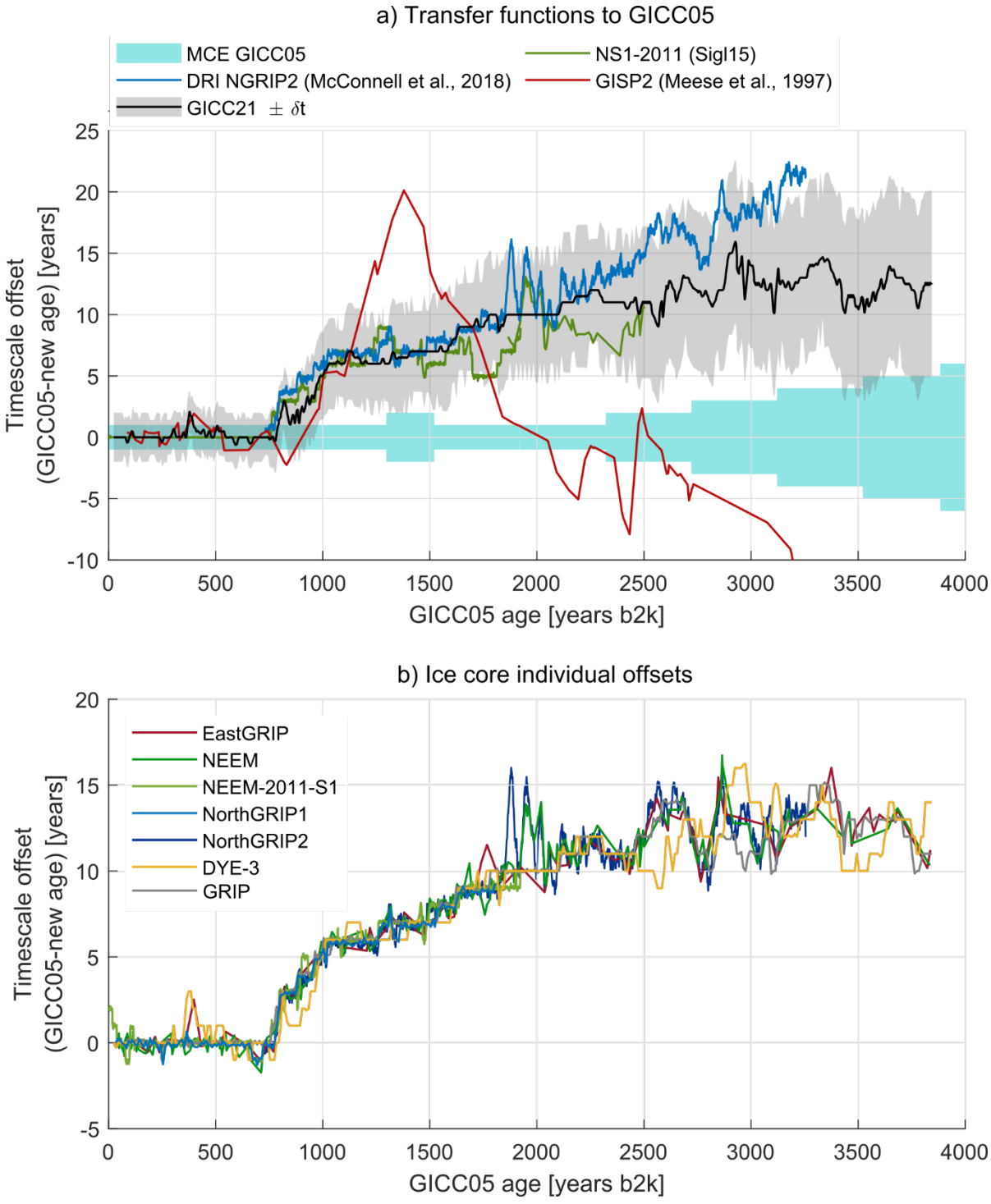

Figure 3.4 Timescale comparison.

(continued caption of Figure 3.4) a) Published timescales and GICC21 compared to GICC05. The shaded areas highlight the uncertainty of both GICC05 (light blue) and GICC21 (grey). The GISP2 timescale was compared using the published match with GICC05 (Seierstad et al., 2014); it agrees with GICC05 at the former Vesuvius tie point, but we observe how it also agrees with the recent revisions until the 1109 b2k eruption, before it spreads to wider offsets. The NS1-2011 timescale (Sigl et al., 2015) agrees with our revision within uncertainties, as well as the DRI_NGRIP2 timescale (McConnell et al., 2018).
b) The individual ice cores have different offsets from GICC05 depending both on the volcanic match and on the layer counting differences. A direct comparison with GICC05 is possible for the ice cores NorthGRIP, GRIP, and DYE-3, for which both GICC05 and GICC21 are annual-layer counted. The NorthGRIP 1 layer comparison stops at 1813 years b2k, corresponding to the end of the IC dataset, but the NorthGRIP 2 comparison continues thanks to the DRI CFA dataset. An indirect comparison was possible for EastGRIP and NEEM, for which published match-point ages were used to interpolate to the new layer-counted ages (Rasmussen et al., 2013; Mojtabavi et al., 2020). The comparison for NEEM-2011-S1 was possible using the matching of the ice core onto GICC05 using the tie points provided in Sigl et al. (2013).

The erroneous attribution of Hekla (1104 CE) explains the steep 4-year offset which was introduced between the Samalas eruption and 1104 CE. In hindsight, the 4 annual layers appear poorly supported by the DYE-3, GRIP and NorthGRIP 1 data (Figure 3.5). After 1100 years b2k, a steady increase is observed until about 2000 years b2k at the age of the previously assigned Vesuvius layer.

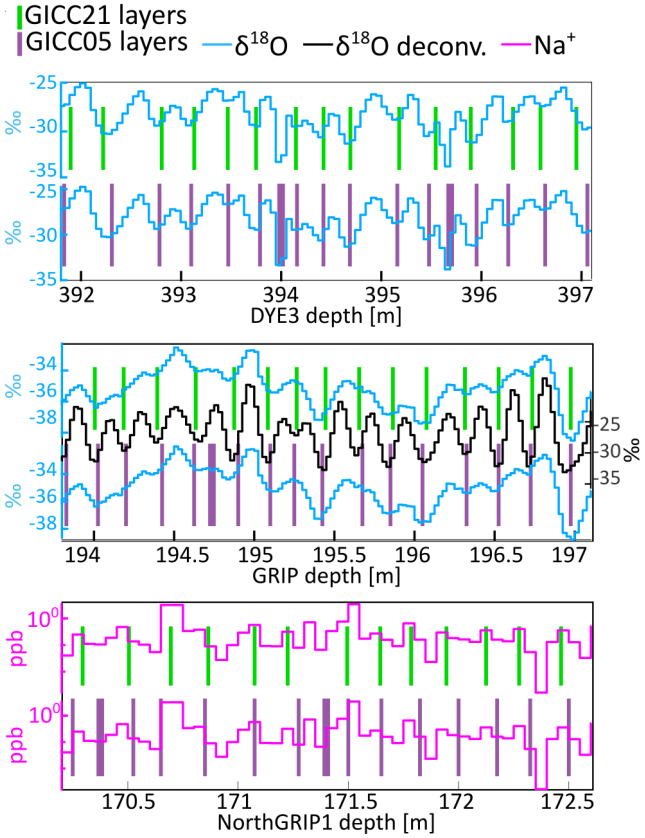

Figure 3.5 Example of GICC05 overcounting between Samalas and 1108 CE in sections of DYE-3, GRIP, and NorthGRIP1.

The top, green bars represent the GICC21 layer boundaries. The bottom, purple bars represent GICC05 layers: they include more layers (thicker purple bars) that are not included in GICC21. For DYE-3, the doubtful features of the isotopes, possibly corresponding to melt layers or measurement issues, suggest that these are not annual layer boundaries. For GRIP, it seems unlikely that a year is found at a local maximum of the isotopes. For NorthGRIP, discrete sodium measurements are not always easy to interpret due to the marginal resolution, however the placement of a layer boundary at a sodium minimum is unlikely.

3.6.1 The offset behavior between 2000 and 3835 years b2k

Beyond 2000 years b2k, the offset stays above 10 years, reaching an average of around 13 years in the last centuries of the timescale. We speculate that the reason for the overall increase in offset is related to a confirmation bias in GICC05 after having acquired the initial 10 years offset, meaning that by deciding to include more layers before Vesuvius, the authors possibly continued to lean towards interpreting melt layers or isotopic fluctuations in DYE-3 as annual layers.

Around the previously attributed Vesuvius match, the NEEM ice core exhibits a divergence from the other ice cores, which was also documented in Sigl et al. (2015). NEEM was matched to NorthGRIP1, which in turn was matched to DYE-3 and GRIP, as the section sits just below where the NorthGRIP1 IC-data stops. We observe that both the DRI_NGRIP2 timescale and our revision of NorthGRIP 2 present a similar feature. We thus conclude that the likely reason for the fluctuation is a previously erroneous transfer of GICC05, because the problem must lie in the ages previously assigned to the NorthGRIP1 match points. Since EastGRIP was matched with fewer match points in this section, the divergence does not arise in the EastGRIP curve.

Between 2500 and 3500 years b2k, three centennial-scale fluctuations are observed, with two notable offset-peaks above 15 years at around 2900 and 3400 years b2k. We argue that these large wiggles in the timescale offset are to be attributed to a difference in layer count within widely separated volcanic markers. The spacing of adequate volcanic tie-points can be as high as 130 years, a fact that called for a heavier use of NH_4^+ markers in our work, and which were not used in GICC05 in this section. For the timespan 2800-3100 years b2k, we analyzed in detail the matching differences between GICC05 and GICC21 (Supplementary Information Figure 3.15) finding that the offset wiggle is explained by shifts of the tie-points, by layer thickness fluctuations of DYE-3, and by interpolated NorthGRIP 1 ages being used to date EastGRIP and NEEM.

3.6.2 The comparison with published ice-core timescales and Holocene chronostratigraphic markers

We found that both GICC21, DRI_NGRIP2 and NS1-2011 have a similar offset to GICC05 within their respective time periods (Figure 3.4a). On the other hand, the GISP2 timescale presents a large divergence from our revision. The GISP2 timescale, however, agrees with our revision until 1109 years b2k, after which the assumption about the Vesuvius tie point produces a large offset-fluctuation, caused by the need to insert and remove layers in order

to compensate for the erroneous tie point. The offset of GISP2 from GICC05 after 3000 years b2k becomes very large and we chose not to plot it.

For the DRI_NGRIP2 timescale (McConnell et al., 2020), we notice a very good agreement until 2250 years b2k, after which DRI_NGRIP2 displays a linear increasing trend in offset, whereas GICC21 shows a more constant offset. On the other hand, the NS1-2011 timescale shows a lower offset between 2000 and 2500 years b2k. Although both are well within the GICC21 uncertainties, the two counteracting offsets between the two timescales might be a sign of widely spaced eruptions and lack of multi-core comparison. Therefore, we conclude that, at least for Greenlandic ice cores, a multi-core comparison is favorable for timescale reconstructions, especially in the case of widely-spaced tie points.

*Table 3.3 GICC21 ages of chronostratigraphic markers in the Holocene which were important for this study. Tephra from eruptions and ^{10}Be from solar proton events (SPE) both provide chronological references when the age of the event is known from historical evidence or other accurate timescales, such as dendrochronology. [a] Only two of the events are used to anchor our timescale. [b] GICC21 ages are reported at the peak of the signal identifying the event, a delay in deposition might occur. [c] Not used as tie point across ice cores. [d] Age from NS1-2011 chronology. [e] Age from indirect historical evidence and tree rings (McConnell et al., 2020) [f] Age from tree rings (Park et al., 2017; Sakurai et al., 2020) [g] GICC05 age of acidity layer * TUNU13 was not used for this study but we verified the match with NEEM-2011-S1 and NorthGRIP to be the same as ours.*

Name, Location	Historical Age (CE/BCE)	GICC21 age (± δt) (CE/BCE) [b]	Reference	Tephra/^{10}Be found in ice core
Katmai, Iceland	1912 CE	1912 ± 2 CE	Coulter et al., 2012	NorthGRIP
[a] Laki, Iceland	1783 CE	1783 ± 2 CE	Fiacco et al., 1994	GISP2
Veiðivötn-Bárðarbunga, Iceland	1477 CE	1477 ± 2 CE	Abbott et al., 2020	TUNU13*
[a] Öræfajökull	1362 CE	1362 ± 2 CE	Palais et al., 1991 Coulter et al., 2012	GISP2 GRIP
Samalas, Indonesia	1257 CE	1259 ± 2 CE	Palais et al. 1992; Lavigne et al., 2013	GISP2
[c] 994 CE SPE (^{10}Be)	994 CE	992 ± 3.6 CE	Sigl et al., 2015 Mekhaldi et al., 2015	NEEM 2011 S1 NorthGRIP, GRIP
Tianchi, Japan	946 CE	946 ± 3.7 CE	Sun et al., 2014	NorthGRIP
Katla, Eldjá, Iceland	939 CE	939 ± 3.8 CE	Zielinski et al., 1995	GISP2
Bárðarbunga, Settlement, Iceland	~877 CE	877 ± 3.9 CE	Grönvold et al 1995; Zielinski et al 1997	GRIP GISP2
775 CE SPE (^{10}Be)	774/775 CE	774 ± 4.1 CE	Sigl et al., 2015; Mekhaldi et al., 2015	NorthGRIP, NEEM 2011 S1 GRIP
UE 88 (former Vesuvius 79 CE)	~88 CE [d]	89 ± 5.4 CE	Plunkett et al., 2022	NEEM-2011-S1
Okmok, Alaska	~43 BCE [e]	43 ± 5.6 BCE	McConnell et al., 2020	NorthGRIP 2
660 BCE SPE (^{10}Be)	665-660 BCE [f]	663 ± 6.8 BCE	O'Hare et al., 2019	NorthGRIP, GRIP
Aniakchak, Alaska (former Thera)	~1645 BCE [g]	1629 ± 7.3 BCE	Pearce et al., 2004	GRIP

We also highlighted the ages proposed by GICC21 of some events detected in ice cores in order to compare to historical ages (Table 3.3). The oldest event is the eruption formerly attributed to Thera (Santorini) by the GICC05 authors, who placed the layer in 1645 BCE. Since then, the origin of the tephra was determined to be Alaskan and the dating of the corresponding acidity peak was questioned, also in relation to comparison to tree-ring data (Pearce et al., 2004; McAneney and Baillie, 2019). According to GICC21, we state the age of this acidity peak to be 1629 BCE (3627.5 years b2k) and we endorse the future search for cryptotephra in ice cores that might indicate a more accurate age for the Thera eruption, which is going to be vital for the archaeological framework of the Late Bronze Age.

3.6.3 Comparison of GICC21 to the tree-ring timescale and the IntCal20 curve

The ice-core timescale can be compared to other timescales and climatic archives to verify their relative consistency and infer leads and lags in the climatic system. The fact that GICC21 was created as independently as possible from other archives makes it possible, for example, to compare to the tree-ring chronology.

In Sigl et al. (2015), a composite of five northern Hemispheric tree-ring chronologies, called 'N-Tree', was created to describe tree-growth anomalies over the last 2500 years in the Northern Hemisphere. Another recent reconstruction of temperature changes from tree rings (Büntgen et al., 2021) can also be used as a comparison until 2000 years ago. These chronologies have virtually no uncertainty since the vast availability of old wood makes tree-ring timescales very accurate thanks to many iterations of cross-dating. By looking at the alignment of ECM with the two reconstructions (Supplementary Information Figure 3.17a and b), we observe that Greenland eruptions align very accurately with some periods of abrupt cooling, providing an indication of the timescale accuracy with respect to tree rings. A comparison to another tree-ring growth reconstruction reaching until 3835 years b2k (Helama et al., 2012) did not lead to conclusive evidence for a better alignment of GICC21 to growth minima with respect to GICC05, either because the resolution of the tree ring data was too low or because no clear minima were seen in the vicinity of the ECM peaks.

We furthermore compared to the bristlecone pine-growth record, compiled by Salzer & Hughes (2007). We found very good correspondence between two growth minima of North-American trees, at 3626 and 3649 years b2k, the first of them corresponding to the Alaskan Aniakchak eruption (Pearce et al., 2004), which again confirms the alignment of the eruptions in ice cores and tree-growth minima (Supplementary Information Figure 3.17c). Finally, a calcium anomaly was reported in tree rings by Pearson et al. (2020) at 3560 years

b2k, speculated to be linked to the eruption of Thera, Santorini, which we find to align with a modest ECM peak in some ice cores (e.g. EastGRIP) (Supplementary Information Figure 3.17c).

Synchronous deposition of cosmogenic radionuclides (^{10}Be and ^{14}C) provides an additional tool for the comparison of ice cores to other archives at lower latitudes. However, the ^{14}C signal is dampened by the carbon cycle and therefore the comparison can only be conducted by backward modelling the ^{14}C to retrieve the original production rates. In this way, GICC05 was compared to the radiocarbon calibration curve IntCal13 (Reimer et al., 2013) by Adolphi & Muscheler (2016), who found that the offset between the timescales increased steadily over the Holocene, reaching about 20 years at 4 ka b2k. This conclusion is supported by GICC21, at least until 3400 years b2k, by observing that the transfer function of GICC21 behaves similarly to the one produced by Adolphi & Muscheler (Figure 3.6a). Furthermore, the solar proton event identified by O'Hare et al. (2019) in NorthGRIP and GRIP, dated through tree-ring evidence, keeps its alignment under the GICC21 timescale and is confirmed at an age of 663 ± 7 years b2k (Table 3.3), providing independent proof for the accuracy of GICC21 for that period.

The transfer curve to IntCal13 is smoothed as a result of the statistical wiggle-matching approach between ^{10}Be and ^{14}C, designed to match unstretched 1000-year long windows in order to avoid over-fitting of spurious peaks (Adolphi & Muscheler, 2016). This implies that beyond 3500 years b2k, the wiggle-matching algorithm is influenced by data older than 4000 years b2k, which could cause the increase in observed offset in the 3500-3800 years window. Since the differences between IntCal13 and IntCal20 are thought to be marginal in the Late Holocene, at least for the purpose of timescale comparisons (Reimer et al., 2020; Muscheler et al., 2020) we refrain from repeating the wiggle-matching. Therefore, after 3500 years b2k, the IntCal-GICC21 offset can be quantified as 7±6 years, which is almost negligible.

To address the finer structure of the offset in the last 500 years of the GICC21 revision, we directly compare the ice-core ^{10}Be concentration measured in the GRIP ice core (Muscheler et al., 2009) and the ^{14}C production signal of the IntCal20 curve, which is obtained by carbon-cycle modelling (Muscheler et al., 2005). Since the underlying production mechanisms are the same, the two radionuclides show common variability. After detrending the signals, we compare the ^{14}C of IntCal20 and the ice-core ^{10}Be, according to GICC21 and to the transfer function by Adolphi & Muscheler. Upon visual inspection (Figure 3.6b), we conclude that there is good agreement between all production signals and that until 3835

years b2k, the offset between IntCal20 and GICC21 is resolved within uncertainties. However, we remark that between 3700 and 3800 years b2k comparative studies of tree-ring and ice-core data should address the inconsistencies observed in the radionuclide production signal. In conclusion, there is no compelling evidence to suggest an offset of GICC21 versus IntCal20.

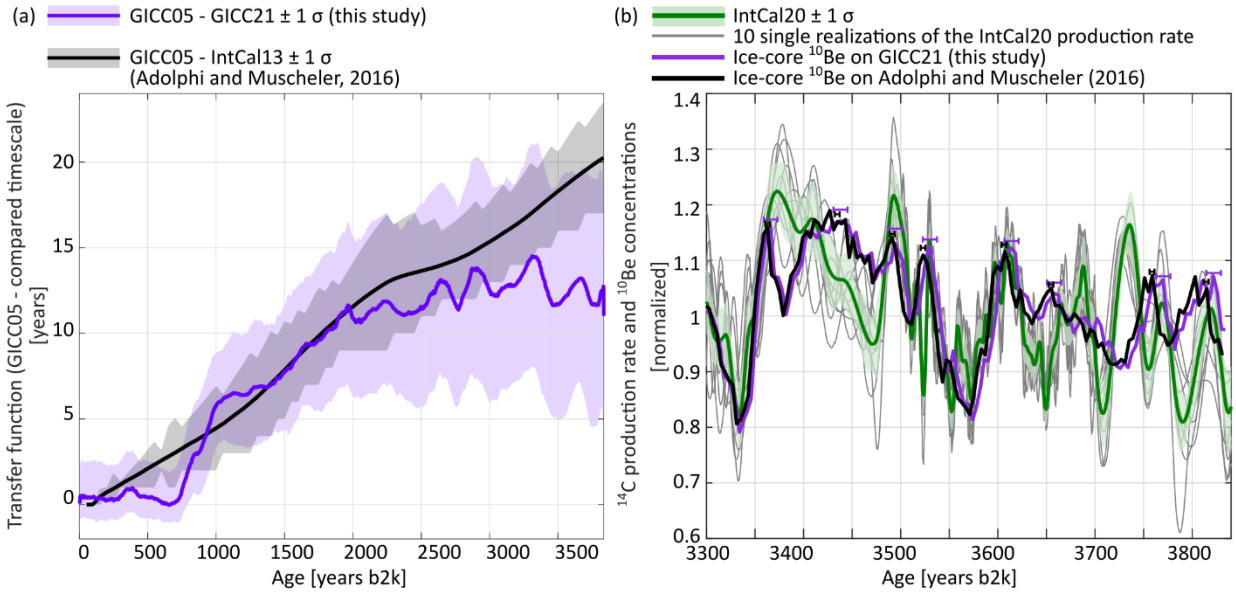

Figure 3.6 (a) Comparison of the transfer function GICC21-GICC05 with the transfer function modelled by Adolphi & Muscheler (2016), based on ^{10}Be data from the GRIP ice core and converted to Δ^{14}C by modelling, and compared it to the Δ^{14}C variations in IntCal13.
The agreement between GICC21 and IntCal is supported by the closeness of the two transfer curves. We observe two notable differences between the transfer curves: between 500 and 1000 years b2k, where the effect of the 1000-year smoothing of the Adolphi & Muscheler approach is evident (used in the ^{10}Be-^{14}C comparison to avoid matching spurious peaks), and possibly between 3400 and 3835 years b2k, where some offset (7±6 years) towards older GICC21-ages is still observed. (b) ^{10}Be concentrations measured in the GRIP ice core (Muscheler et al., 2009) are shown in purple for GICC21 and black for the Adolphi & Muscheler timescales, with horizontal bars highlighting the uncertainties in the peak positioning. The data were smoothed with a 20-year running average and detrended to remove the long term trend. The ^{14}C production rate (green), based on the tree-ring timescale, is obtained from carbon-cycle modelling of the ^{14}C data of IntCal20 (methods outlined in Muscheler et al., 2005). Single realizations of the IntCal20-based production curve show that the position of the peaks underlying IntCal20 can vary slightly, so that the average curve should be handled with care when performing timescale studies (Muscheler et al., 2020). The alignment with IntCal20 is kept within uncertainties throughout the period shown, with possibly GICC21 better aligned in the last century. Any production rate differences between tree-ring data and ice-cores that cannot be resolved within realistic dating offsets (e.g. the period 3700-3740 years b2k) could be explained by under-estimated data uncertainties or by transport and deposition effects on ^{10}Be, since major carbon-cycle changes in this period are unlikely (Muscheler et al., 2004).

3.7 Conclusions

Compared to GICC05, the new GICC21 ice-core timescale shows higher potential for climatic studies and comparison to distant records in the Late Holocene, such as radiocarbon-dated evidence proximal to eruption sites. The timescale offset to GICC05 shows a non-linear behavior, as a consequence of local issues with the layer count and the ice-core comparison. Until 742 years b2k, the two timescales agree within uncertainties, which is convenient for shallow ice-core studies. However, beyond the Samalas eruption (1258 CE, 742 years b2k), the offset increases rapidly because of the mismatch of the Hekla (1104 CE) and the Vesuvius (79 CE) eruptions.

The automated-counting algorithm StratiCounter was applied with success to recognize layers in the ice cores, using the new available proxy data from EastGRIP and NEEM, but nonetheless showed some intrinsic issues, since the algorithm was under-counting layers in some ice cores (EastGRIP, NEEM, and NEEM-S1-2011) and over-counting layers in others (GRIP, NorthGRIP, and especially DYE-3), as demonstrated in the well-constrained age range younger than the Samalas eruption. Hence, we demonstrated the need for a multi-observer manual fine-tuning and applied an empirical statistical approach to show that the rate of the timescale uncertainty envelope can be estimated as about 1 year per century, going back in time from Samalas. A lower bound of 2 years needs to be added to the uncertainty, to account for uncertainties in displacement and delays in the volcanic acidity deposition on the ice sheet. We remark that the existence of a counting bias in each ice core is not a failure of SC, as the task of recognizing layers is challenging regardless of the methodology applied. That is to say that the algorithm cannot overcome the bias which is as much an intrinsic problem with the annual layer record as it is an issue with the layer identification method. Since we demonstrated that ice cores do have site-specific disturbances that affect the layer count, it is clear that a multi-core comparison such as the one conducted in this work is favorable to increase the accuracy of the Greenland ice-core timescale.

The offset of the timescale from GICC05 reaches 13 years at 3835 years b2k, which is significant considering the small timescale uncertainty at this age. The offset has an oscillating behavior between 2000 years b2k and 3835 years b2k, with three important excursions from the mean with amplitudes of about 5 years. This fact we attribute to matching issues related to widely-spaced volcanic eruptions, a finer ammonium-based match in GICC21, and layer thickness fluctuations in DYE-3.

The revision of the timescale was stopped at 3835 years b2k to ensure multi-core comparison. However, since NEEM data improves again for depths larger than 1200 m (corresponding to roughly 8 ka b2k), there is a possibility for a revised Early-Holocene ice-core chronology based on data from EastGRIP, NEEM, and DYE-3, made by a method similar to the one provided here. In contrast, between 3.8 and 8 ka b2k, i.e. within the typical brittle ice section of the cores, where data quality is lower, any timescale revision will have to be constructed by different means or by acquisition of new data from new and old ice cores. We remark that the record of EastGRIP CFA data was acquired with the goal of covering the brittle ice zone part of the Holocene in Greenland, hence this dataset will be key to improving the ice-core timescale in future studies. In the meantime, a timescale-calibration offset should be added when using GICC05 beyond 3835 years b2k (see sec. 3.13).

Comparisons of GICC21 to other timescales provided new insights on some debated issues of ice-core timescales, such as the offset to the IntCal calibration curve. A comparison between several tree-ring growth minima and volcanic acidity spikes supports the conclusion that GICC21 is in good alignment with tree-ring chronologies. Moreover, thanks to the modelling of cosmogenic radionuclides, we were able to compare IntCal20 and GICC21 until 3835 years b2k, concluding that the offset between the two timescales is negligible within uncertainties.

In conclusion, thanks to a good geographical coverage of the central Greenlandic ice sheet provided by the dataset, our improved synchronization of Greenlandic ice cores will allow more precise investigations of the relative timing of climatic events, such as, for example, the climatic response to Holocene volcanic eruptions as reflected in the ice-core signal.

3.8 Supplement

The following documents are provided with the online version of this paper:

1. The GICC21 timescale layer boundaries, the volcanic/ammonium tie-points, and the GICC05-GICC21 transfer function are available in the Timescale Supplement.
2. For more information about the pre-processing and the uncertainty study (sec. 3.5.4) we provide a Straticounter Supplement.
3. The Supplementary Information contains additional figures and text.

Moreover:

4. Straticounter is available at: https://github.com/maiwinstrup/StratiCounter
5. Matchmaker can be obtained by direct communication with SOR.

3.9 Ice-core data availability

All data underlying GICC21 is available for use. As many of the data sets were also used for GICC05 but not released at that time, we have decided to release all hitherto unpublished data and information related to GICC05 and GICC21 together. The publication plans were split according to the ice-core project and are still ongoing.

The CFA data sets from NorthGRIP and NEEM have been documented in a paper by Erhardt et al. (2021) (accepted). The corresponding data files are available at Pangea (https://doi.pangaea.de/10.1594/PANGAEA.935838). EastGRIP CFA data are in the process of being released in a similar way, and a preliminary data file can be obtained from TE until the data files are available at Pangea.

In addition, the following data files have been documented and are currently in review and undergoing curation at Pangea: ECM from DYE-3 (main core, 4B, 18C) and GRIP; yearly resolved isotope data from DYE-3 (main core, 4B, 18C) and GRIP; impurity CFA data from GRIP; impurity IC data from NorthGRIP1; linescan profile from NorthGRIP2; the GICC05 annual layer markings for all cores. The full metadata and documentation for these files are being compiled as a manuscript for ESSD, and the data files are available (with the current preliminary metadata) from SOR until they appear at Pangea in their final form.

Other data underlying the timescale, and where to find it, is listed below:

1) NorthGRIP DEP data from the top are at https://doi.pangaea.de/10.1594/PANGAEA.922308 (Mojtabavi et al., 2022, accepted)
2) NEEM DEP is available at https://doi.pangaea.de/10.1594/PANGAEA.922139 (Mojtabavi et al., 2020)
3) EastGRIP, NorthGRIP, and NEEM Acidity (ECM) are published on the CIC website: https://www.iceandclimate.nbi.ku.dk/data/

3.10 Author contributions

G.S. drafted the paper with comments and corrections from all co-authors. G.S. produced the StratiCounter raw counts and led the fine-tuning, which was performed together with

M.W. and S.O.R, who provided guidance on methodology and on layer recognition. M.W. provided supervision on the use of StratiCounter. S.O.R. produced the manual gap count for the uncertainty study, supervised the general content of the work, and provided ideas regarding the uncertainty formula.

B.V. produced the correlation study for DYE-3, GRIP, and SWG temperatures. A.S. provided suggestions for the IntCal comparison and the tree-ring minima comparison and guidance about volcanic matching and tephra. T.E. and C.J. provided information about the EastGRIP data. C.J. helped with research on ammonium signal in ice cores. T.E. provided useful insight and ideas about the uncertainty and the statistical framework. E.C. provided information about tephra evidence in the Holocene. R.M produced the single realizations of the IntCal20 ^{14}C production rates by carbon-modelling, as well as providing guidance for the IntCal comparison.

3.11 Conflicts of interest

The authors declare that they have no conflict of interest.

3.12 Acknowledgements

3.12.1 Funding

G.S. and S.O.R. acknowledge support via the ChronoClimate project funded by the Carlsberg Foundation.

T.E. and C.M.J. acknowledge the long-term support of ice core research at the University of Bern by the Swiss National Science Foundation (SNSF) (#20Fi21_164190) and the Oeschger Center for Climate Change Research.

3.12.2 People

G.S thanks Hubertus Fischer for his useful comments to the manuscript. Many thanks to the three anonymous referees and to M. Sigl who provided essential comments for the improvement of the manuscript. A special thank you to Joe McConnell for providing the DRI_NGRIP2 timescale and NGRIP2 data and a useful reminder about the importance of b2k/CE age conversions.

3.13 "Appendix A" Transfer function GICC05-GICC21

The transfer function between GICC05 and GICC21 was calculated by, first, acquiring the timescale offsets of each of the ice cores involved in this study. Then, we computed the uncertainty using equation (1). For each year between 0 and 3835 years b2k, a weighted mean of the offset was calculated with the corresponding weighted uncertainty. The transfer function is reported in the Timescale Supplement. For the ice cores EastGRIP, NEEM, NorthGRIP1, NorthGRIP2, and DYE-3 we recommend the direct use of the GICC21 layers and of equation (1) for the uncertainty, in order to convert ages from GICC05. For other cores, which were matched to one or a combination of these ice cores (e.g. GISP2, Rasmussen et al., 2008), we recommend the use of the average transfer function to translate ages from GICC05 to GICC21 until 3835 years b2k. For sections older than 3835 years b2k, we recommend ages of GICC05 to be calibrated by a shift towards younger ages. The amount of calibration needed is 14 years for DYE-3, 12 years for EastGRIP, 11 years for GRIP, and 12 years for any other ice core based on the average transfer curve.

3.14 Supplementary Information for "A multi-ice-core, annual-layer counted Greenland ice-core chronology for the last 3800 years: GICC21"

3.14.1 Top-chronology and remarks about the DYE-3 ice core

The DYE-3 ice core is the best ice core to use for directly comparing our results to GICC05, because its well-preserved isotope signal provided the foundation for GICC05 in the last 4000 years. Hence it is important to match it precisely, even for the top 136 m where the ECM is missing. To match the top part of DYE-3, we used two shallow cores, 4B and 18C, drilled respectively 8 km and 36 km upstream of the main drilling site for climate reconstructions (Vinther et al., 2010). Owing to the close distance between the three ice cores , their $\delta^{18}O$ records could be matched by finding common features in the data (Figure 3.12). The ECM signal of the two shallow cores was in turn matched to NorthGRIP 1 and GRIP. In this way, DYE-3 has been tied to the timescale for the top 136 m.

Vinther et al. (2010) showed that Greenland ice-core isotope signals correlate well with South West Greenland temperature records, and that the inter-core correlations (e.g. between DYE-3 and GRIP) help assess the quality of the cross-dating of the ice cores. To judge the quality of the new top chronology, we repeated the correlation study of DYE-3 with the South West Greenland (SWG) temperature and with GRIP (Table 3.4). The correlation

between isotopes of the DYE-3 main core and GRIP improved by $(0.27 - 0.23)/0.23 \approx 17\%$, a promising result that indicates that the matching between DYE-3 and GRIP has improved. Still, the correlation with SWG temperatures is essentially the same as in Vinther et al. (2010). It is reassuring that the new timescale confirms the link with the SWG temperatures.

Table 3.4 Correlations (ρ) between $\delta^{18}O$ in the DYE-3 ice cores and the SWG temperatures or the GRIP $\delta^{18}O$ over the last 400 years. The correlation between GRIP and all the DYE-3 ice cores (main core 79 and shallow cores 4B and 18C) have almost all increased with the new GICC21 match. No significant change is observed in the correlation between DYE-3 main core (DYE-3 79) and SWG temperatures, and no significant change is observed in the correlation between the shallow cores and SWG temperatures.

	DYE-3 79		DYE-3 4B		DYE-3 18C		GRIP	
	GICC05	GICC21	Vinther et al., 2010	GICC21	Vinther et al., 2010	GICC21	GICC05	GICC21
ρ SWG	0.46	0.47	0.45	0.44	0.35	0.36	0.21	0.20
ρ GRIP	0.23	0.27	0.28	0.31	0.24	0.26		

Fine tuning of DYE-3 was made difficult by the ice core's very different characteristics. Upstream surface undulations (Reeh et al., 1985) lead to low-frequency layer thickness fluctuations at depth (Figure 3.7). Further, many layers of DYE-3 show a double isotopic oscillation during the year, a fact made clear during the top match with the shallow cores 4B and 18C. As shown in Figure 3.12, the DYE-3 ice core was most affected by over-counting, likely because of mid-year local minima. We speculate that mid-year oscillations in the isotopes of DYE-3 are related to melt layers and to the windy conditions that perhaps cause a redistribution of snow in the area. In cases of doubt about where to place the annual layers, we decided to keep the layer boundaries of the GICC05 timescale where possible without creating annual-layer thickness outliers. Finally, DYE-3 also proved to be the most difficult to match, its ECM record being noisy and not strongly resembling that of the other cores, since it also forms spikes because of the influence of high HNO_3 levels (Clausen et al., 1997).

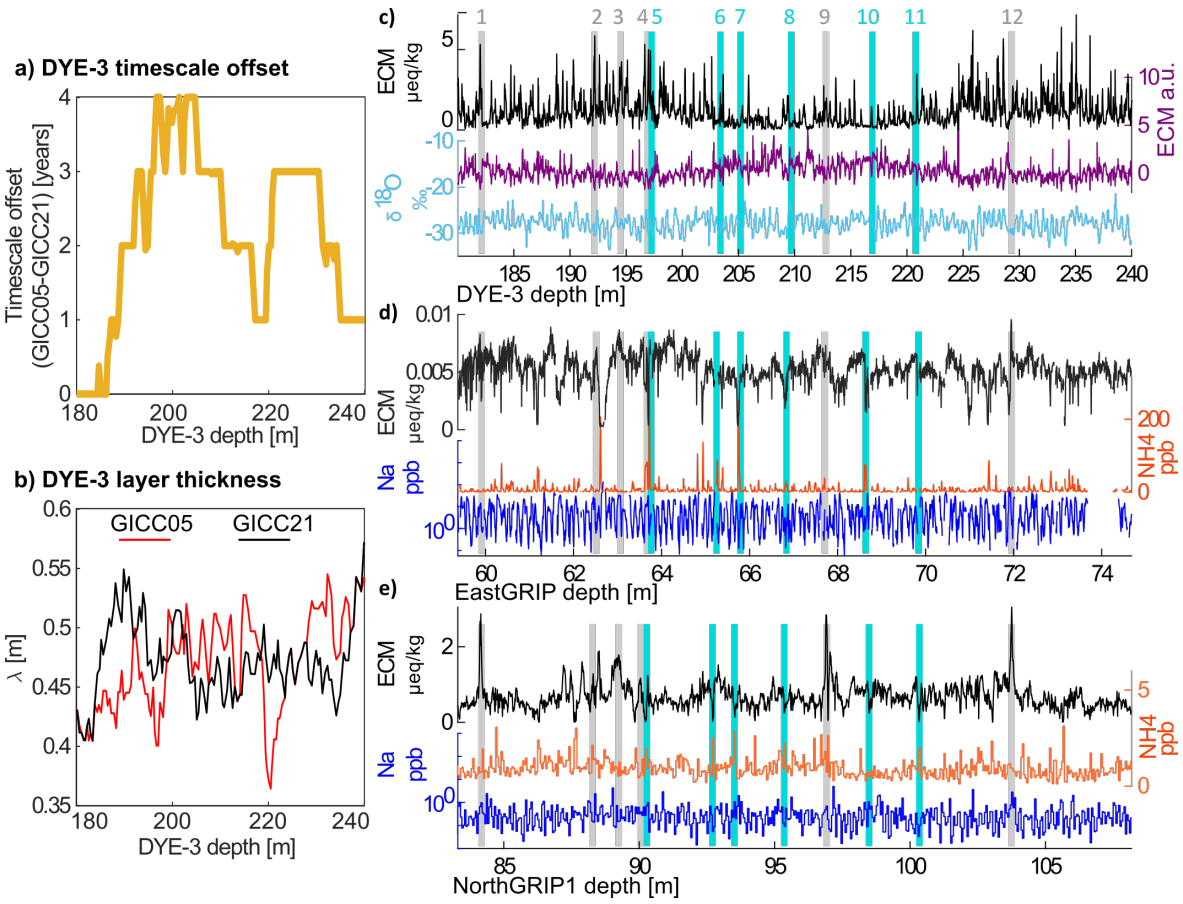

Figure 3.7 a) The first divergence of the timescale offset, at 390-490 years b2k, reported on the DYE-3 depth scale.
Four layers were removed between 190 and 200 m, but they were gradually added back in the earlier part of the timescale. b) The layer thickness in this interval presents a fluctuation towards thicker layers, possibly because of upstream flow effects (Vinther et al., 2006). Between 180 and 240 m, the layer thickness according to GICC05 presents a more gradual increase than according to GICC21, but in turn has a sharp dip at 220 m, which is not present in the GICC21 layer count.
c, d, e) By looking at the actual data, it becomes clear that DYE-3 is very hard to match in this depth range. The fact that the stratigraphy of DYE-3 has been lightly disturbed could have affected the signals, so that both the ECM dips and peaks become almost unrecognizable. The layers present many irregularities that make the fine-tuning more uncertain than usual. d) For EastGRIP, we observed that the broad shape of tie point no.9 caused the match to be revised and placed 2 years later than what was done by Mojtabavi et al. (2020).

3.14.2 Alternative demonstration of the correlation length

The analysis of sec. 3.5.4 (main text) was also performed on sections of 200 and 300 years (numerical results reported in Straticounter Supplement).

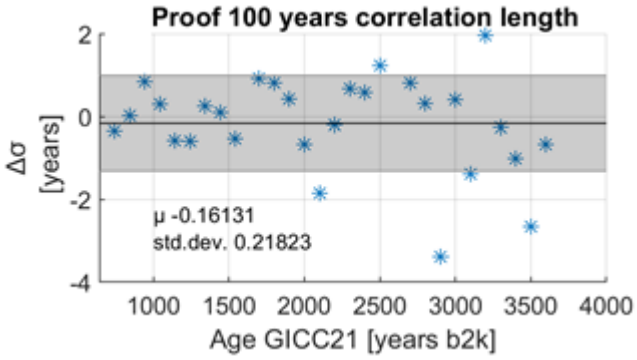

Figure 3.8 Comparison of 100- and 200-year deviations to verify the correlation length.

To analyze if the uncertainty over centuries are uncorrelated, and hence could be added in quadrature, we evaluated the quantity $\Delta\sigma = \delta t_{i,200}{}^2 - (\delta t_{i,100}{}^2 + \delta t_{i+1,100}{}^2)$, shown in Figure 3.8. The meaning of this quantity is that the 200-year deviation from the expected value and the quadrature sum of the 100-year deviation of two adjacent centuries should be approximately the same, if the errors are uncorrelated. The quantity is found to be approximately normally distributed with zero mean (Figure 3.8). Consequently, we find this relationship justified for most 200-year intervals.

3.14.3 Supplementary Figures

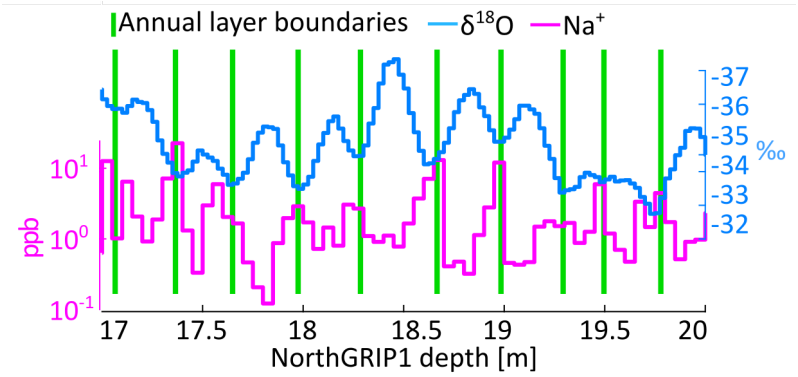

Figure 3.9 Section of NorthGRIP1 data close to the surface, where isotope diffusion is not too strong yet. We highlight the equivalence of choosing Na^+ maxima and $\delta^{18}O$ minima as definition for the start of an annual layer.

Figure 3.10 (next page, top) GRIP spurious layers in deconvoluted $\delta^{18}O$ (red circles).
(a) A spurious oscillation possibly caused by a sharp increase of isotopes at 199 m, which produced a deeper-than-average minimum in the deconvoluted series and a double oscillation in the next layer. Comparison to NorthGRIP and EastGRIP was needed to prove that the layer was an artifact. (b) A rather wide, flat isotope layer produces a small oscillation in the deconvoluted signal, which is again solved by comparison to the two other ice cores.

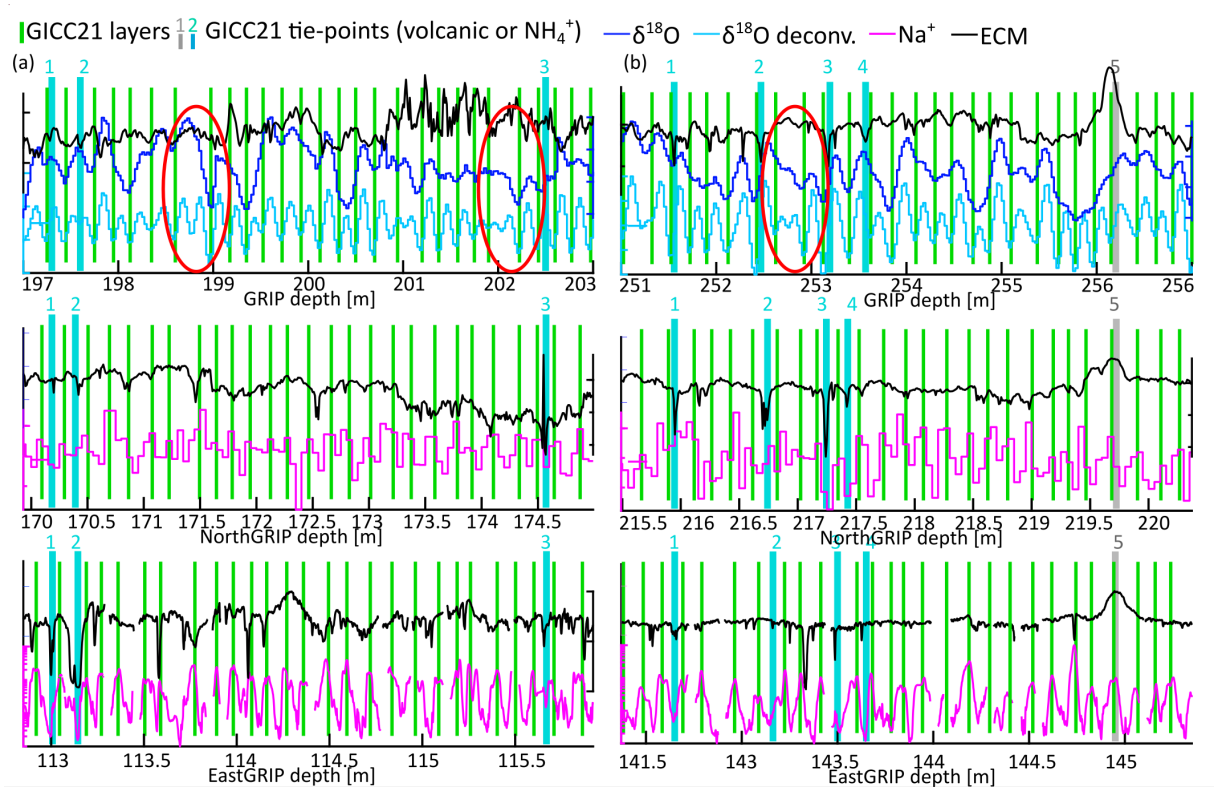

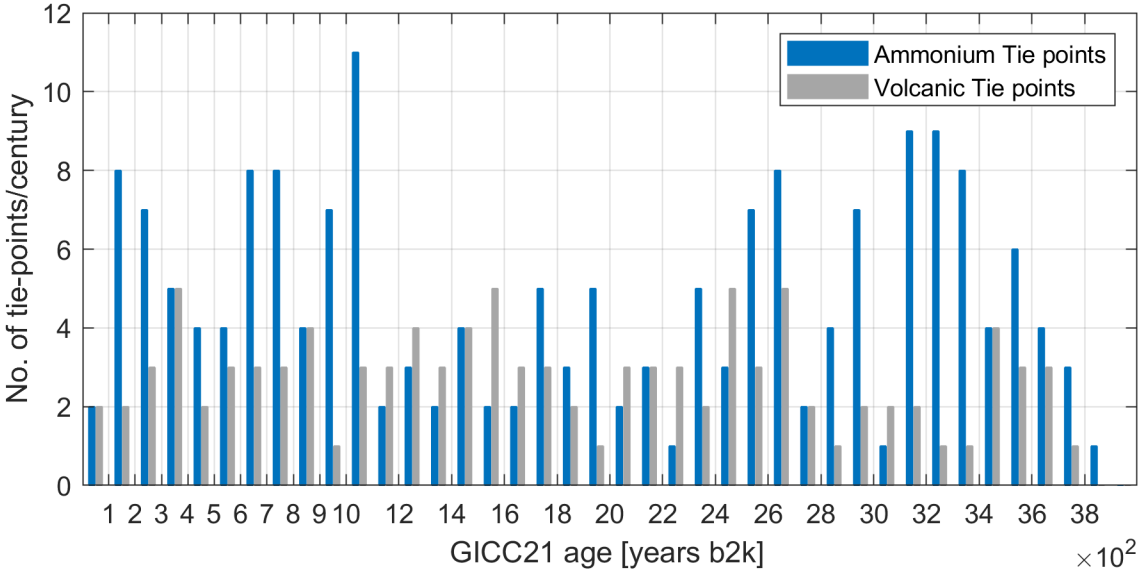

Figure 3.11 Number of tie points per century in GICC21.
The number of ammonium tie points is largest in the most recent millennium of the time scale, where they were supported by the BC signal of NEEM-2011-S1, and in the period after 2500 years b2k, where ammonium is used to support the volcanic match, especially across intervals with less than 2 volcanic tie-points per century. Generally, ammonium tie points are more because we used patterns instead of single peaks.

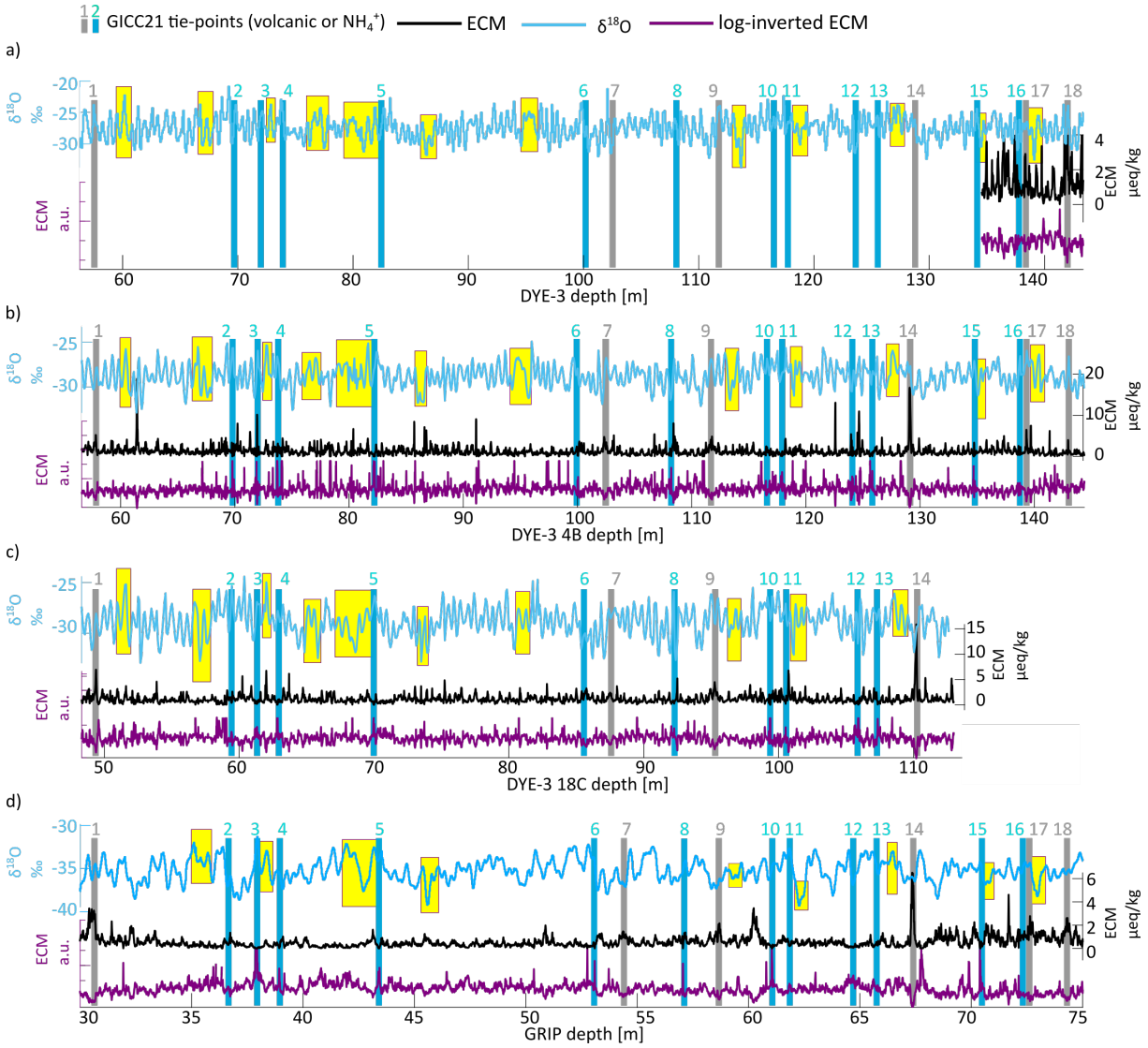

Figure 3.12 Matching the top of DYE-3 using the two shallow cores 4B and 18C. Tie-point n.14 is the Laki eruption (1783 CE). Data for 18C covers only until the Laki eruption, while 4B offers a longer overlap with the start of the ECM signal in DYE-3. Yellow patches highlight some of the common features in the isotopic records that were used to match DYE-3 in absence of ECM measurements. Some of the matched features where also visible in GRIP (although GRIP was not used directly for the isotope-based matching). We observed mid-year oscillations in the DYE-3 isotopic signal, visible for example between tie-points no. 13 and 14, a knowledge we applied to interpret DYE-3 layers further on in the chronology.

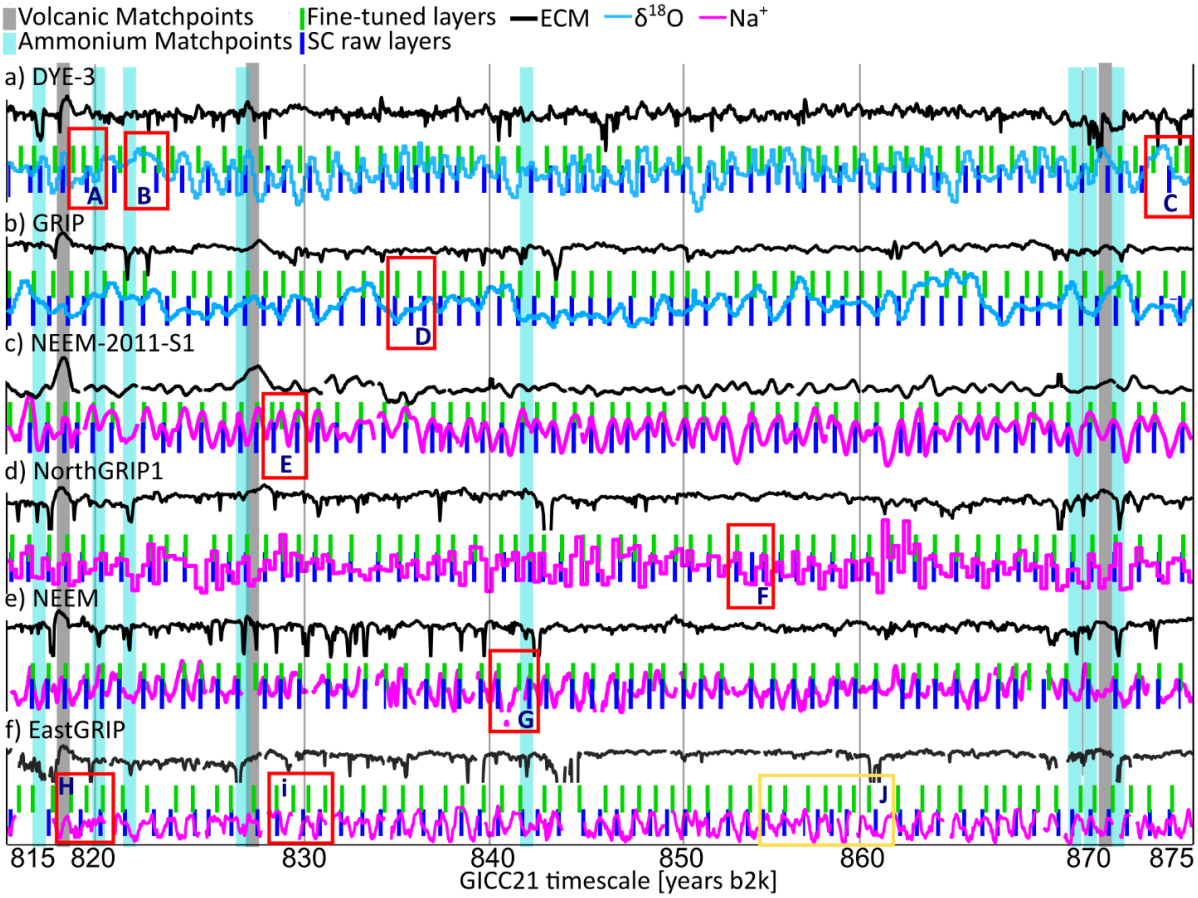

Figure 3.13 Example of the fine-tuning decisional process between 815 and 875 years b2k.
The units of all data are arbitrary, as they were log-transformed and vertically adjusted to better highlight the layer structure and common matching features. Red and yellow rectangles show some examples of where the observers had to intervene because of discrepancies in the layer count between the ice cores. Rectangles A, B, C: in these cases, DYE-3 needed layer addition because SC did not recognize some small isotope features as annual layers. Rectangle D: a spurious isotope oscillation in GRIP was removed from the raw count. Rectangle E: a dubious feature in the data was solved by comparison to NEEM.
Rectangle F: SC counted an extra layer, based on a Ca^{2+} peak (not shown). Rectangle G: SC missed one layer because of the unclear sodium pattern. Rectangle H: An additional layer was inserted because of unclear sodium. Rectangle i: SC did not recognize this annual layer because of the interrupted data. Rectangle J: re-placement of layers did not result in any modification to the count.

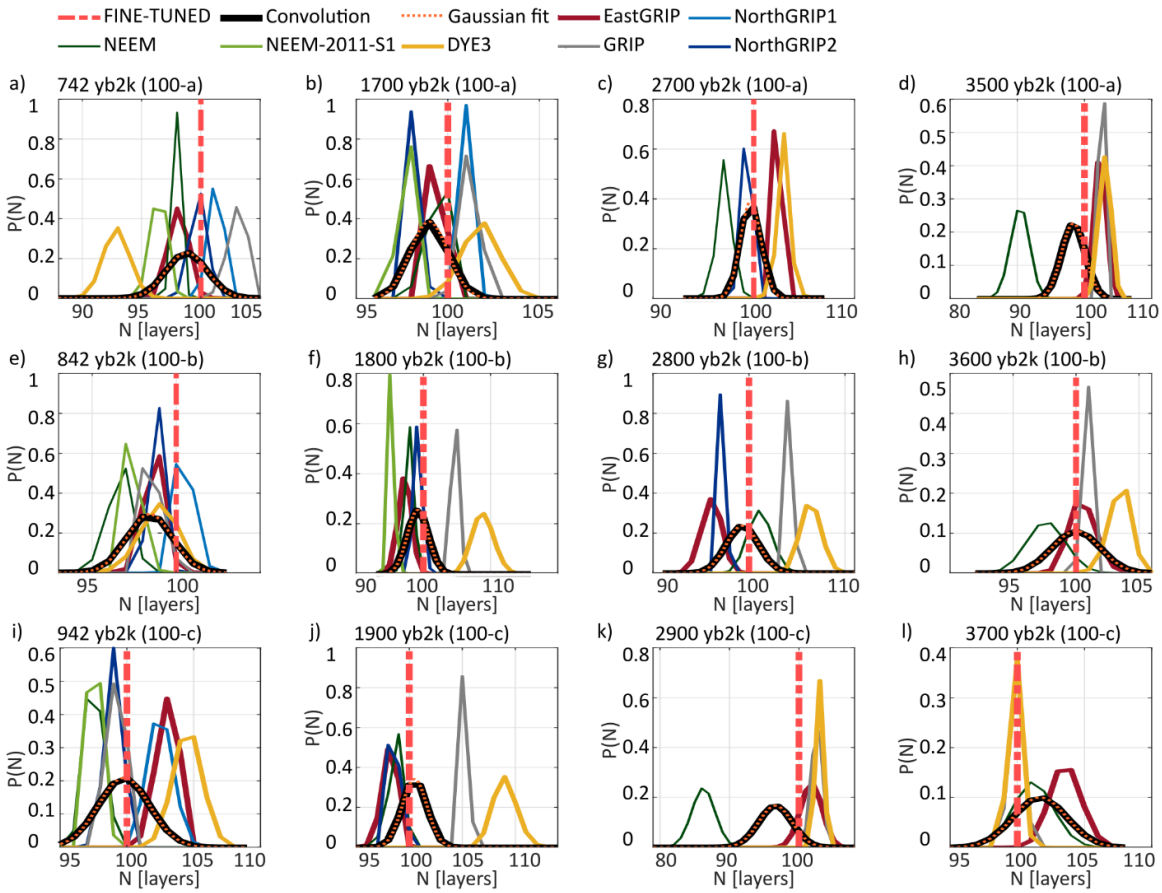

Figure 3.14 Single-core probability density functions (pSC) of the number of years counted by SC in 100-year sections.

All ice cores were corrected for missing layers in data gaps (see Straticounter Supplement). The fine-tuned result (red line, dashed) is often far off some of the single-core probability distributions. In some cases, we observed a systematic over-count by SC of DYE-3 layers, possibly because of melt layers and mid-year isotopic oscillations. However, most of the single-core SC estimates have fewer annual layers than the fine-tuned result. The convolution of the single-core probabilities (black) was fitted to a gaussian (orange) to obtain the parameters listed in Table 3.2.

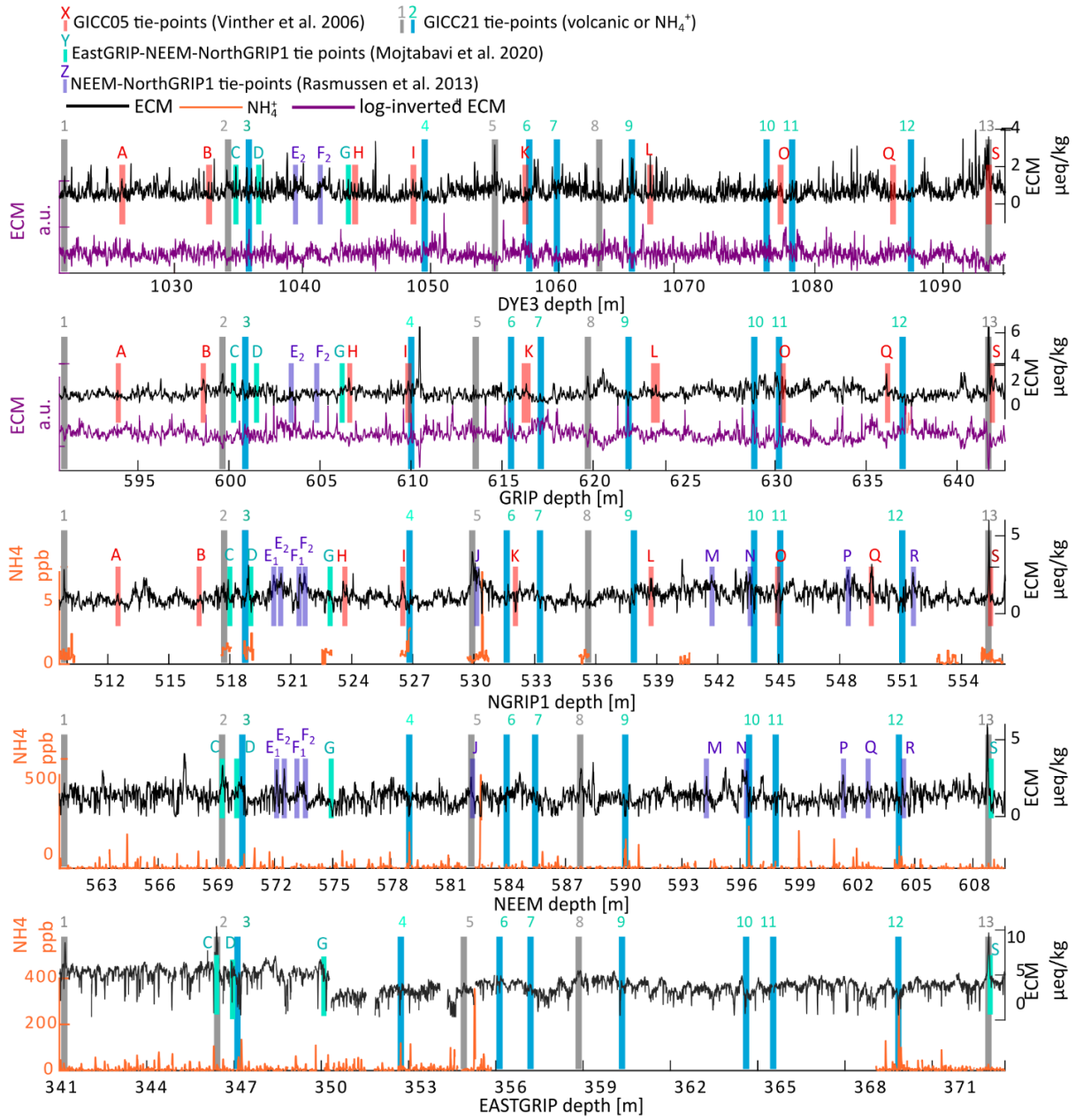

Figure 3.15 Example of a matching problem solved in GICC21 between 2800 and 3100 years b2k. Tie-points of GICC05 are indicated by bars with letters, while tie-points of GICC21 are indicated by numbered bars (see figure legend).

The relative order between the tie-points of GICC21 and GICC05 confirms the interpretation of the offset-wiggle as a result of volcanic mismatch. For example, tie points C and D are slightly shifted in GRIP and DYE-3, causing the steep offset increase at 2800 years b2k. Tie-point K appears between tie points 6 and 7 for GRIP and NorthGRIP, but is between 5 and 6 for DYE-3, explaining why the offset curve of GRIP is flatter in the area. We observe that the match of DYE-3 is affected by layer thickness fluctuations, causing the placement of tie points no. 4-11 to be shifted to the right, similar to Figure 3.7. The problems with EastGRIP and NEEM arise from the match to NorthGRIP1, whose ages result from interpolation from DYE-3 and GRIP, a fact that can be observed by observing the shift of the red and green bars.

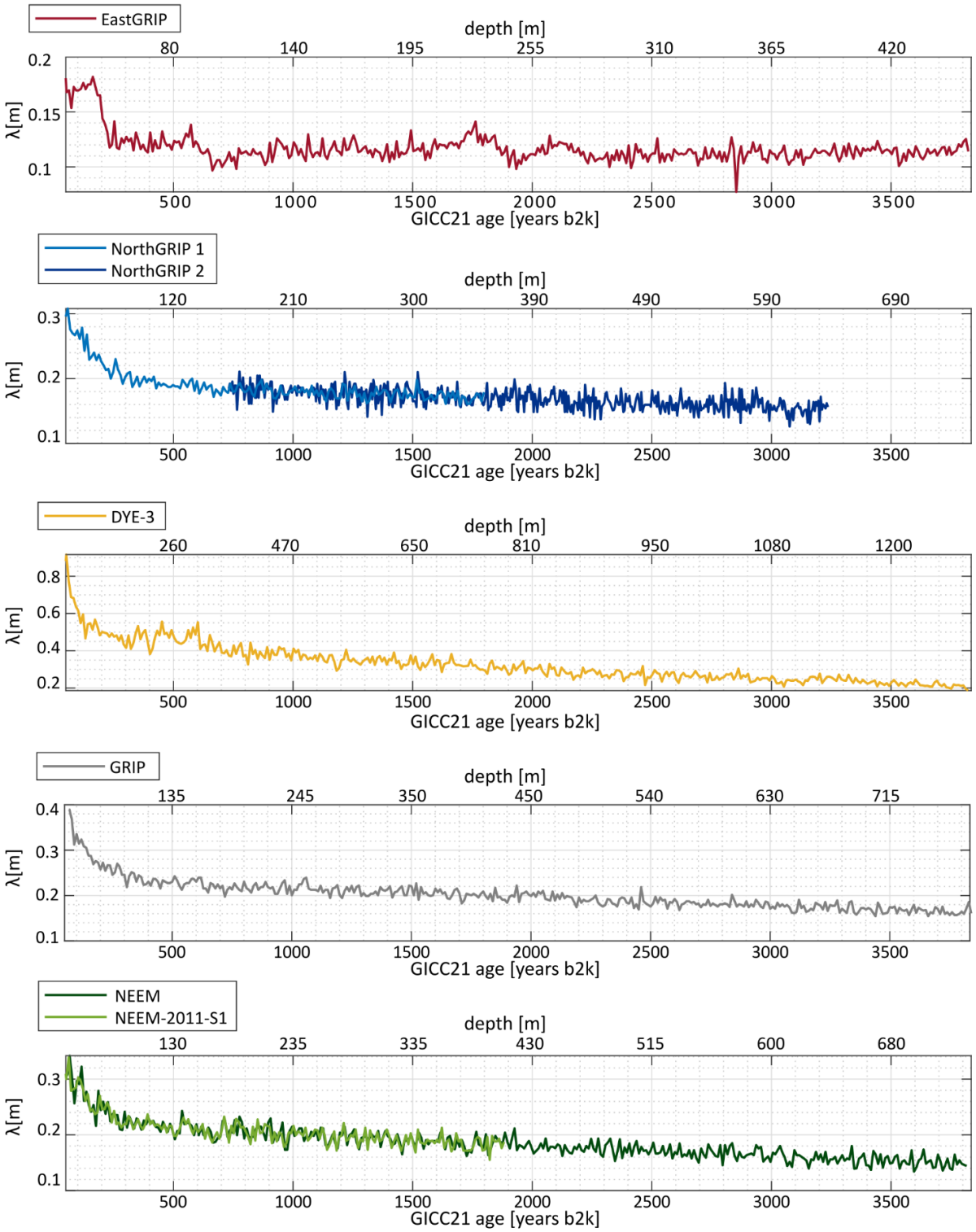

Figure 3.16 The layer thickness of all ice cores from the GICC21 timescale, which provides the basis for reconstructing the accumulation rate of Greenlandic ice cores (Andersen, et al., 2006).

To retrieve the accumulation from the layer thicknesses, one needs to account for thinning due to flow and to model the firn densification. For DYE-3 and EastGRIP, in particular, upstream effects also need to be accounted for, because of high surface velocities that transported the ice away from its original deposition location (Gerber et al., 2021).

EastGRIP exhibits some thickness fluctuations, not only in the very top, but also around 1700 and 2100 years b2k, that will need to be interpreted in view of the high flow speed this core is subjected to, and the potentially complex deformation history for ice coming from upstream, especially if the ice has crossed the shear margins (Gerber et al., 2021). On average, EastGRIP displays an almost constant layer thickness of about 0.11 m, which is an effect of a balance between layer thinning and increased upstream accumulation. For all other cores, the annual layer thicknesses below the firn zone essentially decrease linearly with depth as expected by simple flow models. We again observe the layer thickness fluctuation of DYE-3 at around 500 years b2k. The layer thickness profiles for closely located ice cores are naturally very similar.

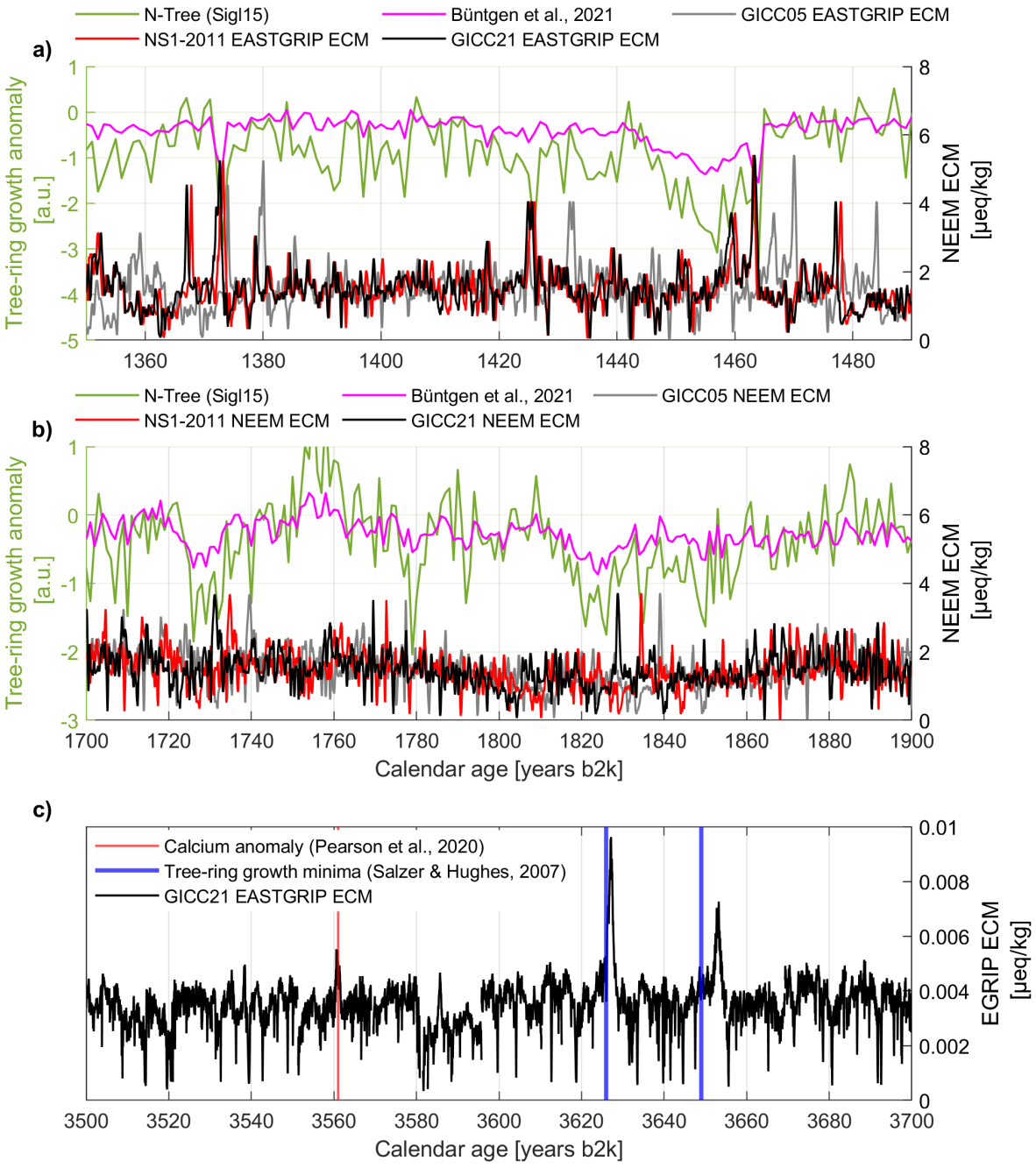

Figure 3.17 (previous page) Comparison of ice-core ECM (NEEM), shifted according to the three compared ice-core timescales, to the N-Tree growth-anomaly record provided in Sigl et al. (2015) and to the average temperature reconstruction by Büntgen et al. (2021).
(a) Between 1360 and 1480 years b2k, we observed good alignment of the ECM-stack with N-Tree local minima, except for when the ice cores are plotted according to GICC05. This fact links the volcanic eruptions evidenced in the Greenland ice sheet with Northern-Hemisphere post-eruption cooling.
(b) In the period 1700-1900, the three timescales do not coincide, as can be observed by the relative delay of the ECM curves.
Some clear N-tree minima are observed here, although the GICC21 peaks (black) are not as clearly related to the minima as in panel a. Two ECM peaks appear somewhat closer to the temperature minima at 1730 and at 1820 years b2k.
(c) The ice-core ECM (EastGRIP) compares well to discrete evidence of tree-ring cooling. One example is the calcium anomaly (star) measured by Pearson et al. in a sample from Turkey, speculated to be linked to the eruption of Thera, Santorini. The other two examples are tree-ring growth minima observed in the North American record by Salzer and Hughes.

3.15 References

Abbott, P. M., & Davies, S. M. Volcanism and the Greenland ice-cores: the tephra record. Earth-Science Reviews, 115(3), 173-191. https://doi.org/10.1016/j.earscirev.2012.09.001, 2012

Abbott, P. M., Jensen, B. J., Lowe, D. J., Suzuki, T., & Veres, D. Crossing new frontiers: extending tephrochronology as a global geoscientific research tool. 10.1002/jqs.3184, 2020

Adolphi, F., & Muscheler, R. Synchronizing the Greenland ice core and radiocarbon timescales over the Holocene–Bayesian wiggle-matching of cosmogenic radionuclide records. Climate of the Past, 12, 15–30. doi:10.5194/cp-12-15-2016, 2016

Adolphi, F., Bronk Ramsey, C., Erhardt, T., Edwards, R. L., Cheng, H., Turney, C. S., . . . others. Connecting the Greenland ice-core and U/ Th timescales via cosmogenic radionuclides: testing the synchronicity of Dansgaard–Oeschger events. Climate of the Past, 14, 1755–1781. https://doi.org/10.5194/cp-14-1755-2018, 2018

Ahlstrøm, A. P., van As, D., Citterio, M., Andersen, S. B., Fausto, R. S., Andersen, M. L., ... & Kristensen, S. S. A new Programme for Monitoring the Mass Loss of the Greenland Ice Sheet. In AGU Fall Meeting Abstracts (Vol. 2007, pp. C11A-0083). https://doi.org/10.34194/geusb.v15.5045 , 2007

Andersen, K. K., Svensson, A., Johnsen, S. J., Rasmussen, S. O., Bigler, M., Röthlisberger, R., . . . others. The Greenland ice core chronology 2005, 15–42 ka. Part 1: constructing the time scale. Quaternary Science Reviews, 25, 3246–3257. https://doi.org/10.1016/j.quascirev.2006.08.002, 2006

Baillie, M. G. Proposed re-dating of the European ice core chronology by seven years prior to the 7th century AD. Geophysical Research Letters, 35(15). https://doi.org/10.1029/2008GL034755, 2008

Baillie, M. G. Volcanoes, ice-cores and tree-rings: one story or two?. Antiquity, 84(323), 202-215. https://doi.org/10.1017/S0003598X00099877, 2010

Barbante, C., Kehrwald, N. M., Marianelli, P., Vinther, B. M., Steffensen, J. P., Cozzi, G., . . . Siggaard-Andersen, M.-L. Greenland ice core evidence of the 79 AD Vesuvius eruption. Climate of the Past, 9, 1221–1232. https://doi.org/10.5194/cp-9-1221-2013 , 2013

Beer, J., Finkel, R. C., Bonani, G., Gäggeler, H., Görlach, U., Jacob, P., ... & Wölfli, W. Seasonal variations in the concentration of 10Be, Cl−, NO3−, SO42−, H2O2, 210Pb, 3H, mineral dust, and σ18O in Greenland

snow. Atmospheric Environment. Part A. General Topics, 25(5-6), 899-904. https://doi.org/10.1016/0960-1686(91)90131-P, 1991

Bourne, A. J., Cook, E., Abbott, P. M., Seierstad, I. K., Steffensen, J. P., Svensson, A., ... & Davies, S. M. A tephra lattice for Greenland and a reconstruction of volcanic events spanning 25–45 ka b2k. Quaternary Science Reviews, 118, 122-141. https://doi.org/10.1016/j.jvolgeores.2014.09.006, 2015

Bronk Ramsey, C. Radiocarbon dating: revolutions in understanding. Archaeometry, 50(2), 249-275. https://doi.org/10.1111/j.1475-4754.2008.00394.x, 2008

Büntgen, U., Allen, K., Anchukaitis, K. J., Arseneault, D., Boucher, É., Bräuning, A., ... & Esper, J. The influence of decision-making in tree ring-based climate reconstructions. Nature communications, 12(1), 1-10. https://doi.org/10.1038/s41467-021-23627-6, 2021

Clausen, H. B., & Hammer, C. U. The Laki and Tambora eruptions as revealed in Greenland ice cores from 11 locations. Annals of Glaciology, 10, 16-22. https://doi.org/10.1017/s0260305500004092, 1988

Clausen, H. B., Hammer, C. U., Hvidberg, C. S., Dahl-Jensen, D., Steffensen, J. P., Kipfstuhl, J., & Legrand, M. A comparison of the volcanic records over the past 4000 years from the Greenland Ice Core Project and Dye 3 Greenland ice cores. Journal of Geophysical Research: Oceans, 102(C12), 26707-26723. https://doi.org/10.1029/97JC00587, 1997

Cook, E., Portnyagin, M., Ponomareva, V., Bazanova, L., Svensson, A., & Garbe-Schönberg, D. First identification of cryptotephra from the Kamchatka Peninsula in a Greenland ice core: Implications of a widespread marker deposit that links Greenland to the Pacific northwest. Quaternary Science Reviews, 181, 200-206. https://doi.org/10.1016/j.quascirev.2017.11.036, 2018a

Cook, E., Davies, S. M., Guðmundsdóttir, E. R., Abbott, P. M., & Pearce, N. J. First identification and characterization of Borrobol-type tephra in the Greenland ice cores: new deposits and improved age estimates. Journal of quaternary science, 33(2), 212-224. https://doi.org/10.1002/jqs.3016, 2018b

Coulter, S. E., Pilcher, J. R., Plunkett, G., Baillie, M., Hall, V. A., Steffensen, J. P., . . . Johnsen, S. J. Holocene tephras highlight complexity of volcanic signals in Greenland ice cores. Journal of Geophysical Research: Atmospheres, 117 (D21). https://doi.org/10.1029/2012jd017698, 2012

Dahl-Jensen, D., Albert, M. R., Aldahan, A., Azuma, N., Balslev-Clausen, D., Baumgartner, M., ... & Zheng, J. Eemian interglacial reconstructed from a Greenland folded ice core. Nature, 493(7433), 489-494. https://doi.org/10.1038/nature11789, 2013

Dahl-Jensen, D., Gundestrup, N. S., Miller, H., Watanabe, O., Johnsen, S. J., Steffensen, J. P., . . . Larsen, L. B. The NorthGRIP deep drilling programme. Annals of Glaciology, 35, 1–4. https://doi.org/10.3189/172756402781817275, 2002

Dansgaard, W., et al., Evidence for general instability of past climate from a 250-kyr ice-core record, Nature, 364, 218–220 https://doi.org/10.1038/364218a0, 1993

Dansgaard, W., Johnsen, S. J., Clausen, H. B., Dahl-Jensen, D., Gundestrup, N. S., Hammer, C. U., ... & Bond, G. Evidence for general instability of past climate from a 250-kyr ice-core record. nature, 364(6434), 218-220. https://doi.org/10.1038/364218a0, 1993

Dansgaard, W., Johnsen, S. J., Clausen, H. B., Dahl-Jensen, D., Gundestrup, N. S., Hammer, C. U., ... & Bond, G. Evidence for general instability of past climate from a 250-kyr ice-core record. nature, 364(6434), 218-220. https://doi.org/10.1038/364218a0, 1993

Erhardt, T., Jensen, C. M., Borovinskaya, O., & Fischer, H. Single particle characterization and total elemental concentration measurements in polar ice using continuous flow analysis-inductively coupled plasma time-of-flight mass spectrometry. Environmental science & technology, 53, 13275–13283. https://doi.org/10.1021/acs.est.9b03886, 2019

Erhardt, T., Bigler, M., Federer, U., Gfeller, G., Leuenberger, D., Stowasser, O., ... & Fischer, H. High resolution aerosol concentration data from the Greenland NorthGRIP and NEEM deep ice cores. Earth System Science Data Discussions, 1-25. https://doi.org/10.5194/essd-2021-324, 2021

Faïn, X., Chappellaz, J., Rhodes, R. H., Stowasser, C., Blunier, T., McConnell, J. R., . . . others. High resolution measurements of carbon monoxide along a late Holocene Greenland ice core: evidence for in situ production. Climate of the Past, 10, 987–1000. https://doi.org/10.5194/cp-10-987-2014, 2014

Fiacco Jr, R. J., Thordarson, T., Germani, M. S., Self, S., Palais, J. M., Whitlow, S., & Grootes, P. M. Atmospheric aerosol loading and transport due to the 1783-84 Laki eruption in Iceland, interpreted from ash particles and acidity in the GISP2 ice core. Quaternary Research, 42(3), 231-240. doi: 10.1006/qres.1994.1074, 1994

Fischer, H., Schüpbach, S., Gfeller, G., Bigler, M., Röthlisberger, R., Erhardt, T., . . . Wolff, E. 0). Millennial changes in North American wildfire and soil activity over the last glacial cycle. Nature Geoscience, 8(9), 723-727. https://doi.org/10.1038/ngeo2495, 2015

Fischer, H., Werner, M., Wagenbach, D., Schwager, M., Thorsteinnson, T., Wilhelms, F., ... & Sommer, S. Little ice age clearly recorded in northern Greenland ice cores. Geophysical Research Letters, 25(10), 1749-1752. https://doi.org/10.1029/98GL01177, 1998

Fuhrer, K., Neftel, A., Anklin, M., Staffelbach, T., & Legrand, M. High-resolution ammonium ice core record covering a complete glacial-interglacial cycle. Journal of Geophysical Research: Atmospheres, 101(D2), 4147-4164. https://doi.org/10.1029/95JD02903, 1996

Fuhrer, K., Wolff, E. W., & Johnsen, S. J. Timescales for dust variability in the Greenland Ice Core Project (GRIP) ice core in the last 100,000 years. Journal of Geophysical Research: Atmospheres, 104, 31043–31052. https://doi.org/10.1029/1999jd900929, 1999

Gautier, E., Savarino, J., Erbland, J., Lanciki, A., & Possenti, P. Variability of sulfate signal in ice core records based on five replicate cores. Climate of the Past, 12(1), 103-113. https://doi.org/10.5194/cp-12-103-2016, 2016

Geng, L., Alexander, B., Cole-Dai, J., Steig, E. J., Savarino, J., Sofen, E. D., & Schauer, A. J. Nitrogen isotopes in ice core nitrate linked to anthropogenic atmospheric acidity change. Proceedings of the National Academy of Sciences, 111(16), 5808-5812. https://doi.org/10.1073/pnas.1319441111, 2014

Gerber, T. A., Hvidberg, C. S., Rasmussen, S. O., Franke, S., Sinnl, G., Grinsted, A., . . . Dahl-Jensen, D. Upstream flow effects revealed in the EastGRIP ice core using a Monte Carlo inversion of a two-dimensional ice-flow model. The Cryosphere Discussions, 1–32. https://doi.org/10.5194/tc-15-3655-2021, 2021

Gfeller, G., Fischer, H., Bigler, M., Schüpbach, S., Leuenberger, D., & Mini, O. Representativeness and seasonality of major ion records derived from NEEM firn cores. The Cryosphere, 8(5), 1855-1870. https://doi.org/10.5194/tc-8-1855-2014, 2014

Gkinis, V, Simonsen, SB, Buchardt, SL, White, JWC and Vinther, BM ater isotope diffusion rates from the NorthGRIP ice core for the last 16 000 years – Glaciological and paleoclimatic implications. Earth and Planetary Science Letters 405(0), 132–141. doi: 10.1016/j.epsl.2014.08.022, 2014

Grieman, M. M., Aydin, M., Isaksson, E., Schwikowski, M., & Saltzman, E. S. Aromatic acids in an Arctic ice core from Svalbard: a proxy record of biomass burning. Climate of the Past, 14(5), 637-651. https://doi.org/10.5194/cp-14-637-2018, 2018

Grönvold, K., Óskarsson, N., Johnsen, S. J., Clausen, H. B., Hammer, C. U., Bond, G., & Bard, E. Ash layers from Iceland in the Greenland GRIP ice core correlated with oceanic and land sediments. Earth and Planetary Science Letters, 135(1-4), 149-155. https://doi.org/10.1016/0012-821X(95)00145-3, 1995

Guillet, S., Corona, C., Ludlow, F., Oppenheimer, C., & Stoffel, M. Climatic and societal impacts of a “forgotten” cluster of volcanic eruptions in 1108-1110 CE. Scientific reports, 10(1), 1-10. https://doi.org/10.1038/s41598-020-63339-3, 2020

Hammer, C. U. Acidity of polar ice cores in relation to absolute dating, past volcanism, and radio–echoes. Journal of Glaciology, 25(93), 359-372. https://doi.org/10.1017/s0022143000015227, 1980

Helama, S., Seppä, H., Bjune, A. E., & Birks, H. J. Fusing pollen-stratigraphic and dendroclimatic proxy data to reconstruct summer temperature variability during the past 7.5 ka in subarctic Fennoscandia. Journal of Paleolimnology, 48, 275–286. https://doi.org/10.1007/s10933-012-9598-1, 2012

Herron, M. M. Impurity sources of F−, Cl−, NO3− and SO4 2− in Greenland and Antarctic precipitation. Journal of Geophysical Research: Oceans, 87(C4), 3052-3060. https://doi.org/10.1029/JC087iC04p03052, 1982

Johnsen, S. Stable isotope homogenization of polar firn and ice. Proc. of Symp. on Isotopes and Impurities in Snow and Ice, Int. Ass. of Hydrol. Sci., Commission of Snow and Ice, I.U.G.G. XVI, General Assembly, Grenoble Aug.—Sept, 1975, IAHS-AISH Publ., 388–392.Retrieved from: http://hydrologie.org/redbooks/a118/iahs_118_0210.pdf, 1977

Johnsen, S. J., Dansgaard, W., & White, J. W. The origin of Arctic precipitation under present and glacial conditions. Tellus B: Chemical and Physical Meteorology, 41, 452–468. https://doi.org/10.1111/j.1600-0889.1989.tb00321.x, 1989

Johnsen, S. J., Clausen, H. B., Dansgaard, W., Fuhrer, K., Gundestrup, N., Hammer, C. U., . . . others. Irregular glacial interstadials recorded in a new Greenland ice core. Nature, 359, 311–313. https://doi.org/10.1038/359311a0, 1992

Johnsen, S. J., Clausen, H. B., Cuffey, K. M., Hoffmann, G., Schwander, J., & Creyts, T. Diffusion of stable isotopes in polar firn and ice: the isotope effect in firn diffusion. Physics of ice core records, (pp. 121–140). doi:10.1144/jgs2013-113, 2000

Johnsen, S. J., Dahl-Jensen, D., Gundestrup, N., Steffensen, J. P., Clausen, H. B., Miller, H., . . . White, J. Oxygen isotope and palaeotemperature records from six Greenland ice-core stations: Camp Century, Dye-3, GRIP, GISP2, Renland and NorthGRIP. Journal of Quaternary Science: Published for the Quaternary Research Association, 16, 299–307. https://doi.org/10.1002/jqs.622, 2001

Jouzel, J., Alley, R. B., Cuffey, K. M., Dansgaard, W., Grootes, P., Hoffmann, G., ... & White, J. Validity of the temperature reconstruction from water isotopes in ice cores. Journal of Geophysical Research: Oceans, 102(C12), 26471-26487. https://doi.org/10.1029/97JC01283, 1997

Kaufmann, P. R., Federer, U., Hutterli, M. A., Bigler, M., Schüpbach, S., Ruth, U., ... & Stocker, T. F. An improved continuous flow analysis system for high-resolution field measurements on ice cores. Environmental science & technology, 42(21), 8044-8050. https://doi.org/10.1021/es8007722, 2008

Laepple, T., Münch, T., Casado, M., Hoerhold, M., Landais, A., & Kipfstuhl, S. On the similarity and apparent cycles of isotopic variations in East Antarctic snow pits. The Cryosphere, 12(1), 169-187. https://doi.org/10.5194/tc-12-169-2018, 2018

Langway, C.C., Oeschger, H. and Dansgaard, W. In: The Greenland Ice Sheet Program in perspective. American Geophysical Union, Washington D.C. 33: 5-8. doi: 10.1029/GM033p0001., 1985

Lavigne, F., Degeai, J. P., Komorowski, J. C., Guillet, S., Robert, V., Lahitte, P., ... & de Belizal, E. Source of the great AD 1257 mystery eruption unveiled, Samalas volcano, Rinjani Volcanic Complex, Indonesia. Proceedings of the National Academy of Sciences, 110(42), 16742-16747. https://doi.org/10.1073/pnas.1307520110, 2013

Legrand, M., McConnell, J., Fischer, H., Wolff, E. W., Preunkert, S., Arienzo, M., ... & Flannigan, M. Boreal fire records in Northern Hemisphere ice cores: a review. Climate of the Past, 12(10), 2033-2059. https://doi.org/10.5194/cp-12-2033-2016, 2016

Lin, J., Svensson, A., Hvidberg, C. S., Lohmann, J., Kristiansen, S., Dahl-Jensen, D., ... & Mulvaney, R. Magnitude, frequency and climate forcing of global volcanism during the last glacial period as seen in Greenland and Antarctic ice cores (60–9 ka). Climate of the Past Discussions, 1-45. https://doi.org/10.5194/cp-18-485-2022, 2021

Lohne, Ø. S., Mangerud, J. A. N., & Birks, H. H. Precise 14 C ages of the Vedde and Saksunarvatn ashes and the Younger Dryas boundaries from western Norway and their comparison with the Greenland Ice Core (GICC 05) chronology. Journal of Quaternary Science, 28(5), 490-500. https://doi.org/10.1002/jqs.2640, 2013

McAneney, J., & Baillie, M. Absolute tree-ring dates for the Late Bronze Age eruptions of Aniakchak and Thera in light of a proposed revision of ice-core chronologies. Antiquity, 93(367), 99-112. https://doi.org/10.15184/aqy.2018.165, 2019

McConnell, R. J., Wilson, A. I., Stohl, A., Arienzo, M. M., Chellman, N. J., Eckhardt, S., . . . Steffensen, J. P. Lead pollution recorded in Greenland ice indicates European emissions tracked plagues, wars, and imperial expansion during antiquity. Proceedings of the National Academy of Sciences, 115, 5726–5731. https://doi.org/10.1073/pnas.1721818115, 2018

McConnell, J. R., Sigl, M., Plunkett, G., Burke, A., Kim, W. M., Raible, C. C., ... & Steffensen, J. P. Extreme climate after massive eruption of Alaska's Okmok volcano in 43 BCE and effects on the late Roman Republic and Ptolemaic Kingdom. Proceedings of the National Academy of Sciences, 117(27), 15443-15449. https://doi.org/10.1073/pnas.2002722117, 2020

McGwire, K. C., McConnell, J. R., Alley, R. B., Banta, J. R., Hargreaves, G. M., & Taylor, K. C. Dating annual layers of a shallow Antarctic ice core with an optical scanner. Journal of Glaciology, 54(188), 831-838. https://doi.org/10.3189/002214308787780021t, 2008

Meese, D. A., Gow, A. J., Alley, R. B., Zielinski, G. A., Grootes, P. M., Ram, M., ... & Bolzan, J. F. The Greenland Ice Sheet Project 2 depth-age scale: methods and results. Journal of Geophysical Research: Oceans, 102(C12), 26411-26423. https://doi.org/10.1029/97JC00269, 1997

Mekhaldi, F., Muscheler, R., Adolphi, F., Aldahan, A., Beer, J., McConnell, J. R., ... & Woodruff, T. E. Multiradionuclide evidence for the solar origin of the cosmic-ray events of AD 774/5 and 993/4. Nature communications, 6(1), 1-8. https://doi.org/10.1038/ncomms9611, 2015

Mojtabavi, S., Wilhelms, F., Cook, E., Davies, S., Sinnl, G., Skov Jensen, M., . . . Rasmussen, S. 1). A first chronology for the East Greenland Ice-core Project (EGRIP) over the Holocene and last glacial termination. Climate of the Past, 16(6). https://doi.org/10.5194/cp-16-2359-2020, 2020

Mojtabavi, S., Eisen, O., Franke, S., Jansen, D., Steinhage, D., Paden, J., . . . Wilhelms, F. Origin of englacial stratigraphy at three deep ice core sites of the Greenland Ice Sheet by synthetic radar modelling. Journal of Glaciology, 1-13. doi:10.1017/jog.2021.137, 2022

Mosley-Thompson, E., McConnell, J. R., Bales, R. C., Li, Z., Lin, P. N., Steffen, K., ... & Bathke, D. Local to regional-scale variability of annual net accumulation on the Greenland ice sheet from PARCA cores. Journal of Geophysical Research: Atmospheres, 106(D24), 33839-33851. https://doi.org/10.1029/2001JD900067, 2001

Muscheler, R. 14C and 10Be around 1650 cal BC. In W. David A. (Ed.), Time's up!: dating the Minoan eruption of Santorini (Vol. 10, pp. 275-284). Danish Institute at Athens. Retrieved from: https://tidsskrift.dk/MoDIA/article/view/126707, 2009

Muscheler, R., Beer, J., Wagner, G., Laj, C., Kissel, C., Raisbeck, G. M., ... & Kubik, P. W. Changes in the carbon cycle during the last deglaciation as indicated by the comparison of 10Be and 14C records. Earth and Planetary Science Letters, 219(3-4), 325-340. doi:10.1016/s0012-821x(03)00722-2, 2004

Muscheler, R., Beer, J., Kubik, P. W., & Synal, H. A. Geomagnetic field intensity during the last 60,000 years based on 10Be and 36Cl from the Summit ice cores and 14C. Quaternary Science Reviews, 24(16-17), 1849-1860. https://doi.org/10.1016/j.quascirev.2005.01.012, 2005

Muscheler, R., Adolphi, F., & Knudsen, M. Assessing the differences between the IntCal and Greenland ice-core time scales for the last 14,000 years via the common cosmogenic radionuclide variations. Quaternary Science Reviews, 106, 81-87.http://dx.doi.org/10.1016/j.quascirev.2014.08.017, 2014

Muscheler, R., Adolphi, F., Heaton, T. J., Ramsey, C. B., Svensson, A., Van Der Plicht, J., & Reimer, P. J. Testing and improving the IntCal20 calibration curve with independent records. Radiocarbon, 62, 1079–1094. https://doi.org/10.1017/rdc.2020.54, 2020

Nakagawa, T., Tarasov, P., Staff, R., Ramsey, C. B., Marshall, M., Schlolaut, G., ... & Yasuda, Y. The spatio-temporal structure of the Lateglacial to early Holocene transition reconstructed from the pollen record of Lake Suigetsu and its precise correlation with other key global archives: Implications for palaeoclimatology and archaeology. Global and Planetary Change, 103493. https://doi.org/10.1016/j.gloplacha.2021.103493, 2021

NEEM community members. Eemian interglacial reconstructed from a Greenland folded ice core. Nature 493, 489–494 https://doi.org/10.1038/nature11789, 2013

Neff, P. D. A review of the brittle ice zone in polar ice cores. Annals of Glaciology, 55(68), 72-82. doi:10.3189/2014AoG68A023, 2014

Neftel, A., Moor, E., Oeschger, H., & Stauffer, B. Evidence from polar ice cores for the increase in atmospheric CO2 in the past two centuries. Nature, 315(6014), 45-47. https://doi.org/10.1038/315045a0, 1985

North Greenland Ice Core Project members. High resolution record of Northern Hemisphere climate extending into the last interglacial period. Nature, 431(7005), 147-151. https://doi.org/10.1038/nature02805, 2004

O'Hare, P., Mekhaldi, F., Adolphi, F., Raisbeck, G., Aldahan, A., Anderberg, E., ... & ASTER Team. Multiradionuclide evidence for an extreme solar proton event around 2,610 BP (~ 660 BC). Proceedings of the National Academy of Sciences, 116(13), 5961-5966. https://doi.org/10.1073/pnas.1815725116, 2019

Palais, J. M., Germani, M. S., & Zielinski, G. A. Inter-hemispheric transport of volcanic ash from a 1259 AD volcanic eruption to the Greenland and Antarctic ice sheets. Geophysical Research Letters, 19(8), 801-804. https://doi.org/10.1029/92GL00240, 1992

Palais, J. M., Taylor, K., Mayewski, P. A., & Grootes, P. Volcanic ash from the 1362 AD Oraefajokull eruption (Iceland) in the Greenland ice sheet. Geophysical Research Letters, 18(7), 1241-1244. https://doi.org/10.1029/91GL01557, 1991

Park, J., Southon, J., Fahrni, S., Creasman, P., & Mewaldt, R. Relationship between solar activity and Δ14C peaks in AD 775, AD 994, and 660 BC. Radiocarbon, 59(4), 1147-1156. doi:10.1017/RDC.2017.59, 2017

Pearce, N. J., Westgate, J. A., Preece, S. J., Eastwood, W. J., & Perkins, W. T. Identification of Aniakchak (Alaska) tephra in Greenland ice core challenges the 1645 BC date for Minoan eruption of Santorini. Geochemistry, Geophysics, Geosystems, 5. https://doi.org/10.1029/2003gc000672, 2004

Pearson, C., Salzer, M., Wacker, L., Brewer, P., Sookdeo, A., & Kuniholm, P. Securing timelines in the ancient Mediterranean using multiproxy annual tree-ring data. Proceedings of the National Academy of Sciences, 117(15), 8410-8415. https://doi.org/10.1073/pnas.1917445117, 2020

Pedro, J. B., Jochum, M., Buizert, C., He, F., Barker, S., & Rasmussen, S. O. Beyond the bipolar seesaw: Toward a process understanding of interhemispheric coupling. Quaternary Science Reviews, 192, 27-46. https://doi.org/10.1016/j.quascirev.2018.05.005, 2018

Plunkett, G., Sigl, M., Schwaiger, H., Tomlinson, E., Toohey, M., McConnell, J. R., . . . Siebe, C. No evidence for tephra in Greenland from the historic eruption of Vesuvius in 79 CE: Implications for geochronology and paleoclimatology. Climate of the Past Discussions, 1–37. https://doi.org/10.5194/cp-2021-63, 2021

Qiao, J., Colgan, W., Jakobs, G., & Nielsen, S. High-Resolution Tritium Profile in an Ice Core from Camp Century, Greenland. Environmental Science & Technology, 55(20), 13638-13645. https://doi.org/10.1021/acs.est.1c01975, 2021

Rasmussen, S. O., Andersen, K. K., Svensson, A. M., Steffensen, J. P., Vinther, B. M., Clausen, H. B., . . . others. A new Greenland ice core chronology for the last glacial termination. Journal of Geophysical Research: Atmospheres, 111. https://doi.org/10.1029/2005JD006079, 2006

Rasmussen, S. O., Seierstad, I. K., Andersen, K. K., Bigler, M., Dahl-Jensen, D., & Johnsen, S. J. Synchronization of the NGRIP, GRIP, and GISP2 ice cores across MIS 2 and palaeoclimatic implications. Quaternary Science Reviews, 27, 18–28. https://doi.org/10.1016/j.quascirev.2007.01.016, 2008

Rasmussen, S. O., Abbott, P. M., Blunier, T., Bourne, A. J., Brook, E., Buchardt, S. L., . . . others. A first chronology for the North Greenland Eemian Ice Drilling (NEEM) ice core. Climate of the Past, 9, 2713–2730. https://doi.org/10.5194/cp-9-2713-2013, 2013

Reimer, P. J., Bard, E., Bayliss, A., Beck, J. W., Blackwell, P. G., Ramsey, C. B., ... & Van Der Plicht, J. IntCal13 and Marine13 radiocarbon age calibration curves 0–50,000 years cal BP. radiocarbon, 55(4), 1869-1887. doi:10.2458/azu_js_rc.55.16947, 2013

Reimer, P. J., Austin, W. E., Bard, E., Bayliss, A., Blackwell, P. G., Ramsey, C. B., . . . others. The IntCal20 Northern Hemisphere radiocarbon age calibration curve (0–55 cal kBP). Radiocarbon, 62, 725–757. https://doi.org/10.1017/rdc.2020.41, 2020

Rhodes, R. H., Yang, X., & Wolff, E. W. Sea ice versus storms: what controls sea salt in arctic ice cores? Geophysical Research Letters, 45, 5572–5580. https://doi.org/10.1029/2018gl077403, 2018

Robock, A., & Free, M. P. Ice cores as an index of global volcanism from 1850 to the present. Journal of Geophysical Research: Atmospheres, 100(D6), 11549-11567. https://doi.org/10.1029/95JD00825, 1995

Röthlisberger, R., Mulvaney, R., Wolff, E. W., Hutterli, M. A., Bigler, M., Sommer, S., & Jouzel, J. Dust and sea salt variability in central East Antarctica (Dome C) over the last 45 kyrs and its implications for southern high-latitude climate. Geophysical Research Letters, 29(20), 24-1. https://doi.org/10.1029/2002GL015186, 2002

Sakurai, H., Tokanai, F., Miyake, F., Horiuchi, K., Masuda, K., Miyahara, H., ... & Moriya, T. Prolonged production of 14C during the~ 660 BCE solar proton event from Japanese tree rings. Scientific reports, 10(1), 1-7. https://doi.org/10.1038/s41598-019-57273-2, 2020

Salzer, M. W., & Hughes, M. K. Bristlecone pine tree rings and volcanic eruptions over the last 5000 yr. Quaternary Research, 67, 57–68. https://doi.org/10.1016/j.yqres.2006.07.004, 2007

Seierstad, I. K., Abbott, P. M., Bigler, M., Blunier, T., Bourne, A. J., Brook, E., ... & Vinther, B. M. Consistently dated records from the Greenland GRIP, GISP2 and NGRIP ice cores for the past 104 ka reveal regional millennial-scale δ18O gradients with possible Heinrich event imprint. Quaternary Science Reviews, 106, 29-46. https://doi.org/10.1016/j.quascirev.2014.10.032, 2014

Sigl, M., McConnell, J. R., Layman, L., Maselli, O., McGwire, K., Pasteris, D., . . . others. A new bipolar ice core record of volcanism from WAIS Divide and NEEM and implications for climate forcing of the last 2000 years. Journal of Geophysical Research: Atmospheres, 118, 1151–1169. https://doi.org/10.1029/2012jd018603, 2013

Sigl, M., Winstrup, M., McConnell, J. R., Welten, K. C., Plunkett, G., Ludlow, F., … Woodruff, T. E. Timing and climate forcing of volcanic eruptions for the past 2,500 years. Nature, 523(7562), 543–549. https://doi.org/10.1038/nature14565 , 2015

Sigl, M., Fudge, T. J., Winstrup, M., Cole-Dai, J., Ferris, D., McConnell, J. R., ... & Sowers, T. A. The WAIS Divide deep ice core WD2014 chronology–Part 2: Annual-layer counting (0–31 ka BP). Climate of the Past, 12(3), 769-786. https://doi.org/10.5194/cp-12-769-2016, 2016

Sjolte, J., Sturm, C., Adolphi, F., Vinther, B. M., Werner, M., Lohmann, G., & Muscheler, R. Solar and volcanic forcing of North Atlantic climate inferred from a process-based reconstruction. Climate of the Past, 14(8), 1179-1194. https://doi.org/10.5194/cp-14-1179-2018, 2018

Smith, C. L., Fairchild, I. J., Spötl, C., Frisia, S., Borsato, A., Moreton, S. G., & Wynn, P. M. Chronology building using objective identification of annual signals in trace element profiles of stalagmites. Quaternary Geochronology, 4(1), 11-21.http://dx.doi.org/10.1016/j.quageo.2008.06.005, 2009

Sun, C., Plunkett, G., Liu, J., Zhao, H., Sigl, M., McConnell, J. R., ... & Hall, V. Ash from Changbaishan Millennium eruption recorded in Greenland ice: implications for determining the eruption's timing and impact. Geophysical Research Letters, 41(2), 694-701. https://doi.org/10.1002/2013GL058642, 2014

Svensson, A., Andersen, K. K., Bigler, M., Clausen, H. B., Dahl-Jensen, D., Davies, S. M., ... & Vinther, B. M. A 60 000 year Greenland stratigraphic ice core chronology. Climate of the Past, 4(1), 47-57. https://doi.org/10.5194/cp-4-47-2008, 2008

Svensson, A., Dahl-Jensen, D., Steffensen, J. P., Blunier, T., Rasmussen, S. O., Vinther, B. M., ... & Bigler, M. Bipolar volcanic synchronization of abrupt climate change in Greenland and Antarctic ice cores during the last glacial period. Climate of the Past, 16(4), 1565-1580. https://doi.org/10.5194/cp-16-1565-2020, 2020

Taylor, K., Alley, R., Fiacco, J., Grootes, P., Lamorey, G., Mayewski, P., & Spencer, M. Ice-core dating and chemistry by direct-current electrical conductivity. Journal of Glaciology, 38(130), 325-332. doi:10.3189/S0022143000002215, 1992

Taylor, K. C., Lamorey, G. W., Doyle, G. A., Alley, R. B., Grootes, P. M., Mayewski, P. A., ... & Barlow, L. K. The 'flickering switch' of late Pleistocene climate change. Nature, 361(6411), 432-436. https://doi.org/10.1038/366549a0, 1993

Torbenson, M. C., Plunkett, G., Brown, D. M., Pilcher, J. R., & Leuschner, H. H. Asynchrony in key Holocene chronologies: Evidence from Irish bog pines. Geology, 43(9), 799-802. https://doi.org/10.1130/G36914.1, 2015

Vidal, C., Métrich, N., Komorowski, JC. et al. The 1257 Samalas eruption Indonesia): the single greatest stratospheric gas release of the Common Era. Sci Rep 6, 34868 (2016). https://doi.org/10.1038/srep34868, Lomb

Vinther, B. M., Johnsen, S. J., Andersen, K. K., Clausen, H. B., & Hansen, A. W. NAO signal recorded in the stable isotopes of Greenland ice cores. Geophysical Research Letters, 30(7). https://doi.org/10.1029/2002GL016193, 2003

Vinther, B., Clausen, H., Johnsen, S., Rasmussen, S., Andersen, K., Buchardt, S., . . . Heinemeier, J. A synchronized dating of three Greenland ice cores throughout the Holocene. Journal of Geophysical Research Atmospheres. https://doi.org/10.1029/2005jd006921, 2006

Vinther, B. M., Buchardt, S. L., Clausen, H. B., Dahl-Jensen, D., Johnsen, S. J., Fisher, D. A., ... & Svensson, A. M. Holocene thinning of the Greenland ice sheet. Nature, 461(7262), 385-388. https://doi.org/10.1038/nature08355, 2009

Vinther, B. M., Jones, P. D., Briffa, K. R., Clausen, H. B., Andersen, K. K., Dahl-Jensen, D., & Johnsen, S. J. Climatic signals in multiple highly resolved stable isotope records from Greenland. Quaternary Science Reviews, 29(3-4), 522-538. https://doi.org/10.1016/j.quascirev.2009.11.002, 2010

WAIS Divide Project Members. Precise interpolar phasing of abrupt climate change during the last ice age. Nature, 520(7549), 661-665. https://doi.org/10.1038/nature14401, 2015

Walker, M. J., Berkelhammer, M., Björck, S., Cwynar, L. C., Fisher, D. A., Long, A. J., ... & Weiss, H. Formal subdivision of the Holocene Series/Epoch: a Discussion Paper by a Working Group of INTIMATE (Integration of ice-core, marine and terrestrial records) and the Subcommission on Quaternary Stratigraphy (International Commission on Stratigraphy). Journal of Quaternary Science, 27(7), 649-659. https://doi.org/10.1002/jqs.2565, 2012

Warming, E., Svensson, A., Vallelonga, P., & Bigler, M. A technique for continuous detection of drill liquid in ice cores. Journal of glaciology, 59(215), 503-506. doi:10.3189/2013JoG12J124, 2013

Westhoff, J., Sinnl, G., Svensson, A., Freitag, J., Kjær, H. A., Vallelonga, P., ... & Weikusat, I. n review). Melt in the Greenland EastGRIP ice core reveals Holocene warming events. Climate of the Past Discussions, 1-36. https://doi.org/10.5194/cp-2021-89, 2021

Whitlow, S., Mayewski, P. A., & Dibb, J. E. A comparison of major chemical species seasonal concentration and accumulation at the South Pole and Summit, Greenland. Atmospheric Environment. Part A. General Topics, 26(11), 2045-2054. https://doi.org/10.1016/0960-1686(92)90089-4, 1992

Wilhelms, F., Kipfstuhl, J., Miller, H., Heinloth, K., & Firestone, J. Precise dielectric profiling of ice cores: a new device with improved guarding and its theory. Journal of Glaciology, 44(146), 171-174. https://doi.org/10.3189/S002214300000246X, 1998

Winstrup, M. An automated method for annual layer counting in ice cores: and an application to visual stratigraphy data from the ngrip ice core (Doctoral dissertation, Københavns Universitet. Niels Bohr Institutet).Retrieved from: https://nbi.ku.dk/english/theses/phd-theses/mai-winstrup/M.Winstrup2011.pdf, 2011

Winstrup, M., Svensson, A. M., Rasmussen, S. O., Winther, O., Steig, E. J., & Axelrod, A. E. An automated approach for annual layer counting in ice cores. Climate of the Past, 8(6), 1881-1895. https://doi.org/10.5194/cp-8-1881-2012, 2012

Winstrup, M., A Hidden Markov Model Approach to Infer Timescales for High-Resolution Climate Archives, Proceedings of the 30th AAAI Conference on Artificial Intelligence and the 28th Innovative Applications of Artificial Intelligence Conference, February 12 – 17,hoenix, Arizona USA, Vol. VI, 4053 (2016), 8 pages. Retrieved from https://ojs.aaai.org/index.php/AAAI/article/view/19084, 2016

Zdanowicz, C. M., Proemse, B. C., Edwards, R., Feiteng, W., Hogan, C. M., Kinnard, C., & Fisher, D. Historical black carbon deposition in the Canadian High Arctic: a> 250-year long ice-core record from Devon Island. Atmospheric Chemistry and Physics, 18(16), 12345-12361. https://doi.org/10.5194/acp-18-12345-2018, 2018

Zielinski, G. A., Mayewski, P. A., Meeker, L. D., Whitlow, S., Twickler, M. S., Morrison, M., ... & Alley, R. B. Record of volcanism since 7000 BC from the GISP2 Greenland ice core and implications for the volcano-climate system. Science, 264(5161), 948-952. doi: 10.1126/science.264.5161.948, 1994

Zielinski, G. A., Germani, M. S., Larsen, G., Baillie, M. G., Whitlow, S., Twickler, M. S., & Taylor, K. Evidence of the Eldgjá (Iceland) eruption in the GISP2 Greenland ice core: relationship to eruption processes and climatic conditions in the tenth century. The Holocene, 5(2), 129-140. https://doi.org/10.1177/095968369500500201, 1995

Zielinski, G. A., Mayewski, P. A., Meeker, L. D., Grönvold, K., Germani, M. S., Whitlow, S., ... & Taylor, K. Volcanic aerosol records and tephrochronology of the Summit, Greenland, ice cores. Journal of Geophysical Research: Oceans, 102(C12), 26625-26640. https://doi.org/10.1029/96JC03547, 1997

4 Applications of the GICC21 in the Holocene

With the GICC21 in place for the Late Holocene and with high-resolution data at hand, both from newer and older ice cores, I would like to add some research material, still in an unpublished preliminary stage, but which might be the basis for future work.
I will start with presenting some additional information about the time scale's agreement with Antarctic time scales. I will then present a study of Greenlandic climate in relation to volcanism. I will conclude the chapter describing my contribution to Paper IV about melt layers at EastGRIP. Some Supplementary Information to this chapter (sec. 4.5) is provided at the end of the chapter.

4.1 The agreement of GICC21 with Antarctic time scales

Having a bipolar record of volcanic tie points is very useful to obtain a global picture of climate. The work by Svensson et al. (2020) unfortunately only records bipolar tie points in the glacial. In the Holocene, we have access to the bipolar tie points by Sigl et al. (2015). They provide a record of volcanic eruptions with associated volcanic forcing, reported on the NS1-2011 time scale. I converted the ages to the WD2014 time scale by using a subset of tie-points reported on the WDC depths (Sigl et al., 2016). In Figure 4.1, the offset of WD2014 to GICC05 follows the ones of NS1-2011 and GICC21.
We also have access to Holocene bipolar tie points from the AICC2012 time scale (Veres et al., 2013). Their bipolar match was constructed between NorthGRIP and each of the Antarctic ice cores and used to constrain the timescale. Hence, it is not surprising that in Figure 4.1 the EDML ages are arranged around GICC05 ages, with a spread of 5-10 years. This indicates that the AICC2012 time scale, in a potential future revision, should be matched directly to the WD2014 time scale where possible.
To assess whether WD2014 and GICC21 agree further beyond 2.5 ka b2k, one would need bipolar tie points between WDC and some of the GICC21 ice cores. The bipolar signal of an eruption in ice cores can be ascertained by tephra (the only reported case of bipolar tephra is the 1257 CE Samalas eruption; Lavigne et al., 2013), by sulfate isotope analysis (Gautier et al., 2019), or by peak similarity and layer counting (Sigl et al., 2015; Svensson et al., 2020). The latter method is the easiest to apply since it mainly requires volcanic proxy records, such as ECM, and an accurate time scale. However, it also implies intrinsic uncertainties arising from the uncertainty of each time scale or from wrongly assuming regional eruptions to be

bipolar, which increase the risks of making a wrong match (Svensson et al., 2020). Hence, this method requires many iterations with multiple observers to decide on a definitive set of bipolar tie points. I did not attempt to conduct such work alone and leave it as a possible future line of research.

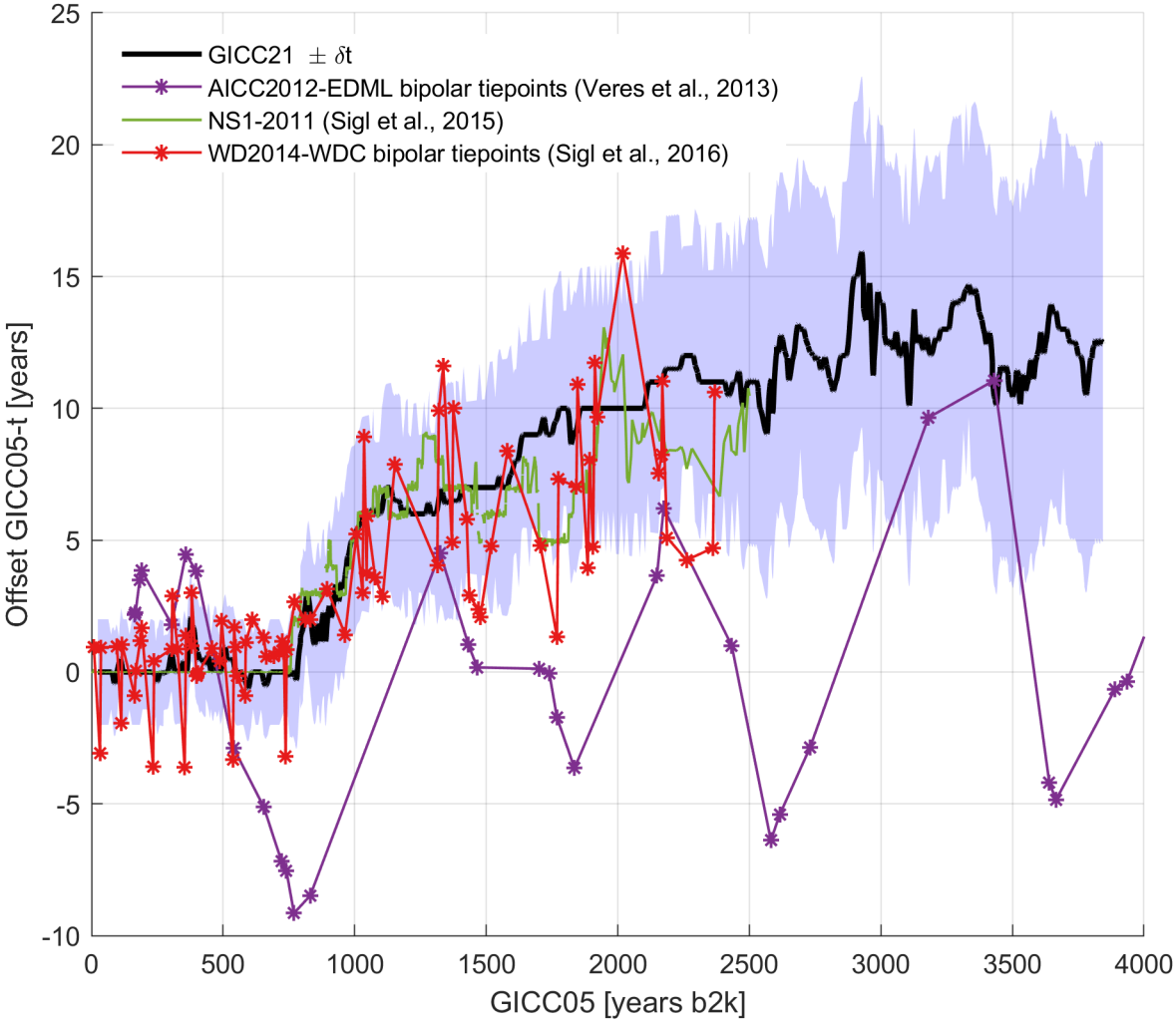

Figure 4.1 Comparison of GICC21 with Antarctic time scales.
The WD2014 time scale (red) agrees well with NS1-2011 and GICC21 until 2.5 ka b2k. The AICC2012 time scale was constrained by GICC05 tie points, the tie points (purple) oscillating around the mean with a spread of about 5-10 years.

The WD2014 chronology between 2.3 and 6 ka b2k suffers from brittle-ice issues, therefore the annual-layer count was constrained using the tree-ring chronology (Sigl et al., 2016).

Thanks to the proven adherence of GICC21 to the tree-ring chronology (Paper III), the two ice-core chronologies are likely to be compatible until 3835 years b2k.

4.2 The behavior of acidity, isotopes, and layer thickness around eruptions

A feature of the GICC21 multi-core timescale is the possibility to average the signals of all involved ice cores with annual resolution. Hence, by aligning the ice-core data on GICC21, I obtained averages of ECM, $\delta^{18}O$, and layer thickness (λ), without distinguishing the ice core's geographic location. I report more details on the stacking method in sec. 4.5.1.
After having obtained the signal stacks, the behavior of Greenlandic ice cores around volcanic eruptions can be investigated. The goal of this section is to understand how post-volcanic climate is registered over Greenland and if we can infer information about the Thera eruption.

4.2.1 Volcanic eruption sources in GICC21

As a first step, we need to understand the nature of the GICC21 volcanic tie points. Sigl et al. (2015) provide a comprehensive record of volcanic activity registered in the ice cores in the recent 2500 years. We will refer to this ensemble of volcanic eruptions as the Sigl Volcanic Forcing (SVF) dataset.

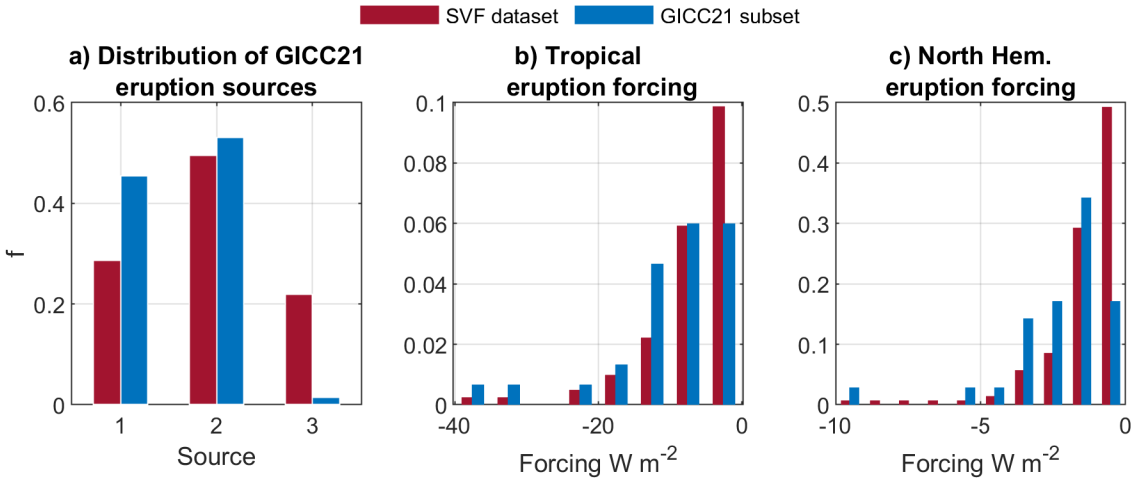

Figure 4.2 The subset of GICC21 tie points also corresponding to an SVF eruption, and analysis of the empirical distributions of volcanic forcing.

(continued caption of Figure 4.2) (a) Normalized[8] *distribution of the source of each eruption (1=tropical, 2=Northern Hemisphere, 3=Southern Hemisphere). For the SVF dataset, at least 20% of the eruptions were from source 3, while GICC21 represents sources 1 and 2, at almost equal ratios. (b) For tropical eruptions, the normalized forcing distribution of the GICC21 subset (blue) has fewer eruptions with low forcing (fewer values in right-most bin) than the SVF dataset (red), indicating that the strength of the eruption must impact the quality of the ECM peaks seen across Greenland.* (c) *An even more drastic picture as (b) can be seen for the Northern Hemisphere eruptions, where low-forcing eruptions are much less used as tie points than eruptions with medium to high forcing.*

Out of the 105 GICC21 volcanic tie points, 75 are younger than 2500 years b2k; out of these latter ones, 66 correspond to a volcanic eruption reported in SVF, representing 23% of the complete record of 283 eruptions. Based on the age proximity of the reported eruptions[9], I inferred the eruption source of our subset of tie points, i.e. if the eruption was from low-latitudes and tropical (T), from the extra-tropical Northern Hemisphere (NH), or the extra-tropical Southern Hemisphere (SH).

In Figure 4.2a, I find that the 66 GICC21 tie points are almost equally divided between T and NH eruptions, implying that both source regions are widely registered over Greenland and provide good matching possibilities for 5 distant drilling locations. In Figure 4.2b and c, I also confirm the expectation that we tend to match eruptions that have a medium to high volcanic forcing. Because for GICC21 we have focused on finding solid tie-points across ice cores, weak signals with irregular shapes were disregarded, especially if located close to better tie points.

Another criterion to evaluate before approaching any quantitative study about post-volcanic climate is the frequency of eruptions. Since we expect the influence on the climate of each eruption to be of the order of one decade (Sigl et al., 2015), we can distinguish eruptions that are clustered, i.e. having less than 10 years between them, and eruptions that are isolated and have no other eruptions in the 10 years before or after them. This criterion should be applied

[8] Normalization by the Matlab option for histogram normalization 'pdf', which computes the normalized bin-height h relative to the count c, the total number of events N, and the bin width w: $h = c/(wN)$.

[9] I first converted the NS1-2011 ages of the SVF record to GICC21 ages, in order to find the eruptions that were recorded within the same year.

irrespective of the eruption's source since it would be difficult to separate the climatic influence of each source when the eruptions happened very close to each other.

After applying the clustering criterion, I find that 55% of eruptions are isolated in the GICC21 tie point dataset by at least 10 years before and after the adjacent eruptions. However, in the SVF dataset, only 33% of eruptions are isolated. Therefore, a clustering criterion to select the isolated GICC21 tie points would, most likely, exclude many cases where the eruptions are clustered.

In conclusion, by comparing the eruptions chosen for GICC21 and the comprehensive SVF record, we can conclude that:

- Matching of many ice cores for GICC21 has naturally selected eruptions that are from tropical or northern-hemispheric origin, at about 50% balance;
- The GICC21 set of tie points represents only about 23% of the volcanic activity recorded at NEEM;
- For GICC21, we have preferably selected eruptions with higher forcing;
- The clustering criterion can only be applied using a complete record of eruptions, such as the SVF dataset.

4.2.2 Post-volcanic climate

For a study of post volcanic climate, we can select what type of eruption we would like to investigate, as there are several options. For once, we can distinguish the origin of the tie points using the SVF dataset. Alternatively, irrespectively of the origin, we can choose to separate the eruptions that are solitary from those that are clustered and only average the climate after the latter eruption of each cluster.

For the most general case, I averaged the Greenlandic stacked signals (ECM, $\delta^{18}O$, λ) around all the 105 eruptions that were identified in GICC21. In Figure 4.3, I show the stacks for 50-year windows around the eruptions. A drop, both in isotopes and layer thickness, lasts for about a decade after the eruption. To assess whether this result is significant I performed 10'000 Monte Carlo iterations in which I sampled data from 105 random ages (details of the analysis can be found in sec. 4.5.2). In each simulation, the amplitude was calculated as the difference of the mean value before and after the eruption. The duration of the minimum was calculated as the length of the longest interval of data significantly below the mean.

The empirical distribution is Gaussian for the amplitude[10], while it is similar to a Poisson distribution for the duration[11], both in the case of the $\delta^{18}O$ data and of the layer thickness. For the latter, I took the precaution of excluding the top 100-years of the chronology from the simulation, because this caused the distribution to have excessive samples in the negative tail of the Gaussian – a residual effect of firn densification.

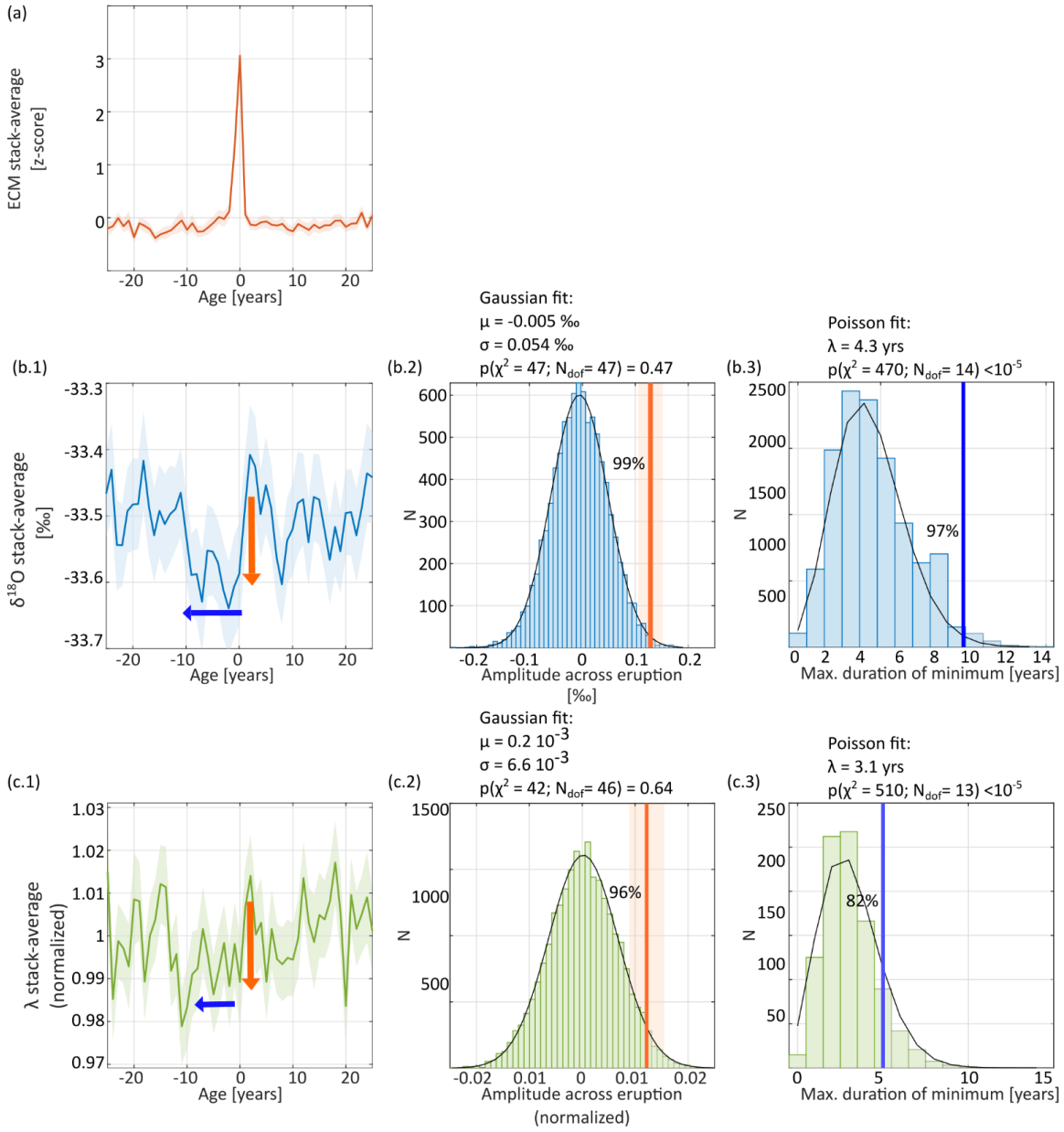

[10] The p-values of the χ^2 test of the fit are above the 0.01 threshold, hence the fit to the Gaussian distribution is accepted.

[11] The p-values of the χ^2 test of the fit are below the 0.01 threshold, but there is a good visual agreement with a Poisson distribution.

Figure 4.3 (previous page) Monte-Carlo study of post-eruptive climate in the climatic record of Greenland until 3835 years b2k.
Left-most panels: signal averages around the 105 eruptions matched in the GICC21 timescale; time is flowing from right to left. Right panels: corresponding Monte-Carlo studies of the significance of the measurement.
(a) The ECM average identifies a common feature in the shape of a sharp peak at 0 years, highlighting the common practice adopted in this work of marking the eruptions at their maximum rather than at the onset. The average duration of the peak is 3 years, starting 1 year before the maximum. (b.1) The $\delta^{18}O$ stack presents a sharp decrease of about 0.12 ‰ (orange arrow), which starts about one year before the maximum of the ECM, at the onset of the eruption. A duration of about 10 years of the post-eruption signal is observed (blue arrow). (b.2) Sampling 105 random events returns a Gaussian empirical distribution of the change of average value before and after the eruption. The measured decrease in $\delta^{18}O$ is located at the 99% percentile (orange line). (b.3) The simulation returns an almost-Poisson distribution of the duration of the minimum. The measured duration is located at the 97% percentile (blue line). (c.1) The layer thickness stack presents a decrease of about 1 % from the mean value and a duration of about 10 years, similar to the isotopic behavior. (c.2) Similar as b.2, but for the layer thickness. The measured decrease is at 96% of the distribution (orange line, shading corresponding to 2σ confidence interval for the measurement). (c.3) Similar as b.3, but for the layer thickness. The measured duration is located at the 82% percentile (blue line).

The measured decrease of $\delta^{18}O$ and layer thickness lie, respectively, at the 99% and the 96% percentiles of the empirical distributions, which I find to be a noteworthy result. The duration of dips in isotopes and layer thickness have percentile values of 97% and 82%, respectively. All findings show the rare occurrence of such a long and deep signal-drop compared to the random sample.
I repeated the study on the GICC05 data, finding non-significant results. Fewer data and a poorer alignment of the ice cores fail to show any minimum in the data (Figure 4.10 in sec. 4.5.2). Nonetheless, using data from NorthGRIP, GRIP, and DYE-3, but aligned on GICC21, I observed a shallow dip in isotopes (not shown for brevity), but not in layer thickness. I

concluded that the extensive dataset and a better alignment are both necessary for reproducing this finding.

In summary, after a volcanic eruption, without selecting the type of eruption, the $\delta^{18}O$ decrease on average by 0.12 ± 0.02 ‰, the layer thickness by 1.1 ± 0.3 % (normalized units, see stacking method in sec. 4), and both display a 10-year-long minimum.

A drop in the water isotopes is generally interpreted as a drop in the temperature, as would naturally occur after a volcanic eruption. However, a concurrent drop in accumulation indicates a more complex dynamic, as the two proxies both reflect the atmospheric impact of volcanic eruptions. Accumulation changes may be caused by a change in the frequency of precipitation events, which is the leading mode of inter-annual variability and closely linked to the NAO by the position of the NA-storm track. As highlighted in Sjolte et al. (2018), there are indications of a positive NAO index after eruptions, associated with low temperatures in Greenland. A hypothetical change in the seasonal distribution of precipitation after volcanic eruptions could even affect the $\delta^{18}O$ independently from the temperature or possibly even counterbalance any cooling, an explanation inspired by the study by He et al. (2021) on Heinrich Event 1.

4.2.3 Post-tropical eruption climate

The study of post-volcanic climate was repeated by selecting only the tropical eruptions in the SVF dataset and visualizing their signature in the stacked data as well as in the single ice cores NEEM, GRIP, and DYE-3. The results shown in Figure 4.4 are similar to what we have seen in Figure 4.3. The dips in isotopes are all about 0.2 ‰ deep and are located on the right tail of the Monte Carlo distributions of Figure 4.3. The layer thickness of DYE-3 does not drop by ~1% but the other ice cores and the stack do.

By selecting the 35 NH eruptions in GICC21, I did not observe any special feature in the averaged records, except for a 10-year drop of the isotopes at NEEM (Figure 4.11 in sec. 4.5.2). By selecting the GICC21 eruptions that are clustered, I did not observe any special feature in the averaged records. However, the clustering study could be repeated, for example by using a more complete dataset of eruptions, by changing the clustering window from 10 years to longer ages, or by conducting a more detailed analysis of the eruption sources.

In conclusion, I am quite confident that the 10-year drop of isotopes is mostly driven by strong, tropical eruptions, which probably affected average temperatures on a large scale and

hence left an impact on the regional climate of Greenland as well as in tree rings (Sigl et al., 2015).

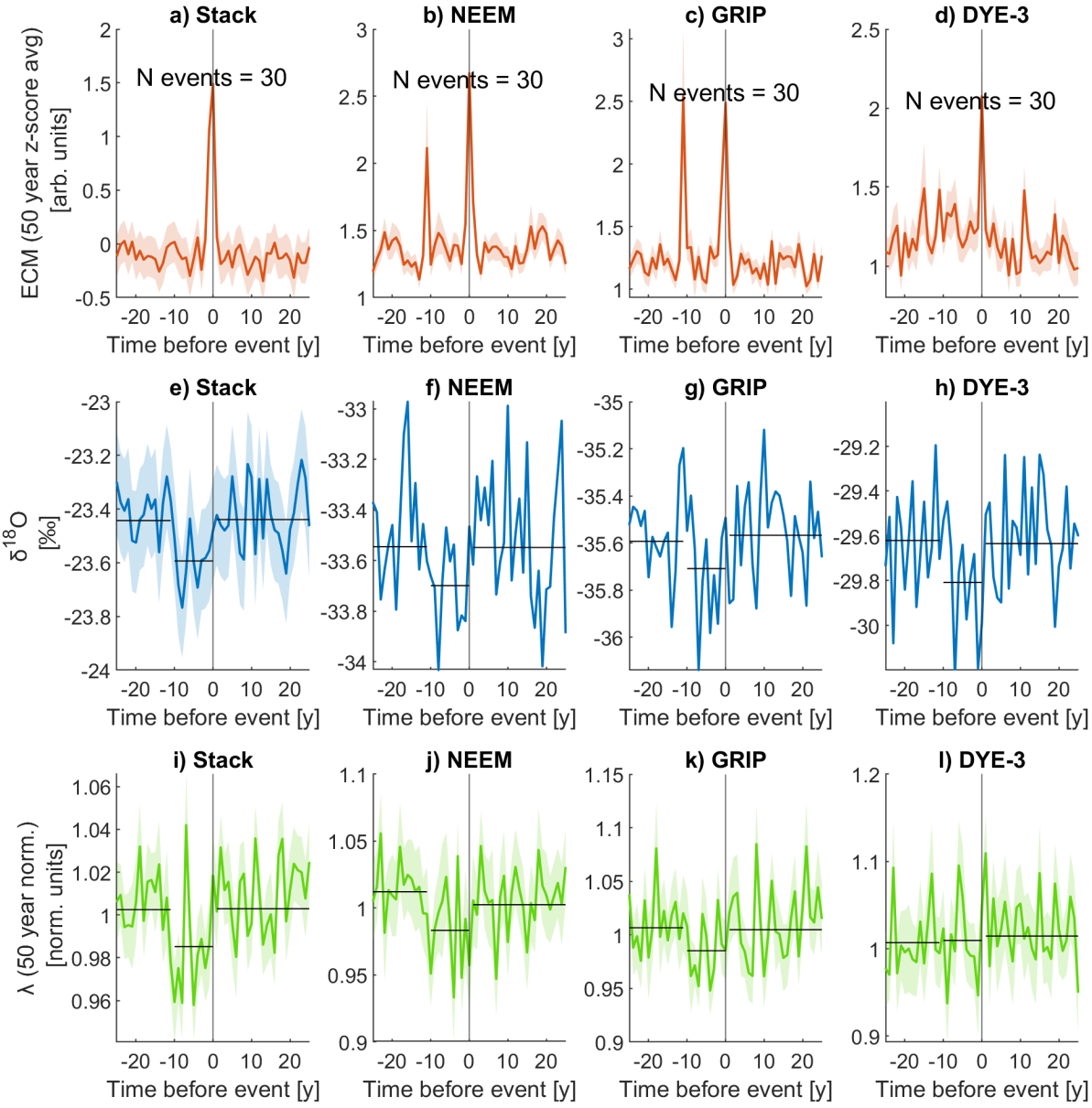

Figure 4.4 Post-volcanic cooling after the 30 tropical eruptions in GICC21. (a-d) ECM signals averaged around the eruptions. (e-h) Corresponding average $\delta^{18}O$ signal of the stack and the single ice cores. A prolonged drop of about 10 years is visible in the datasets; black lines identify the mean signal as computed in the 25-year interval before the eruption, the 10-year interval after the eruption, and the 25 -year interval after that. The drops have an amplitude of about 0.1-0.2 ‰. (i-l) Layer thickness average around the eruptions. Indication of a 10-year minimum is present in the stack as well as in NEEM and GRIP, while DYE-3 does not indicate such a response.

4.3 Perspectives from the GICC21 timescale on Mediterranean eruptions

So far, only two Mediterranean eruptions were thought to have been identified in the Greenlandic ice-core acidity and sulfate records in the last 4000 years: Vesuvius and Thera. However, Mediterranean tephra in ice cores have not yet been found despite continuous sampling (Bourne et al., 2015; E. Cook, personal communication, 2021), and hopes to find tephra in Greenland have been scaled back. The Vesuvius eruption (79 CE) was certainly of large magnitude (VEI[12]=5) and was thought to correspond to the peak now dated 88 CE (Barbante et al., 2013; Plunkett et al., 2022). The second eruption is the debated Minoan eruption on Thera, Santorini. Although the eruption has an estimated VEI of 7 (Johnston et al., 2014), the hopes of finding direct evidence of tephra from Thera in ice cores are rather low (McAneney & Baillie, 2019), because of the dominating circulation patterns that drive the transport of volcanic signal eastward from the Mediterranean region.

In the absence of tephra, by comparing Greenland acidity records and site-specific radiocarbon evidence and by considering that the offset to IntCal20 should have been resolved, I will attempt to provide indirect evidence of the impact of Mediterranean eruptions at the very distant Greenlandic location.

A close observation of all ECM signals at 79 CE on the GICC21 age scale does not indicate that the Vesuvius eruption, although strong, left any prominent acidity signal on the ice sheet (Figure 4.5).

If at least in principle, one didn't know when Vesuvius happened, which is not the case, one would look at radiocarbon evidence found around Vesuvius to reconstruct the age of the eruption. I propose Figure 4.6 as a methodology test: by gathering all evidence available from Greenland, tree-ring temperature reconstructions, and radiocarbon samples from the eruption site, one should be able to pinpoint the age of the eruption.

We note that the year of the Vesuvius eruption aligns with a cooling both in the N-Tree record (Sigl et al., 2015) and in the $\delta^{18}O$ stack, which by no means is conclusive evidence that the eruption was somehow registered in Greenland, but might indicate that there could be potential for further investigation, even given the low acidity signal.

[12] Retrieved from the Smithsonian volcanic database https://volcano.si.edu/volcano.cfm?vn=211020

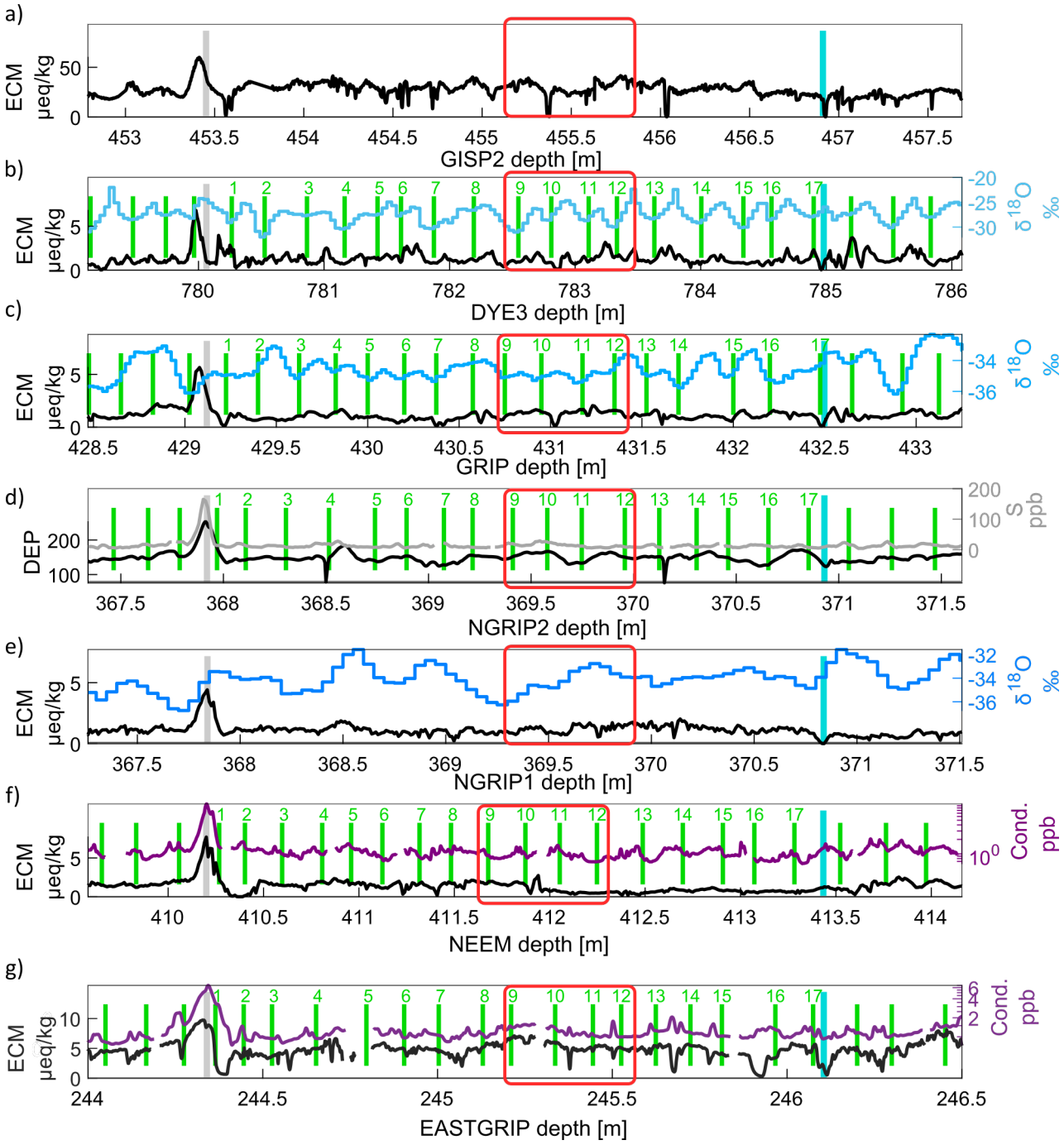

Figure 4.5 Where Vesuvius would be according to GICC21.

Ice-core acidity record showing the 3-year interval (red rectangle) where Vesuvius would lie according to the new chronology. None of the ice cores, unfortunately, register a significant peak in the ECM, in the conductivity (where available: f and g), or the sulfate (d).

Evidence proximal to Vesuvius includes a vase of olive oil, found in Pompeii, which was dated to 1944 ± 50 ^{14}C-years BP (Sacchi et al., 2020). The calendar age of this sample was

calibrated by the OxCal v4 online tool (Ramsey, 2009). As we can see in Figure 4.6, the rather wide distribution of ^{14}C ages prevents an exact identification of Vesuvius in the ice-core stack, because the probability distribution covers multiple ECM peaks in ice cores. By looking at the probability distribution alone, one would still be tempted to attribute tie point no. 4 to Vesuvius, but the layer count and the tephra record can definitively exclude this possibility (Plunkett et al., 2022).

A hypothetical cryptotephra/tephra sample would lie in the region between 9 and 12 years before the 88 CE peak. The search by Plunkett et al. (2022) only involved three samples at a yearly resolution around this latter peak, hence they did not attempt to find Vesuvius anywhere else. Their analysis focused on NEEM-2011-S1, drilled only until shortly after the 88 CE peak, but they endorse a tephra search closer to 79 CE in other ice cores, which could be done with a continuous cryptotephra search (Cook et al., 2018).

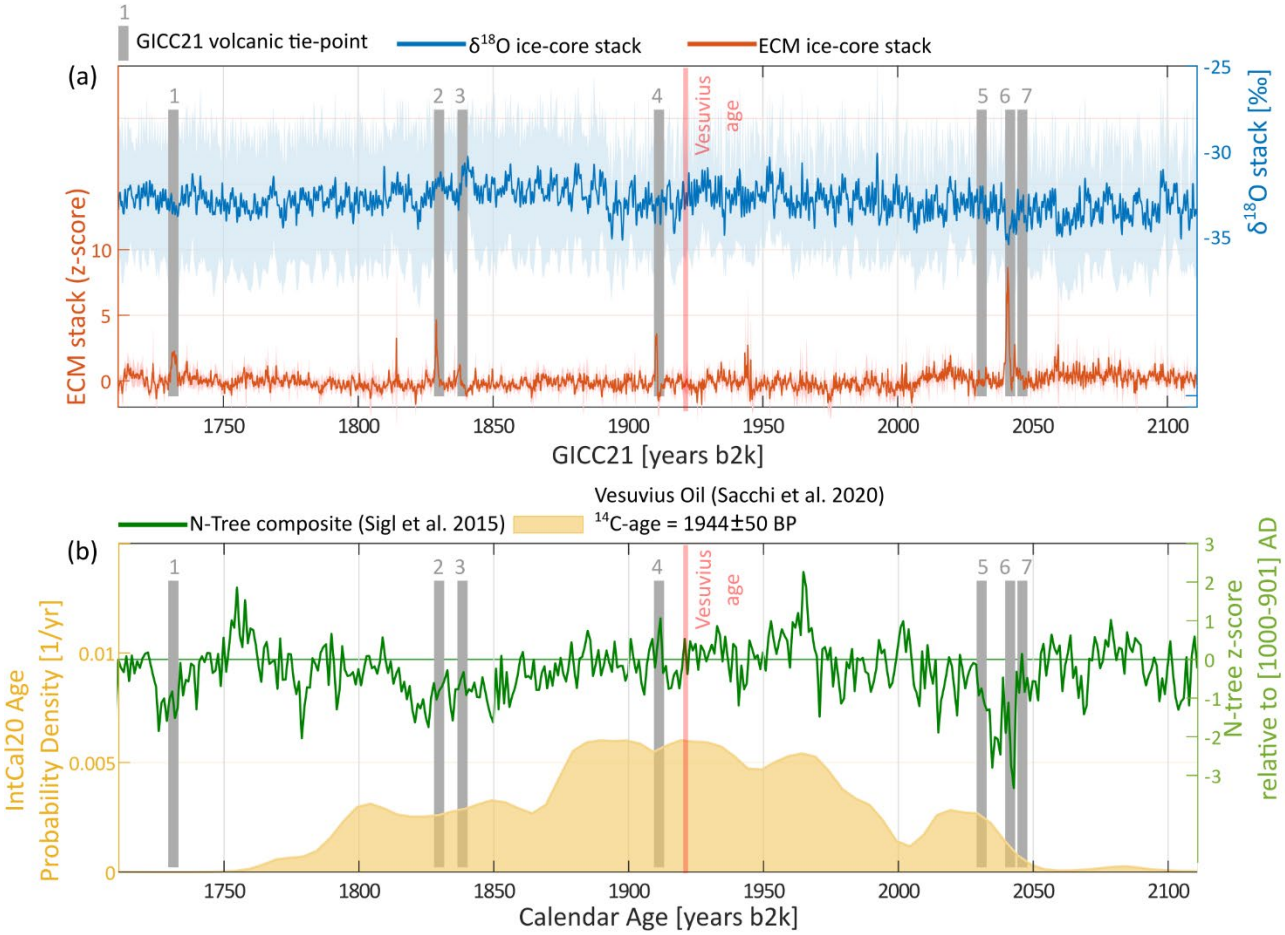

Figure 4.6 Methodology example on the Vesuvius eruption.

The red vertical bar marks where Vesuvius 79 CE should be found in GICC21, while the grey numbered bars indicate tie points used in GICC21. (a) No clear signal can be identified at the Vesuvius age in the ECM-stack of the ice cores. (b) It can be argued that some cooling

in the N-tree record (green) can be observed right after the Vesuvius age, however, no causal relationship is demonstrated by this observation alone. The broad probability distribution of calibrated ages from the radiocarbon-dated sample is not providing an independent age estimation for Vesuvius, of which we know the true age to be 79 CE from direct historical observations.

4.3.1 Perspectives of GICC21 on the Thera eruption

The debate about the exact date of the Thera eruption is still ongoing. The radiocarbon ages for the eruption have recently been found in better agreement with the archaeological attribution to the 16th century BCE (3501-3600 years b2k; Pearson et al., 2018). As discussed in Van der Plicht et al. (2020), the eruption, unfortunately, happened during a plateau in ^{14}C production, which results in a widening of the dating uncertainties. The outer layer of an olive branch found in Santorini, commonly associated with the eruption (Friedrich et al., 2006; Friedrich, Heinemeier, & Warburton, 2009), can be reconstructed according to IntCal20 but shows multi-modality of the age distribution (the ^{14}C age is 3331+/-10 years BP). However, by wiggle matching the olive tree rings to the IntCal20 dataset, the calendar dates for the outer layer are narrowed to the interval 3592-3612 years b2k (68.2% confidence) and 3578-3617 years b2k (95.4% confidence) (Van der Plicht et al., 2020).

Thanks to the demonstrated good alignment between tree-ring chronologies and GICC21, provided in Paper III, data from distant radiocarbon archives and ice cores can be aligned in the Thera range. To clarify whether the GICC21 timescale provides new perspectives on the Thera dating, I produced a comparison between ice-core data and the Thera radiocarbon-dated evidence (Figure 4.7). It is still not possible to assign any Greenlandic signal to the Thera eruption with absolute certainty. However, there is some indication that continuous multi-core cryptotephra searches might be successful.

The Greenlandic volcanic match in the Thera age range relies on 6 ECM tie points, corroborated by sulfate to be volcanic eruptions. According to the olive branch age calibration of its outermost layer, the three eruptions older than 3620 years b2k are excluded from the picture. Specifically, the eruption labeled no.4 in Figure 4.7, now attributed to Aniakchak II (Alaska; Pearce et al., 2004), was formerly attributed to Thera (Hammer et al., 1987). The age of this eruption, according to the revised GICC21, becomes younger by 13 years but is nonetheless outside of the main probability density of the radiocarbon dated olive branch.

Younger ECM peaks, traditionally disregarded as Thera candidates, are found to fall within the range of possible ages. Moreover, thanks to the new ice-core timescale, a volcanic eruption visible in all deep ice cores at 3560 years b2k aligns with a calcium anomaly in Turkish tree rings (Pearson et al., 2020), indicating droughts possibly following an eruption-induced cooling. To my knowledge, tephra evidence for the origin of this volcanic eruption is still lacking.

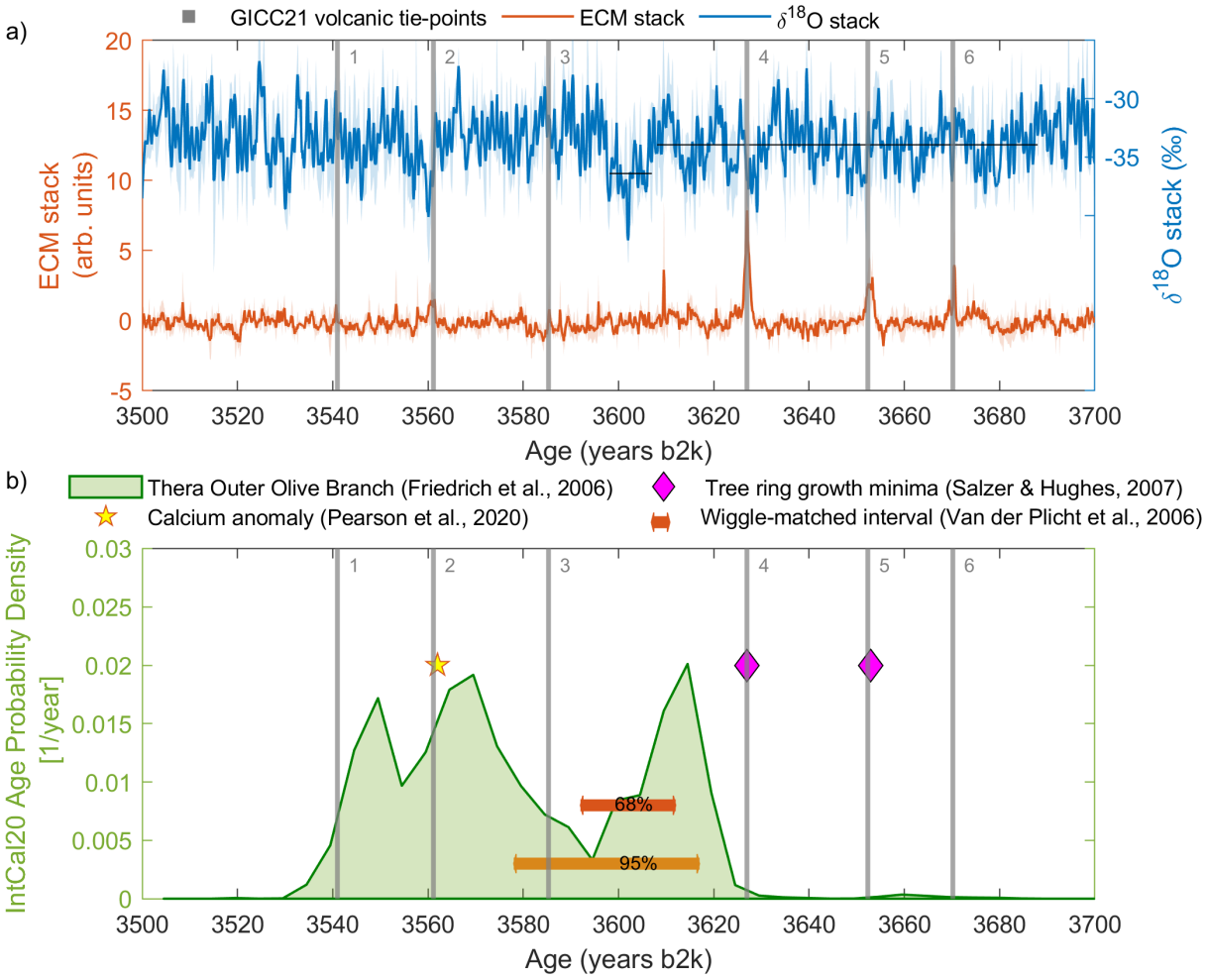

Figure 4.7 Comparison of ice-core data with the radiocarbon-dated olive branch found in Santorini.

The numbered grey bars highlight the synchronized volcanic tie-points used for GICC21. (a) Stacked ECM and isotope record of NEEM, GRIP, DYE-3 (the shading shows the standard deviation of the stack). A cooling period around 3600 years b2k is visible after an ECM peak at 3610 years b2k; black horizontal lines indicate the average value in the 10 years after 3610 and in the 80 years before. (b) The age probability density function of the olive branch is related to the Thera eruption. The three eruptions older than 3620 years b2k (no. 4, 5, and 6) do not overlap with the probability distribution and are therefore less likely

to correspond with the Thera eruption, no. 4 being Aniakchak II. Two tree-growth minima (purple diamonds) reported by Salzer & Hughes (2007) in tree rings from the western USA, were also shown in Paper III to add evidence for the alignment with the tree ring chronology. The red arrows highlight the possible Thera age range by Van der Plicht et al. (2020). It appears that this age range corresponds to the isotope decrease in the ice cores, but not with the calcium anomaly.

It is interesting to observe that over the wiggle-matched age intervals proposed by Van der Plicht et al. (2020), the isotope stack experiences a prolonged decrease, possibly indicating a cooling period. A peak at 3610 years b2k (1610 BCE) is recorded in the ECM stack, right before the cooling. Inspection in the ice cores showed that this ECM peak is mostly visible in GRIP, while minor ECM enhancements can be seen in NEEM and DYE-3 at the same age. The identity of this eruption has not yet been identified.

The $\delta^{18}O$ values decrease at 3610 years b2k for about 9 years by 0.63±0.21 ‰ from the average measured in the 80 years before 3610 years b2k. The drop in isotopes is large compared to the histograms b.2 and b.3 in Figure 4.3, where it would be placed on the far-right end of the Monte-Carlo distribution tails. The average layer thickness (not shown) registers a dip of 3% but only a 3-year long minimum and cannot be distinguished from a random fluctuation, because of its short duration.

A dip in isotopes could be related to other climatic effects, such as the ones induced by solar activity, for example because of a solar minimum. However, by inspecting the data presented in Adolphi et al. (2016), there is no strong indication of a solar minimum in the range 3.5-3.7 ka b2k in the ^{10}Be data of GRIP and GISP2.

In conclusion, multi-modality of the probability distribution and disagreement between radiocarbon ages from different samples prevents a unique identification of a candidate for the Thera eruption in the ice-core ECM. However, a high-resolution search for crypto-tephra grains using scanning electron microscopy (SEM) screening techniques, with particular focus on the ECM peaks at 3560 years b2k and at 3610 years b2k, might offer an answer to whether ashes from Santorini were deposited on the Greenlandic ice sheet.

4.4 Collaboration for Paper IV – "Melt in the Greenland EastGRIP ice core reveals Holocene warming events"

The topic of Paper IV (Westhoff et al., 2021, in review) is mainly an analysis of the melt record of EastGRIP and the description of the general features of melt layers. In addition, we analyzed whether melt layers could be attributed to warm periods in the N-Tree record by Sigl et al. (2015). The hypothesis to test is whether warm years, as recorded by tree rings, are correlated to melt events at EastGRIP, but this is a difficult conclusion to reach. For once, we cannot be sure that the melt layers are recorded in the correct year, because of the percolation of meltwater in deeper snow.

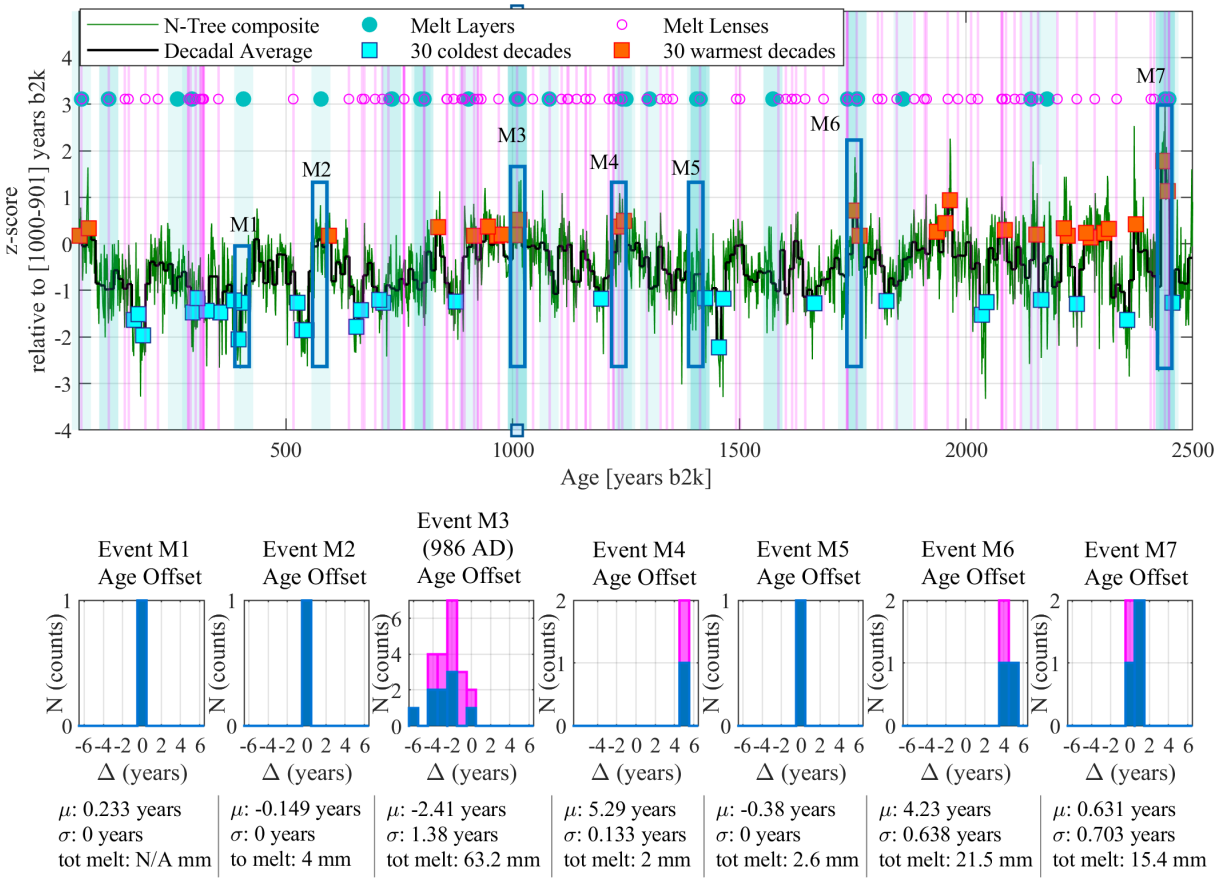

Figure 4.8 Melt at EastGRIP compared to warm years in the tree-ring record by Sigl et al. (2015).

Top panel: Vertical bars highlight the position of melt features at EastGRIP, as described in Westhoff et al. (2021, in review). Seven events of warming are highlighted in blue boxes, corresponding to the histograms below. Histograms (Events M1-M7): distance of melt from tree-ring maximum. Pink bars are lenses (minor melt events) and blue bars indicate melt layers (major melt events).

For Paper IV, GICC21 had not been completed yet, hence the analysis was conducted by aligning EastGRIP on the NS1-2011 timescale and then gathering evidence of melt close to warm years in tree rings. However, previously in this thesis, we have seen that GICC21 and NS1-2011 are very similar.

Figure 4.8 shows the analysis done for Paper IV. The conclusion we draw is that the 986 AD event (M3), which lies at 978 AD according to GICC21 ages, was exceptionally rich in melt layers and likely represents a very warm decade. We also observed that some other very warm years in tree ring records had some melt in their proximity (melt events M1 to M7). Another finding was that melt is Poisson distributed with warmer decades presenting a higher occurrence of melt (Figure 4.9).

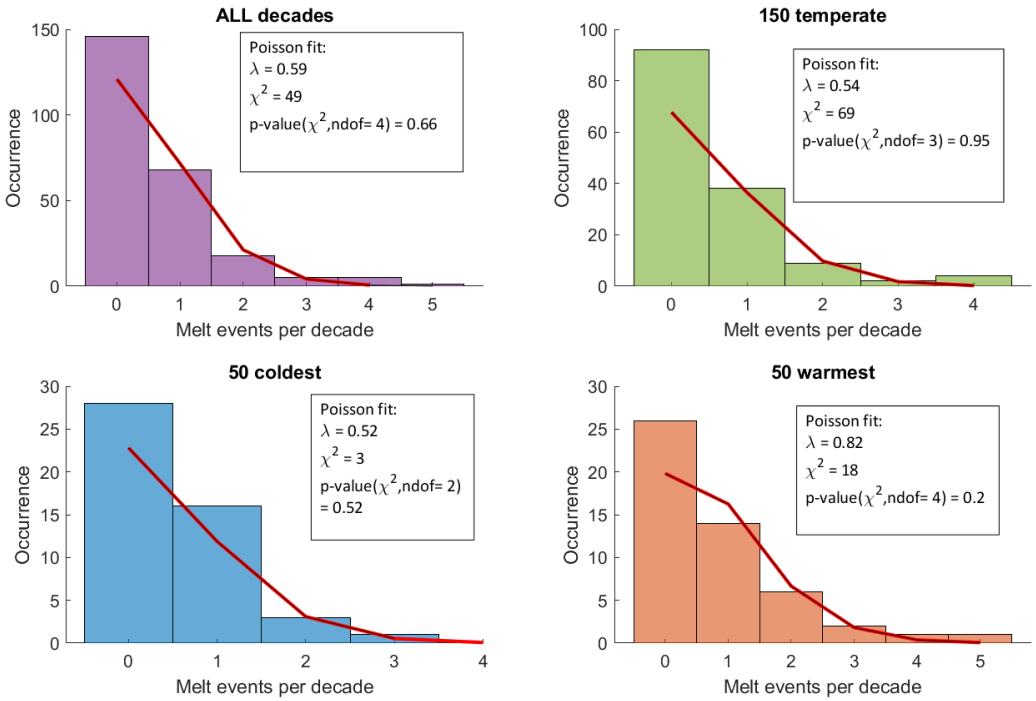

Figure 4.9 Test of Poisson-distributed melt events.

The number of melt events per temperate, cold, or warm decade. The warmest decades have an average of 0.82 melts/decade, compared to the other three cases, where the average is about 0.5 melt events/decade. It thus follows that warmer decades see a higher occurrence of melt at EastGRIP.

As a final experiment, not presented in Paper IV, I tested whether the melt at EastGRIP was most likely to be measured in the summer or the winter season within the corresponding annual layer. This is intended as a test of the percolation of meltwater into older layers since melt most likely happened during the summer months. For this, I simply compared the depth

of the melt layer with the annual signal of sodium at EastGRIP, an indicator of the winter season. I categorized each melt layer according to the relative distance from the sodium minimum. A 'summer melt event' is defined as occurring within ±0.025 m away from the sodium minimum, or else it is a 'winter melt event'[13].

With an occurrence of ~300 events in the summers and ~80 in the winters, the probability of summer occurrence of melt is above 65%, with 99% confidence[14]. This test cannot completely exclude the case of percolation, since it could be that melt was recorded in one of the older summers. In any case, there is a clear indication that melt is preferably located around the sodium minimum.

4.5 Supplementary Information to Chapter 4

4.5.1 Greenland data stacks

To be able to stack the signal of several ice cores at annual resolution, we first need to report each ice core's data on the correct annual average. Hence, for each ice core, we average the signal within each year, making sure that the data points overlapping with a layer boundary are weighted correctly across it. For example, if the annual layer boundary is 2 cm into a 5 cm isotope sample, it will enter the annual averages on each side with 40% and 60%, respectively.

For each ice core, we set a threshold of 80% data coverage within each year, which means that if more than 20% of the data are missing during a certain year, we neglect that core in the averaging.

To do the stacking, we adopted proxy-specific normalizations. Because the calibration of the ECM is not accurate and because volcanic peaks have a highly variable amplitude between ice cores, the ECM data are normalized by z-scores from the millennial average. Fixed,

---

[13] I also define which layers are found in spring and autumn, and discard these events as unclear.

[14] I assumed the problem to follow a binomial distribution, and the null hypothesis to be "melt can happen randomly either in the summer or in the winter" and then verifying if the empirical values are biased. I calculated the posterior probability density of p, which is the single-event probability of obtaining melt in the summer. The posterior probability is conditional to the number of successes (summer melt) and failures (winter melt) counted in the dataset. By integrating the posterior probability over $p<0.45$, $0.45<p<0.55$, and $p>0.55$ one obtains the probability of the 'biased-coin' problem, i.e. if melt is preferentially located in the winter, random, or in the summer.

consecutive windows were used to average the relative amplitude of the volcanic peaks over the slowly-varying background level.

The layer thickness data is normalized by dividing by the centennial means, in order to partially account for thinning and firn densification. On the other hand, isotope data are kept on their original units (‰).

After normalizing, the data from different ice cores are aligned on the common GICC21 (or GICC05) timescale to compute the mean and the variance of the stack. The variance is further divided by the number of ice cores involved in the stacking.

4.5.2 Monte-Carlo protocol

The following Monte-Carlo protocol was used to test the significance of the isotope and layer thickness post-eruption decreases, by iterating the steps 10'000 times:

1. 105 random times were selected between 0 and 3835 years b2k. For the layer thickness only, in order to avoid firn densification effects on the amplitude, the most recent 100 years were excluded;
2. The stacks (isotopes and layer thickness) were selected for 100-years windows centred on each random time;
3. The 105 windows were averaged at annual resolution; a standard error was computed on the average signal;
4. The search for the amplitude and the duration was performed (described in the following).

The amplitude and duration are measured in the same way both for the randomized iterations and for the actual sample. The amplitude is computed as the difference between:

- A_{before} , the average signal in the 50 years before the eruption peak;
- A_{after} , the average signal in the 50 years after the eruption.

The duration of the signal drop is computed by, first, finding all clusters of consecutive data-points that are significantly below average, in a 30 year window around the eruption peak, and then selecting the longest one in terms of duration. This represents a conservative test since the actual measurement has to compete with all the longest minima in the ensemble.

4.5.3 Post-volcanic climate

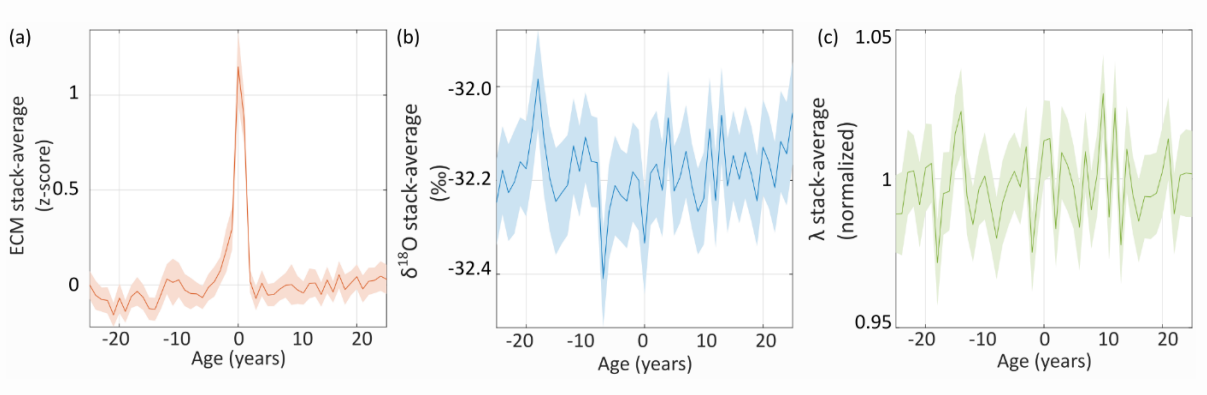

Figure 4.10 Signal stack-averages on the GICC05 timescales around 105 eruptions. The average was calculated around the same eruptions matched in the GICC21 timescale; time is flowing from right to left. Data used for the averages are limited to DYE-3, NorthGRIP, and GRIP, to reproduce the GICC05 data availability and to avoid interpolating GICC05 to annual resolution for the other ice cores. (a) The ECM stack-average is again showing a maximum at 0 years. (b) The $\delta^{18}O$ stack-average does not highlight a significant minimum of more than one year duration. (c) The layer thickness stack-average shows no significant decrease.

4.6 References

Adolphi, F., & Muscheler, R. Synchronizing the Greenland ice core and radiocarbon timescales over the Holocene–Bayesian wiggle-matching of cosmogenic radionuclide records. Climate of the Past, 12, 15–30. doi:10.5194/cp-12-15-2016, 2016

Barbante, C., Kehrwald, N. M., Marianelli, P., Vinther, B. M., Steffensen, J. P., Cozzi, G., . . . Siggaard-Andersen, M.-L. Greenland ice core evidence of the 79 AD Vesuvius eruption. Climate of the Past, 9, 1221–1232. https://doi.org/10.5194/cp-9-1221-2013 , 2013

Bourne, A. J., Cook, E., Abbott, P. M., Seierstad, I. K., Steffensen, J. P., Svensson, A., ... & Davies, S. M. A tephra lattice for Greenland and a reconstruction of volcanic events spanning 25–45 ka b2k. Quaternary Science Reviews, 118, 122-141. https://doi.org/10.1016/j.jvolgeores.2014.09.006, 2015

Cook, E., Davies, S. M., Guðmundsdóttir, E. R., Abbott, P. M., & Pearce, N. J. First identification and characterization of Borrobol-type tephra in the Greenland ice cores: new deposits and improved age estimates. Journal of quaternary science, 33(2), 212-224. https://doi.org/10.1002/jqs.3016, 2018

Friedrich, W. L., Kromer, B., Friedrich, M., Heinemeier, J., Pfeiffer, T., & Talamo, S. Santorini eruption radiocarbon dated to 1627-1600 BC. Science, 312, 548–548. https://doi.org/10.1126/science.1125087, 2006

Friedrich, W., Heinemeier, J., & Warburton, D. Time's up! : dating the Minoan eruption of Santorini : acts of the Minoan eruption chronology workshop, Sandbjerg November 2007, initiated by Jan Heinemeier & Walter L. Friedrich. Danish Institute at Athens. ISBN 978 87 7934 024 4, 2009

Gautier, E., et al. 2600-years of stratospheric volcanism through sulfate isotopes. Nat Commun 10, 466. https://doi.org/10.1038/s41467-019-08357-0, 2019

Hammer, C. U., Clausen, H. B., Friedrich, W. L., & Tauber, H. The Minoan eruption of Santorini in Greece dated to 1645 BC?. Nature, 328(6130), 517-519. https://doi.org/10.1038/328517a0, 1987

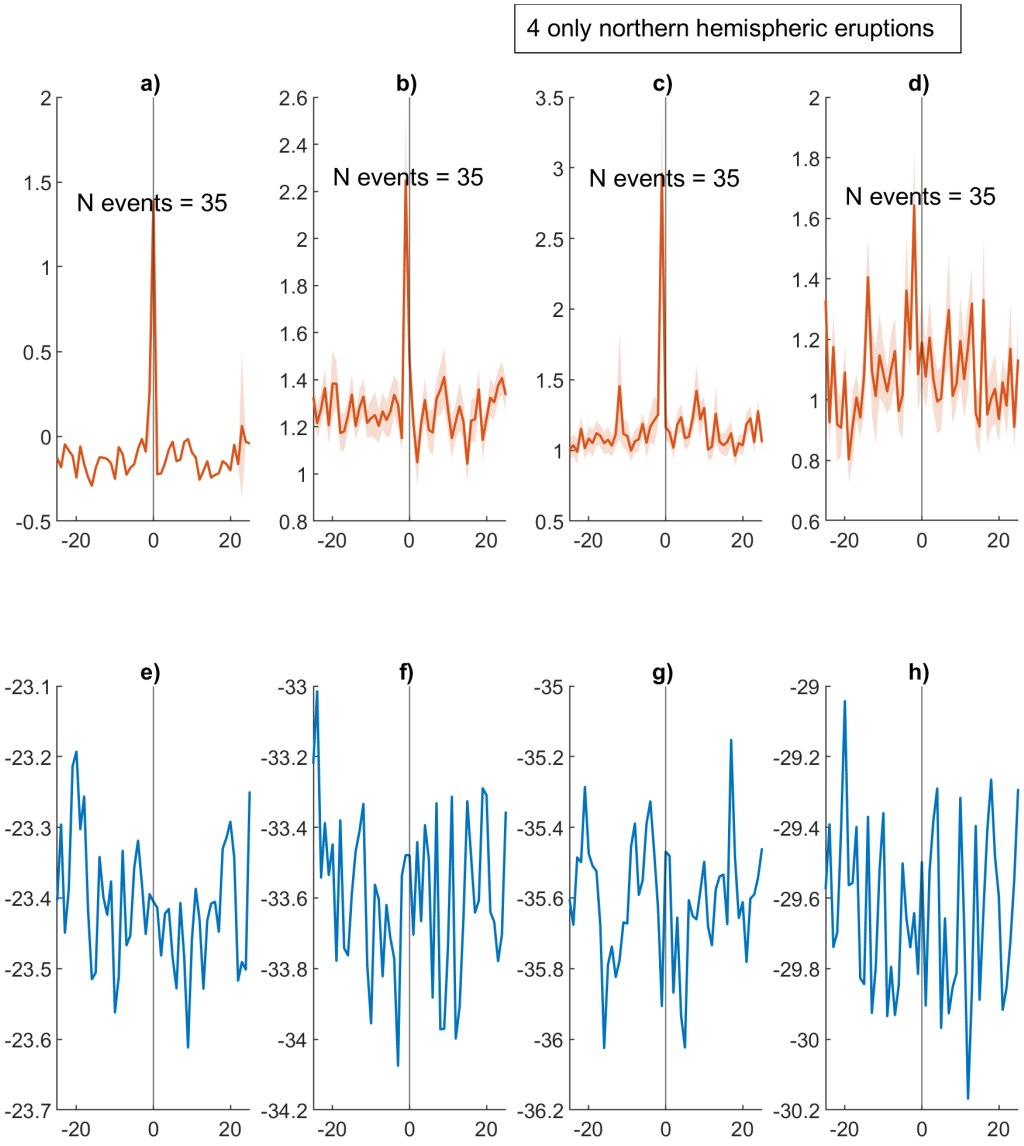

Figure 4.11 D1 The 35 Northern Hemispheric eruptions used for GICC21 do not leave as clear a signature as tropical ones.

He, C., Liu, Z., Otto-Bliesner, B. L., Brady, E. C., Zhu, C., Tomas, R., ... & Severinghaus, J. P. Abrupt Heinrich Stadial 1 cooling missing in Greenland oxygen isotopes. Science advances, 7(25), eabh1007. DOI: 10.1126/sciadv.abh1007, 2021

Johnston, E. N., Sparks, R. S. J., Phillips, J. C., & Carey, S. Revised estimates for the volume of the Late Bronze Age Minoan eruption, Santorini, Greece. Journal of the Geological Society, 171(4), 583-590. doi: 10.1144/jgs2013-113, 2014

Lavigne, F., Degeai, J. P., Komorowski, J. C., Guillet, S., Robert, V., Lahitte, P., ... & de Belizal, E. Source of the great AD 1257 mystery eruption unveiled, Samalas volcano, Rinjani Volcanic Complex, Indonesia. Proceedings of the National Academy of Sciences, 110(42), 16742-16747. https://doi.org/10.1073/pnas.1307520110, 2013

McAneney, J., & Baillie, M. Absolute tree-ring dates for the Late Bronze Age eruptions of Aniakchak and Thera in light of a proposed revision of ice-core chronologies. Antiquity, 93(367), 99-112. https://doi.org/10.15184/aqy.2018.165, 2019

Pearce, N. J., Westgate, J. A., Preece, S. J., Eastwood, W. J., & Perkins, W. T. Identification of Aniakchak (Alaska) tephra in Greenland ice core challenges the 1645 BC date for Minoan eruption of Santorini. Geochemistry, Geophysics, Geosystems, 5. https://doi.org/10.1029/2003gc000672, 2004

Pearson, C. L., Brewer, P. W., Brown, D., Heaton, T. J., Hodgins, G. W., Jull, A. T., . . . Salzer, M. W. Annual radiocarbon record indicates 16th century BCE date for the Thera eruption. Science Advances, 4(8), eaar8241. https://doi.org/10.1126/sciadv.aar8241, 2018

Pearson, C., Salzer, M., Wacker, L., Brewer, P., Sookdeo, A., & Kuniholm, P. Securing timelines in the ancient Mediterranean using multiproxy annual tree-ring data. Proceedings of the National Academy of Sciences, 117(15), 8410-8415. https://doi.org/10.1073/pnas.1917445117, 2020

Plunkett, G., Sigl, M., Schwaiger, H., Tomlinson, E., Toohey, M., McConnell, J. R., . . . Siebe, C. No evidence for tephra in Greenland from the historic eruption of Vesuvius in 79 CE: Implications for geochronology and paleoclimatology. Climate of the Past Discussions, 1–37. https://doi.org/10.5194/cp-2021-63, 2022

Ramsey, C. B. Bayesian analysis of radiocarbon dates. Radiocarbon, 51, 337–360. https://doi.org/10.1017/s0033822200033865, 2009

Sacchi, R., Cutignano, A., Picariello, G., Paduano, A., Genovese, A., & Francesco Siano, G. N. Olive oil from the 79 A.D. Vesuvius eruption stored at the Naples National Archaeological Museum (Italy). npj Science of Food 4, 19. https://doi.org/10.1038/s41538-020-00077-w, 2020

Salzer, M. W., & Hughes, M. K. Bristlecone pine tree rings and volcanic eruptions over the last 5000 yr. Quaternary Research, 67, 57–68. https://doi.org/10.1016/j.yqres.2006.07.004, 2007

Sigl, M., Winstrup, M., McConnell, J. R., Welten, K. C., Plunkett, G., Ludlow, F., … Woodruff, T. E. Timing and climate forcing of volcanic eruptions for the past 2,500 years. Nature, 523(7562), 543–549. https://doi.org/10.1038/nature14565 , 2015

Sigl, M., Fudge, T. J., Winstrup, M., Cole-Dai, J., Ferris, D., McConnell, J. R., ... & Sowers, T. A. The WAIS Divide deep ice core WD2014 chronology–Part 2: Annual-layer counting (0–31 ka BP). Climate of the Past, 12(3), 769-786. https://doi.org/10.5194/cp-12-769-2016, 2016

Sjolte, J., Sturm, C., Adolphi, F., Vinther, B. M., Werner, M., Lohmann, G., & Muscheler, R. Solar and volcanic forcing of North Atlantic climate inferred from a process-based reconstruction. Climate of the Past, 14(8), 1179-1194. https://doi.org/10.5194/cp-14-1179-2018, 2018

Svensson, A., Dahl-Jensen, D., Steffensen, J. P., Blunier, T., Rasmussen, S. O., Vinther, B. M., ... & Bigler, M. Bipolar volcanic synchronization of abrupt climate change in Greenland and Antarctic ice cores during the last glacial period. Climate of the Past, 16(4), 1565-1580. https://doi.org/10.5194/cp-16-1565-2020, 2020

Van Der Plicht, J., Bronk Ramsey, C., Heaton, T., Scott, E., & Talamo, S. Recent Developments in Calibration for Archaeological and Environmental Samples. Radiocarbon, 62(4), 1095-1117. https://doi.org/10.1017/rdc.2020.22, 2020

Veres, D., Bazin, L., Landais, A., Toyé Mahamadou Kele, H., Lemieux-Dudon, B., Parrenin, F., ... & Wolff, E. W. The Antarctic ice core chronology (AICC2012): an optimized multi-parameter and multi-site dating approach for the last 120 thousand years. Climate of the Past, 9(4), 1733-1748. https://doi.org/10.5194/cp-9-1733-2013, 2013

Westhoff, J., Sinnl, G., Svensson, A., Freitag, J., Kjær, H. A., Vallelonga, P., ... & Weikusat, I. Melt in the Greenland EastGRIP ice core reveals Holocene warming events. Climate of the Past Discussions, 1-36. doi: 10.1126/sciadv.abh1007, 2021

5 Synchronizing ice-core and U/Th time scales in the Last Glacial Maximum using Hulu Cave ^{14}C and new ^{10}Be measurements from Greenland and Antarctica

Giulia Sinnl[1], Florian Adolphi[3], Marcus Christl[6], Kees C. Welten [4], Thomas Woodruff [5], Marc Caffee [5], Anders Svensson[1], Raimund Muscheler[2] and Sune Olander Rasmussen[1]

1 Physics of Ice, Climate, and Earth, Niels Bohr Institute, University of Copenhagen, Denmark.

2 Quaternary Sciences, Department of Geology, Lund University, Lund, Sweden

3 Alfred Wegener Institute, Helmholtz Centre for Polar and Marine Research, Bremerhaven, Germany

4 Space Sciences Laboratory, University of California, Berkeley, California, USA

5 Department of Physics and Astronomy, Purdue University, Indiana, USA

6 Laboratory of Ion Beam Physics, ETH Zurich, Switzerland

5.1 Preface to Paper V

The paper reproduced here is awaiting final comments from all co-authors and will soon be submitted to Climate of the Past.

The supplement of the paper is reproduced with the paper (page 144), as it contains figures that are complementing the paper and provide additional information. As it is not yet decided if any of the supplement figures will become part of the publication during review, they should be considered as part of the thesis.

5.2 Abstract

Between 23 and 26 ka b2k (thousand years before 2000 CE) during the last glacial, Greenland experienced a period of extreme cold interrupted by two short-lived warm interstadials. Moreover, ice-core calcium data show two periods, preceding the interstadials, of anomalously high atmospheric dust loading, which are unexplained. At approximately the same time, the Chinese Hulu Cave speleothems exhibit a climatic signal suggested to be

a response to Heinrich Event 2. However, proposed centennial-scale offsets between the polar ice-core time scales and the speleothem time scale hamper the precise reconstruction of the global sequence of climatic events. Here, we examine two new ^{10}Be datasets from Greenlandic (NorthGRIP) and Antarctic (WDC) ice cores to test the agreement between different time scales by taking advantage of the globally synchronous cosmogenic radionuclide production rates.

Evidence of an event similar to the Maunder Solar Minimum is found in the new ^{10}Be datasets, as well as in other radionuclide data from Greenland and speleothems, representing a good synchronization candidate at around 22 ka b2k. We determine the offset between the Greenland ice-core time scale, GICC05, and the WDC Antarctic time scale, WD2014, to be 125±33 years by aligning the ^{10}Be signals. Furthermore, we determine the offset to the Hulu Cave timescale via radionuclide wiggle-matching to be 400 years for GICC05, between 185 and 575 years at 95% confidence, and 235 years for WD2014, between 25 and 425 years at 95% confidence. The uncertainties on the offsets include modelling and resolution uncertainties. The undercounting of annual layers in GICC05 inferred from the offset is hypothesized to have been caused by a combination of under-detected layers for periods with low winter precipitation and uncertain layers arising from unusual patterns in the annual signal during the extremely cold period often referred to as Heinrich Stadial 1.

5.3 Introduction

Paleoclimatic studies need regional climate records with accurate timescales to identify the driving mechanisms of climate change. At present, numerous independent chronologies, based on vastly different methods, are used to date specific climatic archives via, for example, layer counting of the chemical stratigraphy, measuring the U/Th decay, or radiocarbon dating. The uncertainties and inaccuracies of each of those time scales are often difficult to assess and are a major obstacle to a complete and accurate global reconstruction of paleoclimate.

The Last Glacial Maximum (LGM) was the last period when the ice sheets were at their largest extent before the deglaciation into the Holocene, although its precise definition is debatable (Hughes et al., 2013). For terrestrial records of the Northern Hemisphere, Hughes & Gibbard (2015) suggested defining the LGM as the cold period Greenland Stadial 3 (GS-3: 23.3-27.5 ka b2k following Rasmussen et al., 2014) based on the analysis of NorthGRIP

dust and sea-level records. In the present study, we refer to the period 20-25 ka b2k as the LGM for simplicity, being aware that this is not a formal stratigraphic definition.

During this time, a phase of massive discharge of icebergs from the Laurentide ice sheet was recorded in the ice-rafted debris content of North Atlantic marine sediments, defining the occurrence of the Heinrich Event 2 (HE-2; Bard et al., 2000; Peck et al., 2006). HEs happened during some GSs and injected a large amount of freshwater into the ocean, likely causing a more extreme shutdown of the Atlantic overturning meridional circulation (AMOC) and causing prolonged climatic conditions of extreme cold (McManus et al., 2004). The term Heinrich Stadial (HS) is often used to indicate the period affected by the HE. The duration of HS-1, for example, is limited to the 14.5-17.5 ka b2k interval within GS-2.1 (Broecker and Barker, 2007), while for HS-2, a correspondence with the late GS-3 is often argued for, based on speleothem water isotope records (e.g. Li et al., 2021).

Associated with HS-2, one could expect a cooling signal in the stable water isotopes of ice cores ($\delta^{18}O_{ice}$; Jouzel et al., 1997) but this is not the case, either because the ice sheet was not affected by the cooling or because the isotopes reacted non-linearly (Guillevic et al., 2014). For example, it has been suggested that the empirical temperature correlation with $\delta^{18}O_{ice}$ during HS-1 was completely disrupted by precipitation pattern alterations (He et al., 2021) which may also be the case for HS-2.

Mineral dust aerosols (e.g. Ca^{2+}) in Greenland ice cores have their major source in the Eurasian continent and mainly reflect the dryness of the source and wind strength, which are highest in periods of extreme cold (Schüpbach et al., 2018). During the LGM, calcium deposition in Greenland shows two periods of concentration increase (Rasmussen et al., 2014) which could be related to atmospheric reorganization following HE-2. This attribution is still speculative (Hughes & Gibbard, 2015). Also, methane (CH_4) originating from tropical wetland emissions and trapped in the ice cores may have strengthened during HSs and could be used as another descriptor of the HS-2 climate (Rhodes et al., 2015).

The objective of this study is a comparison of three time scales in the LGM. The time scales we are going to examine are the speleothem time scale from Hulu Cave, China (Wang et al. 2001; Southon et al., 2012; Cheng et al., 2016), the time scale for the Antarctic WDC ice core (WD2014; Sigl et al., 2016), and the Greenland ice core chronology (GICC05; Andersen et al., 2006; Svensson et al., 2008).

The Hulu Cave speleothems were dated by U/Th measurements for the period from 15 to 55 ka b2k and contain valuable carbon isotopes (^{14}C; Southon et al., 2012; Cheng et al., 2018)

and climatic proxies, such as stable oxygen isotopes ($\delta^{18}O_{calcite}$; Wang et al. 2001; Cheng et al., 2016). The dead carbon fraction (DCF) of ^{14}C of speleothems from this cave, that is, the estimated amount of older carbon that may contaminate the recorded atmospheric ^{14}C-signal, is very low and assumed to be constant over time (Cheng et al., 2018) making these speleothems excellent candidates for calibration of the IntCal20 curve (Reimer et al., 2020). Throughout the 15 to 42 ka b2k period, the GICC05 was constructed by manually counting annual layers in the electrical conductivity (ECM), continuous flow analysis (CFA) ion records, and visual stratigraphy of the NorthGRIP2 ice core (Andersen et al., 2006; Svensson et al., 2006). The uncertainty of GICC05 was assessed by the number of uncertain layers contributing to the Maximum Counting Error (MCE; Rasmussen et al., 2006). NorthGRIP was synchronized to the GRIP and GISP2 ice cores by identification of volcanic tie points and biomass burning events, and GICC05 was extended to these ice cores by interpolation (Rasmussen et al., 2008; Seierstad et al., 2014).

For Antarctica, the WD2014 time scale was constructed by manual and automatic counting of layers until 31.2 ka b2k in the WDC ice core (Sigl et al., 2016). The data used for counting were ECM and CFA impurity records, however, for the period 15-27 ka b2k, only ECM data were suitable for layer counting because of insufficient resolution of the CFA record. The uncertainty was assessed by comparison to the previous time scale (WAIS Divide Project Members, 2013), as well as by comparing the manual and automated versions of the layer count (Winstrup et al., 2012).

Around 23 ka b2k, the $\delta^{18}O_{ice}$ of Greenland indicates two short-lived Greenland interstadials, also known as Dansgaard-Oeschger events, namely GI-2.1 and 2.2 (Rasmussen et al., 2014). On the other hand, Antarctica experienced warming between 24 and 24.5 ka b2k and cooling for the subsequent millennium, as shown by the Antarctic Isotope Maximum 2 (AIM-2; EPICA Community Members, 2006). Greenlandic and Antarctic $\delta^{18}O_{ice}$ records are hypothesized to be mechanistically coupled by the bipolar seesaw mechanism (Stocker & Johnsen, 2003; Pedro et al., 2018), connecting all GI and AIM stages. According to the current chronologies, the onset of Antarctic cooling, i.e. the peak of the AIM-2 event, can be visually identified in the $\delta^{18}O_{ice}$ of WDC around 23.7 ka b2k (Jones et al., 2017), leading the corresponding onset of GI-2.2 by about 360 years (Rasmussen et al., 2014; Sigl et al., 2016).

By synchronizing Antarctic CH_4 and Greenlandic $\delta^{18}O_{ice}$, the WAIS project members (2015) stated that, on average, the onset of Antarctic cooling lags the onset of the GI warming by

218±92 years. The authors duly excluded the GI-2–AIM-2 pair from their lead-lag analysis, firstly because the GISP2 CH_4 record did not support synchronicity with the GI-2 temperature increase, and, secondly, because the older HS4 and HS5 were similarly associated with higher CH_4 levels. Recently, Svensson et al. (2020) presented a bipolar volcanic match between Greenland and Antarctic ice cores allowing to repeat the GI-AIM synchronization. They find an average of 122±24 years but the pair GI-2–AIM-2 is nonetheless absent from their analysis.

Chemical traces of volcanic eruptions and cosmogenic radionuclides provide synchronization tools that do not rely on the precise identification of climatic match-points and on the assumption of their synchronicity. While aligning GIs across climatic archives returns an overall realistic picture of climate, the assumed synchronicity of GIs across regions prevents from assessing the real leads and lags. Moreover, the climatic tie points may be difficult to identify in the first place. For example, while $\delta^{18}O_{calcite}$ of Asian speleothems show the imprint of HE-2 (Li et al., 2021), they do not represent the brief GI-2.1 and 2.2, hampering synchronization to Greenlandic $\delta^{18}O_{ice}$.

Across the LGM, most studies lack bipolar and inter-regional tie points to allow for an accurate reconstruction of the sequence of events. For example, Svensson et al. (2020) do not report bipolar volcanic tie points over the period 16 to 24 ka b2k. In their study, the evaluation of the time scale offset between WD2014 and GICC05 at 24 ka b2k is 80-90 years, thus bringing the AIM-2 and GI-2.2 closer together. Another inter-regional synchronization effort by Corrick et al. (2020) used climatic horizons to compare the ages of shifts in speleothem and Greenland $\delta^{18}O$, but also lacks tie points over the LGM. Their estimation around GI-3 (27.78 ka b2k) is that GICC05 is 90 years younger than U/Th-dated samples. A comparison between WDC CH_4 and the Hulu and Greenlandic $\delta^{18}O$ found that, at the onset of GI-3, WD2014 is 167 years younger than the Hulu time scale and that GICC05 is younger than WD2014 by about 30 years (Sigl et al., 2016). These studies agree that around GI-3, events are older according to the U/Th time scale than according to the ice-core time scales.

Given the scarcity of climatic and volcanic tie points over the LGM, in this work, we focus on new measurements of cosmogenic radionuclides to connect polar ice cores and the Hulu time scale. The interaction of galactic cosmic rays (GCRs) with the atmospheric parent atoms of ^{10}Be and ^{14}C is modulated by the time-varying helio- and geomagnetic fields. Therefore, the radionuclides recorded in climatic archives may show synchronizable features

in their production history (Steinhilber et al., 2012; Adolphi et al., 2018). The ^{14}C atoms enter the carbon cycle, which causes delay and smoothing of the atmospheric ^{14}C concentration relative to the production signal. However, the connection with the fast-deposited ^{10}Be in ice cores (1-2 years depositional delay; Raisbeck et al., 1981) can be made by the use of carbon-cycle models. The model we apply in this study was used extensively in works by Muscheler et al. (2000, 2004, 2009, 2014) and Adolphi et al. (2014, 2016, 2018) and is based on the box-diffusion model by Siegenthaler (1983). The main assumption that ^{10}Be varies proportionally to the true global production rate of cosmogenic radionuclides may, however, lead to uncertainties. For example, changes in the balance between wet and dry deposition or changes in the transport of ^{10}Be to the ice sheet are possible factors that might alter the signal recorded in ice cores from the true production rate. Similarly, ^{14}C may be affected by changes in the carbon cycle, adding additional signals that are not related to production rate changes.

Currently, the only radionuclide-based tie point in the LGM between ice-core and Hulu Cave records was found by radionuclide wiggle-matching in Adolphi et al. (2018). An offset of 550 years (215-670 years of 95% probability interval) between GICC05 and the Hulu timescale was measured at 22 ka b2k, shortly after the GS-2 onset. Here, we test this result by using new higher-resolution ^{10}Be data from Greenland and adding new Antarctic ^{10}Be data, to verify if the ice-core time scales may have accumulated high dating inaccuracies and to reconstruct the timing of events across the LGM.

5.4 Data and Methods

In this study, we aim at comparing the new cosmogenic radionuclide data with other datasets from Greenland, Hulu Cave, and Antarctica. We also analysed water stable isotope, methane, and calcium data to assess climatic changes. We summarize the relevant datasets, age resolutions, and citations in Table 5.1.

5.4.1 Preparation and measurement of the NGRIP2 samples

The 322 new Greenland ^{10}Be measurements were performed at ETH Zurich on samples from the NorthGRIP2 ice core between 1726.45 m and 1816.51 m depth, which in GICC05 ages corresponds to 20039 to 24774 years b2k (Andersen et al., 2006). The samples have a variable temporal resolution between 7.5 years and 14 years and present some smaller gaps

(see Methods Appendix, sec. 5.10.2), and are the so-far best-resolved published radionuclide dataset for the LGM. The measured ^{10}Be concentrations are shown in Figure 5.1(a).

Table 5.1 Datasets used in this study. Age resolutions are calculated for the period 20 to 25 ka b2k. For the Hulu Cave, two speleothems from the cave, labelled H82 and MSD, were measured for ^{14}C in two separate studies.

Dataset	Location	Proxy	Avg. Age Res. [years]	Reference
NorthGRIP2	75.10N 42.32W	^{10}Be	10	This study
		Ca^{2+}	20	Erhardt et al., 2021
		$\delta^{18}O$	10	NGRIP members, 2004
GRIP	72.58N 37.64W	^{10}Be	27	Yiou et al., 1997; Muscheler et al., 2004
		$\delta^{18}O$	10	Johnsen et al., 1997
GISP2	72.36N 38.30W	^{10}Be	162	Finkel & Nishiizumi, 1997
		$\delta^{18}O$	10	Stuiver & Grootes, 2000
WDC	79.46S 112.085W	^{10}Be	67	This study
		$\delta^{18}O$	10	Jones et al., 2017
		Non-sea-salt-Sulfate (nssS)	1	Buizert et al., 2018
Hulu Cave	32.5N 119.16E	^{14}C	271	H82: Southon et al., 2012
			124	MSD: Cheng et al., 2018
		$\delta^{18}O$	70	Wang et al., 2001
			31	Cheng et al., 2016

5.4.2 Preparation of the WDC samples and measurement

A total of 73 samples from 2453 to 2599 m depth in the WAIS Divide 06A ice core (WDC-06A) were analysed for ^{10}Be concentrations at Purdue University. These samples represent continuous ice-core sections with a cross-section of ~2 cm^2 and a length of ~2 m (varying from 1.89 to 2.12 m), corresponding to ~60-75 years of snow accumulation per sample. See Methods Appendix sec. 5.10.1 for more details. The measured WDC ^{10}Be concentrations are shown in Figure 5.1(d).

5.4.3 Conversion of ^{10}Be concentrations to fluxes

To account for the first-order correction of climatic influences on the ^{10}Be signal (Adolphi et al., 2018), ^{10}Be concentrations need to be converted to fluxes, which requires knowledge of accumulation rates (see Methods Appendix sec. 5.10.3). Accumulation rates for the ice core are reconstructed using the annual layer thicknesses and an appropriate model for the layer thinning. The thinning in the LGM portion of the ice cores can be approximated by a linear function of depth, although there may be uncertainties that relate to the time scale itself.

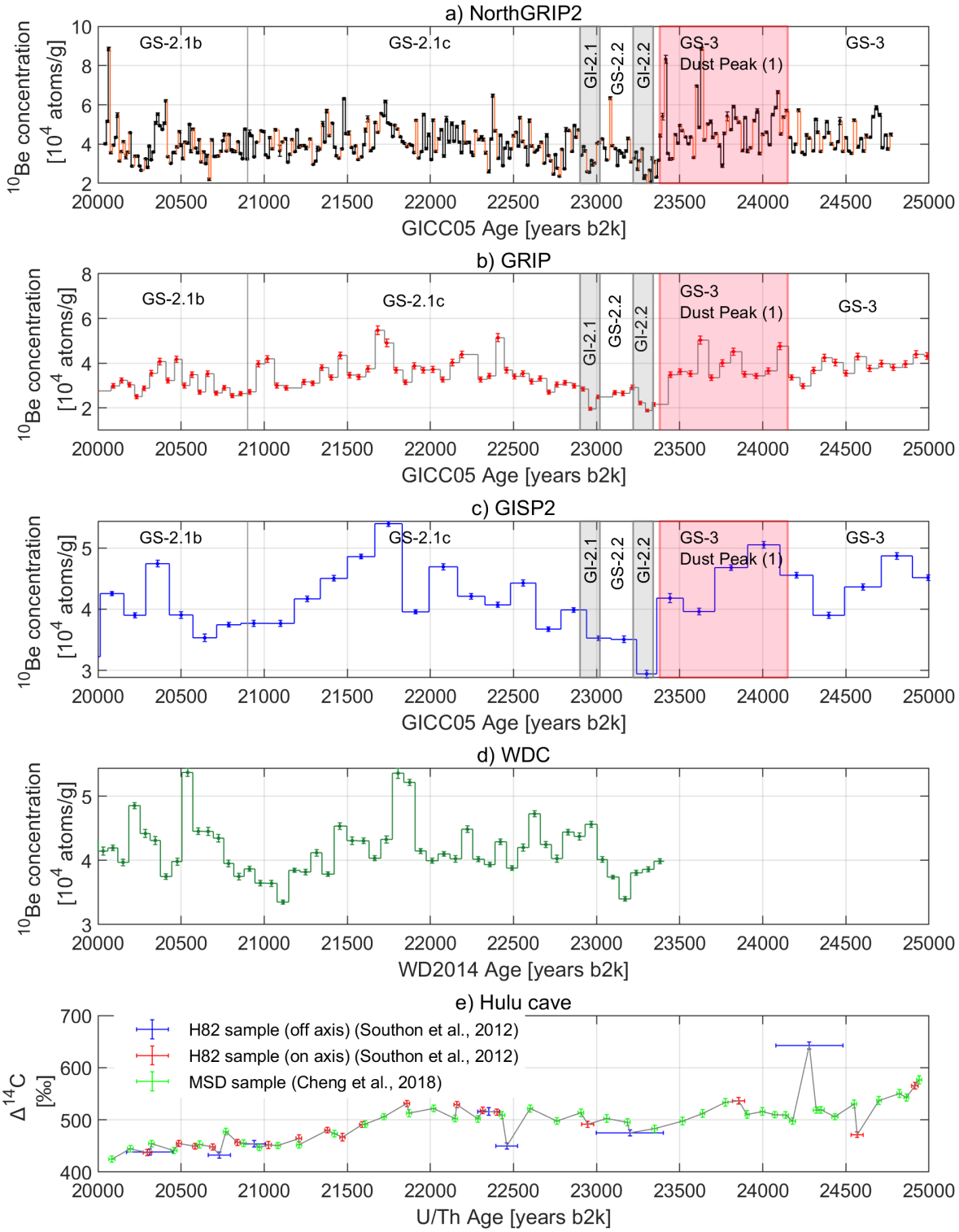

Figure 5.1 Cosmogenic radionuclide data used in this study.
On the GICC05 timescale: (a) NorthGRIP2 ^{10}Be concentrations (orange line indicates discontinuities in data collection); (b) GRIP ^{10}Be concentrations (Yiou et al., 1997; Muscheler et al., 2004). As the data was sampled on alternate ice-core portions of 55 cm, discontinuities in the dataset are present between each 27-year resolved data point (grey lines).
(c) GISP2 ^{10}Be concentrations (Finkel & Nishiizumi, 1997). On the WD2014 timescale: (d) WDC ^{10}Be concentrations.

On the U/Th timescale: (d) Hulu-cave $\Delta^{14}C$ data as reported in three separate datasets. In the following, we refer to the H82 and MSD samples, but we exclude the off-axis H82 measurements by Southon et al., as they show more outliers and wider dating uncertainties.

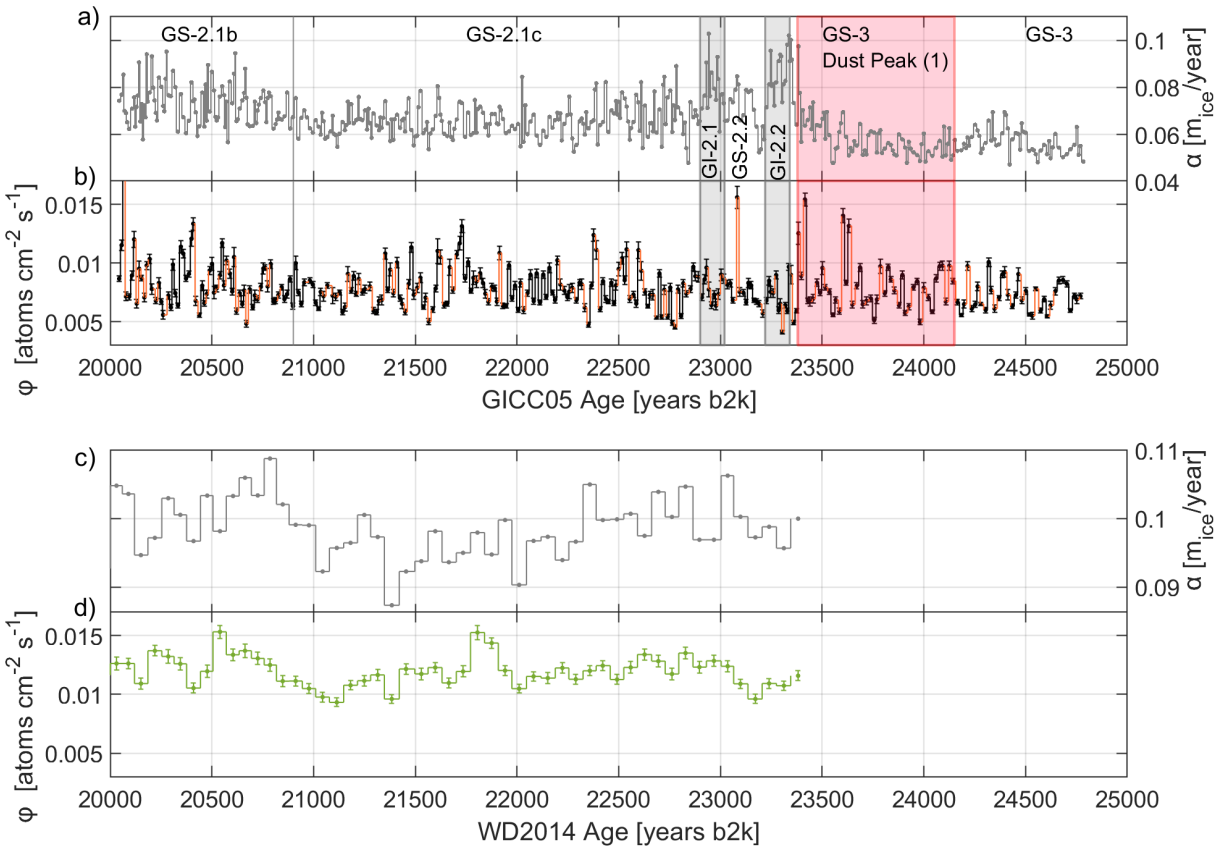

Figure 5.2 Accumulation rates and ^{10}Be fluxes of NorthGRIP2 (a, b) and WDC (c, d).
(a) The accumulation rate of NorthGRIP2 was obtained from the GICC05 layer thicknesses and the strain model (Johnsen et al., 2001) and down-sampled to the same depth-resolution as the ^{10}Be concentrations. The uncertainty on each accumulation rate measurement was estimated from the std. dev. of the data within each depth interval. (b) The fluxes of NorthGRIP2 show less climate-related fluctuations than the concentrations, as expected, and have an average of 0.008 ± 0.002 atoms cm^{-2} s^{-1}. (c) The published accumulation rate of WDC (Fudge et al., 2016) was down-sampled to the same age-resolution of the WDC ^{10}Be concentrations. (d) The WDC ^{10}Be fluxes are shown on the same scaling as the NorthGRIP2 fluxes for comparison. The average WDC flux is 0.011 ± 0.001 atoms cm^{-2} s^{-1}, higher than in Greenland either because of depositional differences between the poles (Heikkilä et al., 2013) or because of accumulation rate or thinning correction inaccuracies.

For NorthGRIP2, the layer thickness is known by direct layer counting (Andersen et al., 2006), while the thinning was modelled by Johnsen et al. (2001). For GRIP and GISP2, the annual layer thickness is interpolated from the volcanic match to NorthGRIP2 (Rasmussen et al., 2008; Seierstad et al., 2014). During interstadials with well-resolved volcanic tie points, it was measured that the two Summit cores (GRIP and GISP2) have a stadial-interstadial accumulation difference that is 10% higher than at NorthGRIP (Seierstad et. al,

2014). Thus, due to the scarcity of volcanic tie points across the LGM, the accumulation difference for GI-2.1 and 2.2 may be underestimated for GRIP and GISP2. The most recent version of thinning functions for the GRIP and GISP2 was used to calculate fluxes in this study (Lin et al., 2021; Hvidberg et al., 1997). For WDC, the accumulation rate was reported by Fudge et al. (2016) as a result of the WD2014 layer thicknesses and modelled thinning (Buizert et al., 2015).

The fluxes of the new datasets are shown in Figure 5.2, together with the modelled accumulation rates. The fluxes of NorthGRIP were checked for residual correlation with climate proxies (Figure 5.14), which shows that the flux-conversion largely removes the climatic influence on ^{10}Be deposition in Greenland.

5.4.4 Carbon cycle modelling and uncertainties

A carbon-cycle model (here Siegenthaler, 1983) is necessary to derive the atmospheric Δ^{14}C signal, i.e. the decay and fractionation-corrected ratio of ^{14}C/^{12}C relative to a standard (Stuiver & Pollach, 1977). The model should be run with parameters that best represent the state of the carbon cycle, with the expectation that any residual anomaly will be related purely to production effects.

To compare the measured and the modelled Δ^{14}C, in this study we will make use of linear detrending, as this largely removes the systematic offsets associated with the unknown carbon cycle history and inventories. By varying the model parameters, some residual effect of the parametrization is observable in the amplitude of modelled Δ^{14}C changes, but not in the timing of the changes, which is most important here.

In the period 20-25 ka b2k, the measured Hulu Cave Δ^{14}C is about 500 ‰ (Figure 5.1e), which is higher than pre-industrial Holocene values, which are below 200 ‰ (Reimer et al., 2020). These higher values may be related to either one or all factors between a lower ocean diffusivity during the LGM (Muscheler et al., 2004), a lower atmospheric ^{12}C budget, resulting in higher ^{14}C/^{12}C ratios (Köhler et al., 2022), or a weaker geomagnetic field. For instance, the ^{10}Be production rates in the LGM are expected to be about 20% higher than today due to the lower geomagnetic field intensity at the time (Muscheler et al., 2004).

The state of the geomagnetic field directly affects both the ^{10}Be and ^{14}C production rates; there may be a disproportion between how much each radionuclide is affected (Masarik & Beer, 2009) but most studies do not find any difference (e.g. Kovaltsov et al., 2012; Herbst et al. 2017). Adolphi et al. (2018) also showed that around a change in the geomagnetic field,

^{10}Be production rates should be amplified by 30% to match the amplitude expected from geomagnetic field reconstructions.

To determine the most appropriate model parameters, we repeat the calibration by Adolphi et al. (2018) since the available ^{14}C data has been updated since then (Reimer et al. 2020). We run the model with different ocean ventilation values around the Laschamps geomagnetic excursion at 41 ka b2k (Figure 5.12). We find that, for values of ocean diffusivity between 25-40% of the pre-industrial Holocene value, the modelled Δ^{14}C match the IntCal20 data best. Moreover, this agrees with Muscheler et al. (2004) who performed a time-dependent adjustment of the ocean diffusivity parameter between 10-25 ka to match the model to the measured Δ^{14}C. In their study, the LGM ocean diffusivity was set to ~1000 m^2/yr, about 25% of the pre-industrial Holocene value.

We find that a 20% production rate amplification of the normalized ^{10}Be and an ocean diffusivity of 25% of the pre-industrial Holocene value produce modelled outputs of about 500 ‰, in agreement with the Hulu-cave measurements, although the model fails to capture the decreasing trend. We note that this is not necessarily a realistic parameter of the state of the carbon cycle, but allows us to match some of the main features seen in the data. We associate no uncertainty with the model parameters since no setup realistically explains all the Δ^{14}C features.

5.4.4.1 *Sensitivity tests: ocean diffusivity changes, accumulation rate uncertainties, measurement uncertainties.*

We performed sensitivity tests to provide an uncertainty boundary for the detrended modelled Δ^{14}C curves. As a first sensitivity test, we investigated how short-term changes in the ocean diffusivity affect the modelled output because during the LGM there have likely been changes in the carbon cycle, because of the GIs and the HS-2 (Bauska et al., 2021). A time-dependent change in ocean diffusivity was induced according to 3 different scenarios, as shown in Figure 5.3b: either an abrupt warming (higher diffusivity: 80% of the pre-industrial value), an abrupt cooling (lower diffusivity: 25% of the pre-industrial value), or a sequence of both. The control scenario is set at 50% of the pre-industrial value. The duration of the events is chosen to reflect changes in the NorthGRIP2 calcium record, while the transition time was set to 200 years. The input signal is a 200-year periodic wave with similar values to the NorthGRIP2 normalized ^{10}Be.

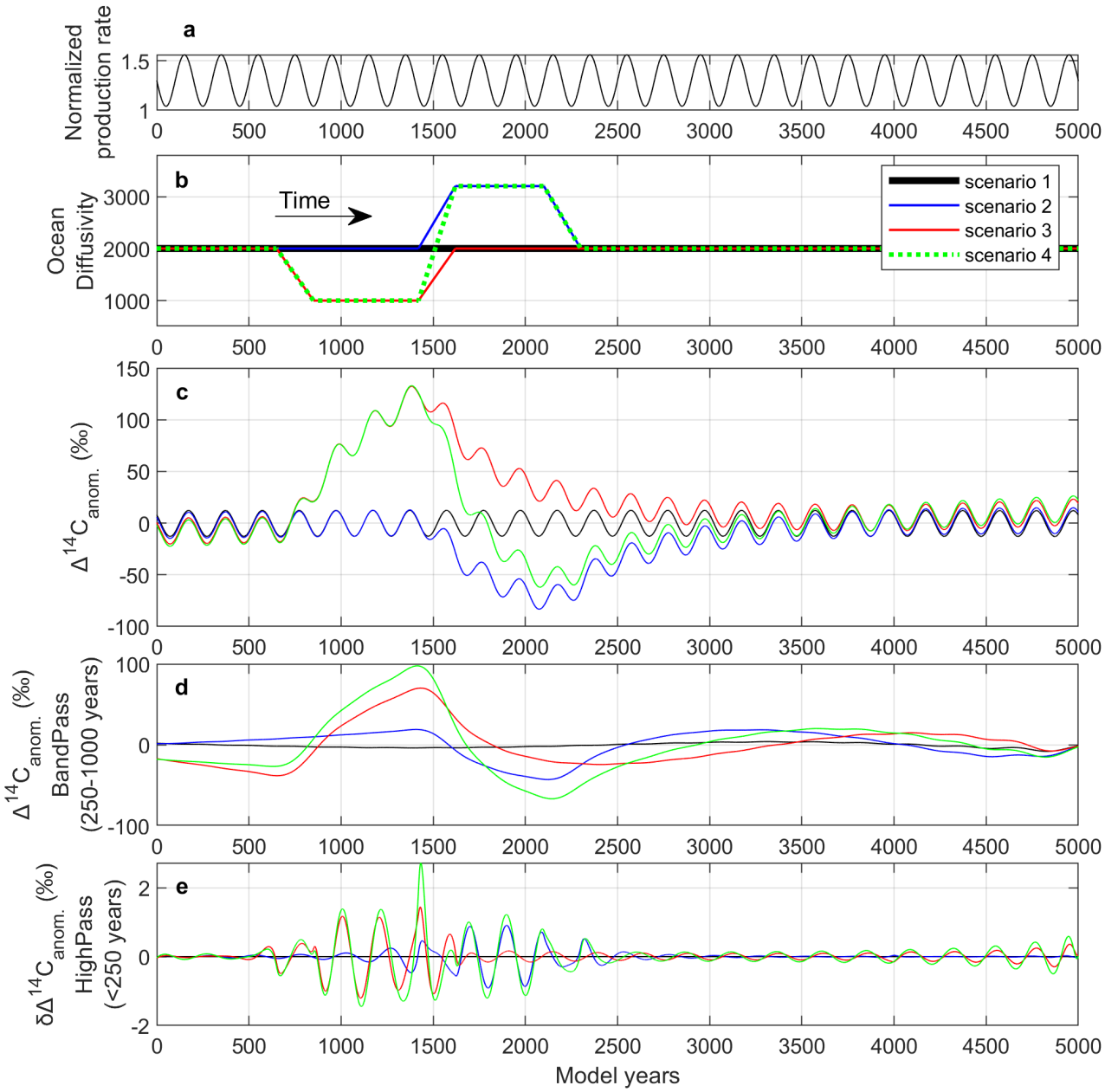

Figure 5.3 Sensitivity tests for time-dependent ocean diffusivity changes.
(a) Normalized production rate input (amplified by 1.2). (b) Scenarios of ocean diffusivity, as described in the text. (c) Modelled output, after linear detrending. (d) Long-term variations of the output (band-pass filtered output with periodicity 250-1000 years). (e) Differences in the short-term variations (high-pass filtered, up to 250-year periodicity) between the control scenario 1 and the other three scenarios (similar as in Adolphi & Muscheler, 2016).

In Figure 5.3c it can be seen that the effects of the perturbations are quite high and span several tens of ‰, after detrending. Thus, any feature in the ^{14}C records that is in the proximity of an abrupt climate change and has a comparable duration is uncertain and should not be used for matching. On the other hand, Figure 5.3e shows that short-term variations of the modelled signal are less affected by the diffusivity perturbations, hence they could, at

least in principle, be used to match signals exceeding 2 ‰ that are much shorter than the climatic transitions.

A second sensitivity test was made to investigate the effect of accumulation rate uncertainties related to the strain model. We performed 2 experimental model runs where we shifted the thinning function (inverse strain) by ±20% of the mean value between 20 and 25 ka b2k, which is a realistic modelling uncertainty between independent studies of the accumulation rate (Adolphi et al., 2018). Changing the strain rate creates an uncertainty of about 3 ‰ between the modelled and detrended $\Delta^{14}C$ curves, as shown in Figure 5.4d. Furthermore, with a similar approach, we quantify the uncertainty deriving from the ^{10}Be measurements to be 1 ‰ (Figure 5.13). Adding these independent contributions in quadrature, we set an uncertainty for our modelled $\Delta^{14}C$ of 5 ‰. This uncertainty serves as an initial parameter for the wiggle-matching algorithm, described in the next section; it furthermore agrees with the comparison of centennial variations of ^{14}C and ^{10}Be during the stable climate of the Holocene (Adolphi & Muscheler 2016). However, longer-term variations, as well as $\Delta^{14}C$ changes in the vicinity of climate perturbations, bear a considerably higher uncertainty.

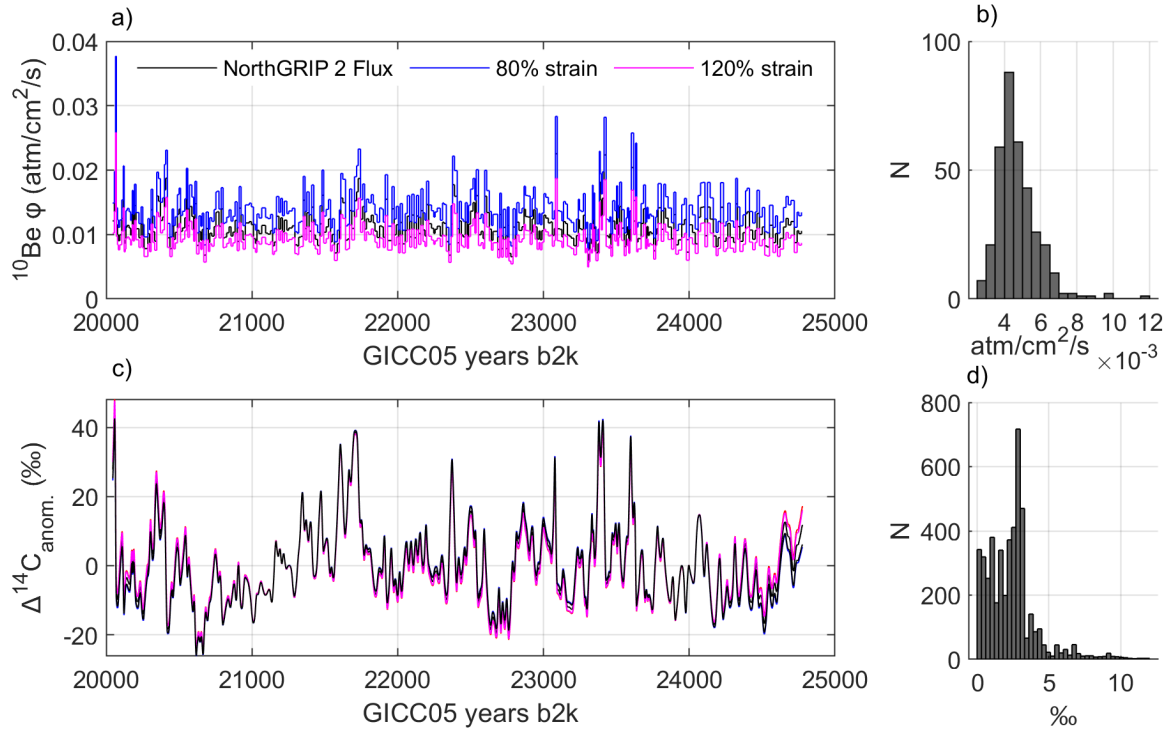

Figure 5.4 Sensitivity test of the effects of accumulation-rate uncertainties on the carbon-cycle modelling.
(a) Two strain-model scenarios produce different flux values. (b) The width of the distribution of differences between the flux curves is about 0.002 atoms/cm^2/s.

(continued caption of Figure 5.4) (c) The modelled $\Delta^{14}C$ curves are detrended, which largely accounts for differences between the scenarios. However, by subtracting each curve from the unperturbed scenario, and keeping the largest offset, we obtain a distribution of the difference between the curves (panel d). Most data points of the three curves lie within 3 ‰ of each other, which can be taken as an uncertainty contribution derived from the ±20% perturbation of the ice accumulation model.

5.4.5 The wiggle-matching algorithm reproduced from Adolphi & Muscheler (2016) and its uncertainty

Along with the visual inspection, an important tool for the quantification of offsets between timescales is the wiggle-matching algorithm, adapted by Adolphi & Muscheler (2016) from the original formulation by Bronk Ramsey et al. (2001), and described in detail therein. The first input for the algorithm is the detrended $\Delta^{14}C$ as modelled from the ice-core ^{10}Be concentrations or fluxes. The second input is the detrended $\Delta^{14}C$ data from the Hulu Cave stalagmite samples. The output of the algorithm is a probability density function of the timescale offsets $\vec{t}_{offset}$.

Following the approach by Adolphi & Muscheler, we investigated the probability within partially overlapping time windows $\overrightarrow{W}$, obtaining a two-dimensional probability matrix $\boldsymbol{P}(\overrightarrow{W}, \vec{t}_{offset})$. This is intended as a way to analyze the offset in a time-dependent fashion since the algorithm does not allow for stretching of the underlying timescales. We summarize the algorithm settings in the Method Appendix.

The position of the time-dependent mode of $\boldsymbol{P}\left(\overrightarrow{W}, \vec{t}_{offset}\right)$ is here defined as the most likely timescale offset $t^*_{offset}(\overrightarrow{W})$. The uncertainty of this estimation is given as the 68 % interval integrated on the 2-dim probability. By performing a time-dependent study of the offset over the time windows $\overrightarrow{W}$, we can first identify if a time-dependent behavior of the offset is justified or, eventually, we can define which time interval is most suited to average the offset over time, by identifying the limits T1 and T2 within which the offset is most stable.

The method for obtaining an average of the offset for each ice-core timescale is derived from the statistical considerations by Adolphi & Muscheler (2016). After applying the wiggle-matching algorithm for each ice-core/Hulu dataset pair, we evaluated if the time-dependency of the offset was motivated. We then computed an initial estimate of the average timescale offset between the visually established T1 and T2 boundaries, for the GICC05 timescale and for the WD2014 timescale. After shifting each ice-core dataset by the proposed average offset, we computed the χ^2 test between the speleothem and ice-

core $\Delta^{14}C$ curves. If the p-value was outside the 0.01-0.99 interval, we repeated the wiggle-matching using the standard deviation of the residuals (RSMD in ‰) for the uncertainty for the modelled $\Delta^{14}C$ curve. Then, we plotted the ice-core $t^*_{offset}(\overrightarrow{W})$ curves, we re-evaluated the boundaries T1 and T2 for averaging, and we average the curves within these intervals.

The uncertainty of our offset evaluation depends on the timescale uncertainties of both ice cores and speleothems, as well as on resolution limitations. Other than establishing the 68% confidence interval for the offset probability $\boldsymbol{P}(\overrightarrow{W}, \vec{t}_{offset})$, we also have to consider the information of running the wiggle matching with multiple ice-core ^{10}Be datasets, including concentrations and fluxes. We applied a Monte-Carlo protocol to estimate the uncertainty and we conducted the following steps:

- For each dataset and window W^*, we model the $\boldsymbol{P}(W^*, \vec{t}_{offset})$ as a Gaussian distribution with 1σ determined from the average lower and upper 34% boundary of the integrated $\boldsymbol{P}(W^*, \vec{t}_{offset})$.
- For each dataset and window W^*, we sample randomly from the Gaussian for 1000 times to derive an ensemble of timescale offsets;
- We compute the overall histogram of the likely offsets, including all datasets and all windows within the established time boundaries T1 and T2;
- We evaluate the 95% confidence interval of the histogram, around the average offset established previously.

In this way, we hope to have included in the uncertainty the information about the resolution of the Hulu Cave, the modelling uncertainties of the ice-core data, and information from multiple ice cores.

5.5 Results

5.5.1 A promising inter-ice-core tie point for ^{10}Be synchronization

Previously used for the matching by Adolphi et al. (2018), a ^{10}Be increase at 21.7 ka b2k (GICC05 ages) is visible in the new NorthGRIP2 data as well in the WDC dataset (Figure 5.1). This radionuclide increase resembles the ^{10}Be signal associated with the Maunder Solar Minimum (1645-1725 CE), which was a period of low solar activity and consequent increase in the global radionuclide production (Berggren et al., 2009; Eddy, 1976). In Figure 5.5, we

compare the Holocene and LGM counterparts of ^{10}Be at NorthGRIP finding similar shapes and duration, which supports the attribution of the ^{10}Be increase to a solar minimum during GS-2, which could explain the co-registration across ^{14}C and ^{10}Be datasets. All signals were normalized over the ±300-year window surrounding the event's peak.

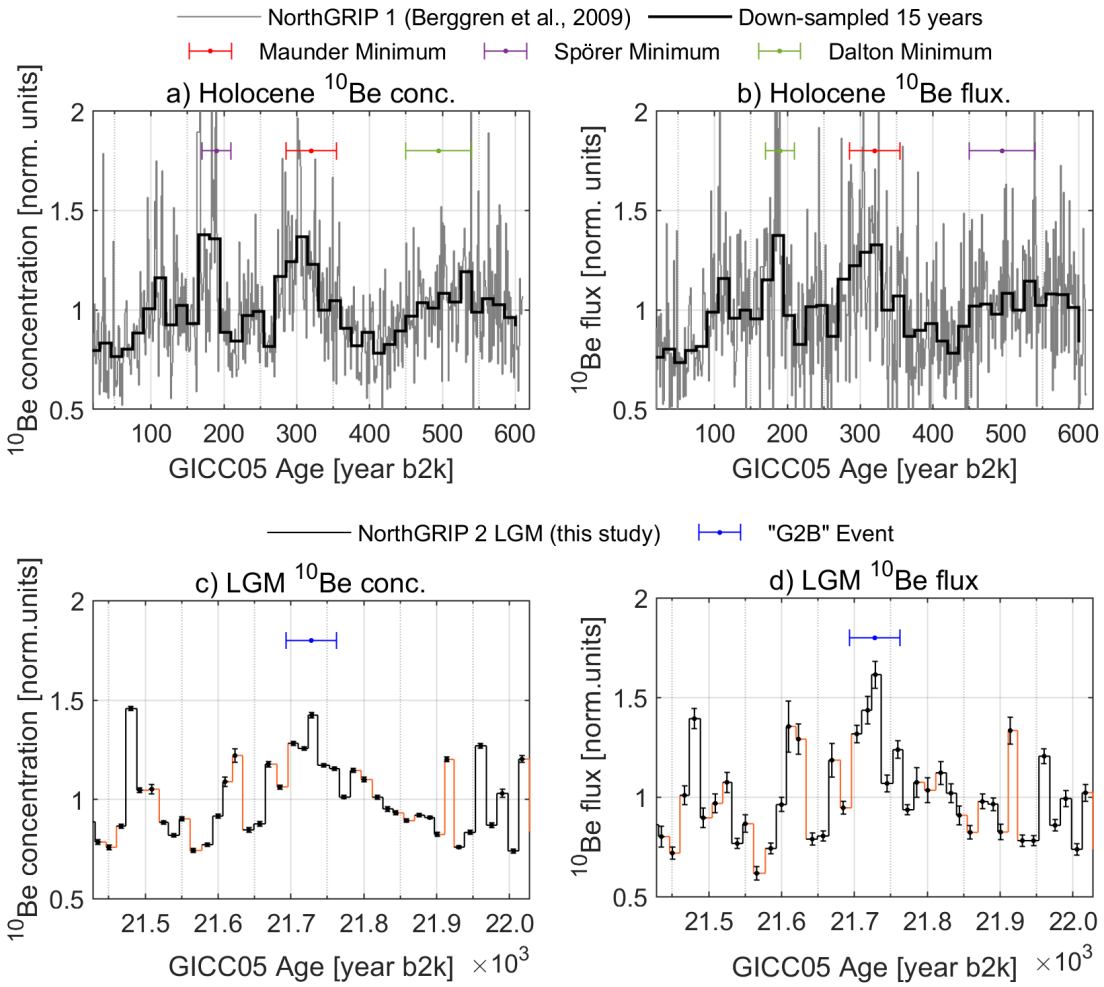

Figure 5.5 Comparison of ^{10}Be ice-core data in the Holocene, around the Maunder Minimum, and in the LGM, around the G2B Event.
By normalizing all data (dividing by their mean) within ±300 years of the central event, we ensure a better visual comparison of the data. (a, b) In the Holocene, the NorthGRIP 1 data by Berggren et al. (2009) are compared to the known duration of the grand solar minima, which were independently recorded in the sunspot observations. The down-sampling to 15 years allows for easier comparison to the LGM dataset below. We can visualize the effect of solar minima as an increase in the ^{10}Be production rate by about 40-50%. The fluxes show a more abrupt increase in time, while concentrations record a more gradual shape. (d, e) In the LGM, the similarity of shape and duration to the Maunder event supports the identification with a solar minimum.

In the Holocene, high accumulation makes the wet deposition mechanism of ^{10}Be predominant over dry deposition, so concentrations may be more representative of the true production rate (Berggren et al., 2009). During the glacial, model runs (e.g. Heikkilä & Smith, 2013) suggest that wet deposition is still predominant, but the abrupt accumulation rate changes observed across GIs require examining the fluxes to separate dilution effects from production effects. We examine both concentrations and fluxes in Figure 5.5, finding that in both cases the LGM and Holocene counterparts are very similar, which may imply a similar accumulation rate pattern caused by a solar event.

Based on the observed similarities in Figure 5.5, we call the ~22 ka b2k increase the "GS-2.1c ^{10}Be Event" (abbreviated G2B Event in the following) but without claiming a certain solar origin of the signal. To support the bipolar synchronization, after resampling the NorthGRIP2 ^{10}Be data on the resolution of WDC, we observe that the two ice cores register similar ^{10}Be amplitudes around the G2B Event. The flux increases 0.003 atoms cm^{-2} s^{-1} at both sites, which represents an increase of 40% and 30%, respectively, from the flux average values at NorthGRIP2 and WDC. The ^{10}Be concentration, on the other hand, increased only 30% (1.3 10^4 atoms/g) and 20% (0.9 10^4 atoms/g), respectively, from the concentration average values at NorthGRIP2 and WDC.

5.5.2 Synchronization between ice cores using ^{10}Be

Having established the G2B Event as a radionuclide production event, we can safely synchronize Greenlandic ice cores by inserting new ^{10}Be tie points between NorthGRIP and the GRIP and GISP2 ice cores. Furthermore, the G2B Event can be used to improve the bipolar matching to Antarctica (Figure 5.6).

We decided to compare the ^{10}Be data on similar resolutions to facilitate the identification of other common production features. Hence, we down-sampled the high-resolution data of NorthGRIP to the same resolution as GRIP and WDC, as ice-core ^{10}Be measurements are averages over the sampling depth intervals and lose variability with decreasing resolution.

In Figure 5.6, the ^{10}Be concentrations from NorthGRIP, GRIP and WDC are shown on their respective time scales together with a set of published non-climatic tie points (Seierstad et al., 2014; Svensson et al., 2020). Between NorthGRIP and GRIP, we observe important similarities in the ^{10}Be data, which leads us to suggest 6 new ^{10}Be tie points: a peak at 20.4 ka b2k, a double peak at 21.5 ka b2k, the G2B Event at 21.7 ka b2k, a single peak at 22.4 ka b2k, and a triple peak structure between 23.5 and 24.2 ka b2k. These tie points cover the previously tie-point-free section across GS-2.1b/c.

The match to WDC, of which the oldest tie point (no. 15) was published by Svensson et al. (2020), is extended with the aid of two additional ^{10}Be tie points that best resemble the Greenlandic signal (no. 4 and no. 7).

The ages of the tie points are summarized in Table 5.2, showing that the timescales of GRIP and NorthGRIP2 are slightly misaligned between 21 and 23 ka b2k by up to 27 years at the G2B Event, probably due to the fact that GRIP ages were interpolated between widely spaced tie points. The uncertainty of this misalignment can be estimated as half the resolution of the GRIP measurements (± 14 years, 1 σ), as this is likely to limit our matching precision. Furthermore, WD2014 and GICC05 are misaligned by 125±33 years at the G2B Event, WD2014 being older; the uncertainty on this offset is given as half the resolution of the WDC data, as this is most likely to impact our matching precision.

To improve the GRIP time scale, we calculated a new depth-depth interpolation between the two Greenlandic ice cores and we obtained a timescale correction, which we apply in the following to the GRIP data. On the resolution of GISP2, ^{10}Be appears to be sufficiently aligned around the G2B Event and the peak at 20.4 ka b2k, hence no time scale correction was applied to GISP2.

Table 5.2 ^{10}Be tie point ages between NorthGRIP, GRIP, and WDC. The internal difference between the Greenlandic cores (δ) reaches 27 years at the G2B Event. Likewise, the difference between WDC and NorthGRIP ages (Δ) indicates older ages for WDC at the G2B Event and the youngest no. 4 tie point.

	GICC05 Age (years b2k)			WD2014 Age (years b2k)	
tie point	NorthGRIP2	GRIP	Δ	WDC	Δ(WDC-NorthGRIP2)
4	20373	20370	3	20541	168±33
5	21372	21347	25		
6	21484	21458	26		
7 (G2B Event)	21710	21683	27±14	21835	125±33
9	22383	22398	-15		
14	24119	24103	16		

The fact that the G2B Event is 27 years older in NorthGRIP2 than GRIP also means that the GRIP accumulation rate needs to be corrected because of the corresponding changes to the layer thicknesses induced by the new tie points. This was done by multiplying the GICC05 timescale of GRIP by a correction function that computes the relative change of the layer thickness between the tie points. For example, since NorthGRIP2 has 1235 layers between tie-points nr. 4 and 7, while GRIP only has 1210 layers, the correction factor for the

accumulation rate between these tie-points is 1.02. Due to these relatively small-magnitude corrections, we do not find it necessary to apply any smoothing to the correction function. In the following, we denote fluxes of GRIP that were corrected in this way as "corrected fluxes" when we need to distinguish them from the previous version used by Adolphi et al. (2018). Although the effect of the accumulation correction is small, in section 5.5.3 we will show that this method has a significant impact on the amplitude of the G2B Event signal in GRIP, making the NorthGRIP and GRIP modelled $\Delta^{14}C$ curves look more alike.

In Figure 5.6, selected climatic proxies are shown to illustrate that a bipolar match across the LGM is already sufficient to change the timing between the two GIs and the AIM-2, bringing the AIM-2 peak to be closer to the GI-2.2 onset (a "before version" of the alignment of the climatic proxies can be found in Figure 5.7). However, the alignment at the G2B Event is not sufficient to alter the order of the GI-2–AIM-2 sequence. What the new alignment shows is that the AIM-2 warming occurs within the dust peak and that the AIM-2 cooling is starting close to the dust peak's termination.

In the WDC isotope data, we fit a curve to the AIM data to determine both the likely age for the onset of the warming slope and the peak on the original WD2014 time scale. We used the Matlab function 'WDC_breakpoint' provided by WAIS project members (2015), which fits the AIM shape with a double-polynomial fit. By 10'000 Monte Carlo iterations, we perturb the $\delta^{18}O$ signal with its noise, 0.4 ‰, i.e. the standard deviation between 24.5 and 25.5 ka b2k. From the distribution of the fitted breakpoints, we obtain the location of the AIM-2 peak as 23715±104 years (1 σ). Similarly, we derive the onset of the AIM-2 warming to be 24272 ± 35 years (1 σ). We also determine the onset of the CH_4 increase at 24060 ± 118 (1σ) years b2k, as the instant at which the signal becomes higher (and remains higher) than 1 standard deviation from the average baseline of the period 24.5-25.5 ka b2k. The uncertainty of the CH_4 onset is quoted from the gas age uncertainty of WD2014 (Fudge et al., 2017), which is only really appropriate to compare CH_4 to the $\delta^{18}O$ signal of the same ice core, WDC. All values are summarized in Table 5.3.

By aligning the two ice-core time scales at the G2B Event, and without stretching the time scales, we shift the GICC05 data by 125 years compared to WD2014 data. We observe that

the AIM-2 peak now happens 250 years before the onset of GI-2.2, instead of 375 years before as was the case on the original time scales.

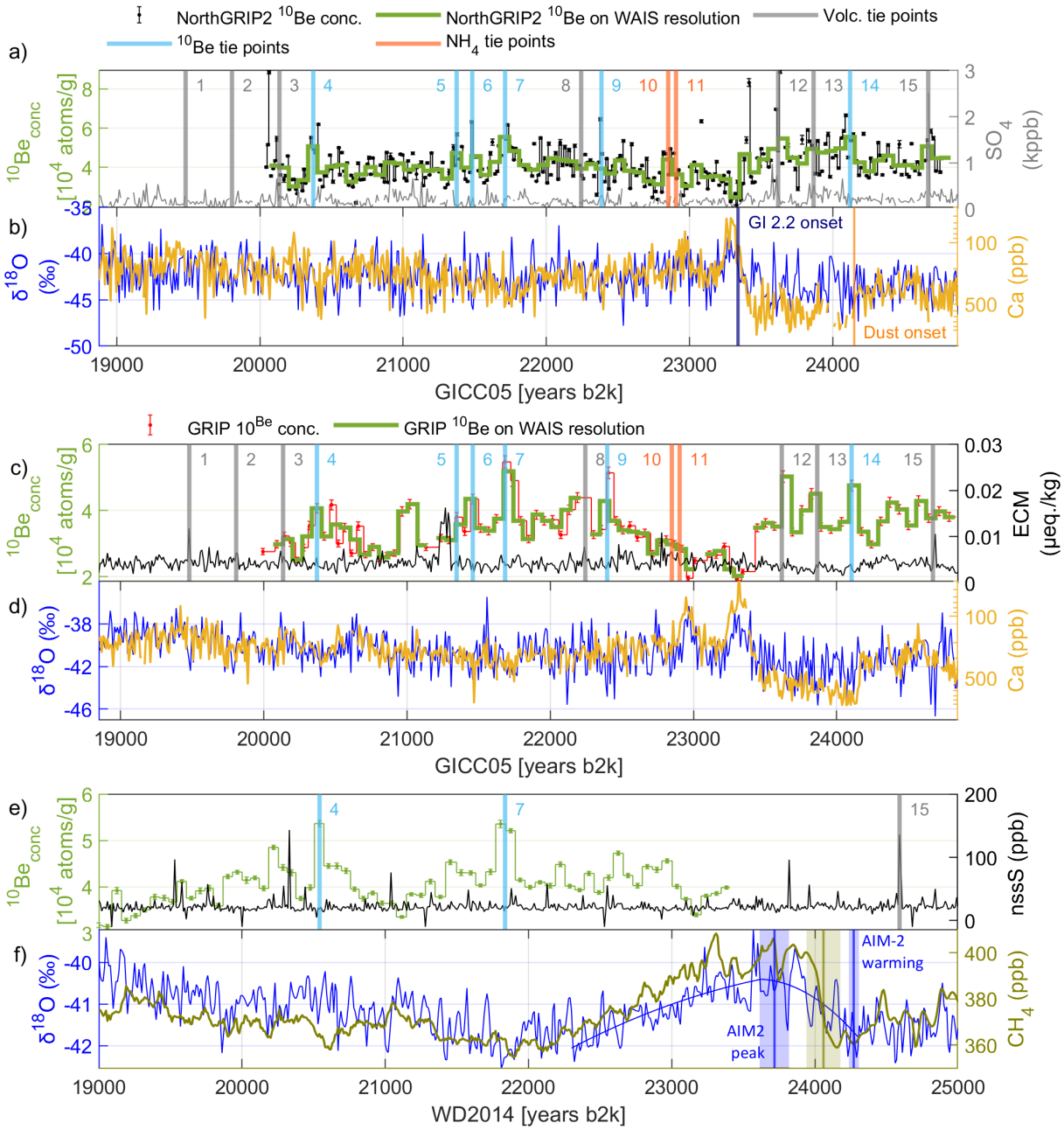

Figure 5.6 Bipolar tie points and climatic proxies. Vertical bars indicate tie point positioning. The data were aligned by tie point 7 (G2B Event), without stretching the timescales. (a) The NorthGRIP2 ^{10}Be concentrations (black) were down-sampled to the WDC resolution (green). The sulfate data (grey) supports the volcanic match, while ammonium data, on which tie points no. 10 and 11 were based, are not shown for clarity.
(b) $\delta^{18}O$ and Ca^{2+} at NorthGRIP (calcium is on an inverted log-scale) qualitatively represent the climate and determine the timing of GIs and the GS-3 dust peak.

(c) GRIP ^{10}Be concentrations (red), having a 27-year resolution, were down-sampled to the WDC resolution (green). ECM (black) represents volcanic tie points, although some eruptions are better visible in the sulfate signal (not shown).
(d) $\delta^{18}O$ and Ca^{2+} at GRIP are similar to NorthGRIP data. (e) WDC ^{10}Be data (green) and nssS (black), on which we base the new bipolar tie points (no. 15 by Svensson et al., 2020). (f) WDC climatic proxies, with CH_4 presented on the gas chronology by Buizert et al. (2015). We observe the occurrence of the AIM-2 warming in Antarctica as an increase of $\delta^{18}O$. The shape of the AIM-2 was calculated by a polynomial fit. The age of the increase of CH_4 by ~50 ppb was also calculated.

Finally, an average of the ^{10}Be fluxes of the three Greenlandic ice cores was calculated by stacking the NorthGRIP2, GRIP (corrected flux) and GISP2 fluxes, using Monte-Carlo bootstrapping (Adolphi et al., 2018). For each iteration, three of the data series are selected with resampling, each dataset is perturbed within its errors, and averaged. The stack is shown in Figure 5.11, with uncertainty bands derived from the standard deviation of the 1000 simulated fluxes.

The assumption behind averaging fluxes is that local accumulation effects are mostly removed by the conversion to fluxes and that the climatic effects on ^{10}Be deposition are the same over Greenland. Stacking the fluxes combines the information from three ice-core locations (or two, if one considers how close GRIP and GISP2 are) and therefore results in a different Δ^{14}C than the interpolation over NorthGRIP data gaps.

5.5.3 Carbon cycle modelling and wiggle-matching

Inspection of the measured Δ^{14}C (Figure 5.7a) and the ^{10}Be-based modelled Δ^{14}C (Figure 5.7 b, c, e) confirms the expectation that a shift of the two ice-core timescales towards older ages is required for a better alignment with the Hulu-cave radionuclides.

We observe two non-climatic tie-points between all Δ^{14}C curves:

1) The G2B Event: a relatively abrupt increase of 30 ‰ in the modelled Δ^{14}C from ^{10}Be, reaching its maximum at 21725 years b2k (GICC05 ages), about 100 years after the maximum is reached in ^{10}Be fluxes. The most likely equivalent of this event is observed in the Hulu Cave data at around 22200 years b2k (U/Th ages), where an increase of about 25 ‰ happens abruptly between two data points which is followed by a slow decrease. In the H82 data by Southon et al., the increase is much less abrupt and spans 4 data points.
2) A smaller peak is observed in the ice-core data at 20400 years b2k (GICC05). In Hulu Cave data, one data point at 20800 years b2k (U/Th) is visible in the MSD dataset, but the H82 sample does not show this peak. In the original ^{10}Be fluxes, this

event is probably caused by the combination of two peaks, one at about the same age and one at 20600 years b2k (e.g. see Figure 5.2). The amplitude of the event is about 40 ‰.

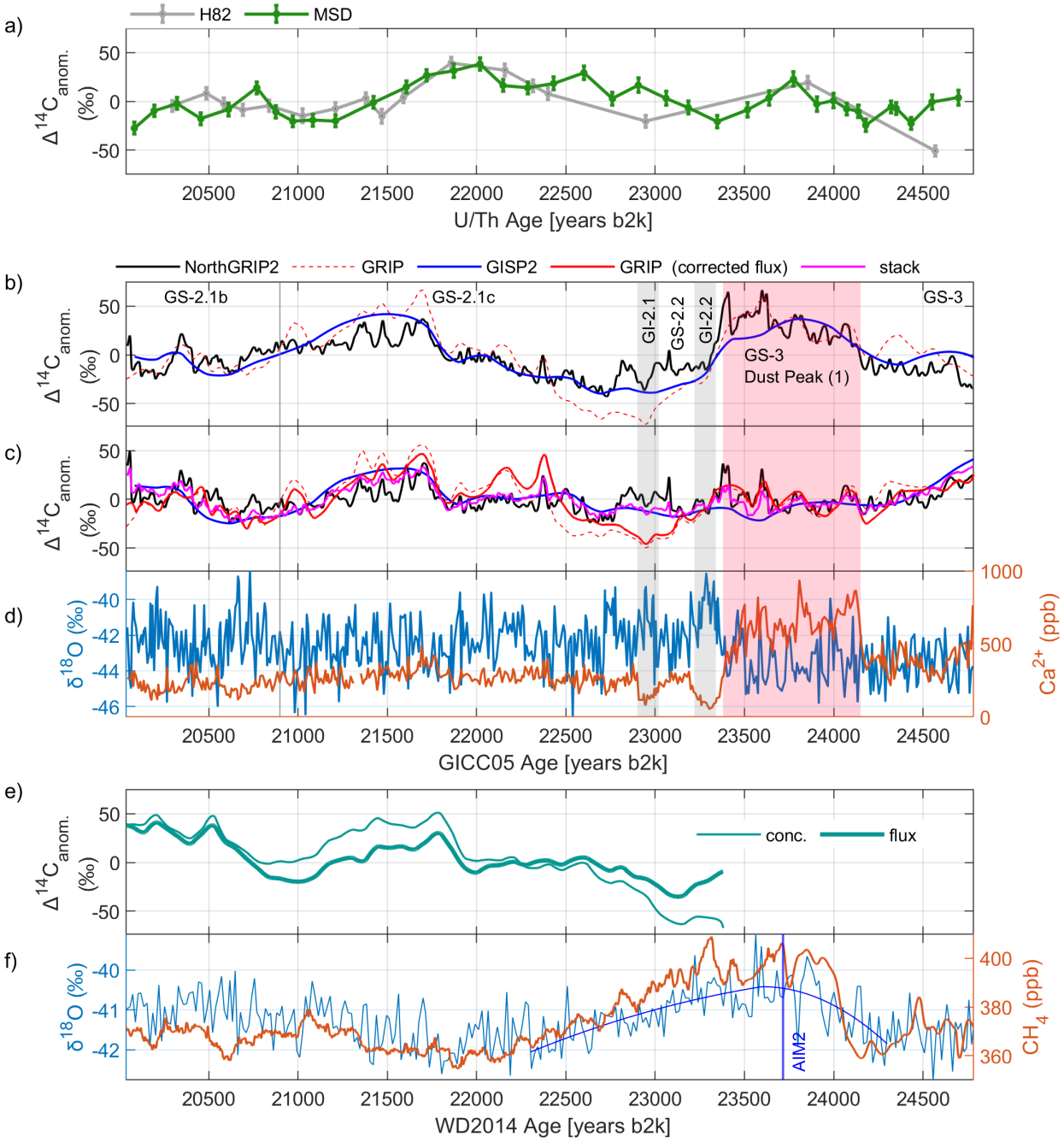

Figure 5.7 Carbon-cycle modelled $\Delta^{14}C$ compared to measured Hulu Cave data and climatic data before synchronization.
(a) Measured Hulu Cave data that will be used for synchronization (H82: Southon et al., 2012; MSD: Cheng et al., 2018). (b) Modelled $\Delta^{14}C$ from Greenland ^{10}Be concentrations (NorthGRIP, GRIP and GISP2 datasets).

(c) $\Delta^{14}C$ from Greenland ^{10}Be fluxes, including the flux stack (magenta). The effect of the flux correction of GRIP is mostly visible around the G2B Event, where the corrected data shows a better agreement with the other cores. (d) Climatic data from NorthGRIP ($\delta^{18}O$ and calcium) contains the signature of the dust peak and the GIs. (e) $\Delta^{14}C$ modelled from WDC ^{10}Be fluxes and concentrations. We can identify the G2B Event and the other peak at 20.5 ka b2k as possible targets for matching. Due to a lower accumulation rate variability than in Greenland, modelled fluxes and concentrations of WDC are much more similar. (f) Climatic data from the WDC core.

We assume that the modelled and the measured $\Delta^{14}C$ should, after detrending, be representative of the same production signal and that the differences we observe in the datasets can be explained by noise, modelling uncertainties, and dynamics affecting the deposition rather than the production of the radionuclides. Therefore, we proceed with the wiggle-matching despite the observed differences.

Based on these considerations, we run the wiggle-matching algorithm exclusively in the 20.5-22.5 ka b2k range (U/Th ages), using data windows of 1300 years with an overlap of 50 years between successive windows. For the U/Th time scale, we use both Hulu datasets but we separate our treatment for the H82 and the newer MSD data (Southon et al., 2012; Cheng et al., 2018). For the WD2014 timescale, we use both the WDC ^{10}Be concentrations and fluxes, modelled to $\Delta^{14}C$, since they are similar after carbon modelling. For the GICC05 timescale, we use all available $\Delta^{14}C$ modelled from concentrations, fluxes, and the flux stack, since they are similar at least around the production features we are going to match.

By averaging the obtained offset curves across the datasets and the interval (Figure 5.15), we estimate the initial time scale offset to be 369 years for GICC05 and 235 years for WD2014, using the MSD dataset exclusively. Following the protocol outlined in the Methods section, we evaluated the χ^2 and the associated p-value between each shifted $\Delta^{14}C$ curve and the Hulu dataset to test the agreement between the $\Delta^{14}C$ curves. For the flux-based datasets, the p-values were satisfactory, except for the GRIP uncorrected fluxes, which we exclude from now on. In the case of the Greenlandic concentration-based curves, because of unsatisfactory p-values ($<<0.01$), we decided to set the $\Delta^{14}C$ uncertainty to the RMSD of each dataset, which is between 12 and 21 ‰, less than the amplitude of the matched features. We repeat the wiggle-matching for these cases.

After having set the uncertainties, we repeat the averaging of the timescale offset (Figure 5.8) between the MSD dataset and the GICC05 ensemble and we apply the Monte-Carlo iteration outlined in the Methods, between 21 and 22.1 ka b2k (the range highlighted in yellow in Figure 5.8a). We obtain the offset estimate of 400 and a 95% confidence interval from 185 to 575 years. The assumption behind this approach is that the offset should only

change slowly with time, which is supported by the flatness of most curves in Figure 5.8 (with exception of the concentration-based offsets of NorthGRIP and GISP2).

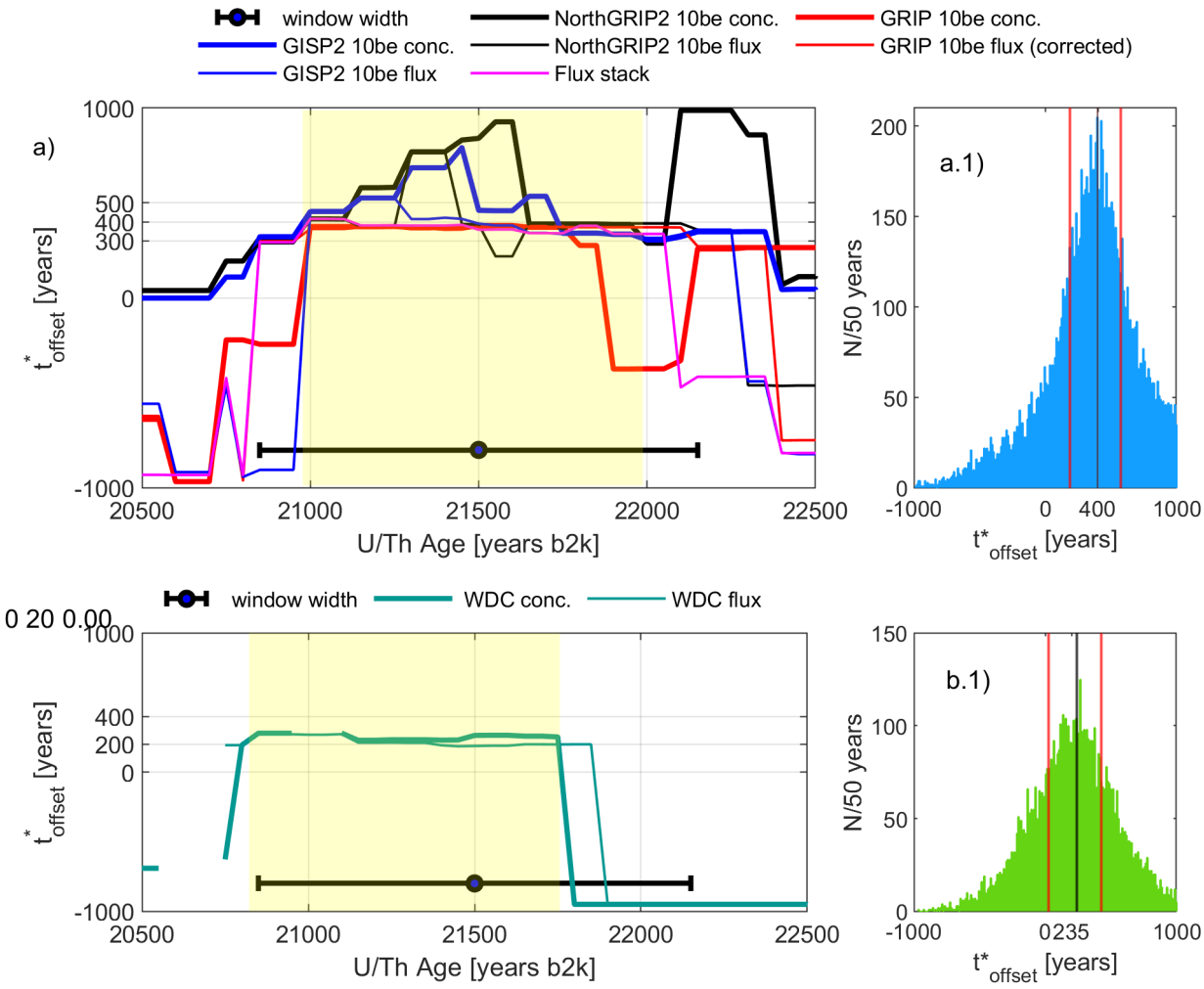

Figure 5.8 Wiggle-matching result around the G2B Event, repeated after enlarging the $\Delta^{14}C$ uncertainties of the concentration-based data, for Greenland (a) and the WDC core (b).
The time scale offset function $t^*_{offset}(\vec{W})$ of each ice-core dataset was calculated as the mode of the underlying 2-dim probability density function, estimated by the algorithm (Adolphi et al., 2016). The window width (horizontal black bar) is highlighted to show that each data-point represents the data comparison within the windows $\vec{W}$. Across the intervals highlighted in yellow, the individual ice-core datasets agree about the offset for each ice-core timescale. We also observe that the offset is not strongly time-dependent, hence we average over the highlighted time interval. (a) For the Greenlandic cores, each curve is also equipped with its 68% confidence interval (not shown for clarity). From these intervals, we sample randomly to obtain the histogram of the offsets within the yellow interval, shown in panel (a.1). From the histogram, we compute the average and the 95% confidence interval. (b) For WDC, the average offset curve of the concentrations and fluxes are the only available datasets for the calculation. The average offset within the interval (yellow) is computed similarly as for GICC05, with the Monte-Carlo histogram shown in panel (b.2).

For the WDC datasets, both flux- and concentration-based curves have p-values above the 0.01 tolerance, hence the estimation did not need to be repeated. We compute the average timescale offset (Figure 5.8) between the MSD dataset and the WD2014 ensemble of flux and concentration-based curves and we apply the Monte-Carlo iteration outlined in the Methods, between 20.8 and 21.75 ka b2k (the range highlighted in yellow in Figure 5.8b). We obtain the offset estimate of 235 and a 95% confidence interval from 25 to 425 years.
The difference between the ice-core offsets represents another estimate of the offset between the polar timescales, which in this way is determined to be ~160 years, close to the offset of 125±33 years obtained by synchronizing the G2B Event in the ^{10}Be fluxes.
Our result for GICC05 is smaller than the 550-year offset obtained by Adolphi et al. (2018) but fully consistent within the uncertainties of their estimate (95% probability interval: 215 – 670 years). For the H82 dataset, our analysis leads to wider and less precise offsets of about 500 ± 200 and 220 ± 500 years, for GICC05 and WD2014, respectively, which partly reproduces the 2018 finding.
In the following, we will assume the U/Th ages to be correct and shift the ice-core time scales accordingly, although, in principle, part of the offset could also be attributed to U/Th being too old because of measurement issues (Corrick et al., 2020).

5.6 Discussion

5.6.1 Climate compared after synchronization

In Figure 5.9 we show the radionuclide and climatic data after the synchronization proposed in section 5.5.3.
To reconstruct the sequence of events during the LGM, we need to define the onset and termination of HS-2. We suggest the onset of HS-2 to be defined by the $\delta^{18}O_{calcite}$ slope in Asian speleothems (Cheng et al., 2021). Here, we measured the onset of the HS-2 signal at Hulu Cave by the same methods used for the AIM-2, combining the WDC_breakpoint function with a Monte Carlo iteration.
By averaging the onset in the two $\delta^{18}O_{calcite}$ onsets at Hulu Cave, one for each dataset, we obtain 24.70±0.04 ka b2k. This is larger, albeit compatible within 2 σ, than the definition by Li et al. (2021) of an HS-2 onset at around 24.48±0.08 ka b2k, based on another speleothem (Furong, China).

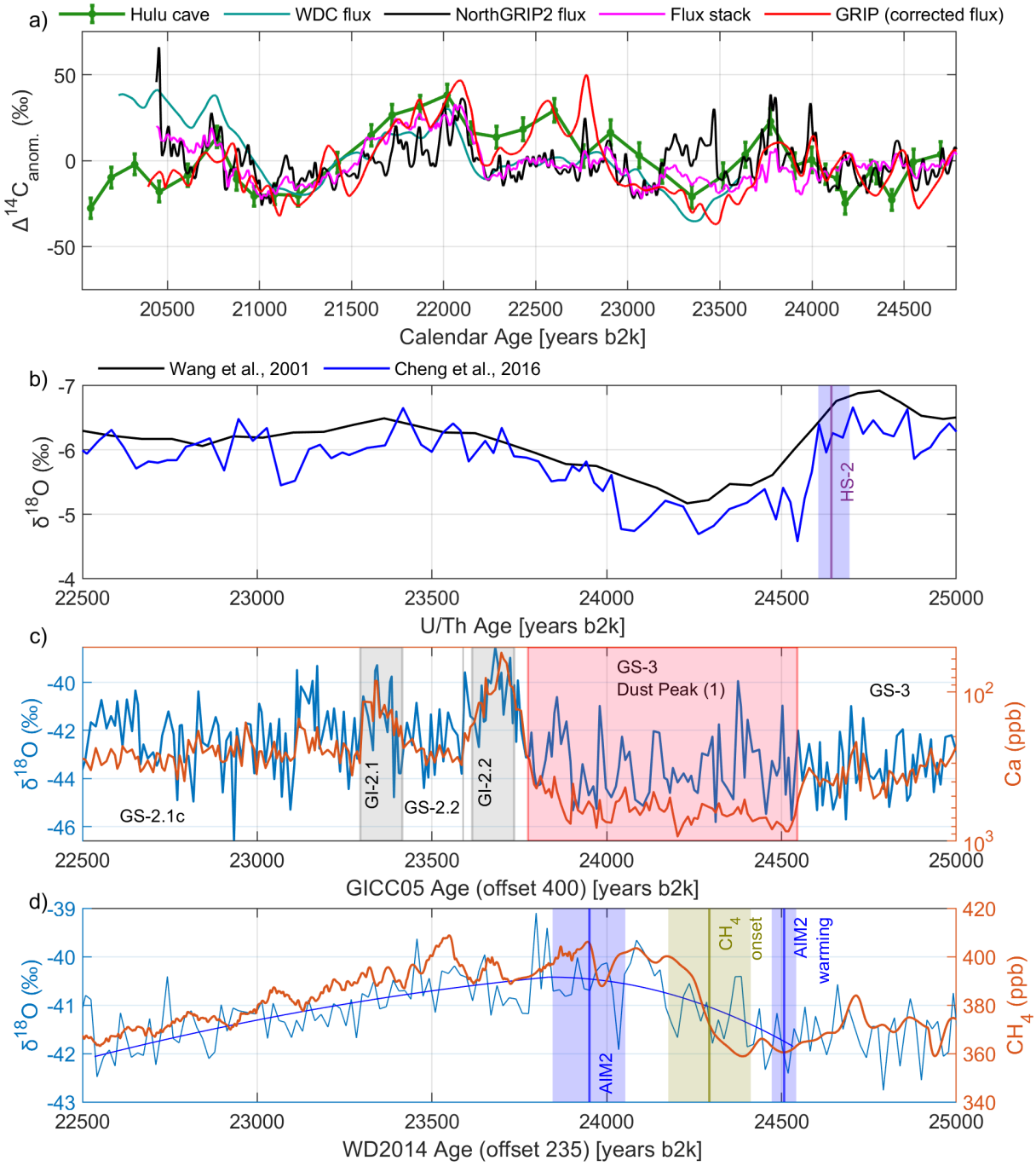

Figure 5.9 Radionuclide and climatic data after the synchronization.
The Greenlandic records were shifted by 400 years towards older ages, the WDC records by 235 years towards older ages. (a) Radionuclide data used for wiggle matching plotted on the synchronized time scales.
(b) Hulu-cave isotopes (reversed y-axis) highlight the suggested onset of HS-2 (Cheng et al., 2016). A lower-resolution dataset is also plotted for comparison (Wang et al., 2001). The termination of HS-2 is not defined, as multiple possibilities arise by comparing the two datasets.
(c) Greenlandic proxy data on the shifted GICC05 time scale. Calcium is presented on an inverted log-axis to better compare to the Hulu record.

(d) The AIM-2 period is shifted enough to align both with the dust peak and the HS-2 in Hulu $\delta^{18}O_{calcite}$. The onset of the methane increase occurs about 330 years after the AIM-2 warming, although we have to consider uncertainties in the gas age reconstruction. The shaded areas describe the uncertainty related to the event without the contribution from the wiggle-matching uncertainty.

Table 5.3 Event onsets and terminations discussed in this work as a consequence of the time scale shifts, with 1σ confidence intervals. The events are listed from oldest to youngest (although overlap may occur because of the uncertainty bounds). The Greenlandic events are ordered, meaning that any uncertainty overlap is an artefact: the uncertainty should rather be applied to the sequence as a whole. In the 'Original Calendar age' column, the onset of GIs and dust terminations are based on the original definition by Rasmussen et al. (2014) with reported uncertainties. At these ages, the MCE is about 600 years. The shape of the AIM-2 and CH_4 at WDC were measured as described in the main text. In the 'Age according to wiggle-matching synchronization' column, GICC05 has been shifted by 400^{+57}_{-26} years, while the WD2014 ages were shifted by 235^{+112}_{-183} years, towards older ages. The uncertainty on the new age was propagated from the original uncertainty and the offset uncertainty.

Event	Archive	Age according to wiggle-matching synchronization (y b2k)	Original Calendar age (y b2k)
HS-2 onset	Hulu $\delta^{18}O$	24641 ± 40	24641 ± 40
AIM-2 (warming onset)	$\delta^{18}O$ WDC	24706^{+128}_{-193}	24272 ± 35
Dust onset	NorthGRIP2 Ca	24545^{+60}_{-27}	24150±10
Methane onset	WDC CH_4	24294^{+162}_{-217}	24060±118
AIM-2 (cooling onset)	$\delta^{18}O$ WDC	23949^{+210}_{-152}	23715±104
Dust termination	NorthGRIP2 Ca	23775^{+60}_{-26}	23380±20
Start of GI-2.2	$\delta^{18}O$ Greenland	23735^{+60}_{-26}	23340±20
Start of GS-2.2	$\delta^{18}O$ Greenland	23615^{+60}_{-26}	23220±20
Start of GI-2.1	$\delta^{18}O$ Greenland	23415^{+60}_{-26}	23020±20
Start of GS-2.1c	$\delta^{18}O$ Greenland	23295^{+60}_{-26}	22900±20

With the time scale correction for WD2014, the onset of the AIM-2 warming occurred synchronously with the HS-2 onset, within the uncertainties determined both by the wiggle matching and by the AIM-2 fit, although a delay would be expected given the centennial-scale response of Antarctic climate to Northern Hemisphere changes (Pedro et al., 2018; Svensson et al., 2020). The AIM-2 cooling onset occurs together with or before the end of the Dust peak in Greenland, which is a similar result one obtains by merely synchronizing the data using the G2B Event tie point (Figure 5.6).

The methane increase in WDC is registered ~330 years after the AIM-2 warming. This strengthens the theory by Rhodes et al. (2015) of an increased southern biogenic methane production as a delayed response to extreme northern-hemispheric cooling. The high

methane levels appear to last between 460 and 800 years, depending on how one defines the end of the methane plateau.

5.6.2 Discussion on causes of the offset for GICC05

In recent work by He et al. (2021) it was observed that, although not reflected by Greenlandic water isotope records, a more complete shutdown of the AMOC likely occurred during Heinrich Stadial 1, producing a period of extreme winter cooling. They concluded that, rather than Greenland not experiencing any cooling during HS-1 (as proposed by Landais et al., 2018), the imprint of the cooling in the $\delta^{18}O$ signal was cancelled by the effect of having less winter snow, and an increase in the summer snow $\delta^{18}O$ level due to the first warming of the deglaciation. The flatness in the water isotope data is, in their analysis, the result of the counteracting effects of Greenland cooling, the HS-1-specific reduction in winter precipitation, and ^{18}O-enriched summer precipitation.

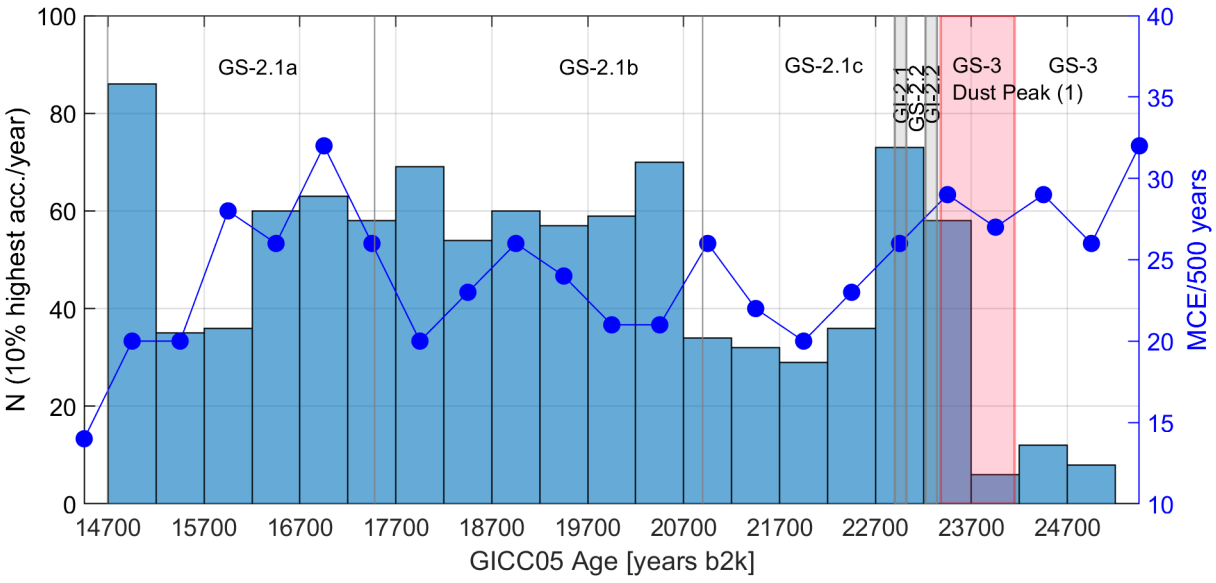

Figure 5.10 Highest accumulation years (histogram) and MCE (dark blue curve) of the GICC05 timescale, both computed on the same 500-years intervals.
The MCE appears rather constant over GS-2, except for some higher values at ~16.7 ka b2k. On the other hand, the thickest layers (>0.09 m/year; corresponding to the 10% thickest layers in the entire period) are located preferentially across GS-2.1b and 2.1a, with a sharp onset at 20.7 ka b2k. The first bin (14.7-15.2 ka b2k) also contains relatively thick layers, possibly an effect of the onset of GI-1. As expected, the thickest layers are often found over the brief interstadials, while over the dust peak the frequency of high-accumulation years is much lower. The thickest layers across GS-2.1b and 2.1a have comparable counts as interstadial periods, which is unclear given that this period was very cold and had very low annual precipitation (Kindler et al., 2014).

As much as the GICC05 layers are concerned, He et al. model a possible scenario over Greenland with a drastic decrease of daily winter precipitation by about 50% at the onset of HS-1. On the other hand, they predict the summer precipitation to increase steadily because of the deglaciation, which is largely unaffected by the AMOC shutdown. This would mean thin and irregular layers at the onset of HS-1, with the summer part of the layer gradually increasing over time.

Acknowledging these results and the 125 years offset between GICC05 and WD2014 at 22 ka b2k and the 400 years offset to the Hulu timescale, we proceed by discussing where the offset could have originated. According to Adolphi et al. (2018), the transfer function from GICC05 to IntCal is near to zero at 13 ka b2k, the closest tie-point younger than the G2B Event. Occurring between these two time horizons, the HS-1 period lasted from about 18 to 14.7 ka b2k, and is most often regarded as ending at the onset of GI-1. The authors of GICC05 resumed the prior subdivision of the corresponding stadial, GS-2.1, in 3 sections (termed a, b, and c) of which GS-2.1a starts at 17.48 ka b2k and ends at the onset of GI-1 (Björck et al., 1998; Rasmussen et al., 2014). The onset of GS-2.1a was originally defined by a 2nd-order water isotope dip but occurs synchronously with an increase in the Greenland ice-core calcium profiles at roughly 17.6 – 17.4 ka b2k.

If GICC05 missed a large number of annual layers across HS-1, the age of the onset of GS-2.1a would move towards older ages by a similar amount. We speculate that the onset of GS-2.1a could correspond to the onset of Heinrich Event 1 (and thus the HS-1 period) and that calcium could be used as a signature of the change of circulation perceived by Greenland during HS-1 as well as HS-2.

Part of the under-counted layers could be recorded in the MCE. The MCE is derived from the number of features that could be annual layers but are not clearly so; it does not properly account for layers not resolved by the data. Within GS-2a the MCE is ~150 years; if we assumed some uncertain layers to have systematically been there, between 150 and 300 years would appear in the chronology. However, according to He et al. (2021), a large number of unresolvable annual layers is a plausible scenario at least in the first part of HS-1 until the increasing summer precipitation alleviated the problem. Therefore, the MCE is probably not faithfully representing the full GICC05 uncertainty in sections where layer thicknesses are very small.

Apart from mis-assigned uncertain layers and layer missed altogether due to marginal data resolution, we can look for another explanation of what could have caused the under-count

of GICC05 layers. The layers that are on the higher end of the thickness distribution could indicate where very low or absent winter precipitation could have made multiple layers appear as one. We highlight the 10% highest accumulation years in Figure 5.10, where we also show the MCE, both per 500-year interval. The accumulation threshold is set at 0.09 m/year by integrating the highest 10% of the empirical distribution of the accumulation between 14.7 and 25 ka b2k. In the accumulation, values are consistently high over the entire GS-2.1b, with high-accumulation years occurring as frequent as in the short interstadials. For the MCE, it appears that observers of GICC05 encountered more issues at the onset of GS-2.1a, whereas the MCE stayed constant over the rest of GS-2.1. Hence, we suggest that a dating bias could have accumulated across GS-2.1a and GS-2.1b due to increased difficulty in identifying annual layers caused by a weakening of the annual signal due to reduced amounts of winter snow. However, we find no pressing evidence that this phenomenon occurs at the onset at HS-1 (17.7 ka b2k).

5.7 Conclusion

In this study, we have presented two new ^{10}Be datasets that allow both a bipolar synchronization and a comparison of Greenland climate to the Hulu speleothem archive, during the 20-25 ka b2k period. The new NorthGRIP ^{10}Be dataset supports a dating offset between GICC05 and U/Th time scales (400 [374-457] years), which is less than the 550-year estimate by Adolphi et al. (2018), albeit consistent within uncertainties. Likewise, an offset was found between U/Th Hulu Cave dates and the WD2014 time scale (235 [53-348] years).

For the WD2014 time scale, the offset can be compared to the uncertainties quoted for the time scale by Sigl et al., (2016). Between 20 and 25 ka b2k, 1σ uncertainties are between 100 and 125 years, which are smaller than the offset we find. This suggests that the authors of WD2014 may have underestimated their uncertainties, similar to GICC05, and that the layer counting in the glacial was likewise challenging. However, the gradual warming observed between 19 and 15 ka b2k (Pedro et al., 2011) likely did not lead to fast changes in the annual layers' expression. The WD2014 issues may thus be mostly related to the admitted low resolution of the data used for counting between 15 and 26 ka b2k (Sigl et al., 2016), which may have limited the accuracy of the time scale.

In terms of the sequence of events between 20 and 25 ka b2k, our time-scale offset does not change their order. However, the onset of the Greenlandic dust peak moved to be roughly

synchronous with the signal in the Hulu speleothem that has been linked to the HS-2 onset. The CH_4 onset in Antarctica also moved closer to the HS-2 onset, supporting the theory by Rhodes et al. (2015) of a long overlap of the methane plateau with the HS periods. The termination of the Greenlandic dust peak and the almost synchronous onset of GI-2.2 were brought closer to the AIM-2 peak, with the dust-peak termination occurring 175 [82,358] years after the AIM-2 onset (uncertainty given as the minimum and maximum distance considering the events' 1σ uncertainties). This may indicate an exception to the average delay of 122±24 years found within other GI-AIM pairs, where the GI generally occurs before the AIM breakpoint (Svensson et al., 2020). It is therefore possible that the very brief GIs did not impact the Antarctic $\delta^{18}O$ signal enough to have propagated the signal in time, and that AIM-2 is the product of the AMOC shutdown of HS-2.

We investigated several possible reasons why GICC05 could have undercounted annual layers across GS-2.1. We find that the MCE of GICC05 alone cannot explain the lack of layers in the GS-2.1, but that either very thin annual layers or missing winter precipitation made it difficult, if not impossible, to resolve the thinnest layers with the available data, and thus made the MCE estimation less robust.

In conclusion, the measurement of ^{10}Be in ice cores from bipolar locations is an essential tool for anchoring time scales together. Given that manual layer recognition has proven to be challenging in the glacial, measuring radionuclides is essential for time scale studies and this practice should continue in the future.

5.8 Acknowledgements

G.S. and S.O.R. acknowledge support via the ChronoClimate project funded by the Carlsberg Foundation.

FA acknowledges support through the Helmholtz Association (grant VH-NG-1501). RM acknowledges support from the Swedish research council (grants DNR2013-8421 and DNR2018-05469).

5.9 Data

^{10}Be data of NorthGRIP and WDC will be made available when this manuscript is submitted, as well as Matlab codes for reproducing the figures.

5.10 Methods Appendix

5.10.1 WDC measurements

Ice samples of 350-400 g were weighed, melted, and acidified with a solution containing ~0.18 mg of Be carrier. The samples were passed through a 30 µm Millipore filter and loaded onto a 3 ml cation exchange column (Dowex 50WX8) from which the Be fraction was eluted and purified following established procedures (Finkel and Nishiizumi 1997; Woodruff et al. 2013). The Be fraction was precipitated as $Be(OH)_2$, transferred to a small quartz vial and heated in a tube furnace at 850 ºC. The BeO was mixed with Nb powder (Alfa Aesar, -325 mesh, Puratronic, 99.99%) and pressed into a stainless-steel cathode. The $^{10}Be/^{9}Be$ ratios of samples and blanks were measured by accelerator mass spectrometry at Purdue's PRIME laboratory (Sharma et al. 2000), relative to well-documented $^{10}Be/Be$ AMS standards (Nishiizumi et al. 2007). The measured $^{10}Be/Be$ ratios of the samples were corrected for an average blank $^{10}Be/^{9}Be$ ratio of $10 \pm 3\ 10^{-15}$ which corresponds to typical blank corrections of 1-2% of the measured values. The blank-corrected values and amount of Be carrier added yield ^{10}Be concentrations ranging from 3.1 to 5.4 10^4 atoms/g (Figure 1d). Typical uncertainties (1σ) in the measured ^{10}Be concentrations are 1.5-3.5%.

5.10.2 NorthGRIP2 measurements

Ice cutting At present, the required minimum weight for each ^{10}Be measurement is around 120 g. About half of the samples, in alternate order, had previously been cut in the shape of gas sticks (section area of 3.5x3.5 cm^2), with a weight of around 600 g per bag (55 cm). The gas sticks were thus cut into 4 parts, resulting in pieces of 13.75 cm, corresponding to a resolution of about 7.5 years. The other half of the samples were cut from the archive piece to have a section area of ~2x3 cm^2. Each bag of these was then cut into two parts, hence each of such pieces weighs around 180 g and corresponds to about 14 years resolution. The campaign was performed with the necessity of keeping the total number of samples at around 320, for cost reasons. Since the total number of cut ice samples was 470, the pieces were selected to alternate between adjacent samples at 7.5 years resolution, to minimize the age gaps; the resulting ^{10}Be data necessarily shows some discontinuities.

Sample preparation and AMS Measurement (ETHZ) Ice samples of 150-180 g were weighed and a solution containing approximately 0.15 mg Be carrier (^{9}Be) was added, as well as 1 mL of Cl carrier (^{35}Cl). The samples were melted, not filtered, and run through

cation exchange columns, from which the Be fraction was extracted. The melted water was further run through anion exchange columns to retain the ^{36}Cl content and stored for future measurement. The resulting $Be(OH)_2$ was heated to obtain BeO and mixed with Niobium powder. Five blank samples of Milli-Q water were also measured for background correction. More details about the most recent preparation protocol which is used at the Lund Laboratory can be found in Adolphi et al. (2014) and Nguyen et al. (2021).

The $^{10}Be/^{9}Be$ ratios of the samples were measured in July 2020 at the AMS facilities at ETH in Zurich (Christl et al., 2013), where a total of 322 measurements was obtained. Measured $^{10}Be/^{9}Be$ ratios were normalized to the ETH Zurich in house standards S2007N and S2010N which in turn have been calibrated relative to primary standards provided by K. Nishiizumi (2007). An average blank correction of $^{10}Be/^{9}Be = 1.3 \pm 0.3\ 10^{-14}$ was applied to correct for ^{10}Be introduced with the Be-carrier. The blank correction corresponds to 2-3% of the measured ^{10}Be ratios. Calculated ^{10}Be concentrations range between 1.8 and 8.7 10^4 atoms/g and were decay corrected using a half-life of $1.387 \pm 0.016\ 10^6$ years. The final uncertainties of the ^{10}Be concentrations were between 1 and 10 %.

5.10.3 From concentrations to fluxes

The concentration to flux conversion, for ice cores, is obtained by simply applying $\varphi = C\rho_{ice}\gamma\alpha$, where φ is the flux, γ is the ^{10}Be concentration, α is the accumulation rate, C is a conversion constant, and ρ_{ice} is the ice density (0.917 g/cm^3). The accumulation rate is usually expressed as m_{ice}/year and the ^{10}Be concentrations in 10^4 atoms/g and, since we want to express the fluxes in units of atoms/cm^2/s, the conversion constant is $3.17\ 10^{-2}$ (dimensionless).

5.10.4 Wiggle-matching algorithm settings

Thanks to the higher resolution of ice-core data with respect to Hulu data and thanks to the carbon-cycle model producing a continuous output, we approximate the ice-core input as a continuous function of time, i.e. we resample it annually. The second input, the Hulu-cave data, is a collection of discrete data points. The uncertainties are about 6‰ for the Hulu Cave data and 5‰ for the ice-core data. The datasets are detrended within each observation window before computing the probabilities. In particular, the ice-core continuous data is first shifted according to the scanned time offset, then detrended with respect to the observation window, and resampled to the Hulu-cave sampling points.

5.11 Supplement to Paper V

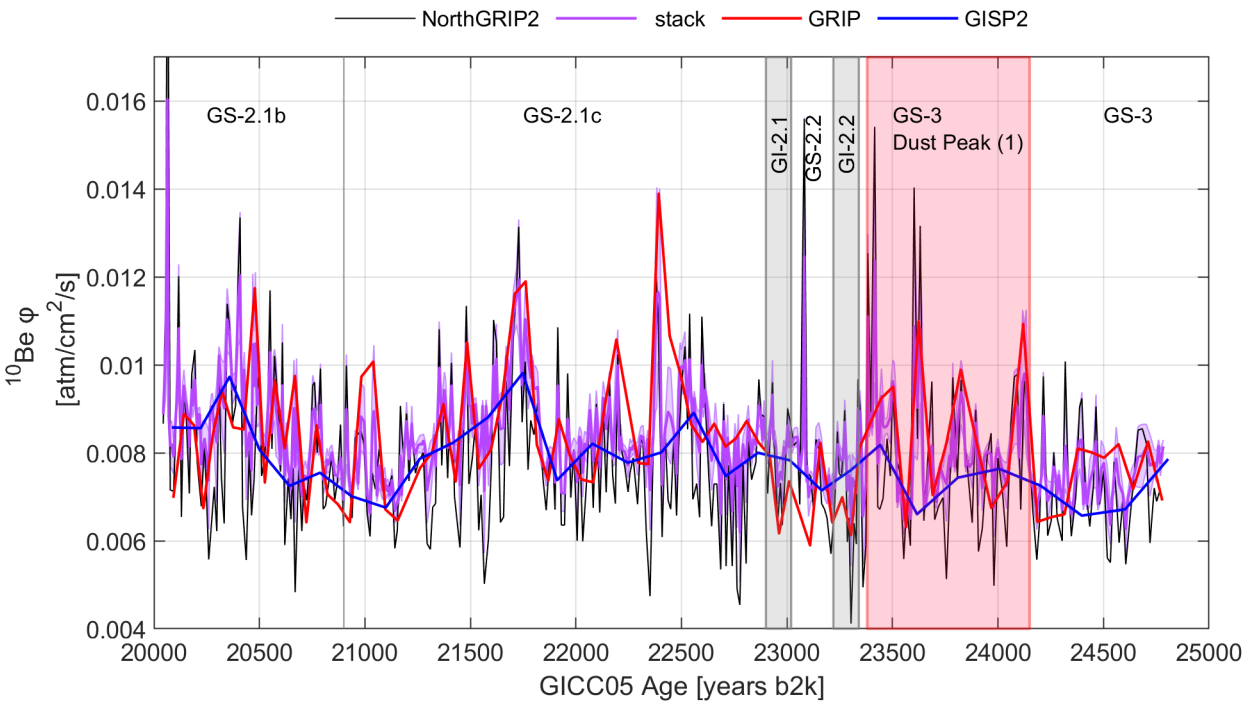

Figure 5.11 Stack of Greenland fluxes in the LGM, used in this study for the wiggle-matching, together with the other datasets.

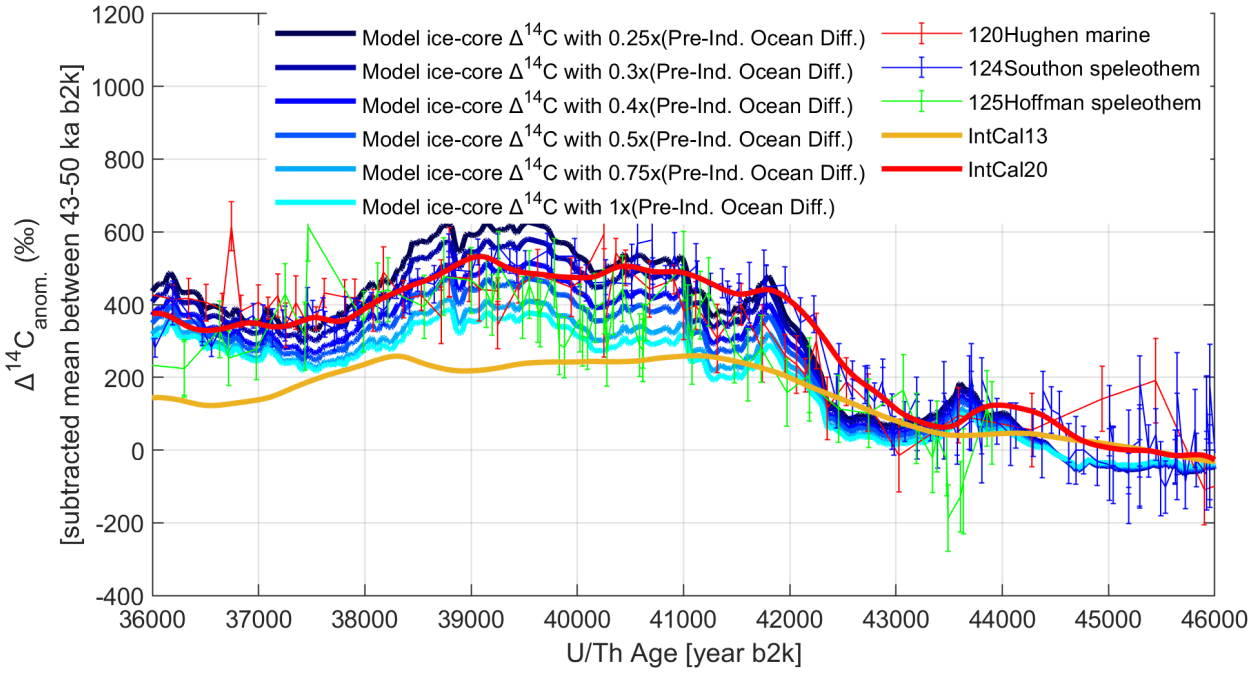

Figure 5.12 Modelling of GRIP data around the Laschamps event.

As a consequence of the lower shielding from GCRs, the geomagnetic excursion caused an increase both in ^{10}Be and ^{14}C production. The average between 43 and 46 ka b2k was subtracted from all datasets. The datasets underlying the IntCal20 curve show increases of about 400 ‰. By using the GRIP ^{10}Be data available at these ages (Yiou et al., 1997), The agreement with the IntCal20 curve and the underlying data is observed to be best for an ocean diffusivity that is ~25-40% of the Holocene pre-industrial value. The timescale of GRIP was shifted by ~200 years according to the timescale offset inferred by Adolphi et al. (2018).

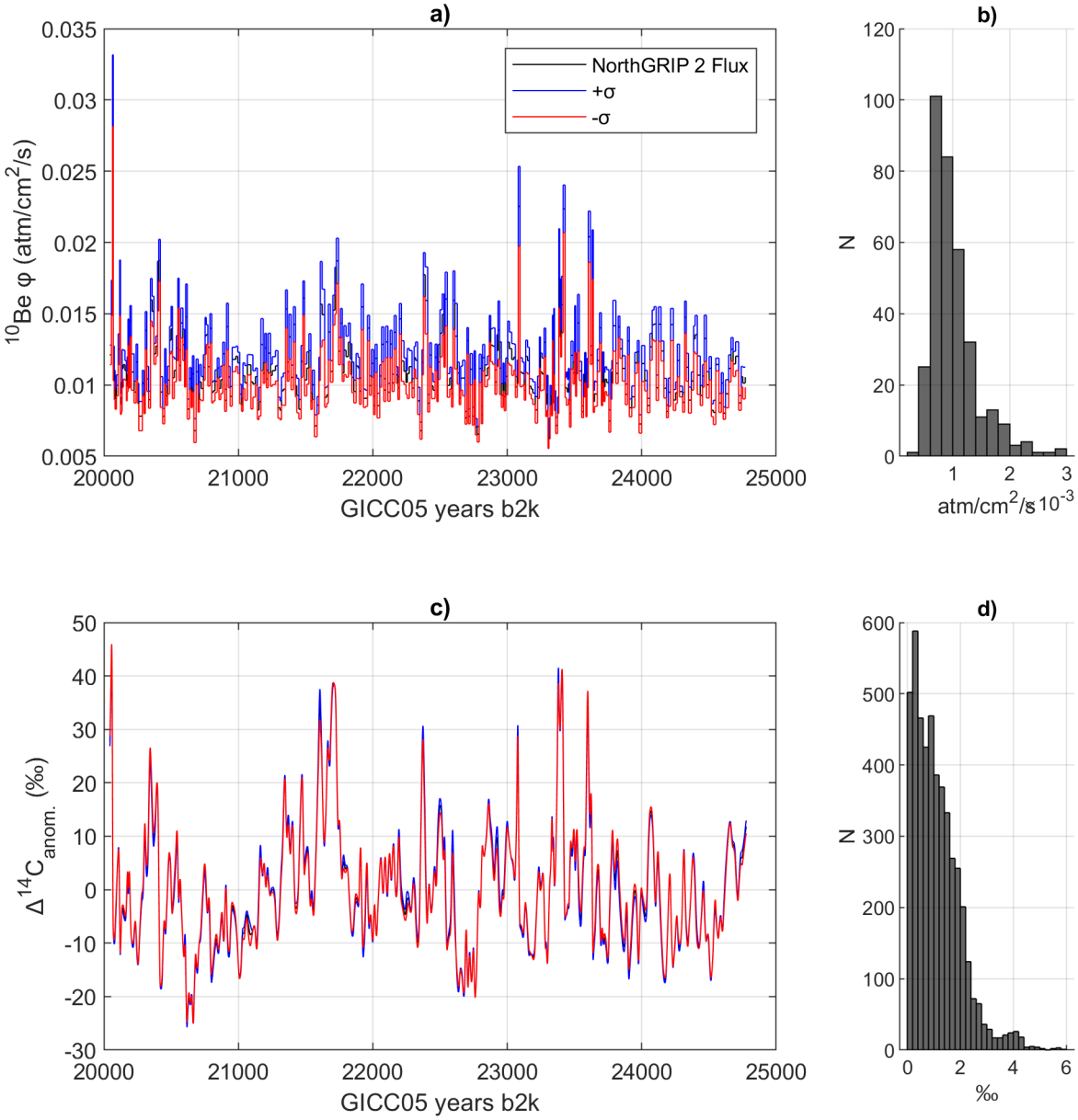

Figure 5.13 Same as Figure 5.4 but for modelling uncertainties derived from the measurement uncertainties of ^{10}Be fluxes, which are propagated from ^{10}Be concentration and the accumulation down-sampling.

We sum ± 1 σ to each measurement to obtain the two curves shown in panel (a), of which panel (b) shows the distribution of differences between the curves. The data are modelled in panel (c) and panel (d) shows that the result has about 1 ‰ uncertainty, encompassing most of the discrepancies between the modelled detrended curves.

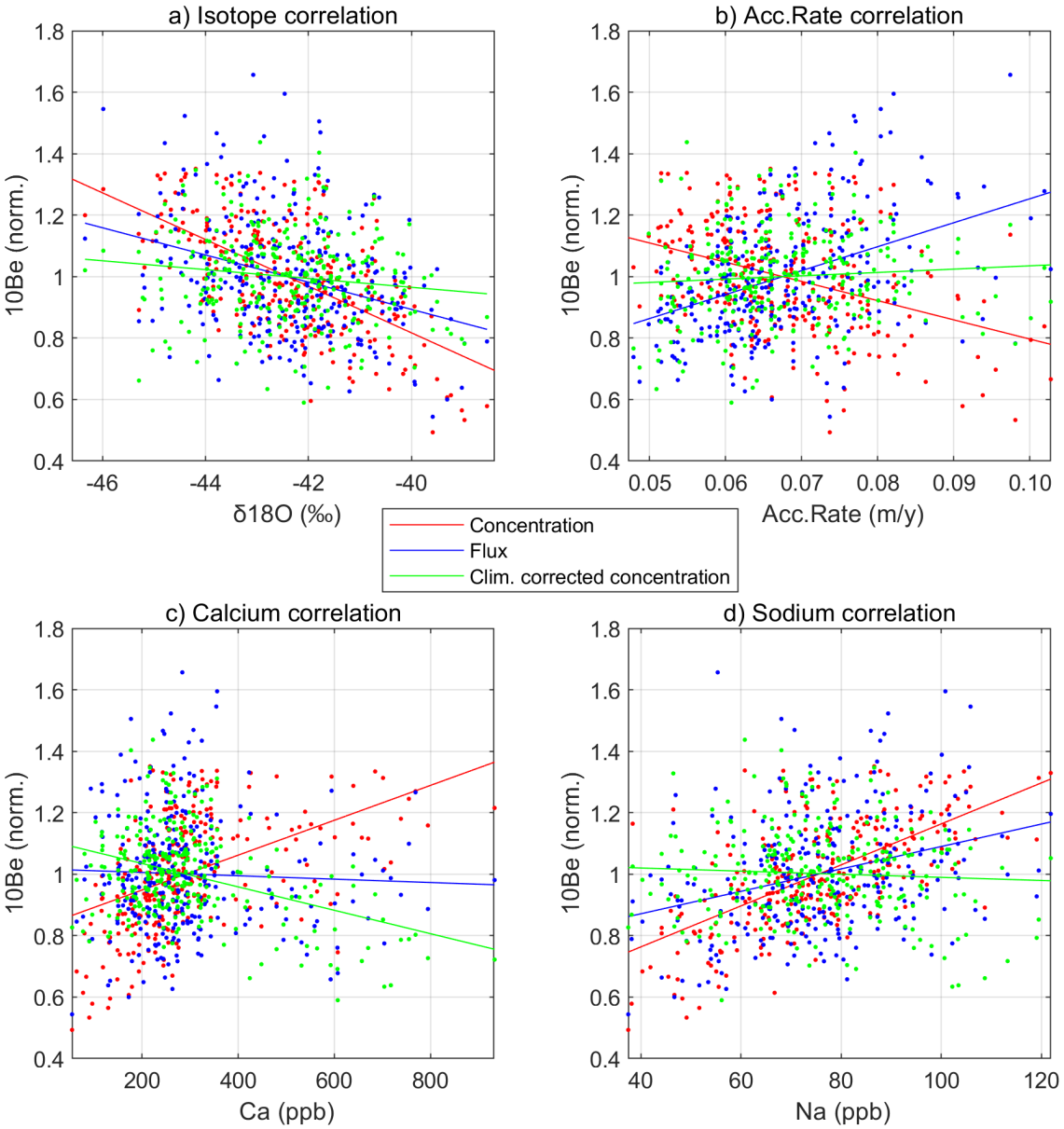

Figure 5.14 Correlation plots of NorthGRIP2 ^{10}Be data with climatic proxies.
Correlation between ^{10}Be concentrations and other proxies are to be expected, since the dilution of ^{10}Be in ice closely follows the amount of precipitation on the ice sheet. Correlations in the fluxes, however, indicate that the conversion does not completely eliminate the dependence of the ^{10}Be signal on the deposition effects. A different conversion from concentrations to production rate was obtained by multi-linear regression analysis of climatic proxies, i.e. by subtracting the linear trend detected in ^{10}Be concentrations against water isotopes, accumulation rates, calcium, and sodium (the mean of the data was added at the end for comparison to the original); this last ^{10}Be data series is called "climate corrected" (Adolphi & Muscheler, 2016).
(a) Correlations of ^{10}Be data series to water isotopes. Residual negative correlations are measured in the fluxes, concentrations, and even in the climate corrected concentrations. This shows that isotope correlate with the ^{10}Be in ways that are very likely influenced by a link of Greenland climate with the Sun's activity.

(b) The accumulation rate is anticorrelated to ^{10}Be concentrations, i.e. inversely proportional, as expected, the concentrations recording the dilution of the signal. After conversion, the fluxes retain a positive correlation, which is possibly a second order effect because of a mixed wet-dry depositional balance that is not accounted for by the simple conversion we have used. (c, d) The correlation to both calcium and sodium is mostly lost in the fluxes. For calcium, the low correlation to fluxes is reassuring us that ^{10}Be atoms did not adhere to dust particles that may have been affecting the signal balance over the dust peak.

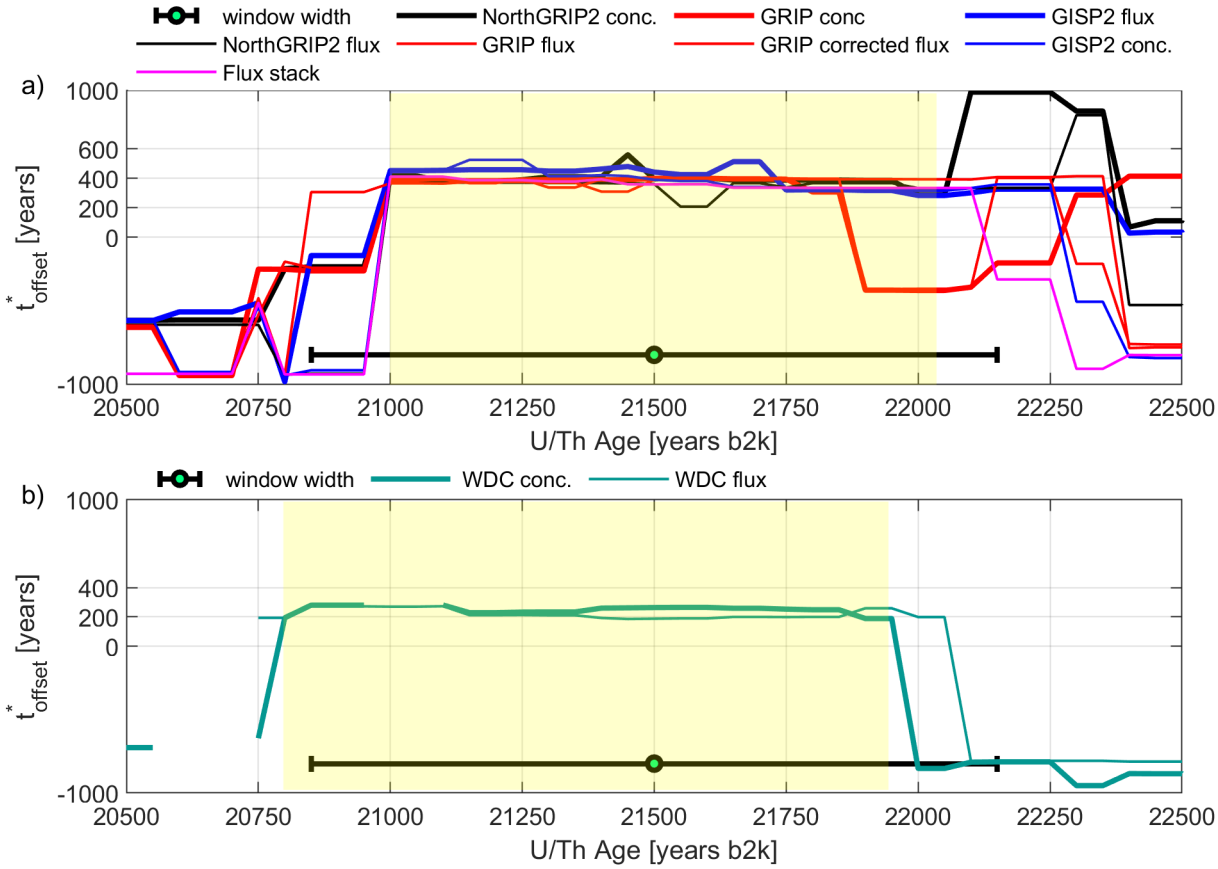

Figure 5.15 Initial wiggle-matching result, before adjusting the $\Delta^{14}C$ uncertainties to satisfy the χ^2 test, for Greenland, 369 years (a), and the WDC core, 235 years (b).
The time scale offset function $t^*_{offset}(\overrightarrow{W})$ was calculated as the mode of the underlying 2-dim probability density function, estimated by the algorithm. The window width (horizontal black bar) is highlighted to show that each data-point represents the data comparison within the windows $\overrightarrow{W}$. Across the intervals highlighted in yellow, the individual ice-core datasets agree about the offset for each ice-core timescale. We also observe that the offset is not strongly time-dependent, hence we average over the entire time interval.

5.12 References

Abreu, J. A., Beer, J., Steinhilber, F., Christl, M., & Kubik, P. W. 10Be in ice cores and 14C in tree rings: separation of production and climate effects. Space Science Reviews, 176(1), 343-349. https://doi.org/10.1007/s11214-011-9864-y , 2013

Adolphi, F., Muscheler, R., Svensson, A., Aldahan, A., Possnert, G., Beer, J., ... & Thieblemont, R. Persistent link between solar activity and Greenland climate during the Last Glacial Maximum. Nature Geoscience, 7(9), 662-666. https://doi.org/10.1038/ngeo2225 , 2014

Adolphi, F., & Muscheler, R. Synchronizing the Greenland ice core and radiocarbon timescales over the Holocene–Bayesian wiggle-matching of cosmogenic radionuclide records. Climate of the Past, 12(1), 15-30. https://doi.org/10.5194/cp-12-15-2016 , 2016

Adolphi, F., Bronk Ramsey, C., Erhardt, T., Edwards, R. L., Cheng, H., Turney, C. S., ... & Muscheler, R. Connecting the Greenland ice-core and U/Th timescales via cosmogenic radionuclides: testing the synchroneity of Dansgaard–Oeschger events. Climate of the Past, 14(11), 1755-1781. https://doi.org/10.5194/cp-14-1755-2018 , 2018

Andersen, K. K., Svensson, A., Johnsen, S. J., Rasmussen, S. O., Bigler, M., Röthlisberger, R., ... & Clausen, H. B. The Greenland ice core chronology 2005, 15–42 ka. Part 1: constructing the time scale. Quaternary Science Reviews, 25(23-24), 3246-3257. https://doi.org/10.1016/j.quascirev.2006.08.002 , 2006

Bard, E., Rostek, F., Turon, J. L., & Gendreau, S. Hydrological impact of Heinrich events in the subtropical northeast Atlantic. Science, 289(5483), 1321-1324. DOI: 10.1126/science.289.5483.1321 , 2000

Bauska, T. K., Marcott, S. A., & Brook, E. J. Abrupt changes in the global carbon cycle during the last glacial period. Nature Geoscience, 14(2), 91-96. https://doi.org/10.1038/s41561-020-00680-2 , 2021

Berggren, A. M., Beer, J., Possnert, G., Aldahan, A., Kubik, P., Christl, M., ... & Vinther, B. M. A 600-year annual 10Be record from the NGRIP ice core, Greenland. Geophysical Research Letters, 36(11). https://doi.org/10.1029/2009GL038004 , 2009

Björck, S., Walker, M. J., Cwynar, L. C., Johnsen, S., Knudsen, K. L., Lowe, J. J., & Wohlfarth, B. An event stratigraphy for the Last Termination in the North Atlantic region based on the Greenland ice-core record: a proposal by the INTIMATE group. Journal of Quaternary Science: Published for the Quaternary Research Association, 13(4), 283-292. https://doi.org/10.1002/(SICI)1099-1417(199807/08)13:4<283::AID-JQS386>3.0.CO;2-A , 1998

Broecker, W., & Barker, S. A 190‰ drop in atmosphere's Δ14C during the “Mystery Interval”(17.5 to 14.5 kyr). Earth and Planetary Science Letters, 256(1-2), 90-99. https://doi.org/10.1016/j.epsl.2007.01.015 , 2007

Bronk Ramsey, C. B., van der Plicht, J., & Weninger, B. ‘Wiggle matching’radiocarbon dates. Radiocarbon, 43(2A), 381-389. doi: 10.1017/S0033822200038248 , 2001

Buizert, C., Cuffey, K. M., Severinghaus, J. P., Baggenstos, D., Fudge, T. J., Steig, E. J., ... & Taylor, K. C. The WAIS Divide deep ice core WD2014 chronology–Part 1: Methane synchronization (68–31 ka BP) and the gas age–ice age difference. Climate of the Past, 11(2), 153-173. https://doi.org/10.5194/cp-11-153-2015 , 2015

Buizert, C., Sigl, M., Severi, M., Markle, B. R., Wettstein, J. J., McConnell, J. R., ... & Steig, E. J. Abrupt ice-age shifts in southern westerly winds and Antarctic climate forced from the north. Nature, 563(7733), 681-685. https://doi.org/10.1038/s41586-018-0727-5 , 2018

Cauquoin, A., Raisbeck, G. M., Jouzel, J., & Bard, E. No evidence for planetary influence on solar activity 330 000 years ago. Astronomy & Astrophysics, 561, A132. https://doi.org/10.1051/0004-6361/201322879 , 2014

Cheng, H., Edwards, R. L., Sinha, A., Spötl, C., Yi, L., Chen, S., ... & Zhang, H. The Asian monsoon over the past 640,000 years and ice age terminations. nature, 534(7609), 640-646. http://dx.doi.org/10.1038/nature18591 , 2016

Cheng, H., Edwards, R. L., Southon, J., Matsumoto, K., Feinberg, J. M., Sinha, A., ... & Ning, Y. Atmospheric 14C/12C changes during the last glacial period from Hulu Cave. science, 362(6420), 1293-1297. DOI: 10.1126/science.aau0747 , 2018

Cheng, H., Xu, Y., Dong, X., Zhao, J., Li, H., Baker, J., ... & Edwards, R. L. Onset and termination of Heinrich Stadial 4 and the underlying climate dynamics. Communications Earth & Environment, 2(1), 1-11. https://doi.org/10.1038/s43247-021-00304-6 , 2021

Christl, M., Vockenhuber, C., Kubik, P. W., Wacker, L., Lachner, J., Alfimov, V., & Synal, H. A. The ETH Zurich AMS facilities: Performance parameters and reference materials. Nuclear Instruments and Methods in Physics

Research Section B: Beam Interactions with Materials and Atoms, 294, 29-38. https://doi.org/10.1016/j.nimb.2012.03.004 , 2013

Corrick, E. C., Drysdale, R. N., Hellstrom, J. C., Capron, E., Rasmussen, S. O., Zhang, X., ... & Wolff, E. Synchronous timing of abrupt climate changes during the last glacial period. Science, 369(6506), 963-969. DOI: 10.1126/science.aay5538 , 2020

Eddy, J. A. The Maunder Minimum: The reign of Louis XIV appears to have been a time of real anomaly in the behavior of the sun. Science, 192(4245), 1189-1202. DOI: 10.1126/science.192.4245.1189 , 1976

EPICA Community Members. One-to-one coupling of glacial climate variability in Greenland and Antarctica. Nature 444, 195–198 https://doi.org/10.1038/nature05301 , 2006

Erhardt, T., Bigler, M., Federer, U., Gfeller, G., Leuenberger, D., Stowasser, O., ... & Fischer, H. High resolution aerosol concentration data from the Greenland NorthGRIP and NEEM deep ice cores. Earth System Science Data Discussions, 1-25. https://doi.org/10.5194/essd-2021-324 , 2021

Finkel, R. C., & Nishiizumi, K. Beryllium 10 concentrations in the Greenland Ice Sheet Project 2 ice core from 3–40 ka. Journal of Geophysical Research: Oceans, 102(C12), 26699-26706. https://doi.org/10.1029/97JC01282 , 1997

Fudge, T. J., Markle, B. R., Cuffey, K. M., Buizert, C., Taylor, K. C., Steig, E. J., ... & Koutnik, M. Variable relationship between accumulation and temperature in West Antarctica for the past 31,000 years. Geophysical Research Letters, 43(8), 3795-3803. https://doi.org/10.1002/2016GL068356 , 2016

Fudge, T. J., & Fudge, T. J. WD2014: Timescale for WAIS Divide Core 2006 A (WDC-06A)" U.S. Antarctic Program (USAP) Data Center. https://doi.org/10.15784/60101 , 2017

Guillevic, M., Bazin, L., Landais, A., Stowasser, C., Masson-Delmotte, V., Blunier, T., ... & Vinther, B. M. Evidence for a three-phase sequence during Heinrich Stadial 4 using a multiproxy approach based on Greenland ice core records. Climate of the Past, 10(6), 2115-2133. https://doi.org/10.5194/cp-10-2115-2014 , 2014

He, C., Liu, Z., Otto-Bliesner, B. L., Brady, E. C., Zhu, C., Tomas, R., ... & Severinghaus, J. P. Abrupt Heinrich Stadial 1 cooling missing in Greenland oxygen isotopes. Science advances, 7(25), eabh1007. DOI: 10.1126/sciadv.abh1007 , 2021

Heikkilä, U., Beer, J., Abreu, J. A., & Steinhilber, F. On the atmospheric transport and deposition of the cosmogenic radionuclides (10Be): A review. Space Science Reviews, 176(1), 321-332. https://doi.org/10.1007/s11214-011-9838-0 , 2013

Herbst, K., Muscheler, R., & Heber, B. The new local interstellar spectra and their influence on the production rates of the cosmogenic radionuclides 10Be and 14C. Journal of Geophysical Research: Space Physics, 122(1), 23-34. https://doi.org/10.1002/2016JA023207 , 2017

Hughes, P. D., Gibbard, P. L., & Ehlers, J. Timing of glaciation during the last glacial cycle: evaluating the concept of a global ‘Last Glacial Maximum’(LGM). Earth-Science Reviews, 125, 171-198. https://doi.org/10.1016/j.earscirev.2013.07.003 , 2013

Hughes, P. D., & Gibbard, P. L. A stratigraphical basis for the Last Glacial Maximum (LGM). Quaternary International, 383, 174-185. https://doi.org/10.1016/j.quaint.2014.06.006 , 2015

Hvidberg, C. S., Keller, K., Gundestrup, N. S., Tscherning, C. C., & Forsberg, R. Mass balance and surface movement of the Greenland Ice Sheet at Summit, Central Greenland. Geophysical research letters, 24(18), 2307-2310. https://doi.org/10.1029/97GL02280 , 1997

Johnsen, S. J., Clausen, H. B., Dansgaard, W., Gundestrup, N. S., Hammer, C. U., Andersen, U., ... & Fisher, D. The δ18O record along the Greenland Ice Core Project deep ice core and the problem of possible Eemian climatic instability. Journal of Geophysical Research: Oceans, 102(C12), 26397-26410. https://doi.org/10.1029/97GL02280 , 1997

Johnsen, S. J., Dahl-Jensen, D., Gundestrup, N., Steffensen, J. P., Clausen, H. B., Miller, H., ... & White, J. Oxygen isotope and palaeotemperature records from six Greenland ice-core stations: Camp Century, Dye-3, GRIP, GISP2, Renland and NorthGRIP. Journal of Quaternary Science: Published for the Quaternary Research Association, 16(4), 299-307. https://doi.org/10.1002/jqs.622 , 2001

Jones, T. R., Cuffey, K. M., White, J. W. C., Steig, E. J., Buizert, C., Markle, B. R., ... & Sigl, M. Water isotope diffusion in the WAIS Divide ice core during the Holocene and last glacial. Journal of Geophysical Research: Earth Surface, 122(1), 290-309. https://doi.org/10.1002/2016JF003938 , 2017

Jouzel, J., Alley, R. B., Cuffey, K. M., Dansgaard, W., Grootes, P., Hoffmann, G., ... & White, J. Validity of the temperature reconstruction from water isotopes in ice cores. Journal of Geophysical Research: Oceans, 102 https://doi.org/10.1029/97JC01283, 1997 , 1997

Knudsen, M. F., Riisager, P., Jacobsen, B. H., Muscheler, R., Snowball, I., & Seidenkrantz, M. S. Taking the pulse of the Sun during the Holocene by joint analysis of 14C and 10Be. Geophysical Research Letters, 36(16). https://doi.org/10.1029/2009GL039439 , 2009

Kovaltsov, G. A., Mishev, A., and Usoskin, I. G.: A new model of cosmogenic production of radiocarbon 14C in the atmosphere, Earth Planet. Sc. Lett., 337–338, 114–120 doi:10.1016/j.epsl.2012.05.036 , 2012

Köhler, P., Adolphi, F., Butzin, M., & Muscheler, R. Toward reconciling radiocarbon production rates with carbon cycle changes of the last 55,000 years. Paleoceanography and Paleoclimatology, 37(2), e2021PA004314. https://doi.org/10.1029/2021PA004314 , 2022

Landais, A., Capron, E., Masson-Delmotte, V., Toucanne, S., Rhodes, R., Popp, T., ... & Prié, F. Ice core evidence for decoupling between midlatitude atmospheric water cycle and Greenland temperature during the last deglaciation. Climate of the Past, 14(10), 1405-1415. https://doi.org/10.5194/cp-14-1405-2018 , 2018

Li, T. Y., Wu, Y., Shen, C. C., Li, J. Y., Chiang, H. W., Lin, K., ... & Edwards, R. L. High precise dating on the variation of the Asian summer monsoon since 37 ka BP. Scientific reports, 11(1), 1-14. https://doi.org/10.1038/s41598-021-88597-7 , 2021

Lin, J., Svensson, A., Hvidberg, C. S., Lohmann, J., Kristiansen, S., Dahl-Jensen, D., ... & Mulvaney, R. Magnitude, frequency and climate forcing of global volcanism during the last glacial period as seen in Greenland and Antarctic ice cores (60–9 ka). Climate of the Past Discussions, 1-45. https://doi.org/10.5194/cp-2021-100 , 2021

Masarik, J., & Beer, J. An updated simulation of particle fluxes and cosmogenic nuclide production in the Earth's atmosphere. Journal of Geophysical Research: Atmospheres, 114(D11). https://doi.org/10.1029/2008JD010557 , 2009

McManus, J. F., Francois, R., Gherardi, J. M., Keigwin, L. D., & Brown-Leger, S. Collapse and rapid resumption of Atlantic meridional circulation linked to deglacial climate changes. nature, 428(6985), 834-837. https://doi.org/10.1038/nature02494 , 2004

Muscheler, R., Beer, J., Wagner, G., & Finkel, R. C. Changes in deep-water formation during the Younger Dryas event inferred from 10Be and 14C records. Nature, 408(6812), 567-570. https://doi.org/10.1038/35046041 , 2000

Muscheler, R., Beer, J., Wagner, G., Laj, C., Kissel, C., Raisbeck, G. M., ... & Kubik, P. W. Changes in the carbon cycle during the last deglaciation as indicated by the comparison of 10Be and 14C records. Earth and Planetary Science Letters, 219(3-4), 325-340. https://doi.org/10.1016/S0012-821X(03)00722-2 , 2004

Muscheler, R. 14C and 10Be around 1650 cal BC:: are there contradictions between tree ring and ice core time scales?. Monographs of the Danish Institute at Athens (MoDIA), 10, 275-284. , 2009

Muscheler, R., Adolphi, F., & Knudsen, M. Assessing the differences between the IntCal and Greenland ice-core time scales for the last 14,000 years via the common cosmogenic radionuclide variations. Quaternary Science Reviews, 106, 81-87. http://dx.doi.org/10.1016/j.quascirev.2014.08.017 , 2014

Nguyen, L., Paleari, C. I., Müller, S., Christl, M., Mekhaldi, F., Gautschi, P., ... & Muscheler, R. The potential for a continuous 10Be record measured on ice chips from a borehole. Results in Geochemistry, 5, 100012. https://doi.org/10.1016/j.ringeo.2021.100012 , 2021

Nishiizumi, K., Imamura, M., Caffee, M. W., Southon, J. R., Finkel, R. C., & McAninch, J. Absolute calibration of 10Be AMS standards. Nuclear Instruments and Methods in Physics Research Section B: Beam Interactions with Materials and Atoms, 258(2), 403-413. https://doi.org/10.1016/j.nimb.2007.01.297 , 2007

North Greenland Ice Core Project members. High resolution record of Northern Hemisphere climate extending into the last interglacial period. Nature, 431(7005), 147-151. https://doi.org/10.1038/nature02805, 2004

Peck, V. L., Hall, I. R., Zahn, R., Elderfield, H., Grousset, F., Hemming, S. R., & Scourse, J. D. High resolution evidence for linkages between NW European ice sheet instability and Atlantic Meridional Overturning Circulation. Earth and Planetary Science Letters, 243(3-4), 476-488. https://doi.org/10.1016/j.epsl.2005.12.023 , 2006

Pedro, J. B., Van Ommen, T. D., Rasmussen, S. O., Morgan, V. I., Chappellaz, J., Moy, A. D., ... & Delmotte, M. The last deglaciation: timing the bipolar seesaw. Climate of the Past, 7(2), 671-683. https://doi.org/10.5194/cp-7-671-2011 , 2011

Pedro, J. B., Jochum, M., Buizert, C., He, F., Barker, S., & Rasmussen, S. O. Beyond the bipolar seesaw: Toward a process understanding of interhemispheric coupling. Quaternary Science Reviews, 192, 27-46. https://doi.org/10.1016/j.quascirev.2018.05.005, 2018

Raisbeck, G. M., Yiou, F., Fruneau, M., Loiseaux, J. M., Lieuvin, M., Ravel, J. C., & Lorius, C. Cosmogenic 10Be concentrations in Antarctic ice during the past 30,000 years. Nature, 292(5826), 825-826. https://doi.org/10.1038/292825a0 , 1981

Rasmussen, S. O., Andersen, K. K., Svensson, A. M., Steffensen, J. P., Vinther, B. M., Clausen, H. B., ... & Ruth, U. A new Greenland ice core chronology for the last glacial termination. Journal of Geophysical Research: Atmospheres, 111(D6). https://doi.org/10.1029/2005JD006079 , 2006

Rasmussen, S. O., Seierstad, I. K., Andersen, K. K., Bigler, M., Dahl-Jensen, D., & Johnsen, S. J. Synchronization of the NGRIP, GRIP, and GISP2 ice cores across MIS 2 and palaeoclimatic implications. Quaternary Science Reviews, 27(1-2), 18-28. https://doi.org/10.1016/j.quascirev.2007.01.016 , 2008

Rasmussen, S. O., Bigler, M., Blockley, S. P., Blunier, T., Buchardt, S. L., Clausen, H. B., ... & Winstrup, M. A stratigraphic framework for abrupt climatic changes during the Last Glacial period based on three synchronized Greenland ice-core records: refining and extending the INTIMATE event stratigraphy. Quaternary Science Reviews, 106, 14-28. https://doi.org/10.1016/j.quascirev.2014.09.007 , 2014

Reimer, P. J., Austin, W. E., Bard, E., Bayliss, A., Blackwell, P. G., Ramsey, C. B., ... & Talamo, S. The IntCal20 Northern Hemisphere radiocarbon age calibration curve (0–55 cal kBP). Radiocarbon, 62(4), 725-757. doi:10.1017/RDC.2020.41 , 2020

Rhodes, R. H., Brook, E. J., Chiang, J. C., Blunier, T., Maselli, O. J., McConnell, J. R., ... & Severinghaus, J. P. Enhanced tropical methane production in response to iceberg discharge in the North Atlantic. Science, 348(6238), 1016-1019. DOI: 10.1126/science.1262005 , 2015

Schüpbach, S., Fischer, H., Bigler, M., Erhardt, T., Gfeller, G., Leuenberger, D., ... & Wolff, E. W. Greenland records of aerosol source and atmospheric lifetime changes from the Eemian to the Holocene. Nature communications, 9(1), 1-10. https://doi.org/10.1038/s41467-018-03924-3 , 2018

Seierstad, I. K., Abbott, P. M., Bigler, M., Blunier, T., Bourne, A. J., Brook, E., ... & Vinther, B. M. Consistently dated records from the Greenland GRIP, GISP2 and NGRIP ice cores for the past 104 ka reveal regional millennial-scale δ18O gradients with possible Heinrich event imprint. Quaternary Science Reviews, 106, 29-46. https://doi.org/10.1016/j.quascirev.2014.10.032 , 2014

Sharma P., Bourgeois M., Elmore D., Granger D., Lipschutz M. E., Ma X., Miller T., Mueller K., Rickey F., Simms P. and Vogt S. RIME lab AMS performance, upgrades and research applications. Nuclear Instruments and Methods B172, 112-123. https://doi.org/10.1016/S0168-583X(00)00132-4 , 2000

Siegenthaler, U. Uptake of excess CO2 by an outcrop-diffusion model of the ocean. Journal of Geophysical Research: Oceans, 88(C6), 3599-3608. https://doi.org/10.1029/JC088iC06p03599 , 1983

Sigl, M., Fudge, T. J., Winstrup, M., Cole-Dai, J., Ferris, D., McConnell, J. R., ... & Sowers, T. A. The WAIS Divide deep ice core WD2014 chronology–Part 2: Annual-layer counting (0–31 ka BP). Climate of the Past, 12(3), 769-786. https://doi.org/10.5194/cp-12-769-2016 , 2016

Southon, J., Noronha, A. L., Cheng, H., Edwards, R. L., & Wang, Y. A high-resolution record of atmospheric 14C based on Hulu Cave speleothem H82. Quaternary Science Reviews, 33, 32-41. https://doi.org/10.1016/j.quascirev.2011.11.022 , 2012

Steinhilber, F., Abreu, J. A., Beer, J., Brunner, I., Christl, M., Fischer, H., ... & Wilhelms, F. 9,400 years of cosmic radiation and solar activity from ice cores and tree rings. Proceedings of the National Academy of Sciences, 109(16), 5967-5971. https://doi.org/10.1073/pnas.1118965109 , 2012

Stocker, T. F., & Johnsen, S. J. A minimum thermodynamic model for the bipolar seesaw. Paleoceanography, 18(4). https://doi.org/10.1029/2003PA000920 , 2003

Stuiver, M., & Polach, H. A. Discussion reporting of 14C data. Radiocarbon, 19(3), 355-363. doi:10.1017/S0033822200003672 , 1977

Stuiver, M., & Grootes, P. M. GISP2 oxygen isotope ratios. Quaternary Research, 53(3), 277-284. doi:10.1006/qres.2000.2127 , 2000

Svensson, A., Andersen, K. K., Bigler, M., Clausen, H. B., Dahl-Jensen, D., Davies, S. M., ... & Vinther, B. M. The Greenland ice core chronology 2005, 15–42 ka. Part 2: comparison to other records. Quaternary Science Reviews, 25(23-24), 3258-3267. https://doi.org/10.1016/j.quascirev.2006.08.003 , 2006

Svensson, A., Andersen, K. K., Bigler, M., Clausen, H. B., Dahl-Jensen, D., Davies, S. M., ... & Vinther, B. M. A 60 000 year Greenland stratigraphic ice core chronology. Climate of the Past, 4(1), 47-57. https://doi.org/10.5194/cp-4-47-2008 , 2008

Svensson, A., Dahl-Jensen, D., Steffensen, J. P., Blunier, T., Rasmussen, S. O., Vinther, B. M., ... & Bigler, M. Bipolar volcanic synchronization of abrupt climate change in Greenland and Antarctic ice cores during the last glacial period. Climate of the Past, 16(4), 1565-1580. https://doi.org/10.5194/cp-16-1565-2020 , 2020

Wagner, G., Beer, J., Masarik, J., Muscheler, R., Kubik, P. W., Mende, W., ... & Yiou, F. Presence of the solar de Vries cycle (∼ 205 years) during the last ice age. Geophysical Research Letters, 28(2), 303-306. https://doi.org/10.1029/2000GL006116 , 2001

WAIS Divide Project Members. Onset of deglacial warming in West Antarctica driven by local orbital forcing. Nature, 500(7463), 440-444. https://doi.org/10.1038/nature12376 , 2013

WAIS Divide Project Members. Precise interpolar phasing of abrupt climate change during the last ice age. Nature, 520(7549), 661-665. https://doi.org/10.1038/nature14401 , 2015

Wang, Y. J., Cheng, H., Edwards, R. L., An, Z. S., Wu, J. Y., Shen, C. C., & Dorale, J. A. A high-resolution absolute-dated late Pleistocene monsoon record from Hulu Cave, China. Science, 294(5550), 2345-2348. DOI: 10.1126/science.1064618 , 2001

Winstrup, M., Svensson, A. M., Rasmussen, S. O., Winther, O., Steig, E. J., & Axelrod, A. E. An automated approach for annual layer counting in ice cores. Climate of the Past, 8(6), 1881-1895. https://doi.org/10.5194/cp-8-1881-2012 , 2012

Woodruff T. E., Welten K. C., Caffee M. W. and Nishiizumi K. nterlaboratory comparison of 10Be concentrations in two ice cores from Central West Antarctica. Nuclear Instruments and Methods in Physics Research, B294, 77–80. https://doi.org/10.1016/j.nimb.2012.08.033 , 2013

Yiou, F., Raisbeck, G. M., Baumgartner, S., Beer, J., Hammer, C., Johnsen, S., ... & Yiou, P. Beryllium 10 in the Greenland ice core project ice core at summit, Greenland. Journal of Geophysical Research: Oceans, 102(C12), 26783-26794. https://doi.org/10.1029/97JC01265 , 1997

6 Conclusive Remarks and Outlook

For the field of paleoclimate studies to keep up with the fast pace of new discoveries it is important that the chronologies are maintained in good shape. The inter-regional comparison of climatic archives continues to prove useful in understanding the Earth's paleoclimate.

In this thesis, I have inspected the GICC revision in the Holocene and I have provided indications of how much accumulated error there is in the LGM. Now that the GICC21 revision has been started and that the radiocarbon calibration curves have been updated, I believe a revision of AICC2012 could also be initiated.

The GICC21 timescale should be extended to the Mid and Early Holocene. The procedure of manual fine-tuning and multi-core comparison should be continued. From a methodological standpoint, the SC algorithm could be improved to solve the problem with the undercount over data gaps (see 3.5.3) and to generally improve the algorithm's performance, a task that may require a heavier intervention into the algorithm than what I have personally attempted. In addition, the SC algorithm could be modified in such a way to count multiple parallel ice-cores together.

The lack of NEEM and NorthGRIP CFA data over the brittle zone may be an obstacle for the Mid Holocene chronology, but the useful EastGRIP dataset will be vital for closing the gap in the Holocene chronology (Jensen, 2020). The coastal ice core from Renland (RECAP) may also prove useful in this context. This ice core has a preserved Holocene annual-layer record because of its shallowness (~400 m), preventing the formation of brittle ice. The RECAP ice core was not used for the GICC21 because of the sufficient high quality of the other ice cores, while Renland has thin and irregular layer patterns. The RECAP ice core has previously been dated using mixed approaches over the Holocene (Simonsen et al., 2019). At least some of the RECAP layers could ameliorate the GICC in the Mid Holocene, but a fine-tuning procedure is likely to be repeated for incorporating this ice core into the GICC.

More ^{10}Be measurements over the Holocene could prove useful for the update of the GICC. By inspecting IntCal20, promising radionuclide production features could be measured in ice-core ^{10}Be to provide a verification of the ice-core alignment with tree rings in the Mid and Early Holocene (e.g. Brehm et al., 2022). A bipolar match to the Antarctic timescale WD2014 over the Holocene would be useful to compare the Polar regions further back in time, as would be the inclusion of more tree-ring growth records into a composite to provide better insight about the alignment of ice cores and tree rings around volcanic eruptions.

I provided evidence that the isotope records in Greenland cool down for about 10 years after strong tropical eruptions, more than is usually estimated from Greenland surface temperature (Box et al., 2009) but compatible with modelling on a larger scale (Kobashi et al., 2017) and with the tree-ring analysis by Sigl et al. (2015). This study was possible thanks both to the GICC21 accuracy and to the wealth of ice-core data. The water isotope signal of EastGRIP may provide additional answers, once released. More analysis would be needed to test if these results also apply for northern-hemispheric eruptions (e.g. strong Icelandic eruptions) and if the clustering of eruptions is relevant for Holocene climate change in Greenland.
No Mediterranean tephra has ever been found in Greenlandic ice cores, and the quest for the identification of the Thera eruption remains open. The GICC21 timescale would allow a very precise dating of Thera with a tightly constrained uncertainty, which could help solve the long-lasting debate about the age of this eruption. It is currently not possible to connect any specific acidity spike in ice cores with this eruption, because of the multi-modality of the radiocarbon dated evidence, which indicates several possible ages. A measurement of sulfate isotopes may reconstruct whether any of the ECM peaks comes from a bipolar eruption (Gautier et al., 2019), and two candidates for a crypto-tephra search in Greenlandic ice cores were suggested in this thesis, at 3540 years b2k and ~3600-3610 years b2k.

In the glacial, the GICC05 will need to be revised as well, but the challenge of layer recognition might be hard to overcome. It would be advisable to gather more data in sufficiently high resolution from recently drilled ice cores, such as NEEM or EastGRIP, and to repeat the layer counting over GS-2 and 3.
The aid of the ^{10}Be data has been fundamental in closing the synchronization gap between Greenland, Antarctica and Hulu Cave over the LGM. Next, bipolar volcanic tie points across the LGM may be found by counting annual layers in the eruption intervals, with the aid of the two independent ^{10}Be tie points.
After synchronizing the three independent timescales of Hulu, GICC05, and WD2014, the sequence of events around GS-3 has become clearer. The signature of the HS-2 was almost synchronous in Greenlandic dust, Hulu oxygen isotopes, and WDC water isotopes, followed by the methane record of WDC about 300 years later. It appears that, in the case of AIM-2, the onset of the warming is more related to the beginning of HS-2 than to the onset of the D-O events in Greenland. One possible explanation of this sequence of events lies in a powerful shutdown of the AMOC during HS-2, which initiated warming in Antarctica similar to what

the bipolar-seesaw mechanism predicts. To strengthen this interpretation, one would need a chronologically accurate average of Antarctic isotope records, or at least a comparison of the AIM-2 signature in other parts of the Antarctic ice sheet. I expect and hope that more detailed studies of Heinrich Stadial 2 will become possible thanks to the inter-regional synchronization we have provided in Paper V.

6.1 References

Box, J. E., Yang L., et al. Greenland Ice Sheet Surface Air Temperature Variability: 1840-2007. Journal of Climate, 4029-4049. https://doi.org/10.1175/2009JCLI2816.1, 2009

Brehm, N., Christl, M., Adolphi, F., Muscheler, R., Synal, H. A., Mekhaldi, F., ... & Wacker, L. Tree rings reveal two strong solar proton events in 7176 and 5259 BCE. Nat. Commun. 13. 1196 https://doi.org/10.21203/rs.3.rs-753272/v1, 2022

Gautier, E., et al. 2600-years of stratospheric volcanism through sulfate isotopes. Nat Commun 10, 466. https://doi.org/10.1038/s41467-019-08357-0, 2019

Jensen, C. M. Continuous high-resolution aerosol record from the East Greenland Ice Core Project covering the entire Holocene (Doctoral dissertation, Institute for Climate and Environmental Physics and Oeschger Centre for Climate Change Research, University of Bern). https://boris.unibe.ch/158023/, 2021

Kobashi, T., Menviel, L., Jeltsch-Thömmes, A., Vinther, B. M., Box, J. E., Muscheler, R., . . . others. Volcanic influence on centennial to millennial Holocene Greenland temperature change. Scientific reports, 7, 1–10. https://doi.org/10.1038/s41598-017-01451-7, 2017

Sigl, M., Winstrup, M., McConnell, J. R., Welten, K. C., Plunkett, G., Ludlow, F., … Woodruff, T. E. Timing and climate forcing of volcanic eruptions for the past 2,500 years. Nature, 523(7562), 543–549. https://doi.org/10.1038/nature14565 , 2015

Simonsen, M.F., G. Baccolo, T. Blunier, A. Borunda, B. Delmonte, R. Frei, S. Goldstein, A. Grinsted, H.A. Kjær, T. Sowers, A. Svensson, B. Vinther, D. Vladimirova, G. Winckler, M. Winstrup and P. Vallelonga. East Greenland ice core dust record reveals timing of Greenland ice sheet advance and retreat. Nature Communications. doi: 10.1038/s41467-019-12546-2, 2019